Machine and Process Development for the Robust Machining of Microstructures on Free-Form Surfaces for Hybrid Optics

Final report of BMBF collaboration project »ERANET-OPTICALSTRUCT«

Prof. Christian Brecher (Editor)

Fraunhofer Institute for Production Technology IPT

SPONSORED BY THE

Federal Ministry
of Education
and Research

Bibliographic information published by Die Deutsche Bibliothek.
Die Deutsche Bibliothek lists this publication in the Deutsche Nationalbibliographie; detailed bibliographic data are available at http://dnb.ddb.de.

Editor: Christian Brecher

Machine and Process Development for the Robust Machining of Microstructures on Free-Form Surfaces for Hybrid Optics

Printed on acid-free paper

Wissenschaftsverlag des Instituts für Industriekommunikation und Fachmedien
an der RWTH Aachen
Steinbachstr. 25, 52074 Aachen
URL: www.apprimus-verlag.de, E-Mail: info@apprimus-verlag.de

Printed in Germany

ISBN 978-3-940565-79-2

The German partners of this research and development project were funded by the German Federal Ministry of Education and Research (BMBF) within the Framework Concept ”Research for Tomorrow’s Production” (funding numbers 02PG2620, 02PG2621, 02PG2622 and 02PG2623) and managed by the Project Management Agency Forschungszentrum Karlsruhe (PTKA).

The authors are responsible for the contents of this publication.

Authors

Prof. Christian Brecher (Fraunhofer IPT)

Michael Merz (Fraunhofer IPT)

Frank Niehaus (Fraunhofer IPT)

Claus Richterich (ModuleWorks)

Kari Rinko (Oy Modines)

Erik Schalle (Eschenbach)

Dr. Kai Schmidt (LT Ultra)

Dr. Marc Stautner (ModuleWorks)

Antonio Ventura-Traveset (Unimetrik/DataPixel)

Manfred Zavelberg (Fraunhofer IPT)

Table of Contents

Formulas, Symbols and Abbreviations

A	m²	Area
a_p	µm	Depth of cut
ADC		Analog/Digital converter
ADE		Abstract data encapsulation
API		Application programming interface
BRAM		Block RAM
CAD		Computer aided design
CAM		Computer aided manufacturing
CAP		Computer aided planning
CMM		Coordinate measurement machine
DAC		Digital/Analog converter
DDR		Double data rate
DO		Diffractive optics
DOE		Diffractive optic element
DLL		Dynamically linked library
DPRAM		Dual ported RAM
ECAP		Equal channel angular processing
EDX		Energy dispersive X-ray
EMF		Electromotive force
f	µm/rot	Feed rate, infeed
F	N	Force
FOV		Field of view
FPGA		Field programmable gate array
FT/ST		Fast Tool / Slow Tool
FTS		Fast Tool Servo
GUI		Graphical user interface
HAL		Hardware abstraction layer
HMI		Human machine interface
HV		Vickers hardness
IC		Integrated circuit
IGES		Initial graphics exchange specification

I/O		Input/Output
JTAG		Joint test action group - IEEE 1149.1
k	N/µm	Stiffness
LAN		Local area network
LCD		Liquid crystal display
LED		Light emitting diode
NC		Numerical control
Ni		Nickel
NiP		Nickel-phosphorus
NRS		Non-rotationally symmetric
NRZ		Non return to zero
NURBS		Non-uniform rational B-splines
OFHC		Oxygen free high conductive
OpenGL		Open graphics library
P		Phosphorus, proportional (control)
PC		Polycarbonate, personal computer
PCI		Peripheral component interconnect
PCIe		Peripheral component interconnect express
PDMS		Polydimethylsiloxane
PI		Proportional-integral (control)
PLC		Programmable logic control
PMMA		Polymethylmethacrylate
PTB		Physikalisch-Technische Bundesanstalt
Ra		Surface roughness
RAM		Random access memory
RPC		Remote procedure call
rs		Rotationally symmetric
s	µm	Stroke
SDRAM		Synchronous dynamic RAM
SEM		Scanning electron microscope
SOAP		Simple object access protocol
SPM		Scanning probes microscopy

STEP		Standard for the exchange of product model data
t	s	Time, process time
TTL		Transistor/transistor logic (voltage level specification)
U	V	Voltage
UBUS		Universal bus
UMAC		Universal motion and automation controller
UP		Ultra-precision
USB		Universal serial bus
UV		Ultra-violet
v_c	m/min	Cutting speed
VHDL		Very high speed integrated circuit hardware description language

1 Preface

Complex optical components are essential for advanced products. Examples range from miniature lighting systems for display technology in mobile phones and laptops, or ophthalmologic lenses to highly sophisticated LED-based lighting units for the automotive industry. Although the manufacturing of free-form surfaces or micro-structures is nowadays more or less possible, the machining of complex structured free-form surfaces has not yet been satisfactorily solved. Typically, lithography has been used to generate such finite structures. However, the process is expensive and limited to selected geometries. Diamond machining is an alternative process, but has to be optimized for microstructuring.

In this context, the project »ERANET-OPTICALSTRUCT« aimed to establish a complete process chain for the production of free-form surfaces for hybrid optics for the very first time. A new ultra-precision machining system, equipped with a hybrid Fast Tool Servo system, has been developed and several tests were performed to enable the machining of high quality microstructures on free-form surfaces (hybrid optics) and their replication. The characterization of the microstructures was conducted by a novel miniature tactile sensor.

Following results were achieved:

- A new generation of machine tools and control strategies for highly-dynamic ultra-precision machining
- Innovative process alternatives for complex structured free-form surfaces based on this new machining technology
- A miniaturized, tactile measuring system with a tip of 20 nm radius for the characterization of microstructures
- Innovative optical applications and products based on hybrid optics

The developments of »ERANET-OPTICALSTRUCT« in the field of highly dynamic axes, for example, now allow for the combination of a Fast Tool Servo (FTS) with a dynamic long-axis, a so-called Slow Tool servo, to a hybrid system FTS. Thus, higher dynamics in machining than the state of the technology are possible. This represents roughly a doubling of the possible working frequencies, and consequently, a significant process time reduction. A new hybrid control technology with an integration of a Fast and a Slow Tool is now functional, and allows for new opportunities for the manufacturing of hybrid optics.

The consortium was composed of European technology leaders from Belgium, Finland, Germany, The Netherlands, and Spain as part of the MNT ERA-NET of the European Commission for Micro- and Nanotechnology in order to enable innovative transnational collaboration. The German partners in this project have been funded by the German Federal Ministry of Education and Research (BMBF) within the

framework concept »Research for Tomorrow's Production«. Thanks to all partners for their cooperation and commitment.

Forschungszentrum Karlsruhe GmbH

Project Management Agency Forschungszentrum Karlsruhe (PTKA)

Stefan Scherr

September 2009

Opticalstruct

BETREUT VOM

Projektträger
Forschungszentrum
Karlsruhe (PTKA)

2 Introduction

2.1 Topical Background

Complex optical components are essential functional elements in modern products. Examples are miniaturized illumination systems for mobile phones or notebook displays, bi-focal glasses or contact lenses with diffractive structures or technical highly challenging optics for LED headlights in the automotive industry (**Figure 2.1**).

Figure 2.1: LED headlights for automotive applications (Courtesy: Audi)

The demand for optics with increasing functionality requires the development of more complex optical elements. Examples are hybrid lenses that combine refractive optics with diffractive microstructures. Typically, optical systems use the principle of refraction. Light is refracted passing a lens due to the different refraction indices of the lens material and the surrounding media (air in most cases) along the continuous outline of the lens. In contrast to refractive optics, many microstructured optics are based on diffraction. Structures in the range of the wavelength of the used light bend and re-direct the beam of light. By combining diffractive and refractive functions to hybrid optical systems a high potential of cost saving and light weight design is possible due to the integration of multiple functions into one optical element.

During the development phase of innovative optical systems the optic designers are supported by powerful software, which enables the design and layout of complex diffractive as well as hybrid optics. Though the design of complex optics is possible, certain and efficient process chains for the machining of these optics are not available in industry.

First applications of hybrid optics can be found in high end camera objectives. Standard objectives use combinations of single lenses (achromatic lenses) for the correction of the chromatic aberration. Additional correction lenses increase the number of lenses, the size as well as the weight. Furthermore, the combination of many lenses decreases the imaging quality. These issues can be solved using hybrid optics. A diffractive structure at the backside of a refractive lens is enabling the color correction usually realized by achromatic lenses. Due to the integration of different

functions into one hybrid lens, the size and the weight of the camera objective could be reduced by a third.

The replication of hybrid optics by injection molding for mass production of optics often requires mold inserts that combine microstructures with free-form surfaces. This is not only necessary for polymer lenses with free-form shapes, but also for lenses with a spherical geometry. The shrinkage of the polymer lenses in the molding process has to be considered in the design and machining of the according molds. The compensation leads to molds with free-form shape. These free-form molds need to be microstructured for the production of hybrid optics by injection molding.

Microstructures with optical functionality are not only interesting for hybrid optics. Fields of application with high potential can be found in illumination techniques. As successor of the light bulb, light emitting diodes (LED) gain in importance and offer a three to five times higher light efficiency [lm/W]. Combined with innovative optical design LED systems are used for illumination of buildings, in automotive, or display technologies. Examples are illustrated in **Figure 2.2**. The main task of such illumination optics is the conversion of the point light source of a high-power LED into a planar light source with directed light outcoupling on a maximal area. Due to the directed light outcoupling, disturbances of the environment by a light source, so called »light pollution«, can be reduced. The intelligent outcoupling of such light sources illuminates only the areas that shall be illuminated. Hence, the use of light is very specific and a high energy efficiency is reached.

Figure 2.2: Examples for illumination systems (Courtesy: Fraunhofer IPT, Modines, LG)

The planar light source is reached by special light guiding foils which carry a microstructure. The structures consist of v-shaped grooves or blazed gratings and have dimensions below 10 µm. Typically, lithography is used to generate these finite structures but this process is expensive and limited in producible geometries (2.5 D geometries). Especially sloping geometries, like blazed gratings, are difficult to manufacture by lithography and the resulting surface quality is poor. Furthermore, this technique is limited to flat surfaces, due to focusing issues in production. Microstructuring of free-form surfaces is not solved with lithography, yet.

As an alternative, ultra-precision machining using diamond tools enables the machining of high quality surfaces. Ultra-precision turning machines allow for the machining of continuous groove structures on the face of a workpiece or on the circumference of a drum. Additionally with a Fast Tool Servo (FTS) system, the groove structures can be machined discontinuously while the groove lengths and distances are varied. The FTS enables a nearly free programming of structures and offers a high flexibility at low costs. **Figure 2.3** shows a FTS system during the machining of a non-rotationally symmetric surface (faceted mirror).

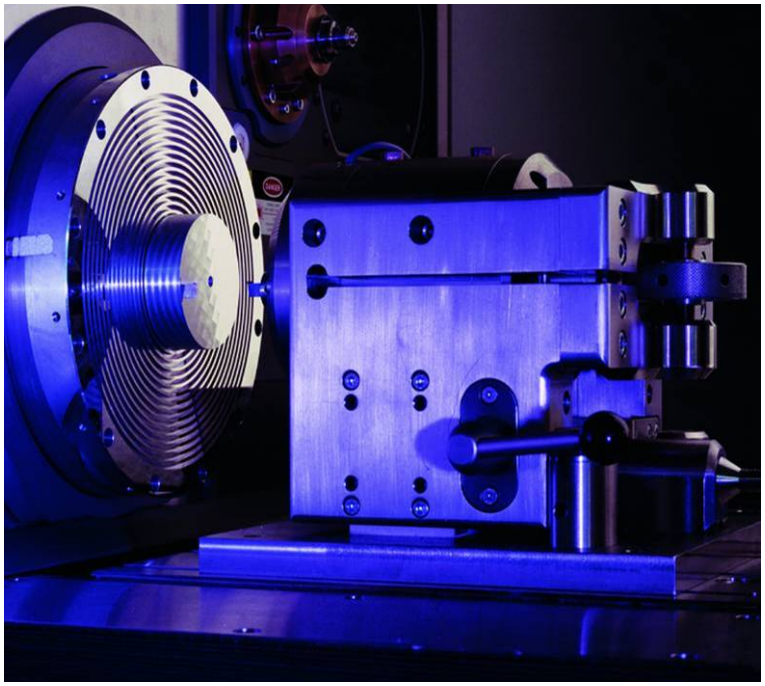

Figure 2.3: Fast Tool Servo system mounted on ultra-precision lathe

Over the past years, diamond machining has been examined and optimized mainly for the manufacturing of transmissive and reflective optics with continuous surface geometries as well as for free-form geometries. The machining of microstructures using diamond tools has different and more complex requirements but can be realized.

Ultra-precision machining enables the manufacturing of high quality surfaces, which can be produced cost effectively and very flexibly. Structures like V-grooves with dimensions in the single digit micrometer range are machinable and the use of Fast Tool Servo systems allows for the machining of non-rotationally symmetric geometries. Hence, this machining technology is promising for the manufacturing of hybrid optics.

2.2 Aim of the Project

The aim of the project »ERANET-OPTICALSTRUCT« was to enable the complete process chain for polymer hybrid optics. This chain starts with the optical design, the flexible machining of mold inserts by diamond cutting and ends with the manufacturing of the final product by replication process.

The main issues of the project were a flexible machine system as well as a robust machining process. Therefore, new possibilities have been discussed for the microstructuring of free-form surfaces based on existing rudiments of the ultra-precision machining using diamond tools. Exemplary, **Figure 2.4** is showing the principle of a hybrid optic consisting of a refractive free-form surface with an overlaid diffractive, discontinuous microstructure.

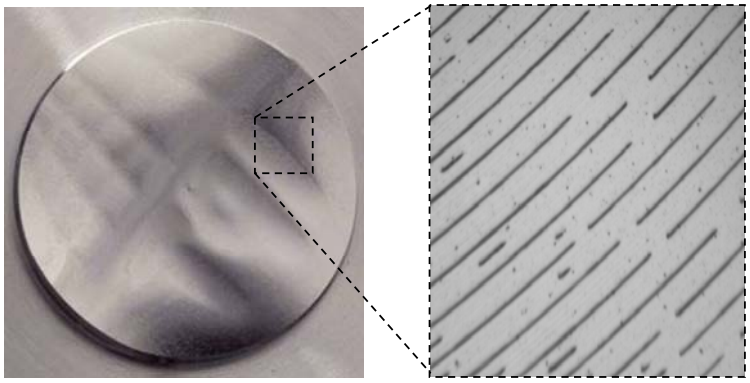

Figure 2.4: Principle of hybrid optic: free-form surface with discontinuous microstructure

The research defined at the beginning of the project should qualify the diamond machining process as only machining technology for the manufacturing of hybrid optics having refractive macro geometry combined with diffractive microstructures. Based on the geometry requirements defined by the optical design, the necessary process technology for the robust and reproducible manufacturing by diamond machining of replication masters should be developed. Therefore, an ultra-precision turning machine has been equipped with dynamic axes for the machining of free-form surfaces as well as microstructures. The machine control has been enhanced by a CAD/CAM interface. As the final process step, the replication of optics has to be considered, because the manufactured microstructures have to be replicable. For the characterization of the machined and replicated work pieces furthermore a new miniaturized measurement system has been developed.

Following, the general aims of the research project »ERANET-OPTICALSTRUCT« are summarized:

- New machine and control techniques for highly dynamic ultra-precision machining
- Innovative process strategies based on the new machine technology
- Material characterization regarding capability for ultra-precision microstructuring
- Development of new innovative hybrid optics based on the new machining possibilities
- Optimized replication processes for microstructures and hybrid optics
- New measurement systems for the characterization of microstructured optics

3 Project Consortium

The project »ERANET-OPTICALSTRUCT« is part of the MNT ERA-Net program, which supports research in the field of micro- and nanotechnology. Due to the special structure of the MNT ERA-Net program, it allows for European research consortia where each partner is funded by its national organization. The consortium of »ERANET-OPTICALSTRUCT« consists of four German partners financed by the Federal Ministry of Education and Research Germany (BMBF) as well as one Finish and one Spanish partner funded by their national agencies (see **Figure 3.1**). Furthermore, the project is supported by a Dutch and a Belgian company that do not get financial support and participate as associated partners in the project.

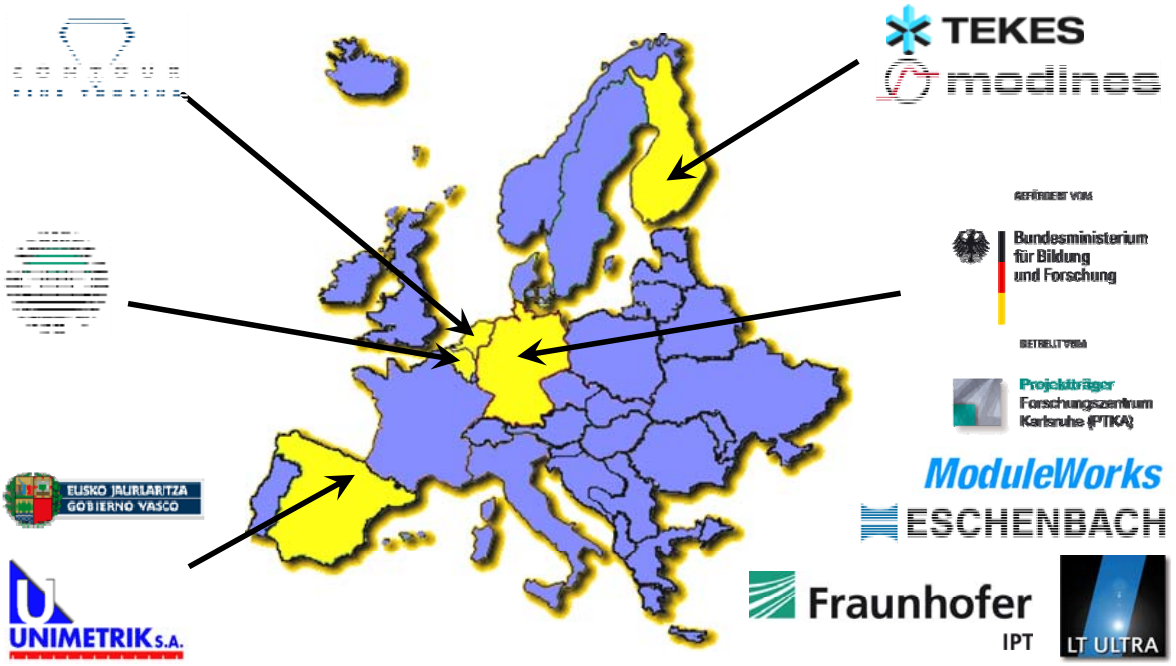

Figure 3.1: European consortium and funding organizations

The project coordinator is the company LT Ultra-Precision Technology GmbH (LT Ultra) which has taken care of the development of the ultra-precision machine as well as in close cooperation with the Fraunhofer Institute for Production Technology IPT (Fraunhofer IPT) for the development of a hybrid FTS system (**chapter 6**). Within the project Fraunhofer IPT has developed a piezo-driven Fast Tool Servo system (**chapter 6.2**) as part of the hybrid FTS and has taken care of the control of the machine system (**chapter 7**). Furthermore, Fraunhofer IPT has worked on the process development to qualify diamond machining for micro structuring processes (**chapter 5.1-5.4**). Since the machining results are strongly depending on the material and the diamond tool, Fraunhofer IPT has worked closely together with the associated partners Kanigen Works Benelux (Kanigen) in the field of nickel-phosphorus coatings and Contour Fine Tooling (Contour) for the development of new diamond cutting tools with a large clearance.

There are two companies in the consortium that develop optical systems. They define the requirements and replicate the resulting work pieces. While Eschenbach

Optik (Eschenbach) has worked in the field of polymer consumer and technical optics (**chapter 4.1, 5.5**), Oy Modines (Modines) has developed illumination systems for displays or buildings based on LED technology (**chapter 4.2, 5.6**).

Due to the fact that the description of these optics, especially free-form optics, is getting more and more complex, a customized CAD/CAM system is required to support the data processing. Fraunhofer IPT has implemented the geometry data chain including the data formats used in the control system (**chapter 8.1**). The graphical user interface (GUI) has been specified on the basis of the process results by Fraunhofer IPT and has been implemented together with ModuleWorks (**chapter 8.3**). As part of the GUI, ModuleWorks has implemented the CAD/CAM data chain and a removal simulation (**chapter 8.2, 8.4**).

To ensure the quality of structured work pieces and hybrid surfaces machined by Fraunhofer IPT using the developed machine equipped with the new hybrid FTS (**chapter 10**), the company Unimetrik has developed a miniature tactile measurement probe for the characterization of the machined microstructures (**chapter 9**).

Only the cooperation of all the different subjects allows for the realization of the project aims. Contact information of each company in the project consortium can be found at the end of this document in chapter 13.

4 Development of New Optical Components

4.1 Hybrid Optics for Automotive LED Headlights

During the past few years, plastic lenses are used in more and more applications. Additional to classic purposes such as sensor and safety engineering as well as visual aids or magnification devices, plastic lenses are increasingly used in the field of illumination. The reason for this is the rapid technical development of the LEDs, that offers many new possibilities for illumination systems.

The main advantages of plastic compared to glass optics are low weight and low costs. Further plastic optics offer a large freedom of design. Apart from applying functional elements for the assembly it is possible to mold optical components with Fresnel- and microstructures. The disadvantage is that only a few plastics are suitable for optical applications. The higher the requirements, such as the need for thermal resistance, the more limited is the choice of suitable plastics. Optical values such as transmission and refraction index differ from plastic to plastic depending on the temperature and the thickness of the lens. But since the temperature loads in LED lighting systems remain small the limitations in use of plastic lenses are reduced. Also certain wavelengths in LED lighting systems can determine negative effects in the used plastic materials. The appearance of the plastic can be cloudy and the transmission quality is decreased.

Some examples of plastic lenses for lighting purposes are shown in **Figure 4.1**.

Figure 4.1: Photograph of various lenses for lighting purposes

The design freedom of optical surfaces made of plastic offers opportunities to compensate for certain disadvantages. Structures on the optical surface can perform the widest variety of optical tasks:

- Poor dispersion of polycarbonate lenses can be corrected
- Light can be directed to illuminate specific areas
- Softening light for concealing color edges
- Reducing the center thickness of the lens

In the field of automotive, the use of LED is increasing. Headlight systems for illuminating the road in the dark or for decorative purpose during daytime are based on LED. Sophisticated plastic lenses allow for a precise light distribution on the road. Therefore, the blinding of oncoming traffic has to be absolutely avoided. The complexity of headlight lenses is characterized by their large size and by their combination with microstructures. Microstructures in the form of wave structures or facets with a height of about four micrometers ensure a homogenous illumination of the road. The light distribution of the dipped beam as well as the light-dark boundary are clearly defined by regulations which have to be strictly adhered during the development of headlights.

In today's LED headlights, the plastic lens takes care of the dipped headlight and spot modes. In doing so, a defined area at a given distance must be intensely illuminated. The realized optical system is based on projection and the plastic lens is used as secondary optic. The light source can be one or several LED, as can be seen in **Figure 4.2**.

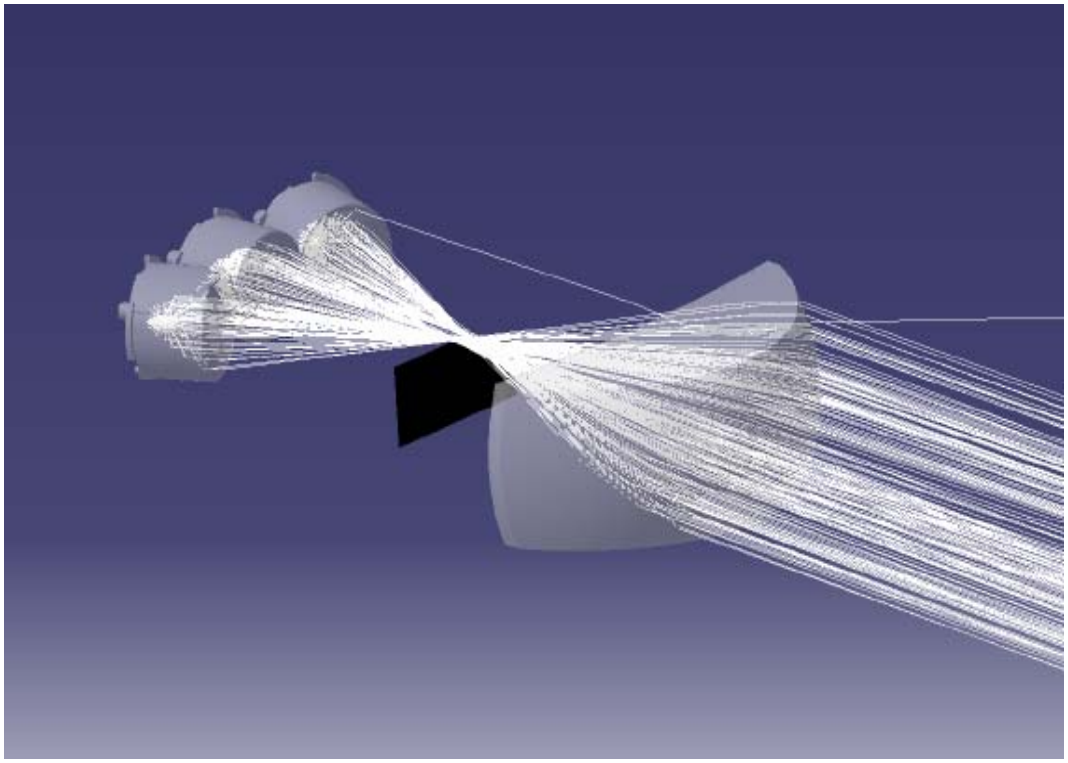

Figure 4.2: Principle of a LED projection system for the low beam light spot

Figure 4.3 shows the contours of the illumination area as well as the allocated field lines of the intensities. The 15°-kink at the top of the illuminated area is characteristic and ensures that oncoming drivers on the left side of the road are not blinded. Furthermore, it increases the illumination of the road on the right side. In the projection system of the LED headlight the light-dark boundary with the 15°-kink will be created with an aperture.

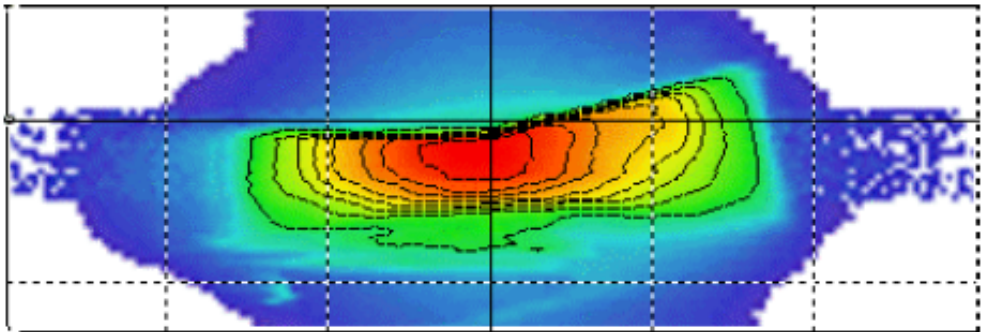

Figure 4.3: Characteristic light distribution of dipped headlight-spot

To achieve the ideal light distribution with plastic lenses several considerations have to be done to compensate for the disadvantages of the plastic. The most significant disadvantages are inhomogeneities within the lens as well as the high degree of dispersion of the polycarbonate material which has been used in this case. Undesired scattered light and color fringes on the edges of the illuminated area are the consequence.

Figure 4.4 shows the light distribution by a non-optimized lens. Scattered light is clearly viewable in the area above the 15°-kink and in the target area in particular. The color fringes on each edge are not clearly evident from this grayscale image.

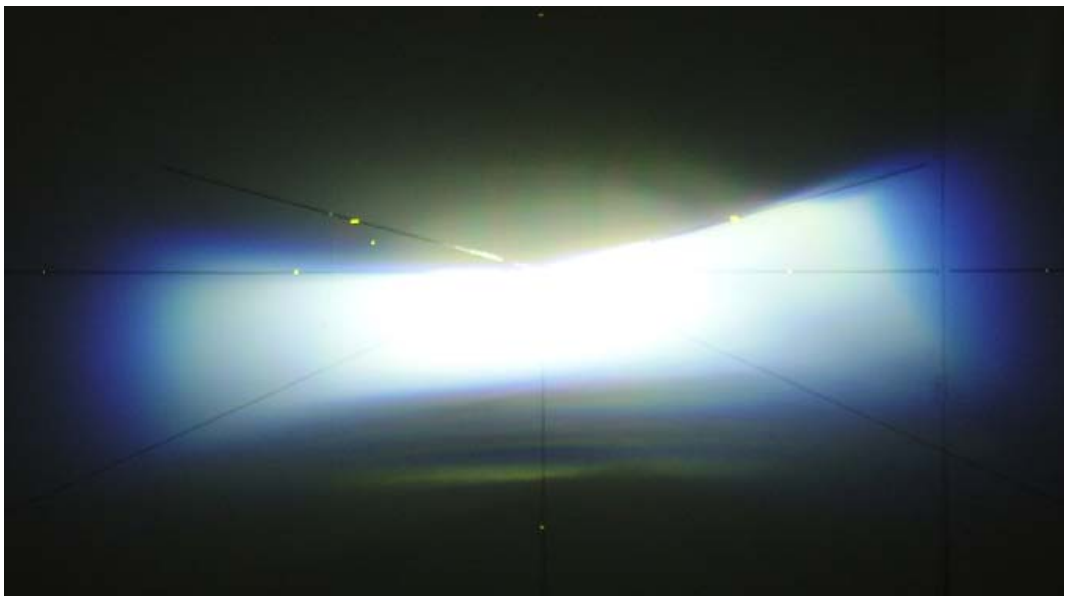

Figure 4.4: Light distribution from a non-optimized lens

To minimize the aberration and to obtain an illumination that is conform with the regulations, the optical surface of the lens has to be microstructured. This is extremely challenging since the lens is manufactured by the injection molding

process. Apart from a precise shape of the optical surfaces, the microstructures have to be replicated accurately.

The shrinkage that occurs in the injection molding process can be up to 100 µm, dependent upon the thickness of the lens. This shrinkage has to be corrected in the mold insert to achieve the desired degree of precision. Due to the correction the mold inserts get a free-form shape that has to be microstructured to attain proper lighting characteristics. The programming and processing required for producing such mold inserts is correspondingly demanding. The optimized interaction of Fast and Slow Tool Servo in the ultra-precision machine is crucial.

Figure 4.5 shows the light distribution of an optimized lens in the light channel. Clearly the reduction of scattered light in the area of the light-dark boundary can be seen. The contour of the illumination is more similar to the required reference contour. The more accurate exposition of the light-dark line shows the better result of the optimized lens.

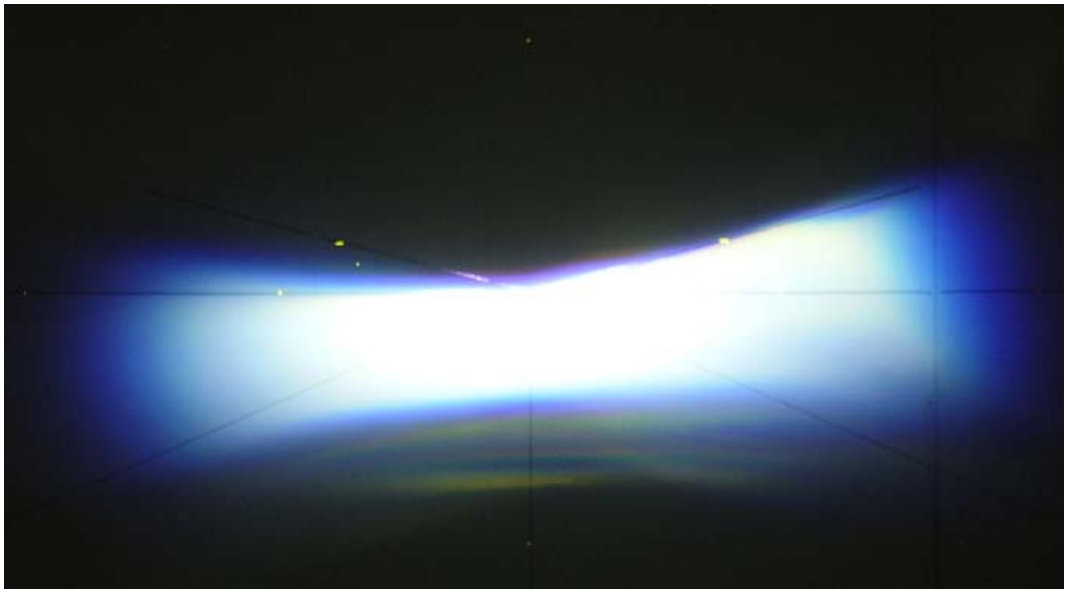

Figure 4.5: Light distribution from an optimized lens

There is a huge challenge for all participants in manufacturing thick-walled lenses with high precision for applications in automotive LED headlights. From the beginning a close collaboration is necessary to produce such a lens in high quality. This is starting in the optical design, where the specifics of plastic materials in processing and application have to be considered. Further in the machining process of the mold inserts with optical surface finish. The usage of the combined Fast and Slow Tool Servo to a hybrid FTS, as an add-on-component for the ultra-precision machine, makes it possible to machine microstructures on optical free-form surfaces in a high precision. The precise replication of the microstructures combined with a high shape accuracy of the lens surfaces by the injection molding process needs a high degree of experience. Nevertheless, the results introduce a new and important field of application for plastic optics.

4.2 Diffractive Optical Elements for Illumination Application

Today, »green« technology is one of the most commonly used phrases, that can be directly related to global energy saving. The illumination industry has risen to the challenge to improve several lighting systems, products and components, in order to minimize total power consumption. There is great demand for such lighting systems. LED lighting is encompassing a new type of »green« technology illumination where a lot of effort and prospects are being focused. However LED technology is a point light source, which is not able to provide the preferred or required lighting performance by itself. Thus advanced optics are needed, such as optical diffraction gratings.

Diffractive optics (DO) have several special features and benefits, compared to conventional refractive optics. However there are only few industrialized applications available. One reason for this, is fabrication, which may cost too much or is unable to generate preferred forms or profiles. The most critical structure features are nano-scale, under 150 nm, as well as 3 - 8 micron-scale. Recently, fabrication techniques and technologies, such as micro machining, has been investigated and developed to such a degree, that high quality surface relief grating profiles can be fabricated.

A diffractive optic element (DOE) can comprise different surface profiles, depending on the application. In terms of illumination performance, the most requested characteristics are a) efficient light outcoupling at a controlled angle in the light guide application and b) efficient light collimation, light directed with a lens application. **Figure 4.6** shows different grating profiles.

Figure 4.6: Different grating profiles for different applications

The grating type must be selected carefully for each type of application, depending on the required performance. Generally DO elements can be divided into two sections: 1) lightguide elements and 2) transmissive elements. These elements cover a vast array of different product applications.

One major application is display illumination. This comprises backlights and frontlights for micro, medium and large size LCDs, reflective displays and even advertisement displays. The most important features are efficiency (performance), cost, and thickness. Conventional refractive optics cannot offer any more new solutions. Thus, a new approach was required. Diffractive gratings can improve the efficiency by direct collimation, decrease the final cost through the use of roll-to-roll

manufacturing, minimize thickness without additional films, and thus, offer a small profile thickness. This basic concept is described in **Figure 4.7**.

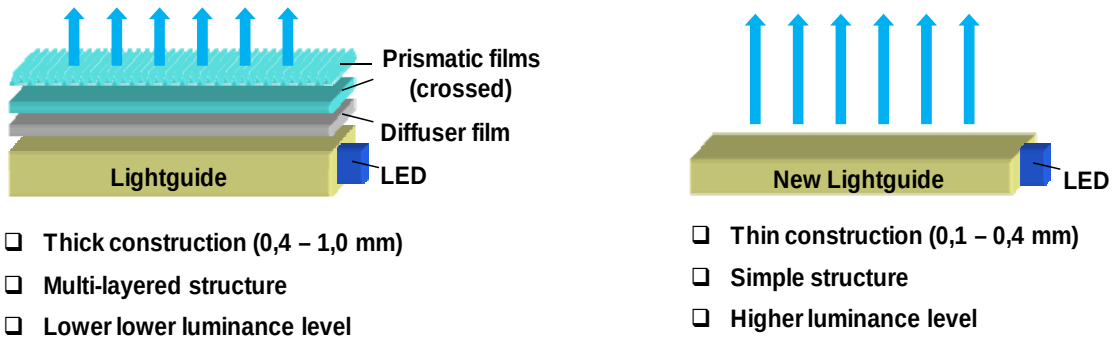

- Thick construction (0,4 – 1,0 mm)
- Multi-layered structure
- Lower lower luminance level

- Thin construction (0,1 – 0,4 mm)
- Simple structure
- Higher luminance level

Figure 4.7: Comparison of conventional backlight vs. new backlight

Other types of consumer electronics can also utilize DO lightguide elements. Several light indicators, signal lighting, etc. are preferred. One application is the keypad lightguide in mobile devices, which should be as efficient as possible in terms of minimized power consumption. A thin lightguide solution is suitable for this application.

General LED lighting is one potential application for DOE. There are several requirements, but one interesting topic is the replacement of halogen lighting with an LED illuminator. Today, many LED illuminators are either unsuitable for this purpose, or further improvements are required. Typically refractive lenses are big with a complex 3D form. The performance of an LED illuminator with three LEDs was unsatisfactory, due to non-uniform illumination and three shadows. Furthermore, the cost of injection molding is not cheap, due to its long cycle time and high material volumes. A DO lens, however, which is flat and thin, has lower production and material costs. Additionally, uniform performance can be achieved with more acceptable efficiency. **Figure 4.8** shows the above mentioned two lenses for the same illumination purpose.

Figure 4.8: Refractive 3D-lens with complex form vs. DO lens with flat and thin form

In this project three applications were selected in order to prepare DO based demonstrators. **Figure 4.9** is showing selected applications: 1) collimating lightguide

for micro displays, b) efficient lightguide for keypad illumination, c) lens for LED illuminators (halogen replacement).

Figure 4.9: Selected applications for the project demonstrators

Nowadays white light LEDs are in great demand. This fact sets a clear condition for the grating design. In accordance with above-mentioned issues, a grating size between 3-8 microns, with a periodic blazed grating profile was selected. **Figure 4.10** shows the features of blazed grating performance in light directional coupling.

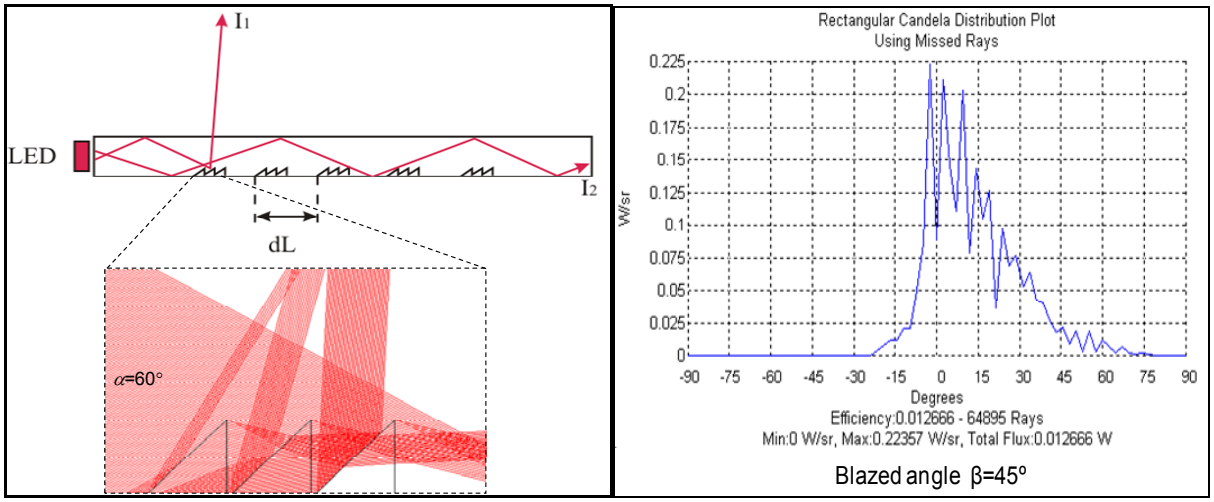

Figure 4.10: Ray tracing in lightguide grating pixel and blazed grating profile simulation

This type of grating profile has interesting optical characteristics. The periodic blazed grating profile can provide efficient light directing performance, which is a much required feature in many different applications.

The most advanced benefits of DOE are:

- Special optical performance, e.g. light collimation
- Low material volume and weight
- Product and production cost, e.g. thin DO lens vs. refractive lens
- Productivity, utilizing the roll-to-roll method

Additionally, thin and planar elements can be utilized in 3D format. With high volume products, DOE offers the best features to optimize all production phases in terms of energy saving and cost reduction, and are a direct route to »Green Technology«.

5 Process Development for Micromachining and Replication

In the scope of »ERANET-OPTICALSTRUCT«, microstructures are produced by two different manufacturing principles. On the one hand the microstructures are machined using diamond cutting tools. On the other hand structured molds are used for the replicative production of microstructures in polymers. In both cases the manufacturing of structures has to be robust and fulfill the requirements and tolerances defined by the optical designer.

Robust in that context means that the manufacturing process is running stable over a long time and is not easy to influence. Thinking about a machining process the result should not be influenced by a bad chip removal or by inclusions or porosities in the material. Hence, the expression »robust« includes not only the process but also the material, the tool, and the machine. In that context, the production of microstructures by replication seems to be less complicated and the preferred way to manufacture microstructures. But of course appropriated tools are needed for the replication which are ideally machined by diamond cutting if optical surface quality is needed.

Hence, in the following sections the requirements and optimization of both the mold machining by diamond cutting tools and the replication process are illustrated.

5.1 Requirements for Manufacturing of Microstructures

Since the diamond machining is a crucial part in the manufacturing process of high quality optical microstructures, in the following influences on and disturbances of this machining process are explained. This is done with respect to the microstructures (blazed gratings) used in display illumination systems (see chapter 4.2).

Figure 5.1 shows the main influences on the structure quality of the mold insert. Beside the picture of the mold insert itself, two detailed pictures can be seen at the right side. One shows the arrangement of the different grooves varying in length and distance. The second one is about the structure geometry. It shows the 45°-v-groove geometry with burr free groove tips and perfect slanted surfaces, which have the strongest effect on the optical function of the structure. The critical influences on the structure are the material, the process, and thermal effects. Beside these influences the machine and the condition of the cutting tool influence the structure accuracy and quality. But these effects are not just related to microstructuring processes.

In contrast to the machining of metal optics and mold inserts with continuous surfaces (spheres, free-forms), the material properties have a strong influence on microstructuring processes. Due to the anisotropy and grains in polycrystalline materials, like OFHC copper (oxygen free high conductive copper), the cutting conditions change during the machining of micro-grooves. This results in changing burr formation along the groove. Aluminum is another common material for diamond machining but has hard and brittle inclusions that disturb the structures by break

outs. Hence, micro machining requires homogeneous materials without any material defects.

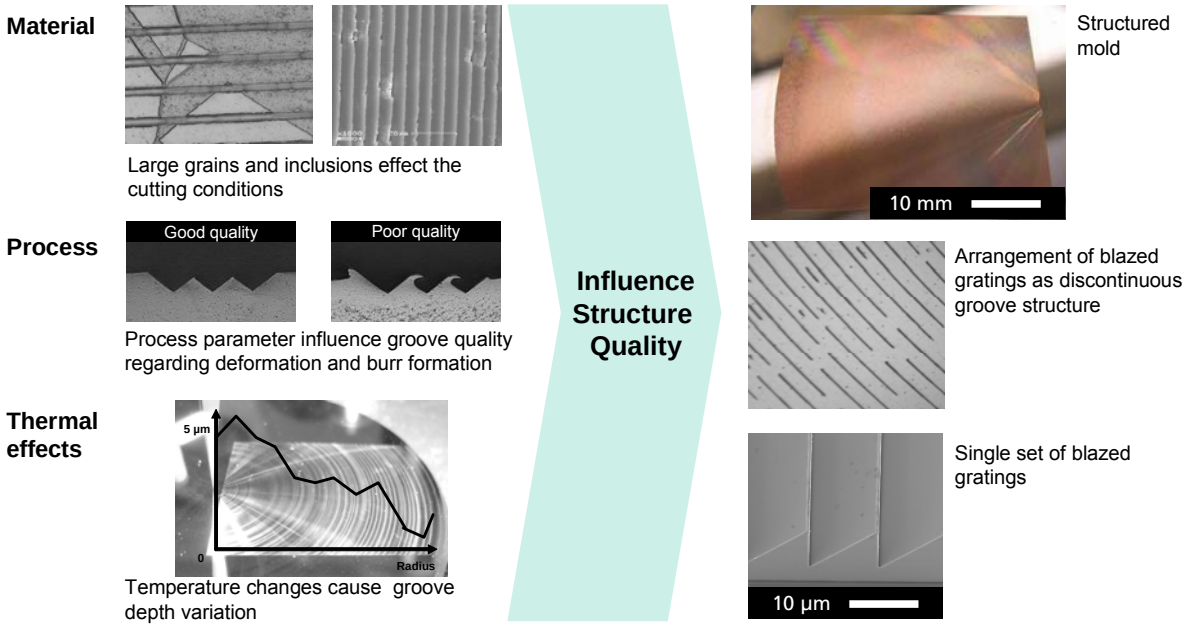

Figure 5.1: Critical influences on structure quality

Furthermore, the process parameters affect the quality of the grooves. Especially the burr formation and form accuracy is influenced. Good groove qualities and sharp, burr free edges can only be achieved by machining parameters adapted to the material. Since the machining of microstructures can be time consuming with process times up to several days the conditions for machining have to be very stable and constant. Changing room temperatures cause variations of the tool length, axial drifts of the work piece, or the work holding spindle which are affecting directly the depth of the machined structure. Hence, a sufficient control and monitoring of the temperatures during the machining process is needed.

In the scope of »ERANET-OPTICALSTRUCT«, the mentioned main influences are examined thoroughly by several machining tests using diamond cutting tools. Furthermore, precautions are done in the development of the mechanical components like the ultra-precision machine and the Fast Tool Servo (see chapter 6.2). The integration of thermal sensors allows for the compensation of temperature changes using the machine control. Additionally, optimizations have been done regarding the replication of microstructures by the use of injection molding as well as step-embossing.

5.2 Process Optimization for Microstructuring using Diamond Cutting Tools

The quality of optical microstructures machined by diamond cutting tools (plunge-cut process) is not only characterized by form accuracy and surface quality but also by burr formation. Therefore, different tests and examinations have been done to identify the influences on the burr formation and to optimize the process.

5.2.1 Machining Process and Test Structures

The process examination is done with two different structures that are shown in **Figure 5.2**. A 90°-v-groove structure has been chosen for first examinations regarding the effect of cutting parameters. The structure consists of a single groove and a set of three grooves. In that way different angles at the edges of 90° and 135° are achieved. The single groove can be used to check the groove depth by measuring the width of the groove from the top view using a microscope. The 90°-v-grooves have a depth of 15 µm and a width of 30 µm.

A second structure consists of blazed gratings having a groove angle of 45°, which are arranged in a saw tooth shape. Again, the test structure consists of a single groove and a set of grooves. values between 7 and 10 µm have been adjusted for the pitch.

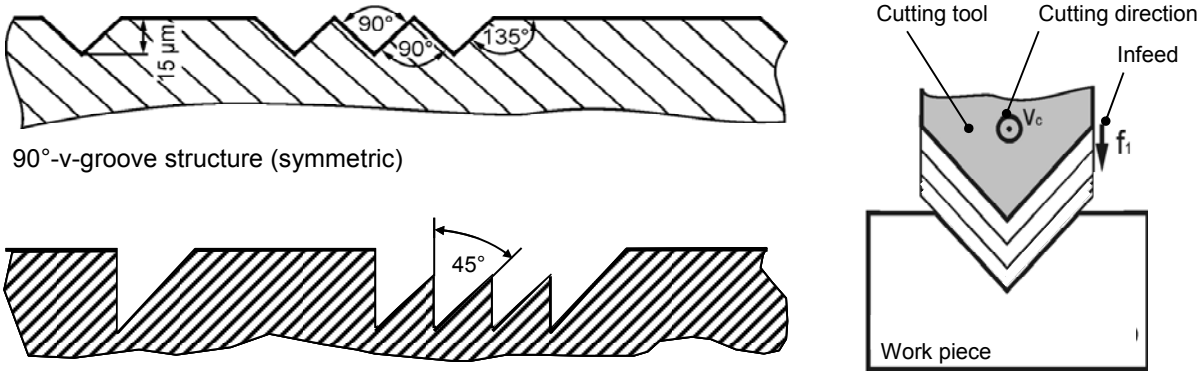

Figure 5.2: Definition of test structure and cutting process

The grooves are machined in a plunge cut process. Concentric rings are the result. In plunge cutting the tool moves in Z-direction. After the required depth of the groove is reached, the tool is moved backward. The infeed speed of the tool is defined as a feed rate f in micrometer per rotation [µm/rot]. In plunge cutting processes the feed rate equals the depth of cut. In that way, the time for structuring is strongly depending on the spindle speed and the depth of the grooves.

5.2.2 Test Machining

The machining of the test parts made of different materials have been conducted on an ultra-precision lathe. Two tools have been set in the machine (see **Figure 5.3**). A radius tool has been used for the machining of the planar surface, while the V-

shaped tool has been used for the machining of the grooves. The diameter of the test parts is 30 mm and they have a height of 15 mm. An adapter has been used for the clamping at the vacuum chuck of the spindle (see Figure 5.3, right).

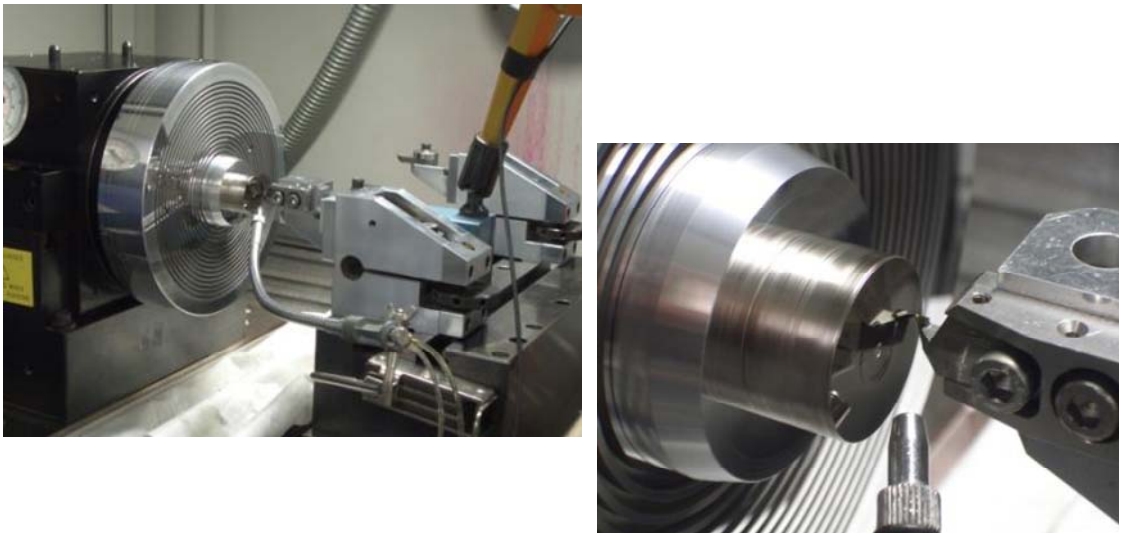

Figure 5.3: Test set-up in an ultra-precision turning machine

After the machining, the samples have been examined in a SEM (scanning electron microscope). Detailed pictures have been made using the SEM. Furthermore, the SEM has been used for EDX-analysis (energy dispersive X-ray) to determine the composition of the NiP-coatings examined in chapter 5.3.2 (see **Figure 5.4**). In the lower part of Figure 5.4 the preparation of the test sample for the production of cross sections is shown. Cut-outs of the structures have been embedded into a polymer. After that, the cross-section has been grinded and polished. Pictures of the cross sections have been taken by using an optical microscope.

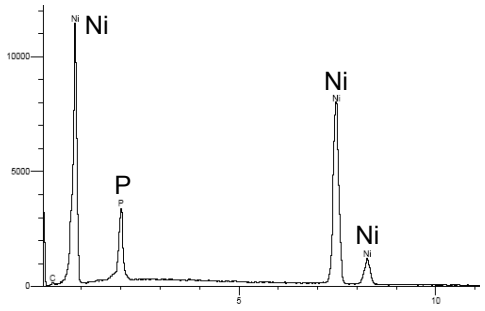

Result of EDX-Analysis

Prepared samples for examination of cross section of structure

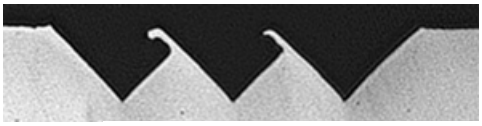

Cross section of structure

Figure 5.4: Analysis processes for test parts

5.2.3 Process Parameter Studies

Process parameter studies have been conducted to check the effect of the main parameters in a plunge cut turning process. The parameters cutting speed v_c and infeed f (depth of cut) have been varied in a certain range. The cutting speed has been changed between 5 and 100 m/min. The depth of cut has been varied between 0.2 and 3 µm. The material of the test work piece has been OFHC copper and a 90°-v-groove tool has been chosen.

After the machining, the copper plate has been cut into pieces and the cross sections have been polished to evaluate the form accuracy and the burr formation. This cross sections are shown in **Figure 5.5**. The overview of the cross sections shows that the cutting speed has no significant influence on the burr formation. The first row of the table shows that the burr keeps more or less constant when changing the cutting speed from 5 to 100 m/min. The same can be noticed for a larger depth of cut.

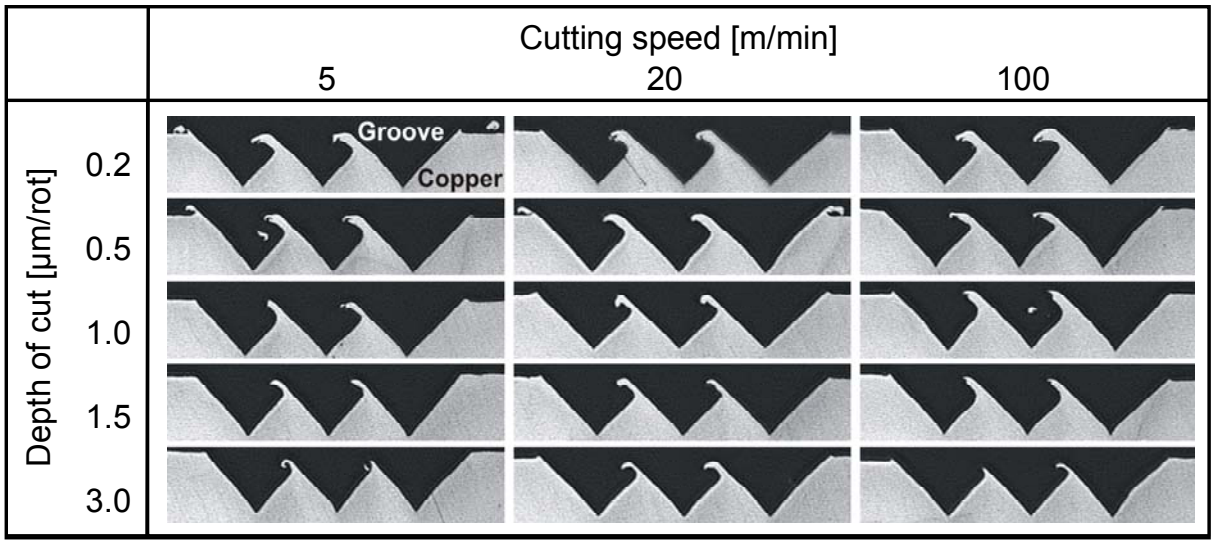

Figure 5.5: Influence of cutting speed and depth of cut on the burr formation (90°-v-groove)

The columns of Figure 5.5 show a different behavior of the burr. The burr formation is changing strongly with the variation of the depth of cut. Large and thick burrs can be seen on the groove tips for a depth of cut of 0.2 µm/rot while they are getting thinner by increased depth of cut. The results show also a dependency of the angle at the edge of a groove. The 90° transition between each groove shows more burr than the larger angle (135°) at the transition to the flat work piece surface.

While the results above show that the burr is reduced by increasing the depth of cut a different effect could be seen in cutting blazed gratings in a nickel-phosphorus (NiP) coating (see **Figure 5.6**). The microscope pictures on the left side in Figure 5.6 show the top view of a single 45°-v-groove which are machined with different depth of cut (variation between 0.1 and 1.5 µm/rot). With increasing depth of cut the generation of burr at the left groove corner is getting stronger. This can be recognized by the undefined groove edge. Beside the burr formation, also the accuracy in shape of the v-grooves is influenced significantly by variation of the infeed speed. Figure 5.6 (right) shows the cross sections of four blazed gratings arranged in an array. The

structures are machined at different infeed speeds. While the structure is significantly deformed at 1.5 µm/rot, the smaller infeed of 0.1 µm/rot shows the perfect geometry and only small burrs are remaining. Again, smaller infeed speeds are preferable.

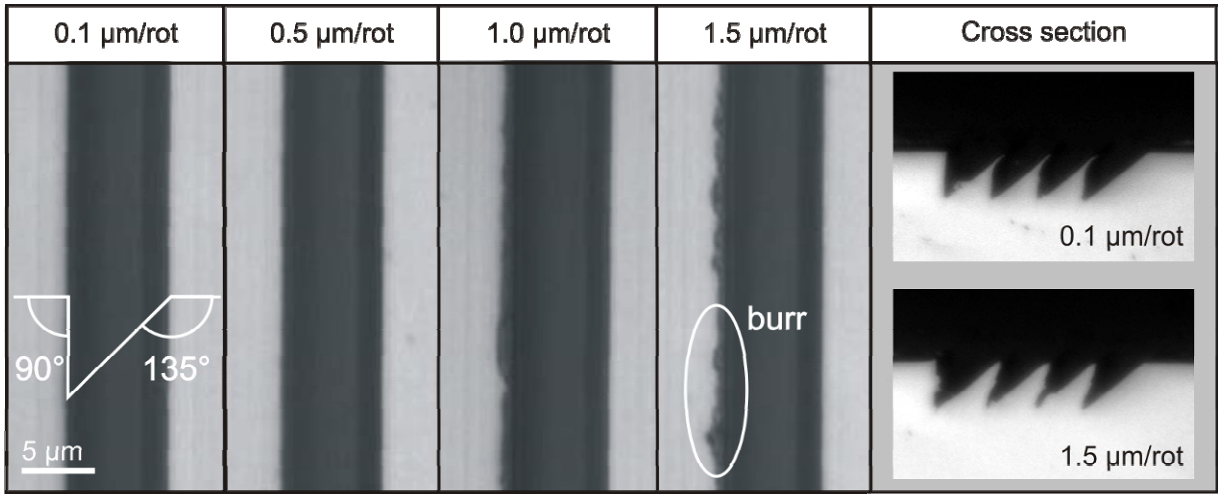

Figure 5.6: Microscope pictures of burr formation at 45°-V-grooves for different depth of cut (left), cross sectional views (right)

The two experiments show that the depth of cut or the infeed speed have a strong influence on the burr formation as well as on the accuracy of the groove geometry. But the test showed further that the best depth of cut is depending on the material properties. While the groove quality is getting enhanced due to increased infeeds (from 0.2 up to 3 µm/rot) in copper the burr formation in a NiP coating is getting worse by a larger depth of cut. This phenomenon can be explained by the minimum depth of cut, that is depending on the material and the cutting edge radius.

The minimum depth of cut is the smallest cutting depth that allows the removal of material in form of chips. If the cutting depth falls below this limit, the material is not removed anymore but strongly deformed. This effect is called »ploughing« and is depending on the ductility of the material. This means for the experiments above that the chosen depths of cut for copper are already close to the minimum cutting depth and by increasing the depth of cut a more stable cutting process is possible. Since the NiP coating is less ductile and harder than copper the minimum depth of cut is much smaller.

Summarizing it can be defined that the cutting speed has no significant influence on the burr formation. The depth of cut or infeed has to be adjusted to an optimum value depending on the ductility of the material.

5.2.4 Influences by Structure Geometry

It has been proven that not only the process parameter influence the groove quality but also the structure geometry (angle and symmetry) as well as the absolute structure depth. These effects on the structure quality are explained in the following.

Geometry angle and absolute structure depth

The parameter studies, introduced in chapter 5.2.3, showed, beside the dependency of the cutting depth, the influence of the angle of the groove edges. This angle varies related to the groove angle, the groove orientation and the arrangement of single grooves into an array structure.

SEM pictures of the 45° test structure are shown in **Figure 5.7**. Each picture shows four sets of blazed gratings machined with different infeeds. Different burr formation can be seen. Burr and sharp, thin corners appear as bright lines in SEM pictures. Remarkable is that only the single grooves next to the groove array are burr free. The groove tips in the array have always some kind of burr at the top. This can be explained by the fact that small angles at the groove edges tend to generate more burr. The edges along the single groove (90° and 135°) are much more stable than the 45°-transition between grooves arranged in the array. A reason might be the missing support of the surrounding material if sharp-edged corners have to be machined in plunge cutting processes. Hence, a single 45°-v-groove can be machined burr free using an infeed of 0.5 µm/rot while for thinner groove tips the infeed has to be reduced stronger.

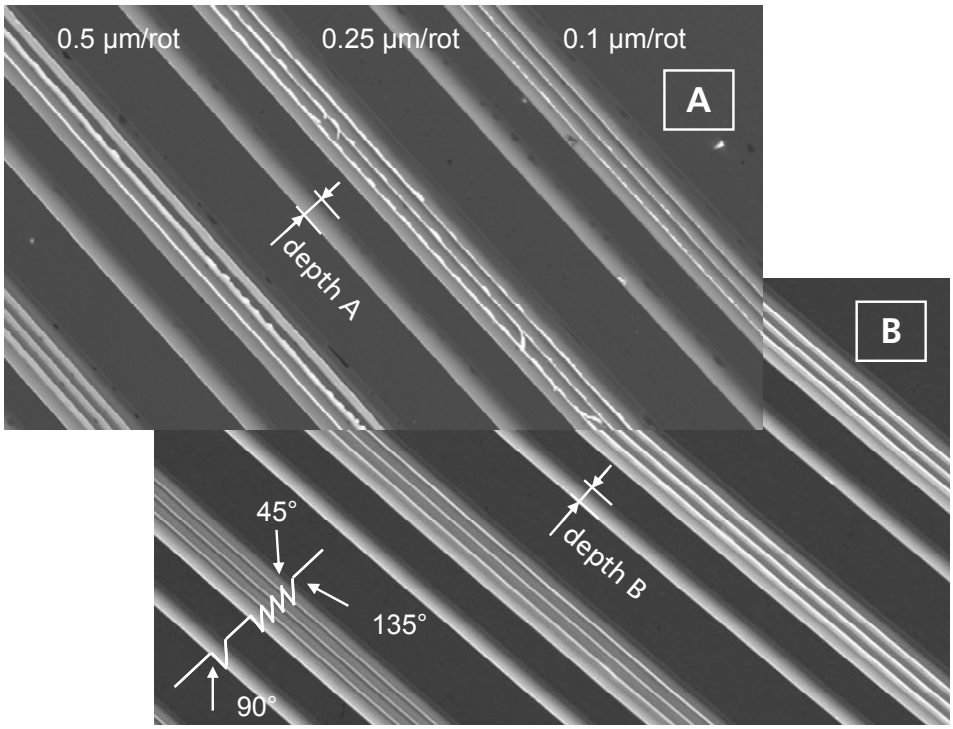

Figure 5.7: SEM pictures of blazed gratings (pitch: 7 µm) machined in NiP with different depths of cut

Furthermore, the SEM pictures in Figure 5.7 show another effect on the burr formation. The absolute groove depth in picture A and B is different. The grooves in

picture A are cut deeper into the material. This can be measured by the width of the single grooves. The single groove in A is wider and consequently deeper than the grooves in B. This does not influence the structure geometry itself as long as a minimum groove depth is realized, but the burr formation is totally different. In picture B the burrs are very homogenous (straight and linear bright lines at the groove tips) whereas the burrs in A are frazzle and look like torn off.

To examine this occurrence and the effect of the absolute structure depth more tests have been done. While the absolute structure depth describes the depth of the groove according to the work piece surface, the relative structure depth is the result of the groove geometry and the groove pitch. This is described by the cross sections in **Figure 5.8**, (right). The burr size at the top of the groove tips is increasing the deeper the structure is cut into the material or in other words the larger the absolute groove depth is getting.

The SEM pictures in Figure 5.8 show that the burr size is rising with an increase in absolute structure depth until the burr is breaking off leaving frazzle structure tips. At an infeed of 0.25 µm/rot and an absolute depth of 15 µm the burr is breaking off partly at the groove tips. The quality of the groove tips is comparable with the structures in Figure 5.7, picture A. The breaking burr can be found already at 9 µm absolute depth at higher infeed speed. Measurements of the burr size on the tip of the structure proved that the height of the burr nearly equals the difference between the absolute and the relative structure depth. Hence, perfectly sharp pointed tips can only be machined, if the absolute equals the relative structure depth.

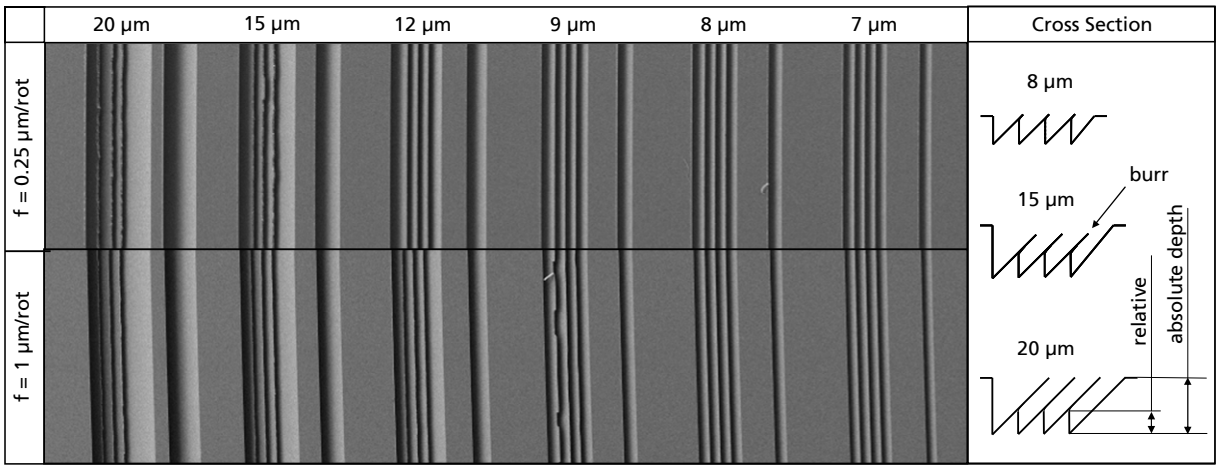

Figure 5.8: SEM picture of structures with different absolute structure depth

Figure 5.9 shows detailed SEM pictures of groove tips machined with different cutting parameters at different absolute groove depths. If the absolute and relative groove depth match (7 µm), the 45°-tip between two grooves is almost perfect and free of burr. Using the same cutting parameters (f = 0.25 µm/rot) but an absolute depth of 20 µm the groove tips are undefined and frazzle. In this conditions the grooves cannot be used in a replication process. The tip of the grooves has a width of about 1 µm. The effect is similar, if larger infeeds (1 µm/rot) are used for the machining.

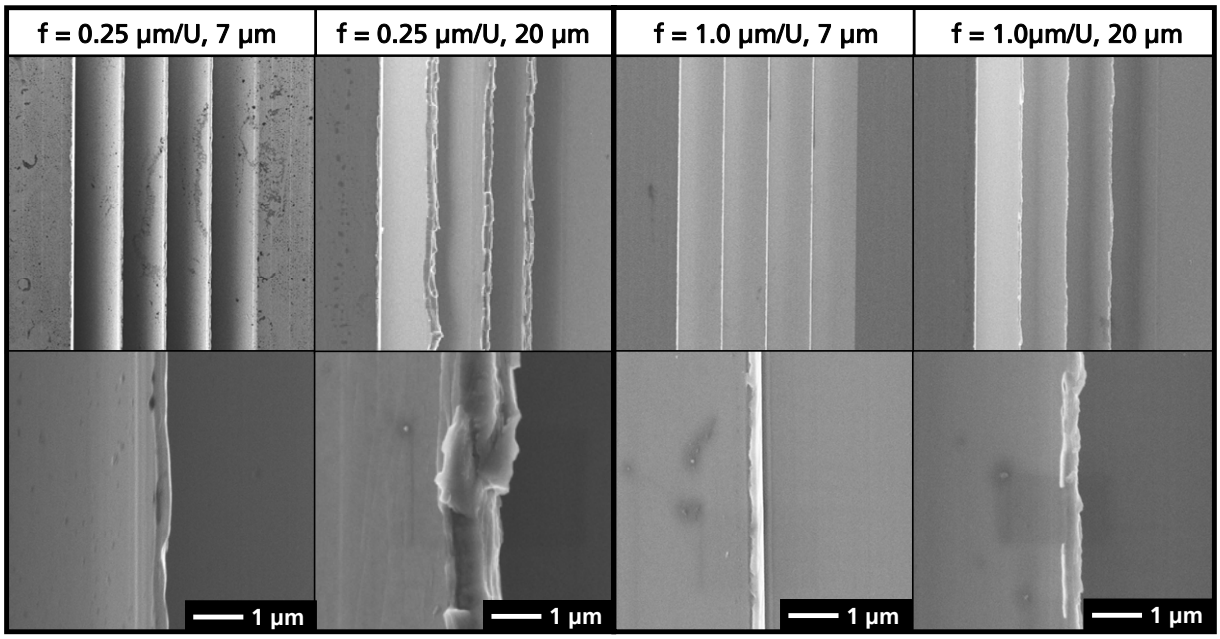

Figure 5.9: Detailed pictures of structure tips with different absolute structure depth

Influence of groove symmetry

Depending on the desired functionality, the geometry and the shape of the microstructures are varying. Prismatic 90°-v-groove structures with a symmetric cross section are used for example in display technology. In contrast, the blazed gratings used for illumination systems of Modines have an asymmetric cross section (see Figure 5.2). Regarding the machining process, these different geometries do not just affect the shape of the cutting tool but also the plunge cut process and the according machining strategy.

In the scope of the conducted experiments, two different shapes of burr could be observed at the groove tips when machining blazed gratings (see **Figure 5.10**). The different shapes of burr have been caused by different machining directions. It can be distinguished between the direction »vertical flank« and »slanted flank«.

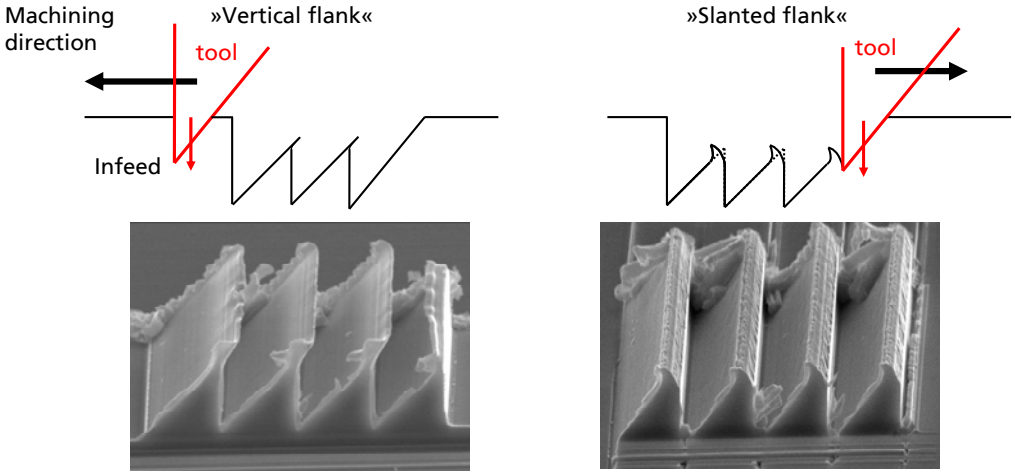

Figure 5.10: Burr formation depending on the machining direction

The different directions are illustrated in Figure 5.10 with sketches and the according SEM picture. Using the direction »vertical flank«, the tool cuts into the full material

and is supported at the left and the right side. If the opposite direction is used for machining the grooves, the tool cuts at the edge of the structure into the material. The material next to the prior machined groove offers no support and bends over while the tool moves forward. After a certain depth the material is stable enough to withstand the cutting forces. The generated deformation is quite large and cannot be called just burr anymore.

Hence, for machining asymmetric groove structures the direction of machining has to be considered and chosen in a way, that the tool cuts into the material like shown in Figure 5.10 (left). The burr generated at the groove tips is significantly thinner and offers the possibility to use a de-burring step (see chapter 5.2.5), if there is no chance to avoid the burr.

The minimum depth of cut has been mentioned already in the chapter about the influence of the right infeed to avoid burrs (see chapter 5.2.3). For the machining of grooves having an asymmetric cross section the minimum depth of cut has to be considered as well. Using an infeed direction normal to the surface and cutting an asymmetric 45°-v-groove the depth of cut differs between both flanks at the cutting tool. Theoretically, there is no cutting at the vertical flank of the groove, but small deviation in the tool setting may cause material deformation resulting in significant burrs. Hence, it is necessary to move the tool under a certain angle into the material during the cutting. In that way, the cutting depth can be adjusted to the same value on both tool flanks and defined cutting is possible. In **Figure 5.11** the result of this consideration is shown. The SEM pictures show single asymmetric 45°-v-grooves that are machined alternating with different infeed strategies.

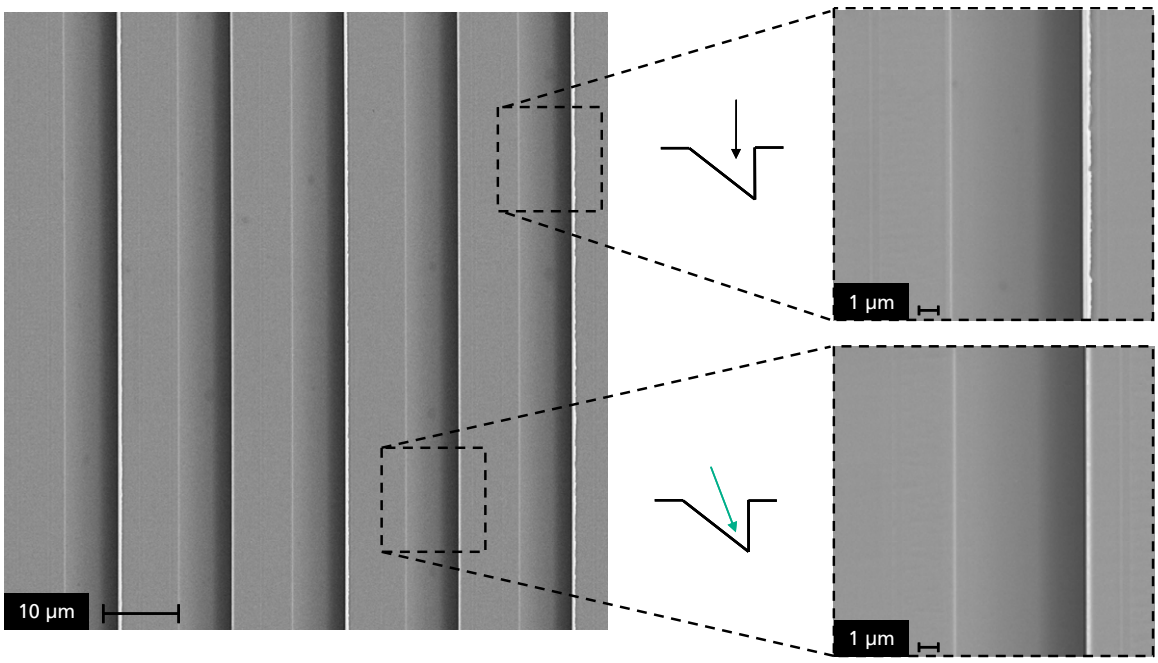

Figure 5.11: Effect of infeed direction on burr formation along the rectangular groove edge

Again, the bright lines at the groove edges in the SEM picture (see Figure 5.11) indicate the burr. Using the adapted infeed direction the vertical flank of the v-groove is straight and homogenous showing no burr.

5.2.5 In-Process De-Burring Strategies

Several advices and optimization possibilities have been introduced in the chapters before to prevent and reduce burr formation in the microstructuring process. But there can be structure requirements that do not allow a burr free machining. Therefore, de-burring strategies shall be present in this chapter.

Two de-burring strategies are illustrated in **Figure 5.12**. Aim of the de-burring is to remove the burr at the tip of the structures. Preferable the thin burr, like shown in Figure 5.10 (left), can be removed with this de-burring step. Using »Strategy I« the tool moves back into the prior produced groove with a certain distance above the structure tip. Then the tool will be moved down into the groove with about 0.5 µm distance to the steep flank of the groove. »Strategy II« works similar. Instead of a backward movement with a security distance to the structure tip the tool is moved directly at the aimed structure height.

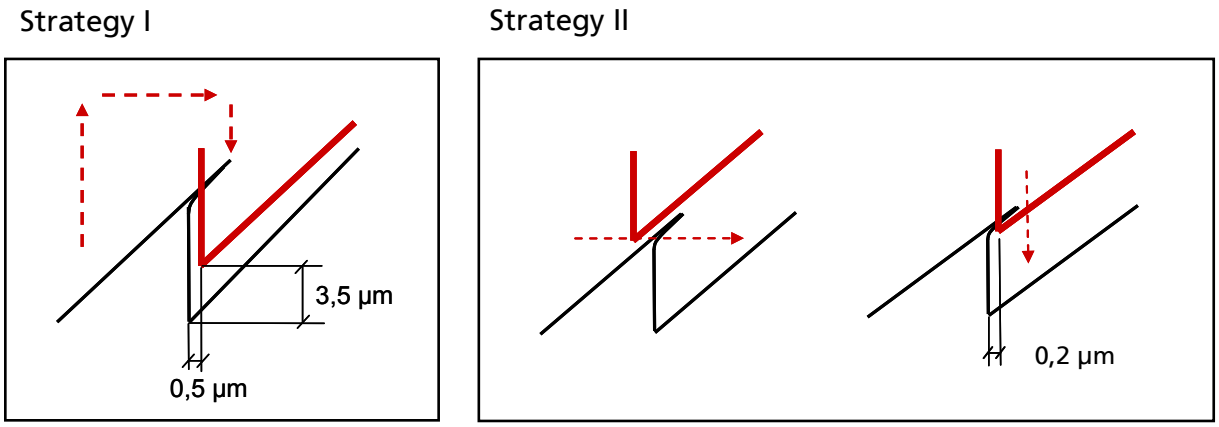

Figure 5.12: Tool movement for de-burring strategies

After the de-burring the machining of the next groove goes on. In that way, the tool movement can be compared with a »pilgrim step« (two forward, one back, etc.). It is absolutely necessary to do the de-burring during the structuring process. De-burring of the whole structure after finishing the structuring is not advisable since variations in the position after two or three days machining occurs. This does not allow small gaps of half a micron to the steep flank, which are required for a good de-burring result.

Exemplary the results of de-burring »Strategy I« are documented with SEM pictures in **Figure 5.13**. The de-burring tests are done at structures having 20 µm absolute depth (relative depth/pitch: 7 µm) and are machined with a infeed of 0.25 and 1 µm/rot. The detailed pictures in the lower part show the significant increase in quality of the edges. The frazzle appearance of the tips is completely gone. Better results may be achieved if the gap between the tool and the steep flank is reduced further.

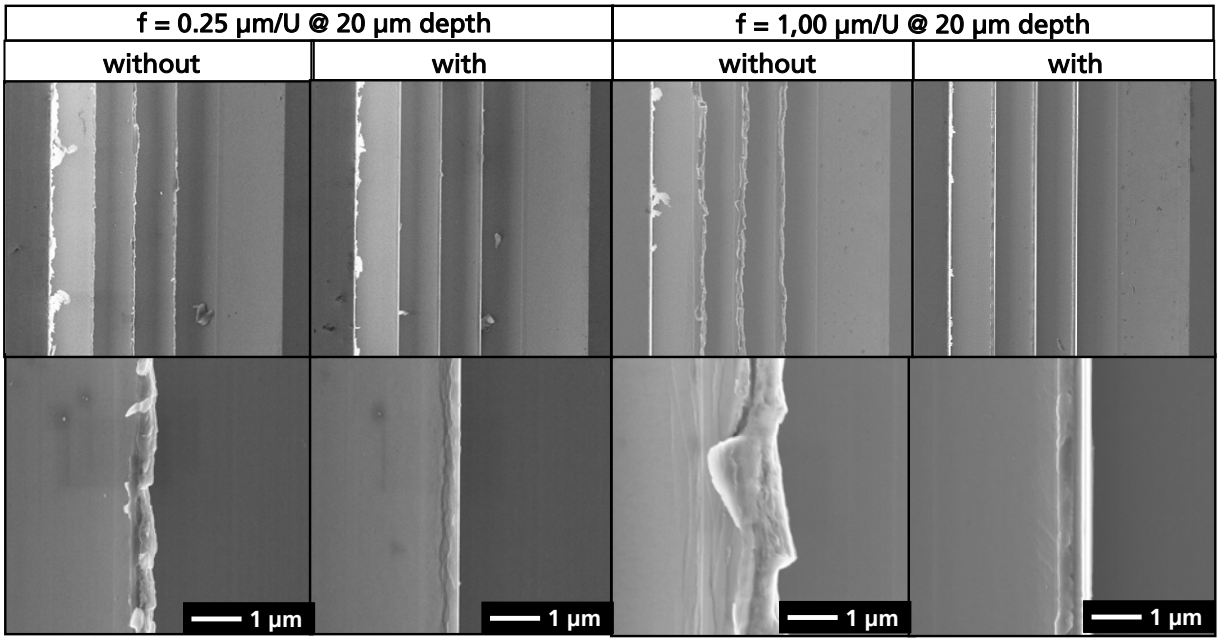

Figure 5.13: Resulting groove tips using de-burring strategies (Strategy I)

5.2.6 Machining of Structures for Step-Embossing

Considering the boundaries described above, the machining of nearly burr free structures can be achieved by a plunge-cut process using diamond cutting tools. **Figure 5.14** shows a SEM picture of blazed gratings machined in NiP-coating. The structure angle, except the first one, is 45° and the pitch is below ten micrometers. It can be seen that the burr at the groove tips is reduced to a minimum. The slanted flanks of the grooves are very smooth and the bottom is machined sharp. The dimensions of the stamping tool are about 40 x 50 µm².

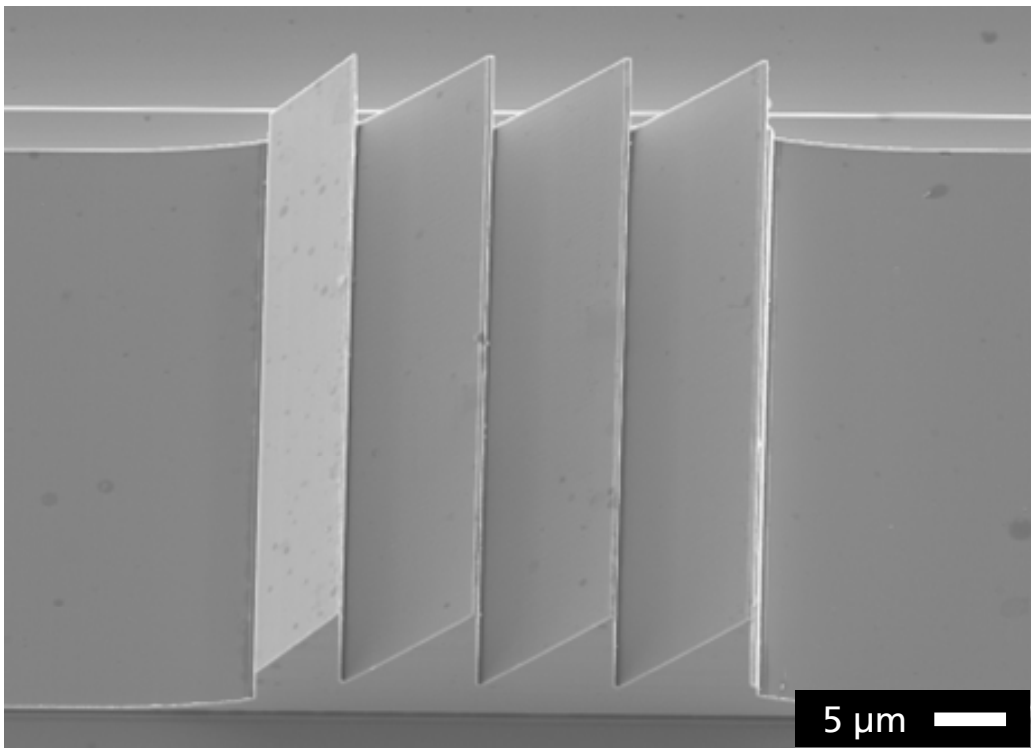

Figure 5.14: Stamping tool with blazed gratings (width: 40 µm, length: 50 µm)

5.3 Materials for Microstructuring Processes

5.3.1 Material Requirements

In the field of micromachining, the material has a strong influence on the machining result. In macro machining the grain size is neglectable compared to features on the work piece or the cutting edge radius of the tool. But the smaller the to be machined details, the more important is the homogeneity of the material. In micro and ultra-precision machining structures and details are machined that have dimensions in the range of below 50 µm or even below one micrometer for medical applications.

Typically, OFHC copper is used in ultra-precision machining. The polycrystalline material has, in standard condition, grain sizes in the range of 300 µm and is strongly anisotropic. The material properties, for example the Young's modulus, is changing with the orientation of the grain. Hence, during the chipping the cutting conditions for the tool (cutting edge radius: 50 nm) are changing continuously. The resulting surface characteristic of a planar surface, machined by using radius cutting tools, show small plateaus with height variations of a few ten nanometer. Every plateau represents a different grain.

The effect can also be realized in microstructuring process using diamond cutting tools. The changing properties of the different grains result in a different burr formation along for example micro grooves (see **Figure 5.15**).

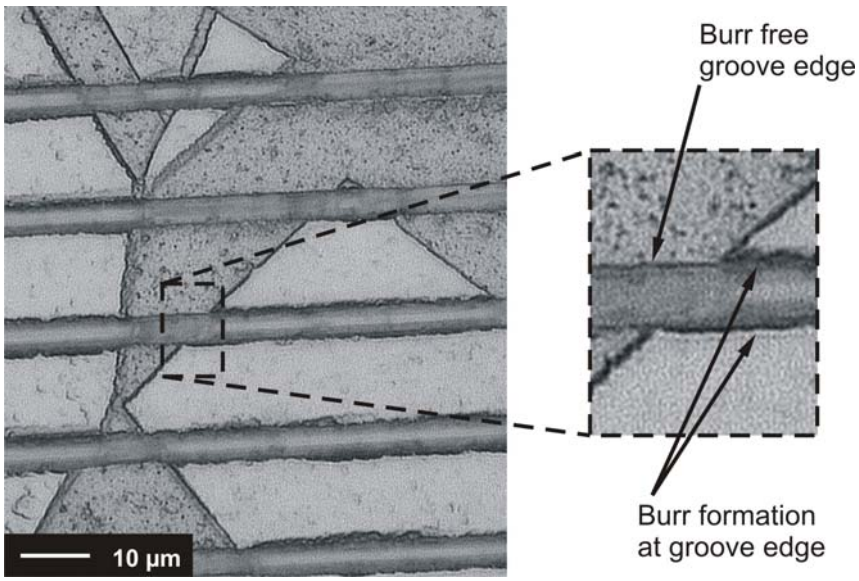

Figure 5.15: Grain structure of OFHC copper influences burr formation along micro grooves

In that way, it is very hard to optimize the machining process since there are no constant conditions. The same is valid for other polycrystalline materials like aluminum, whereas in aluminum further hard inclusions can be found disturbing the machining. Single crystal materials are not very suitable. Silicon is well known in micro technology but is hard to machine. Tools with negative rake angle (-20°) are needed to achieve a ductile machining. Nevertheless, strong tool wear can be noticed which is not allowed, if larger areas have to be microstructured. Copper is also available as single crystal. There is less tool wear than in machining silicon but it

is not very suitable if microstructuring using turning processes is applied. Due to the rotation of the work piece the orientation of the single crystal is changed continuously so that the cutting properties change accordingly.

Hence, materials that offer significant smaller grains are required. Preferable several times smaller than the structure dimensions or even amorphous materials, like nickel-phosphorus (NiP) coatings without any grain structure.

Fine crystalline aluminum is produced by the company RSP Technology. Due the manufacturing process the aluminum gets a fine crystalline structure. The used melt spinning process allows for very high cooling rates during the solidification of the melted material (see **Figure 5.16**, left). In that way, grain sizes of about 2 µm as well as high percentage of alloying elements can be reached. The alloying elements can have another effect on grain refinement or can increase the hardness. The metal belt produced by the melt spinning is then chopped into pieces and consolidated into bulk material.

Figure 5.16, right, shows another fine crystalline material. The copper is strongly deformed by the ECAP (equal channel angular processing) process material. The raw piece is pushed through an angled channel by high forces. The refinement of the grains is achieved by shear deformation. The procedure is repeated several times while the orientation of the material is changed each time. In that way grain sizes of one or two micrometers are possible. Unfortunately, just small samples can be produced by this technology so far. Furthermore, the more pure the copper is the more reactive is the material and grain growth is starting easily.

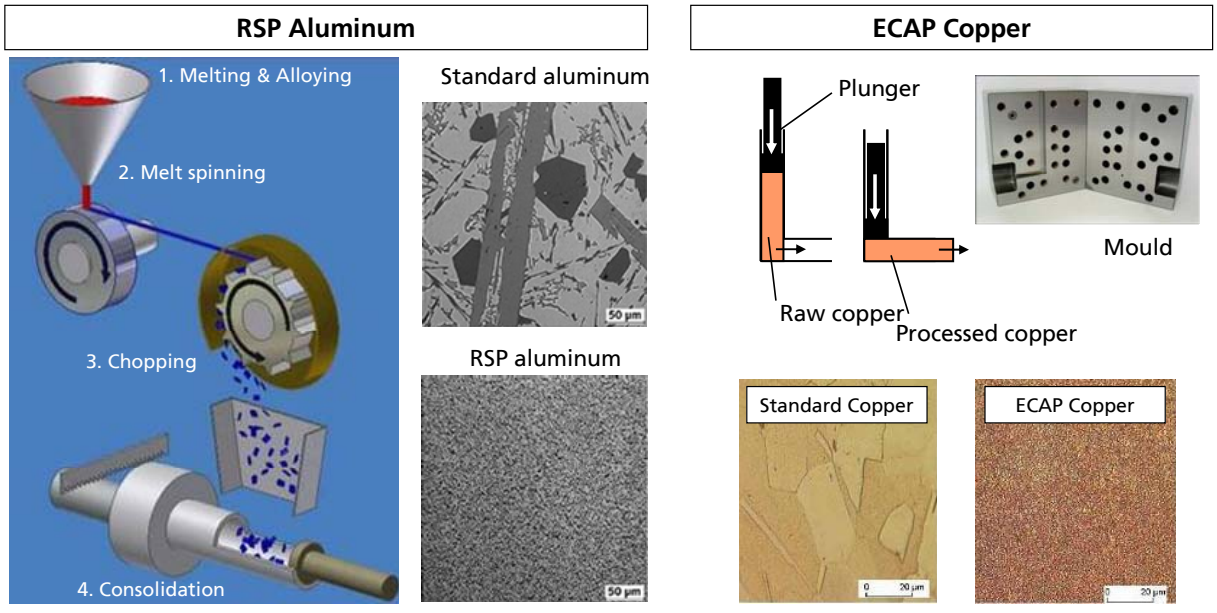

Figure 5.16: Fine crystalline aluminum produced by melt spinning process (left, courtesy: RSP Technology) and copper made by ECAP process (right)

The results of microstructuring using different materials are described in the following chapters. The examined materials are aluminum alloys, copper materials, and electroless NiP-coatings by Kanigen. The main parameter has been the depth of cut

(infeed) since it has according to chapter 5.2.3 the strongest influence on the burr formation.

5.3.2 Nickel-Phosphorus Coatings

Nickel coatings are widely used to protect steel components against corrosion. The coating happens in a chemical or so called electroless process. The result is a layer of nickel-phosphorus (NiP) alloy that is plated with a constant thickness (between one and 120 µm) on the workpiece outline (see **Figure 5.17**). Since several years this material is used for diamond machining. Pure nickel cannot be machined due to chemical wear of the diamond cutting edge. But the alloy of nickel (Ni) and phosphorus (P) is machinable, if a P-content of at least 8% is applied. Larger contents of about 12% reduce the tool wear further. The structure of the coating is amorphous, which makes the NiP-coatings very interesting for microstructuring processes. Furthermore, NiP-coatings offer greater hardness than other non-ferrous materials, like copper or brass. Hence, this material is used preferable for inserts in replication processes like injection molding.

Since the thickness of the electroless coatings is limited to about 100 µm a galvanic coating process has been developed which is capable to deposit NiP-layers. Layers of several 100 µm in thickness are possible, but the layer does not follow the outline of the work piece (see Figure 5.17). The deposition is depending on the strength of the electric field which is concentrated at the edges of the work piece. Hence, the work pieces have to be pre-machined before the ultra-precision machining can start. Beside the costs, this is one big disadvantage of the galvanic process.

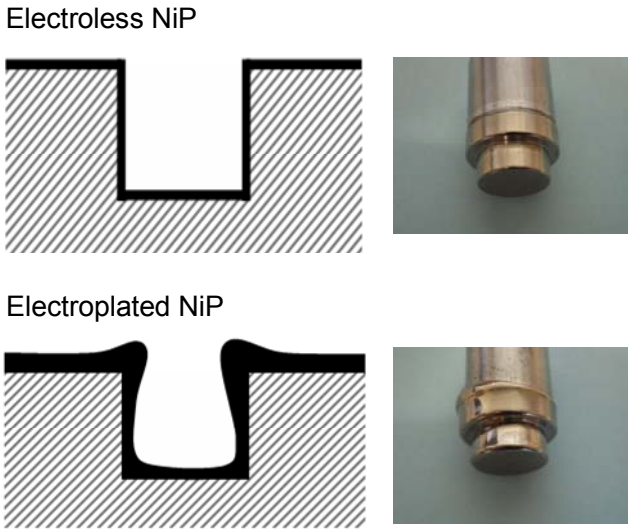

Figure 5.17: Difference in electroless and electroplated nickel-phosphor (NiP)

In the scope of »ERANET-OPTICALSTRUCT«, mainly the behavior of electroless NiP-coatings is examined in strong cooperation with the associated partner Kanigen Works Benelux. The coating is in general capable for the machining with diamond cutting tools but the influences of different phosphorus contents and heat treatments on the quality of microstructures have not been examined so far.

Against this background, Kanigen plated 32 different test parts which have been examined at Fraunhofer IPT. The coating process that Kanigen is using is defined specific in its procedure. So that strong variations of the process to influence actively the Phosphor content in the NiP-layer has not been possible. Nevertheless, the Phosphor content in the nickel coating is influenced by several parameters, that vary slightly over the life time of bath. Therefore, the samples have been coated at eight different times. Furthermore, there are small differences regarding the speed of the coating process. Kanigen possesses automatic and manual coating lines that work with different coating speeds (see **Figure 5.18**). Thermal treatment of the coated work pieces at low temperatures can improve the adhesion of the coating as well as the hardness of the coating. Higher temperatures in the range of 300 °C can change the texture of the coating. The coating changes from amorphous to crystalline. This is not preferred for micro machining applications. To enable the traceability of the results there are always two test parts available for each parameter. Figure 5.18 shows also the test parts coated by Kanigen. The front and backside differ in quality because hydrogen bubbles produced in the coating process may disturb the surface. But the important fact is that the front surface which will be structured is without any disturbances.

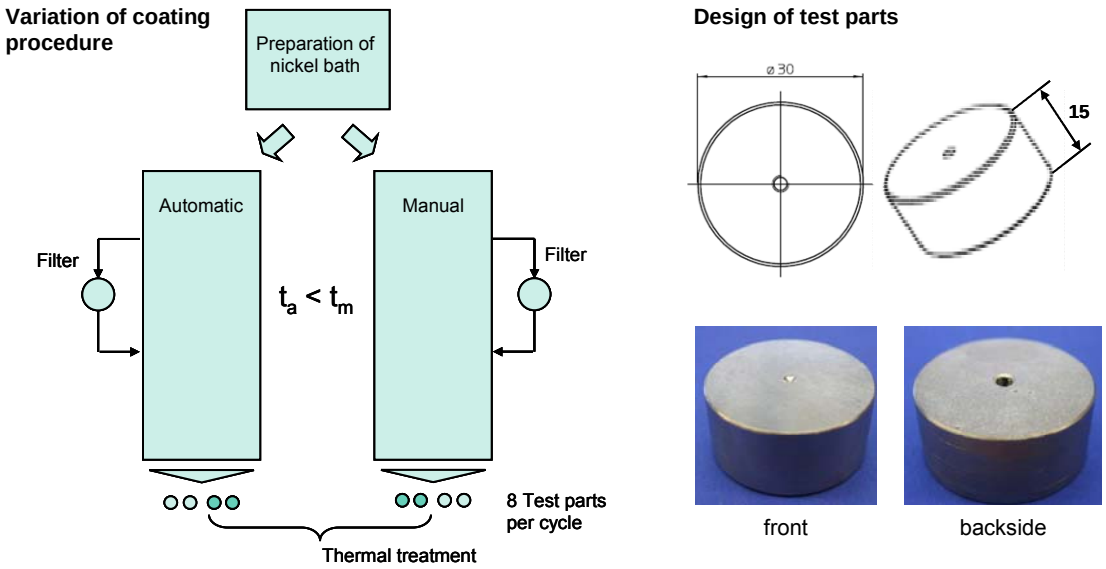

Figure 5.18: Variation of coating process using manual and automatic line (left), design of test part (right)

The analysis of the NiP-coatings has been started with the examination of the phosphorus content by EDX-analysis. In preparation for the EDX analysis the samples have been machined by diamond turning. The average phosphorus content could be determined to 8.5 % (see **Figure 5.19**). The EDX analysis has appointed uncertainties but a more secure determination is just possible by destructive testing. Nevertheless, the examination could prove a quite constant phosphorus content for all parts. No significant difference between the automatic and the manual production line could be found. In the later machining of the microstructures no significant variation of the burr formation could be detected due to a variation of the P-content in the coating. The process parameter and settings showed a stronger influence.

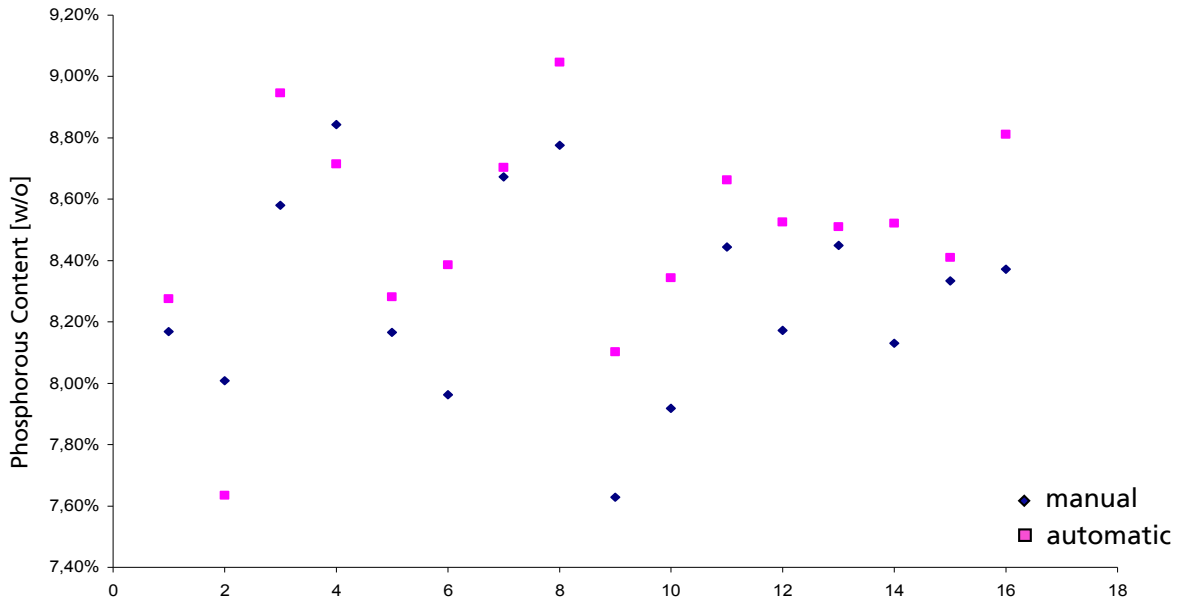

Figure 5.19: Results of EDX-analysis: Phosphorus content of the samples

The hardness of the coating has been measured by a Vickers hardness tester. The test force has been adapted to thin layers. The hardness varied between 560 and 610 $HV_{0,1}$. The measurements did not show the typical decrease of the hardness by increasing phosphorus content in the coating. The increase of the hardness due to the thermal treatment can be seen in the graph in **Figure 5.20**. Most of the samples with thermal treatment feature a higher hardness than the others.

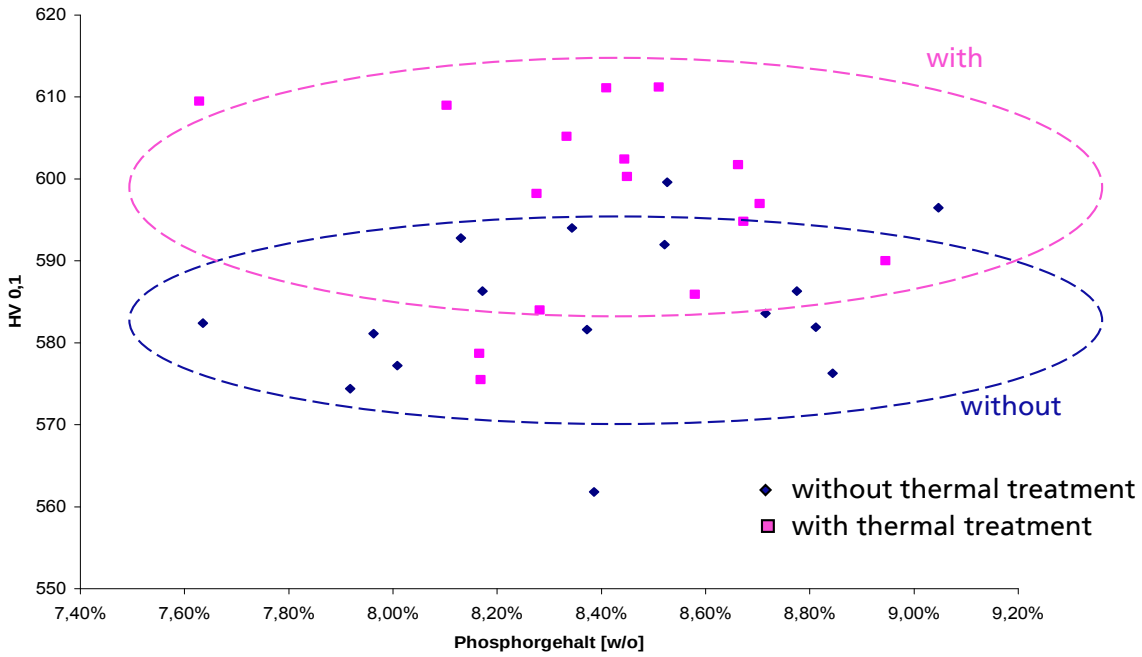

Figure 5.20: Surface hardness referring to phosphorus content and treatment

Beside the small test parts for the examination of the coating and the process parameter studies, also a large plate with a diameter of 100 mm has been coated by Kanigen and machined at Fraunhofer IPT. **Figure 5.21** shows the plate before and after the machining. Beside the planar machining, also 90°-v-grooves can be seen on

the plate on the left. At the planar surface a roughness of 2.8 nm Ra has been achieved.

Figure 5.21: NiP-coated workpiece (diameter: 100 mm): before and after machining

After the first general test of the machinability of the Kanigen NiP-coating, the material has been examined in microstructuring. Therefore, the test structure (45° blazed gratings, pitch: 7 µm) has been machined considering the absolute structure depth (see chapter 5.2.4). Preliminary examinations proofed that NiP requires small infeeds in the range of 1 µm per rotation to achieve groove structures in good quality. Hence, for the examination of the two different NiP-coatings (electroplated and electroless) infeeds between 0.05 µm and 1.5 µm were chosen. An overview of the results, that are documented by SEM pictures, is shown in **Figure 5.22**.

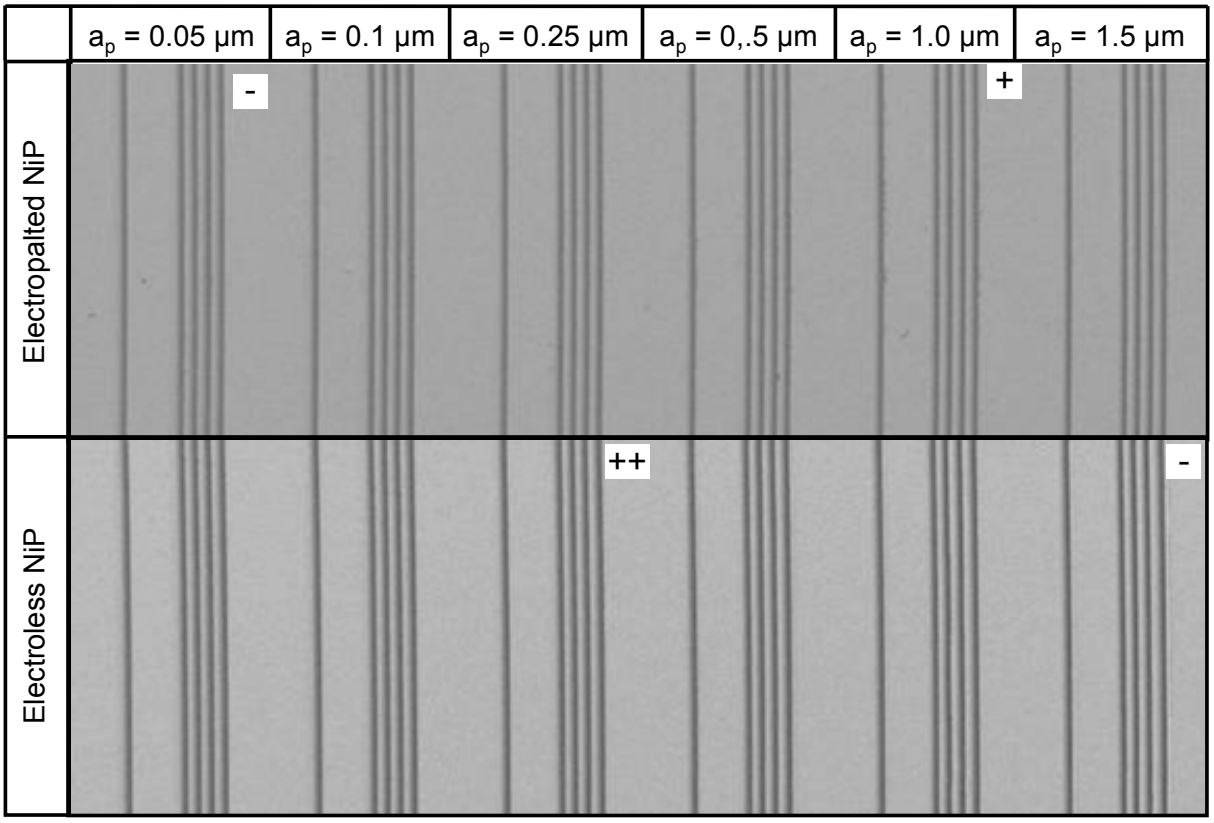

Figure 5.22: Overview of microstructuring of NiP-coatings with blazed gratings

The quality of the grooves regarding burr and deformation is labeled using the symbols »--«, »-«, »o«, »+«, »++« ranging from very bad to very good. In general the

quality is good and no defects or irregularities in the structure can be seen in the overview in Figure 5.22. The results in electroplated NiP are not that good compared to the electroless NiP by Kanigen. Very good results could not be realized for the electroplated NiP. The best result has been achieved at a depth of cut of 1 µm. The electroless NiP showed better results at 0.25 µm and with increasing depth of cut the burr formation has been increased.

A detailed view of the structures is given in **Figure 5.23**. There the burr formation at the tip of the structures in the groove array can be seen more clearly. The electroless NiP-coating by Kanigen has at 0.25 µm nearly no burr at the structure tips. The tips are very straight.

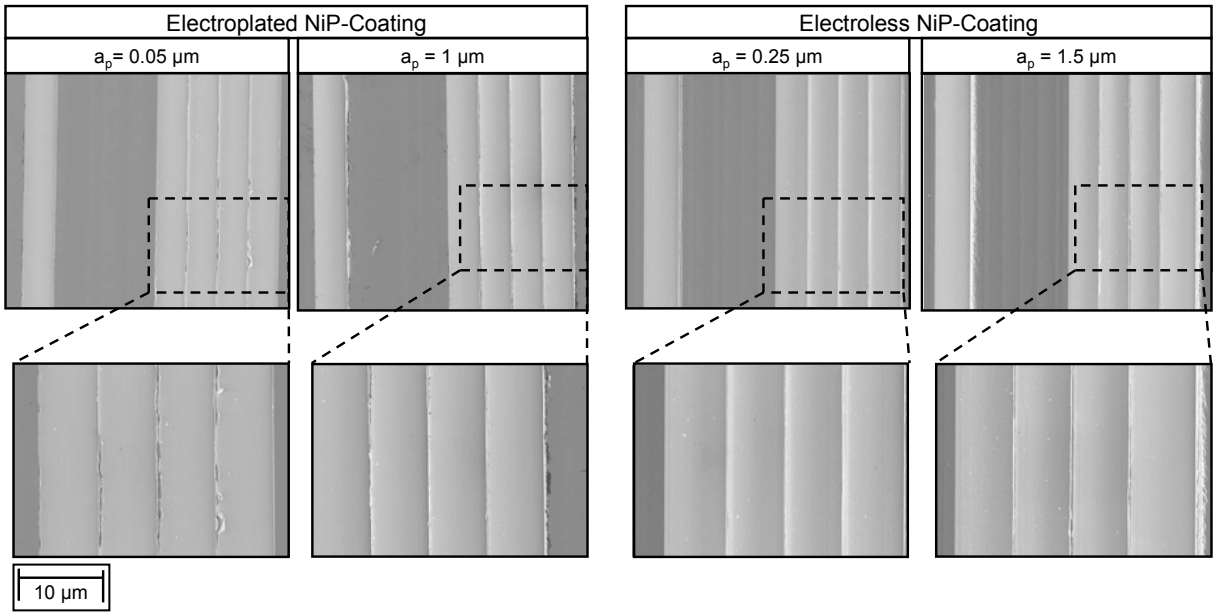

Figure 5.23: Detailed views of blazed gratings machined in NiP coatings

Summarizing the results of the test machining of the nickel-phosphorus (NiP) coatings, it can be said that the material does not generate any significant defects in the structure. Burr free structures without deformations can be machined. To prevent burrs depth of cut in the range of 0.25 should be adjusted.

5.3.3 Aluminum Materials

Aluminum materials are very common in the field of ultra-precision machining. Aluminum offers a high reflectivity for mirror systems and is used even for large telescopes. Furthermore, aluminum is due to its low density used for dynamic applications like scanner optics. Aluminum is a polycrystalline material. For optical applications aluminum alloys are used that offer a very low silicon content (< 1%). This element produces hard inclusions in the soft aluminum matrix. Depending on the cutting conditions the inclusions can be torn out or break. Consequently they influence the surface negatively. This is valid for continuous surfaces but even more critical in microstructuring processes.

In the scope of the »ERANET-OPTICALSTRUCT«, three different alloys have been examined: Certal (AW-7075), RSA-905, and RSA-6061. While Certal is a standard

alloy the RSA materials are fine crystalline materials produced by RSP Technology (see Figure 5.16). The RSA-6061 equals AW-6061 in the composition but offers a fine grain structure. The RSA-905 is a special alloy developed by RSP Technology. The results of the microstructuring tests are illustrated in **Figure 5.24**. As before, the test structure consists of a single and set of blazed gratings with a depth of 7 µm. The machining took place with depth of cut between 0.1 and 1.5 µm. The overview shows directly the differences between the materials. Certal has large inclusions in the aluminum matrix that appear as light grey spots in the SEM pictures. Such inclusions cannot be detected in the fine crystalline materials of RSP Technology. The inclusions in Certal have dimensions up to 15 µm and influence clearly the structuring result, while the effect of the inclusions at the planar surface is neglectable. In the shown picture the structure possesses a large defect for a depth of cut of 0.1 µm which makes the structure unusable. Compared to NiP-coatings larger infeeds are needed for good results regarding the burr formation. Best results have been achieved in Certal using a depth of cut of 1.5 µm.

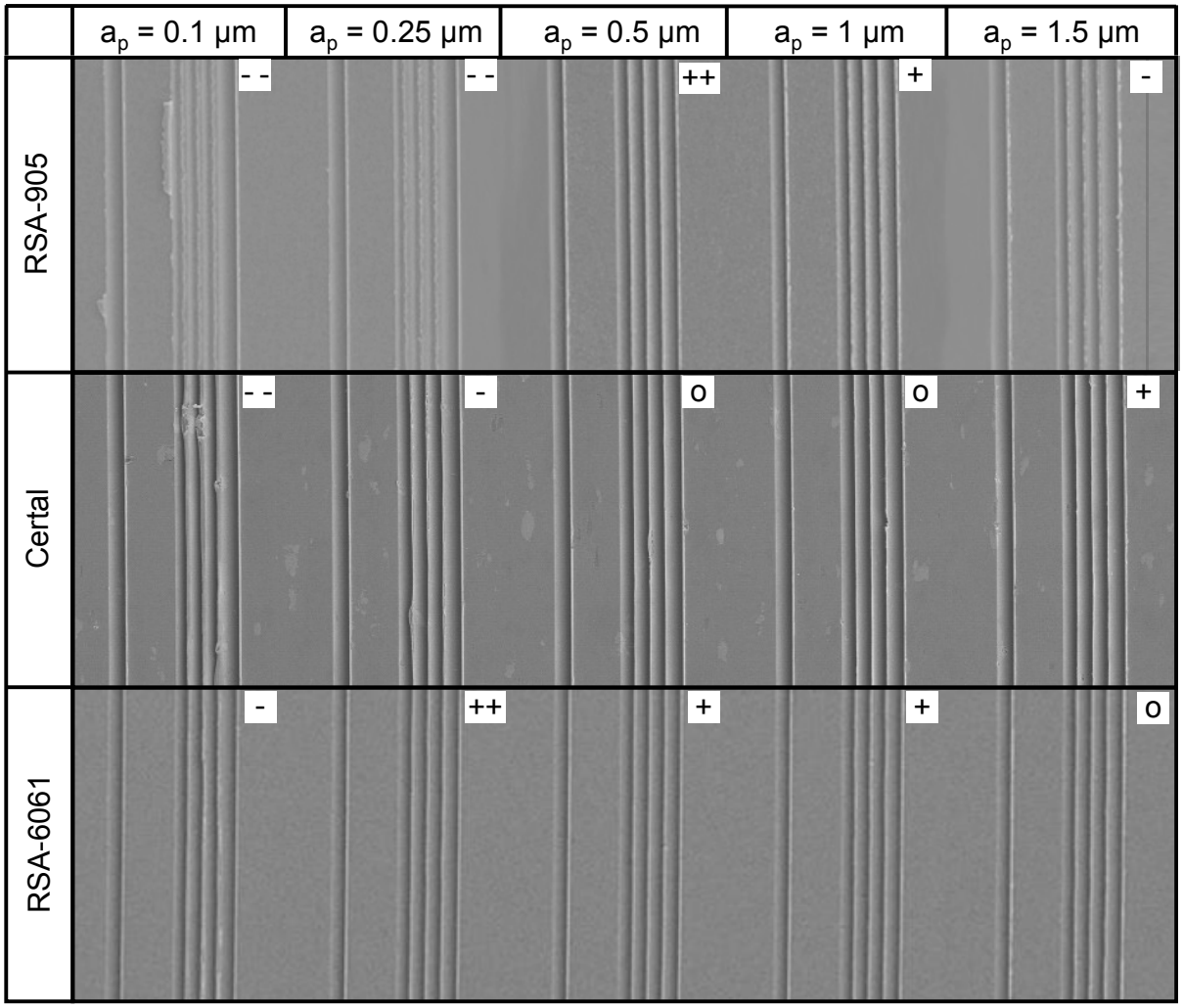

Figure 5.24: Overview of microstructuring of aluminum alloys with blazed gratings

The effect of the fine grained material can be seen directly in Figure 5.24. The surface appears more homogenous and no large breakouts can be seen. Furthermore, the generated burr seems to be more frazzle than burr in standard

aluminum. The RSA-905 shows the best results for 0.5 µm depth of cut. Lower infeeds show more deformations and burrs since the cutting depth is very low (ploughing effect). Higher infeeds (1.5 µm) generate more burr as described in chapter 5.2.3. A similar behavior can be observed for the RSA-6061 which should be machined with an infeed between 0.25 µm and 0.5 µm.

A difference between both RSA materials can be seen in the detailed views shown in **Figure 5.25**. Both materials have fine grains with dimensions below two micrometer, which can also be recognized by the speckled appearance of the surface. But in RSA-6061 a small breakout can be seen at the groove flanks. This defect is not that big compared to the Certal, where failure influences three grooves (see Figure 5.25, left), but it cannot be tolerated for optical applications.

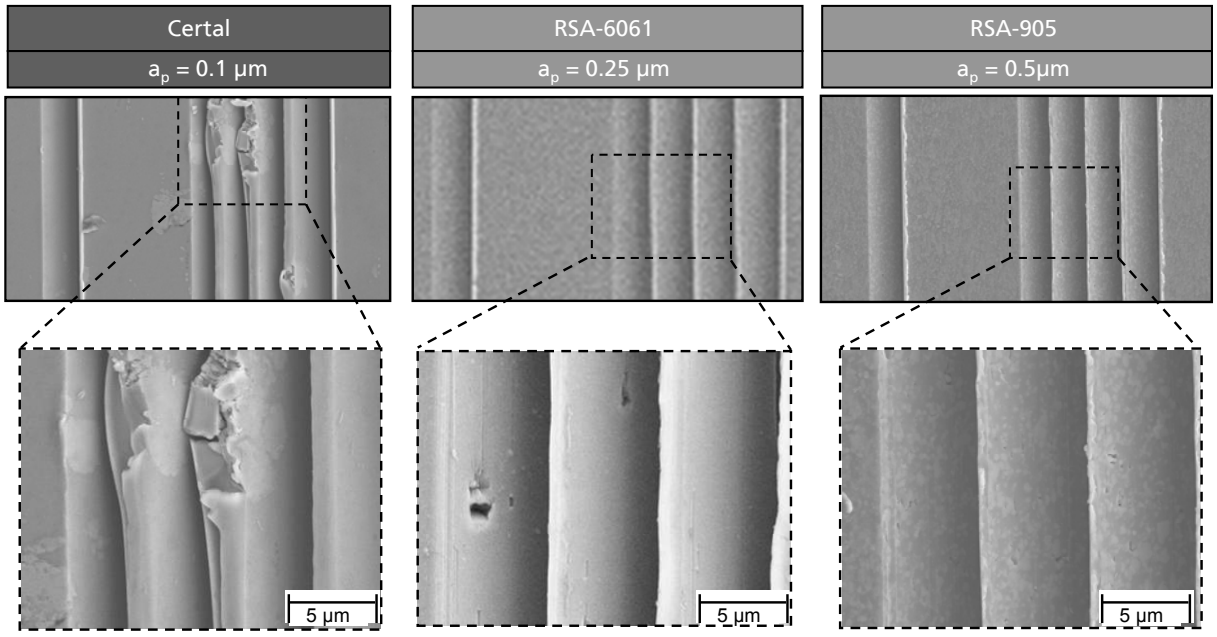

Figure 5.25: Detailed views of blazed gratings machined in aluminum alloys

Hence, fine grained aluminum materials are preferable to use for microstructuring application compared to the standard aluminum material. But, as Figure 5.25 shows, even small grains can break out of the bulk material. The best results has been achieved with RSA-905 using infeed rates of 0.5 µm during the machining of the test structures. The results regarding burr formation are comparable with the NiP-coatings.

5.3.4 Copper Materials

In ultra-precision machining Copper is mainly used for laser mirrors due to its very good heat conduction (nearly twice the number of aluminum). To achieve high surface qualities OFHC copper is typically used for UP-machining which is very pure and good to machine. Unfortunately, as described before in chapter 5.3.1, the polycrystalline and anisotropic characteristics of copper influence the micromachining processes. For this background, beside the OFHC copper, electroplated and ECAP copper have been examined in the scope of »ERANET-OPTICALSTRUCT«.

The result of the structures machined in copper materials can be seen in **Figure 5.26**. The examined electroplated copper is very soft and tends to deform. The single structures bend because of the cutting forces. The effect gets stronger the smaller the infeed is. Better results can be achieved with infeeds larger than one micrometer. Very good result can not be achieved with the used process parameters. In contrast to former examinations (see Figure 5.5) the quality of the grooves machined in OFHC copper has been good at very low depths of cut (< 0.25 µm). With increasing depth of cut the burr formation increased. Good results can be achieved with the ECAP copper at an infeed between 0.25 and 0.5 µm. At the characteristic of the burrs, for example at a depth of cut of 1.5 µm, the fine grained structure can be noticed. The burrs are very frazzle and not homogenous.

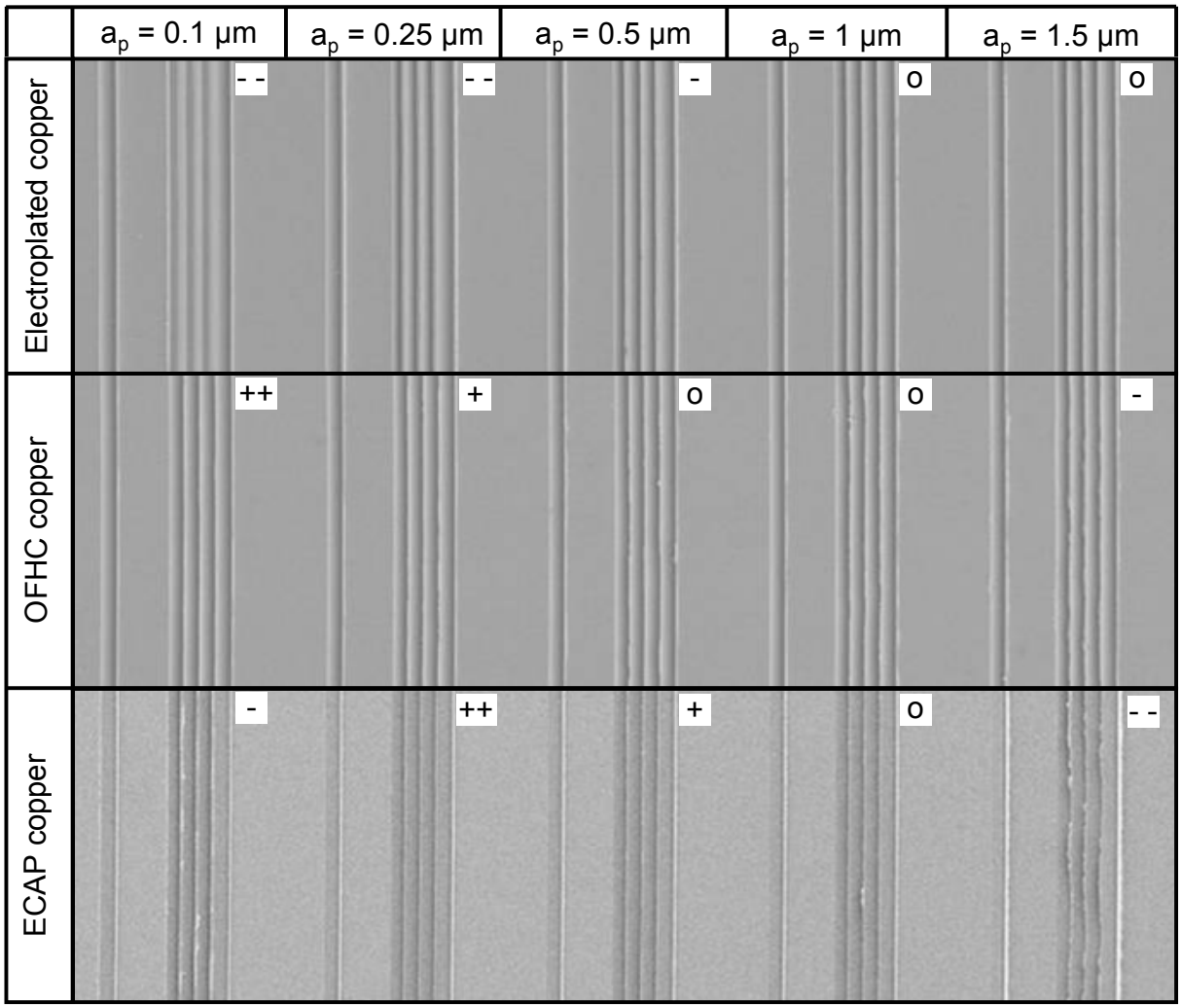

Figure 5.26: Overview of microstructuring of copper materials with blazed gratings

Figure 5.27 gives a more detailed insight in the structure results. The results for low depth of cut in OFHC copper are very good. The variation of the burr formation that can be seen for a depth of cut of 1.5 µm indicates the dependence on the material properties caused by the grain structures. In homogenous materials like NiP-coatings the burrs are more or less constant structure by structure if the same cutting parameters are used (see Figure 5.10). As described before, the burrs of the ECAP copper are a bit frazzle which can be explained by the fine grained structure. The

SEM picture of the electroplated copper shows the strong deformation of the blazed geometry mentioned before (indeed 0.1 µm). The grooves are machined from the left to the right side and the material structures are bend by the cutting forces into the groove that has been machined before. Hence, the last groove appears wider than the other grooves in the top view. The sketch below the pictures explains the deformation. Low infeeds cause also for other materials (ECAP copper) deformations of the structure, but for the examined electroplated copper nearly for all parameters deformation can be recognized.

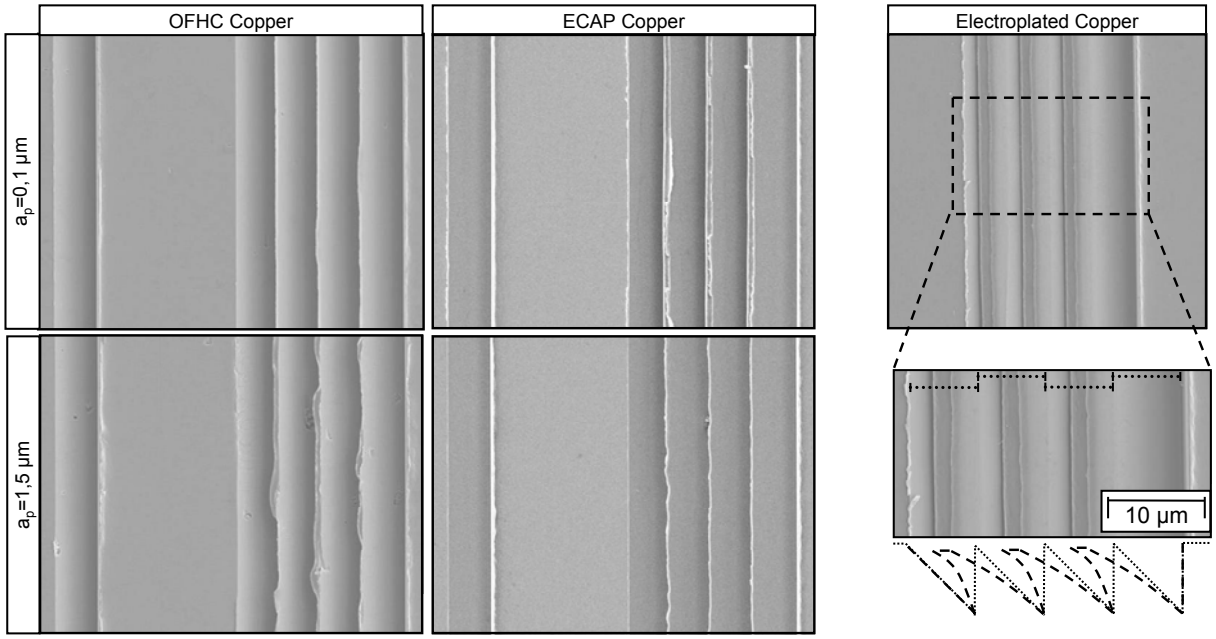

Figure 5.27: Detailed views of blazed gratings machined in copper materials

Summarizing the results of the examined copper materials it can be said that the fine crystalline ECAP copper indicates its capability for microstructuring processes, but the available material is limited in dimension. The results of OFHC copper confirmed the issues with the grains, although sufficient groove qualities could be reached for infeeds with 0.1 µm. Since the material properties of electroplated coatings are strongly depending on the process parameters during the coating may a different electroplated copper shows better results in the deformation.

5.3.5 Summary of Material Examination

Standard materials like non-ferrous metals that are used for metal optics for years are not suitable, if structure details go down to sizes of a few micrometers. The polycrystalline composition of copper provokes changing cutting conditions, because each grain has different orientations and properties. Thus, different burr formation along the groove, which is cut through several grains, can be noticed (see Figure 5.15).

Another issue are inclusions. Alloying elements, like silicon, generate hard inclusions in aluminum that disturb the groove structure. Brittle particles break due to cutting forces out of the bulk material. **Figure 5.28** shows this effect for an aluminum that is common in ultra-precision machining. Fine crystalline aluminum alloys with small

grain sizes in the range of one micrometer minimize the issue of inclusions. Due to the special production process, the maximum grain size is limited for the aluminum as well as for the inclusions to dimensions in the range of one or two micrometer. In that way, a uniform composition of the material is guaranteed, offering constant cutting conditions. Nearly amorphous materials like nickel-phosphorus (NiP) coatings offer even better properties. As shown in Figure 5.28, the structure is very smooth and no texture can be found on the flanks of the v-grooves.

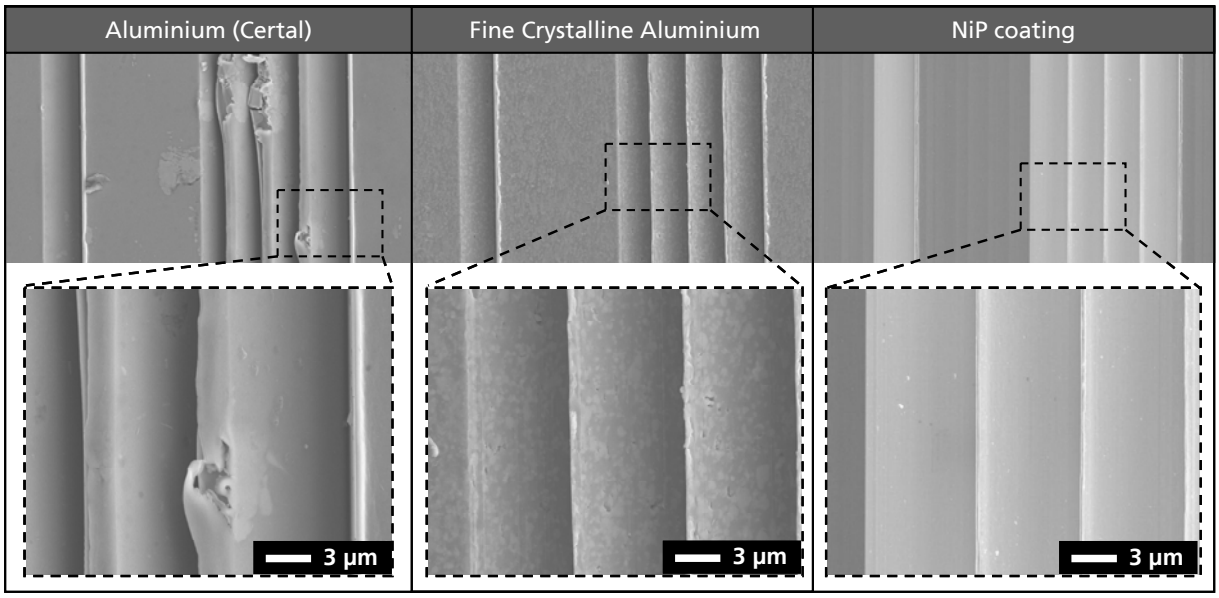

Figure 5.28: Material comparison for diamond machining of blazed gratings

Furthermore, NiP-coatings offer a sufficient hardness which is important for replication by embossing processes. Additionally, structures produced in NiP can easily be copied by electroforming. For this reason, NiP-coatings are considered as most suitable for the manufacturing of microstructures. Nevertheless, NiP-materials exist only as coating with a maximum thickness of several hundred micrometers. Hence, in some cases the RSA-905, which showed also good results, can be used if a coating cannot be applied.

5.4 New Diamond Tools for Fast Tool Servo Machining

The machining of non-rotationally symmetric work pieces using Fast Tool Servo (FTS) systems is beside dynamic limitations often limited by the clearance angle of the used diamond cutting tools. In that way, the inclinations of a free-form surface, the shape of micro lenses or slopes in micro grooves are restricted to the maximum clearance angle of the cutting tool. State of the art are tools with clearances of 18° (with controlled waviness). This limit is defined by the geometry of the diamond crystal. A diamond can be grinded and polished with high quality just in certain directions and angles. It is not possible to grind through particular crystal planes reaching a high quality cutting edge with a controlled waviness. The crystal geometry prevents larger clearance angles than twenty degrees in a conventional grinding and manufacturing process of diamond radius tools.

To illustrate the consequences of the limitations in tool manufacturing a groove structure and a micro lens array are described in **Figure 5.29**. Due to the clearance angle the tool has to follow a certain slope (clearance angle plus <2°) while it is cutting into the material to avoid damage of the cutting edge or of the work piece surface. This means for groove structures that a certain part of the groove does not offer the target depth. This is especially critical for short grooves (< 50 µm). In the given example just 5 µm have the targeted depth of 5 µm. The end of the groove is just limited by the dynamics of the FTS. The faster the tool can be moved out of the material by the FTS the steeper the end of the groove is. The sketched micro lens array defines the maximum size of a lens with a radius of 2.5 mm. Just a depth of 130 µm can be reached at a lens opening diameter of 1.6 mm.

- Clearance angle of diamond cutting tool limits the infeed angle

Examples:

- Linear groove
  - Clearance angle: 20°
  - Length: 20 µm
  - Depth: 5 µm
  - Usable length: 5 µm

- Lens array
  - Clearance angle: 20°
  - Radius: 2,5 mm
  - Max. depth: 130 µm

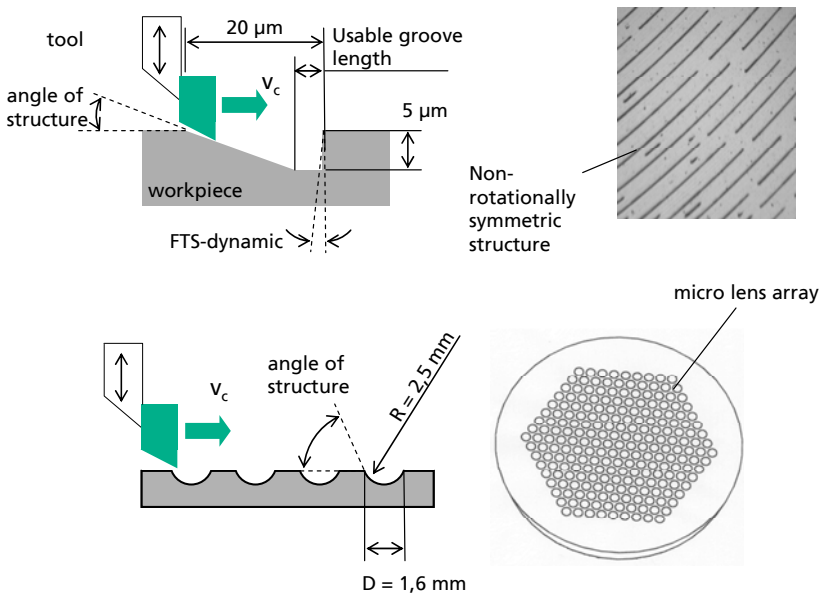

Figure 5.29: Material comparison for diamond machining of blazed gratings

Nevertheless, the market requires cutting tools with larger clearance angles than 20°. Especially micro lens arrays need large aspect ratios for most applications. A maximum angle of 30°- 40° at the edge of a lens is common. Furthermore, there are strong limitations in machining discontinuous micro grooves.

Hence, Contour developed a new way of producing diamond cutting tools. Now it is possible to manufacture a radius tool with a clearance angle of 40° and controlled waviness. The tools are shown in **Figure 5.30** in a test machining setup as well as in SEM pictures.

The new tool has a radius of 450 µm and a rake angle of zero degree. The first test has been conducted in machining a rotational symmetric sphere. In that way the stability and condition of the cutting edge over a large bow of the cutting edge could be characterized. The material of the work piece is OFHC copper. The part has an outer diameter of 80 mm and the sphere has a radius of 70 mm. A surface roughness of 2.3 nm Ra (measured with white light interferometer) has been achieved at the flat frame of the sphere. This test proved the capability of the new tool.

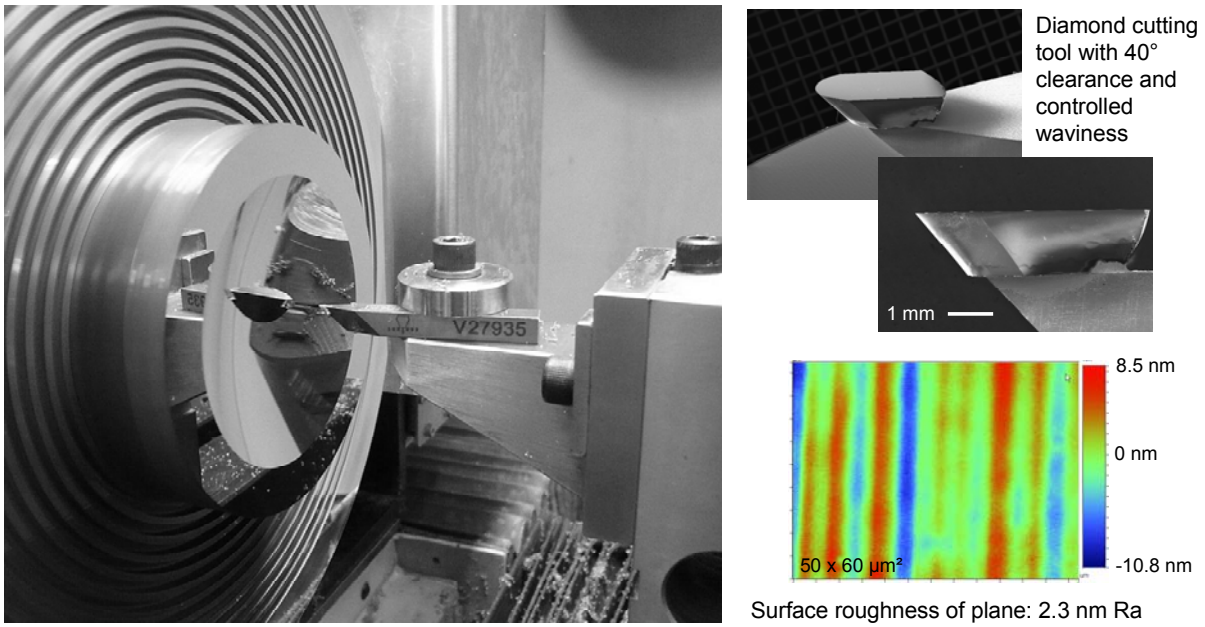

Figure 5.30: Machining of sphere using new 40° clearance tool (left), SEM pictures of cutting edge (upper right)

A micro lens array has been the second test geometry for the new tool (see **Figure 5.31**). The array consists of four lenses arranged at a diameter of 12 mm. Each lens has a radius of 6 mm and a depth of about 0.8 mm. Due to the aspect ratio of the lens (depth to sphere radius) the maximum structure angle at the boundary of the lens is 30°. Hence, a clearance of ten degrees between the lens surface and the clearance surface of the tool is remaining. The machining has been taken place using a spindle speed of 75 rpm and for the finishing cut a feed rate of 0.3 mm/min has been adjusted. As material the aluminum Certal has been used.

Figure 5.31: Machining of micro lens array requiring large clearance tool (Lenses are arranged on diameter 12 mm)

Hence, it has been proven that the new diamond cutting tool of Contour is able to produce optical surface quality and is in general able to withstand the stress and strains that occur in Fast Tool Servo machining. The cutting edge is still fragile and

first break outs could be detected after several machining cycles in the lens array. Nevertheless, this is an important result since by the availability of this new tool having a clearance angle of 40° former limitations in machining free-form surfaces are eliminated.

5.5 Replication of Hybrid Optics by Injection Molding

Exact replication of optical components and structures using the injection molding process is a great challenge. Basically, producing optical components by injection molding does not differ from the production of other technical, plastic components. **Figure 5.32** shows the inside of an injection molding machine with a handling system for the lens removal. The major difference has to do with the geometry of the components. Whilst other technical moldings can be designed to suit the plastic and the process, with optical components the optical design dictates the geometry. Often thick-walled lenses having a great variation in thickness are the result of the optical design. An additional requirement is the high degree of shape accuracy required for the optical surfaces and structures that, depending on size and application, have dimensions of a few micrometers.

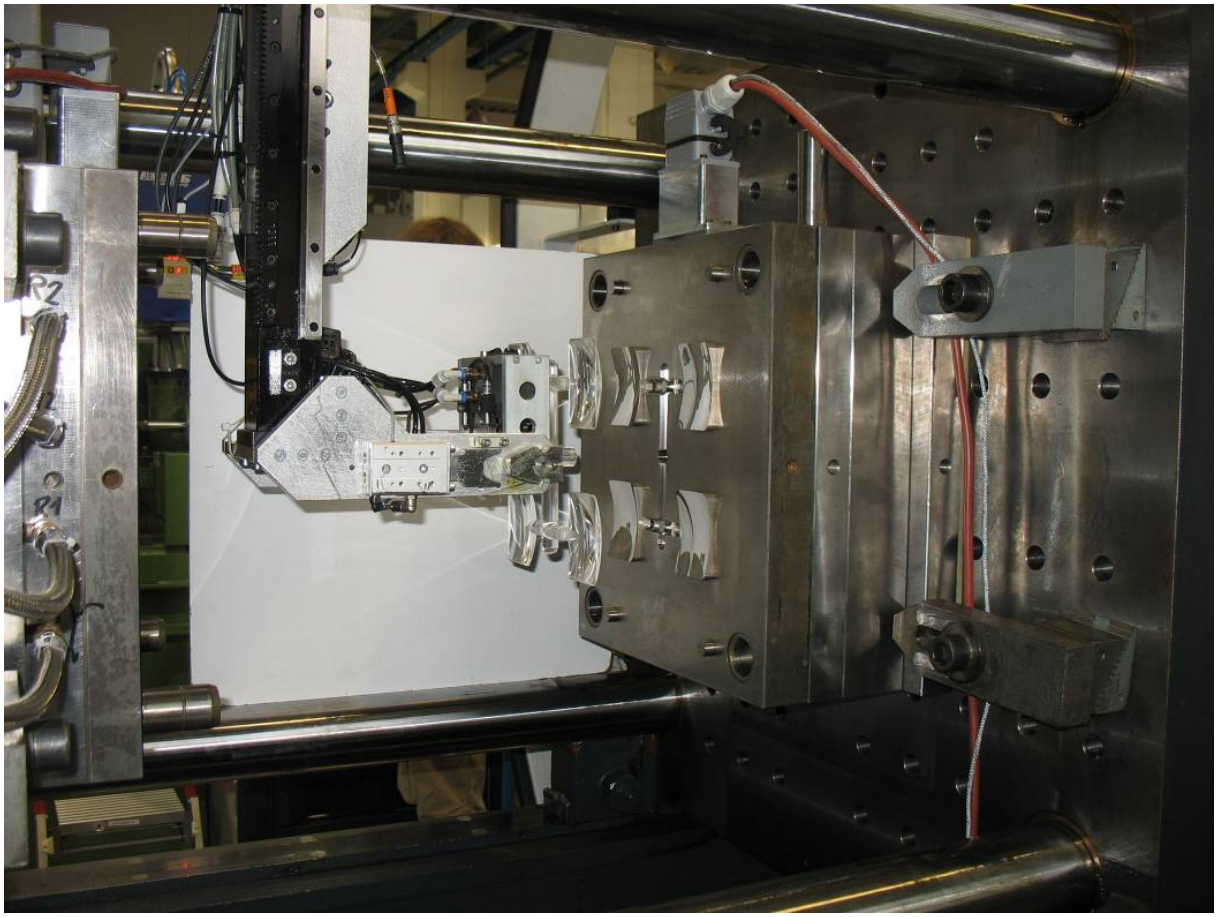

Figure 5.32: Production of lenses with microstructures in a four-cavity tool

The main objective in the scope of the project »ERANET-OPTICALSTRUCT« has been to investigate the individual influencing parameters that determine the quality of molded structures.

These parameters are listed in the following:

- Geometry of the lens (curvature of the optical surface, center thickness, outer contour)
- Geometry of the structures (depth, pitch, flank angle)
- Material characteristics (ease of flow, shrinkage, molding characteristics)
- Injection molding machine process parameters
- Process engineering (injection molding, injection embossing, variotherm process)

Within the project different test series have been done to examine the correlation of the influencing parameters and the relevance on the replication accuracy of hybrid lenses. Therefore test parts with different structure geometries and lens shapes have been defined. The used molding tools are multifunctional and allow depending on the test series injection embossing or variotherm operation.

The following sections describe test series and their main results regarding the replication of microstructures and the effect of variothermal tempering.

5.5.1 Replication of Microstructures

For the first trials a prototype mold has been constructed and built. This mold has been designed as an injection embossing mold. The used optical mold inserts are nickel plated steel inserts.

In order to investigate the influences of the structure geometry on the molding characteristics a test work piece with a simple geometry has been chosen. It has been a flat disc with a diameter of 27 mm and a thickness of 3.6 mm. **Figure 5.33** shows a replicated work piece with different microstructures as concentric rings.

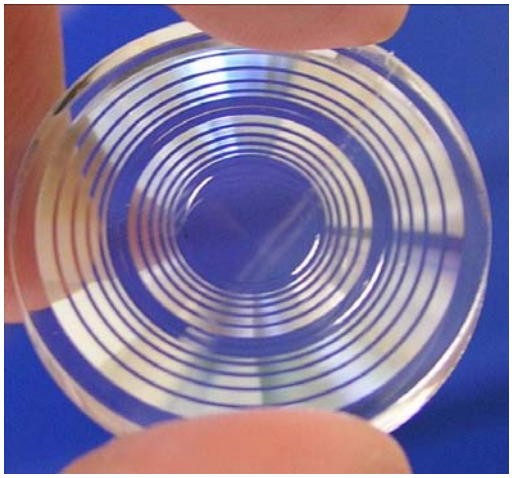

Figure 5.33: Test work piece for the replication of microstructures

Design of experiment

For the molding trials specific test structures have been defined. To obtain results that can be measured and characterized, simple structures have been chosen. The main task during the first trials has been the qualitative evaluation of the molding accuracy.

In **Figure 5.34** and **Figure 5.35** the two test structures, a diffractive and a v-groove structure, are presented. The diffractive structure has a constant step heigt of half a micrometer while for the 90°-v-groove structure two depths of 10 µm and 50 µm have been chosen.

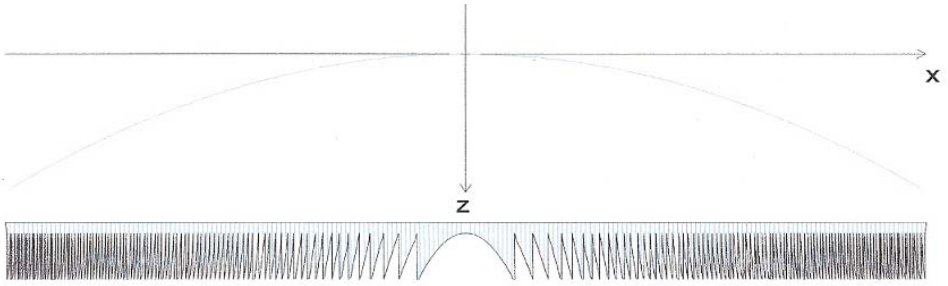

Figure 5.34: Diffractive structure (D = 27 mm, 95 zones, step height: 0,5 µm, steepest angle: 0,4°)

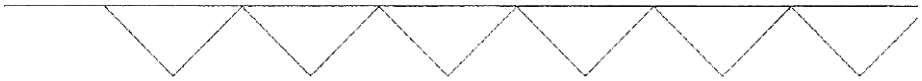

Figure 5.35: 90°-v-groove structure

Standard PMMA and PC materials with different flow characteristics have been used for the trials. They are listed in **Figure 5.36**.

Thermoplastic material	Trading name	Manufacturer	Melt Flow Index
PMMA	Plexiglas 8N	Evonik Röhm	3.6 g/10 min
PMMA	Sumipex LG 35	Sumitomo	35.0 g/10 min
PC	Lexan 123R	Sabic	17.5 g/10 min

Figure 5.36: Materials selected for trials

Certain process parameters of the injection molding machine have been specified as further variables in the test series. **Figure 5.37** illustrates the parameter that influence mainly the replicated structure quality. The range of variation of the process parameters depends on the characteristics of the material being processed, the geometry of the lens, the features and performance of the injection molding machine as well as on the physical dependency of the individual process parameters on each other.

The tool temperature is the most important parameter to influence the quality of optical lenses. It affects strongly the molding accuracy of optical surfaces and microstructures as well as the cooling time. The cooling time is further influenced by the thickness of the lens. Injection and dwell pressure, injection velocity, and embossing gap are parameter that are mainly depending on the lens geometry. Their impact on the molding accuracy of optical surfaces and microstructures is not very

high. The melt temperature is a value which is depending on the material used for the replication and the effect on the replication result is rather low.

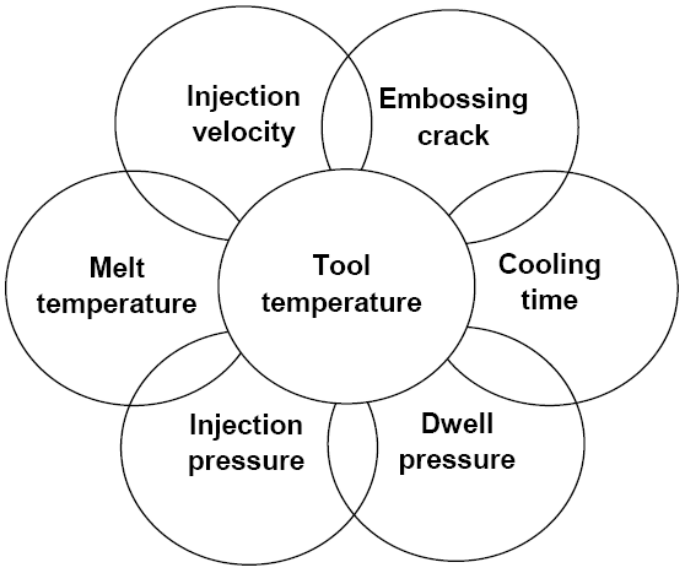

Figure 5.37: Optimized process parameters in the trials

The test series have been done by replicating the above described structures using the materials Plexiglas 8N, Sumipex LG 35 und Lexan 123R. Following procedure has been applied:

- **Initial situation:** First adjustment of injection parameters. The test part needs to be visually alright which means that the planar surfaces have to be even. Afterwards the form accuracy of the microstructures have been measured.
- **Optimization:** Variation of the previously defined process parameter according the test sheet. Measurement and documentation of the form accuracy of the microstructures.
- **Best result:** Analysis and evaluation of the documented results. Repetition of molding tests with promising parameters to check the repeatability of the earlier achieved form accuracy.

Following the results of the test series for the diffractive and the v-groove structure are described.

Results of Molding the Diffractive Structure

The diffractive structure seems to be an easy structure for the replication since the structure depth is low. Nevertheless, during the machining of the structured mold insert using diamond cutting tools some issues occurred that influenced the aimed structure depth of 0.5 µm. The step height varied from center to periphery from 0.543 µm to 0.432 µm. The reason for the form deviation could not be established, even by conducting turning tests with various parameters on the ultra-precision lathe. Therefore, the measured values of the mold insert in the centre and at the periphery

were defined as reference values for analyzing and assessing the measurement results.

In all test trials the diffractive structure generally has been molded with good results after optimizing the process parameter. The mold temperature and dwell pressure have been the significant parameters to achieve a high replication quality.

Sumipex LG 35, with a melt flow index of 35 g/10 min, is a low viscous material. This is the reason for achieving really good results in molding of the diffractive structure. Already the first machine set up produced results with high form accuracy. With further optimization of the process parameter the first results using Sumipex LG 35 could not be improved clearly.

Plexiglas 8N has a melt flow index of 3.6 g/10 min. This is really high viscous. Nevertheless, the shape accuracy of the microstructure from injection molded parts has been quite well. To obtain a comparable result, as achieved with Sumipex LG 35, the parts had to be injection embossed.

Lexan 123R, with a melt flow index of 17.5 g/10 min, is a medium viscous polycarbonate. Parts injection molded using Lexan 123R achieved structure depths comparable to the Sumipex LG 35 samples. However, the achieved form accuracy of the structure geometries in Lexan 123R has been remarkable poorer. The slanted surfaces of the diffractive structure showed a kink close to the structure tip.

Figure 5.38, **Figure 5.39**, and **Figure 5.40** show the measurement results of the best achieved part quality for each material. The measurements have been done using a confocal 3D-surface measurement device by the company nanofocus. Each picture shows a part of the primary profile of the diffractive structure. The given measurements of the structure depth are the mean values.

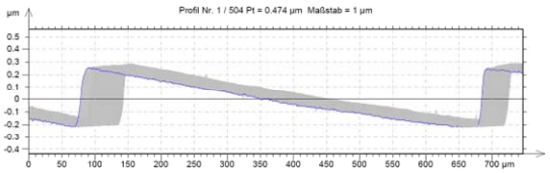

Primary profile – centre: 0,486 µm

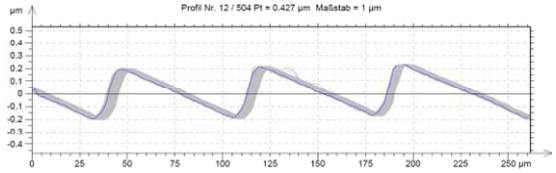

Primary profile - periphery: 0,426 µm

Figure 5.38: Best results with Sumipex LG 35

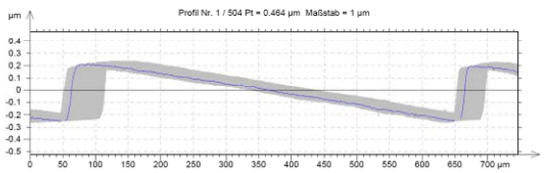

Primary profile – centre: 0,465 µm

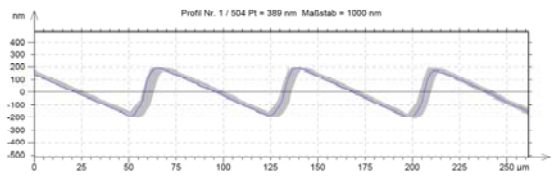

Primary profile - periphery: 0,389 µm

Figure 5.39: Best results with Plexiglas 8N

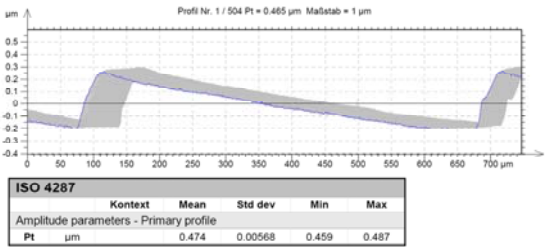

Primary profile – centre: 0,474 µm

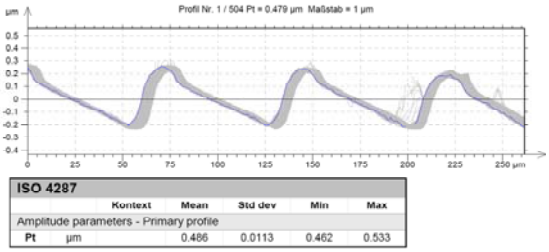

Primary profile - periphery: 0,486 µm

Figure 5.40: Best results with Lexan 123R

Results of Molding the 90°-V-Groove-Structures

Aim of the replication trials of the 90°-v-groove structures has been to evaluate the quality of the compared to the diffractive structure significantly larger structures having dimensions of 10 µm and 50 µm. The measurements of the structure have been done using a 2D tactile measurement probe of Taylor Hobson. The criteria have been the replicated structure depth and the shape accuracy compared to the mold insert.

The mold insert for the 90°-structure have been machined by diamond turning. Due to the machining process the aimed structure depth does not match exactly with the aimed values. Measurements proofed a depth of 47.3 µm for the larger structure and 6.7 µm for the 10 µm structure. The measured dimensions have been defined as the reference values for the characterization of the replicated test samples.

The conclusions on the molding characteristics of the various materials indicate similar tendencies compared to the diffractive structure. The low viscous Sumipex LG 35 achieved also for the replication of the 90°-v-groove structures the best results regarding the accuracy. But the high viscous Plexiglas 8N surprisingly achieved quite good results.

However, the best molding results for the 10 µm and 50 µm structures were exclusively obtained using the injection embossing process. But it is interesting to note that injection embossing achieved not significantly better results than the standard injection molding process. The improvement due to the injection embossing are in the range of maximal two percentage points. Thus, the effort regarding time and costs needed to implement the embossing technology is not justified by the quality of the results.

It also has to be emphasized that these investigations have not considered the molding precision of the entire optical surface nor the inner stresses of the parts produced. For these quality attributes, embossing technology can bring decisive advantages, depending on the geometry of the component.

Figure 5.41 and **Figure 5.42** set out the achieved degree of molding precision as a percentage of the reference value (step height of mold insert: 47.3 µm / 6.7 µm).

During the optimization step, the results are based on the injection molding process. The data of the best results could only be achieved with injection embossing.

Target: 47.3 µm	Sumipex LG 35	Lexan 123R	Plexiglas 8N
Best result	98%	97%	94%
Optimization	97%	97%	93%
Initial situation	89%	96%	91%

Figure 5.41: Comparison of the ratio of the mold insert for the 50 µm deep 90°-v-groove-structures with injection results in percent

Target: 6.7 µm	Sumipex LG 35	Lexan 123R	Plexiglas 8N
Best result	94%	90%	92%
Optimization	92%	88%	89%
Initial situation	91%	88%	83%

Figure 5.42: Comparison of the ratio of the mold insert for the 10 µm deep 90°-v-groove-structures with injection results in percent

The variance from target height for the 50 µm structure is arranged between 0.7 µm and 2.7 µm in the best results. The variance from the 10 µm target depth is 0.42 µm to 0.55 µm.

In **Figure 5.43** and **Figure 5.44** the measured profiles of the 50 µm and 10 µm structure illustrate the accuracy in shape of a single tip between two v-grooves. These are the measurement results from replication trials using Sumipex LG 35.

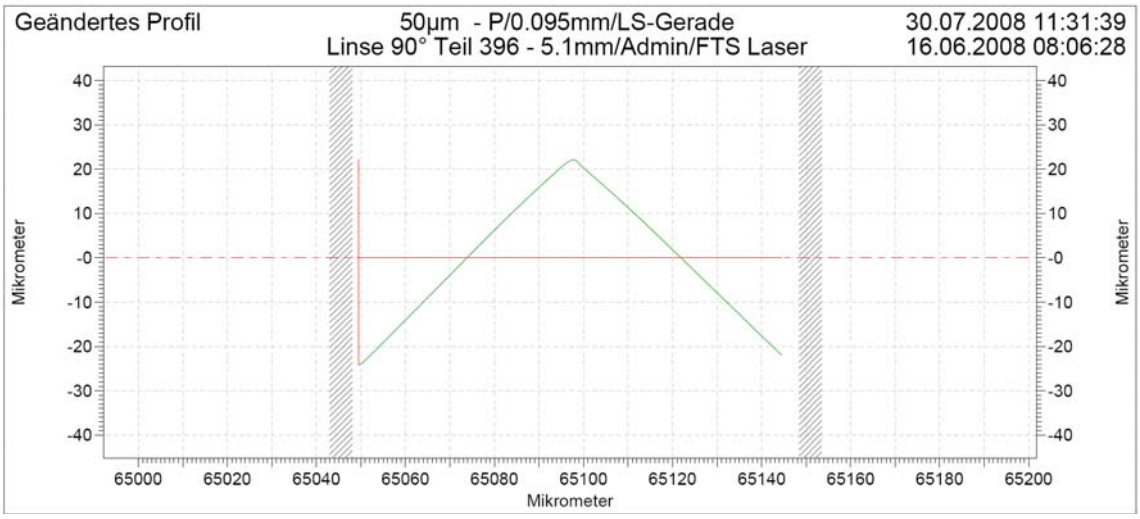

Figure 5.43: Measured 50 µm structure step height (result 46,3 µm)

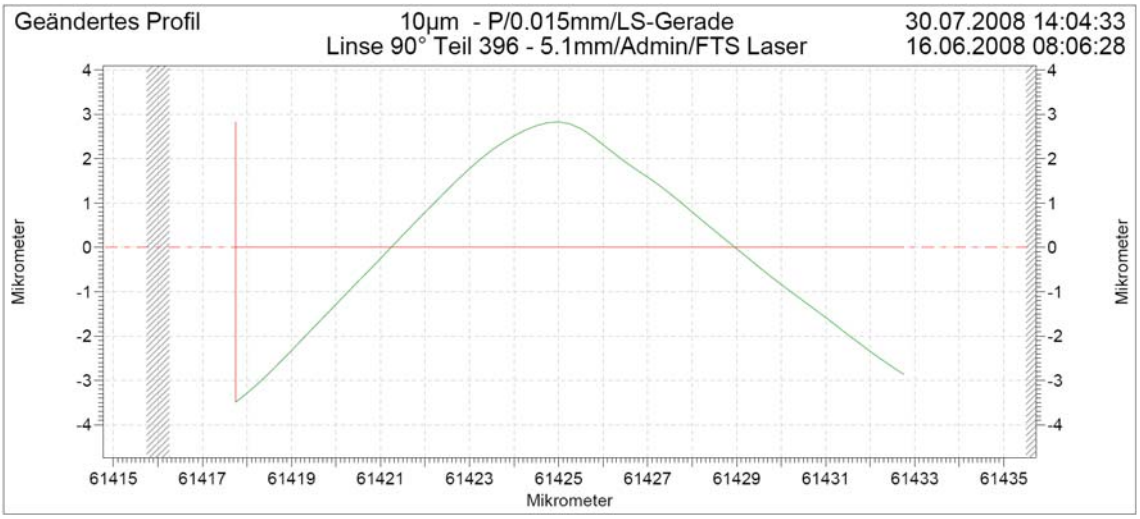

Figure 5.44: Measured 10 µm structure step height (result 6,3 µm)

Conclusion

The described trials show, that excellent results can be achieved just by injection molding. Embossing achieves no remarkable improvement, although the test part geometry (flat disc with 3.6 mm thickness) is very suitable for embossing.

The fact that excellent molding results can be achieved with easy flowing materials has been confirmed in these examinations. However, high viscous materials like Plexiglas 8N enable good results in shape accuracy as well.

Further optimization of the accuracy of molded structures can only be achieved, if the flow resistance is remarkable reduced during the injection phase. From a process engineering point of view, this is only possible by variothermal tempering.

5.5.2 Variothermal Tempering

With variothermal tempering the optical surfaces of the mold inserts will be heated to above the glass transition temperature of the plastic material. Therefore a better molding behavior can be achieved during the injection and dwell pressure periods. With subsequently cooling of the mold inserts the required de-molding temperature will be achieved faster. The entire heating and cooling process takes place within the injection molding cycle.

For the variotherm trials a new molding tool has been conceived and constructed which enables the heating and cooling of the mold inserts. Additionally, the test work piece has been changed to a thick-walled lens that is due to its large volume more critical regarding temperatures. The cavity is now larger (65 x 25 mm²) and has square outer contour. The optical effective surfaces are planar/aspherical and the center thickness is 19 mm. Regarding the replication quality of the microstructures the thick-walled lens generates more influences compared to the flat disc before. The shrinkage of this lens geometry will be one aspect. Further, injection molding process parameters which mainly affect the shape accuracy of the lens can have a larger impact on the accuracy of the microstructures.

At the time this report has been produced, the trials have not been completed. So far the results relate to a diffractive structure with a constant step height of 1,08 µm (see **Figure 5.45**). This has been designed for a specific illumination application. The aim has been to correct the inadequate dispersion of polycarbonate by deflecting the light beam.

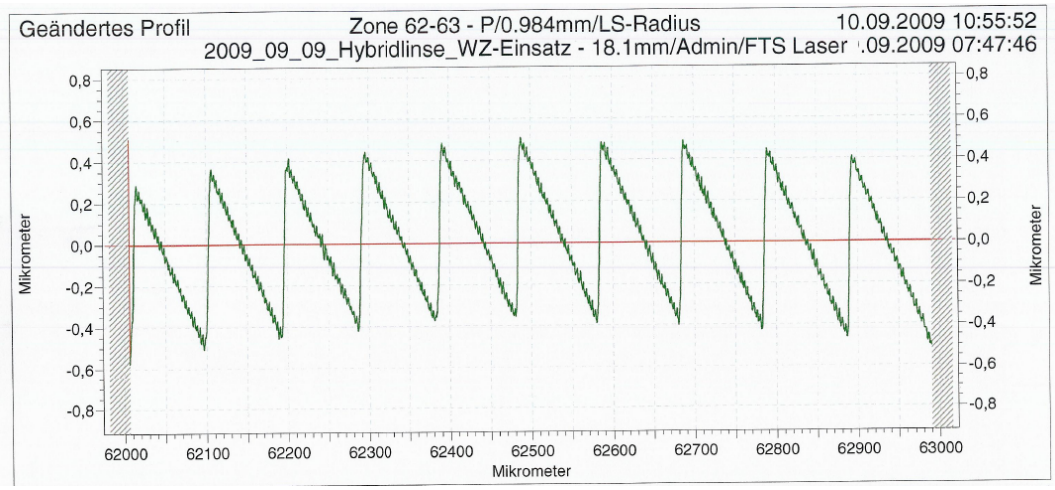

Figure 5.45: Talysurf assessment of optical tool insert

In the beginning the injection molding trials have been realized without using variothermal tempering. First test results have shown that a similar quality as in the trials with the flat disc can not be achieved. The significantly larger volume (and thus also quite different shrinkage ratio of the lens) has a great effect on the microstructure molding accuracy. The molded microstructures have a step height of 0.73 µm (instead of 1.08 µm). This is a deviation of 33% compared to the targeted structure height. The deviation of the lens shape is about 30 µm (peak to valley).

The next trials have included variothermal tempering. The variotherm functionality is now another parameter that influences the form accuracy of the microstructures. The test trials are supplemented by different variothermal temperature courses that are defined by various temperature altitudes and the cycle times. An adaptation of the form of the mold inserts has not been intended, just the effect of the variothermal tempering has been examined.

The initial results using variothermal tempering have been very promising. The form deviation of the lens has been reduced to 20 µm while the quality of the microstructures has been significantly increased. Along the whole lens geometry the microstructure has had a constant step height of 1.01 µm (see **Figure 5.46**) which is close to the step height of the mold insert. Hence the variothermal tempering increased the form accuracy of both the lens shape and the microstructure. Further corrections of the geometry of the optical surface of the mold insert will enhance the quality of the replicated lenses significantly.

The trials involving variothermal tempering are not yet complete. Further improvement potential has been identified during the trials in terms of tool engineering and optimization of the process parameters in particular.

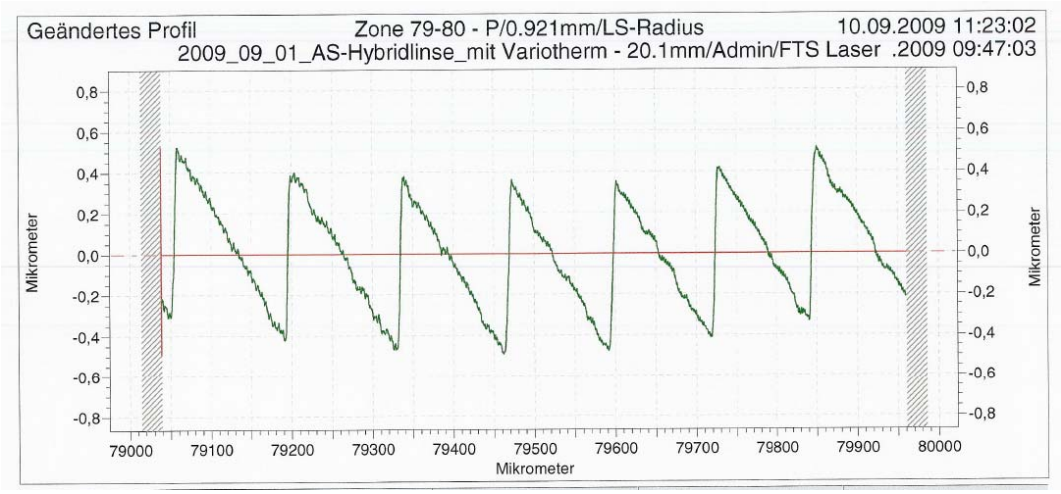

Figure 5.46: Talysurf assessment of injected lens with variothermal tempering

5.5.3 Summary of Results

Summarizing, it can be defined that excellent results can be achieved in producing microstructures by injection molding even in combination of thick-walled lenses (see **Figure 5.47**). However, the quality of the results depends on the design of the microstructures and the shape of the optically functional surfaces. Also the choice of the plastic material has an effect on the molding results. By the optimization of the process parameters plus special technologies like variotherm, or, with restrictions, also injection embossing, an optimal repeatable process can be achieved. Furthermore, the possibility to machine microstructures on optical free-form surfaces by the use of the combination of Fast and Slow Tool axes to a hybrid FTS is essential for these very good replication results. Simultaneously, the mathematical correction of the mastering surface (mold insert) for the compensation of shrinkage enables the replication of plastic lenses for demanding applications by injection molding.

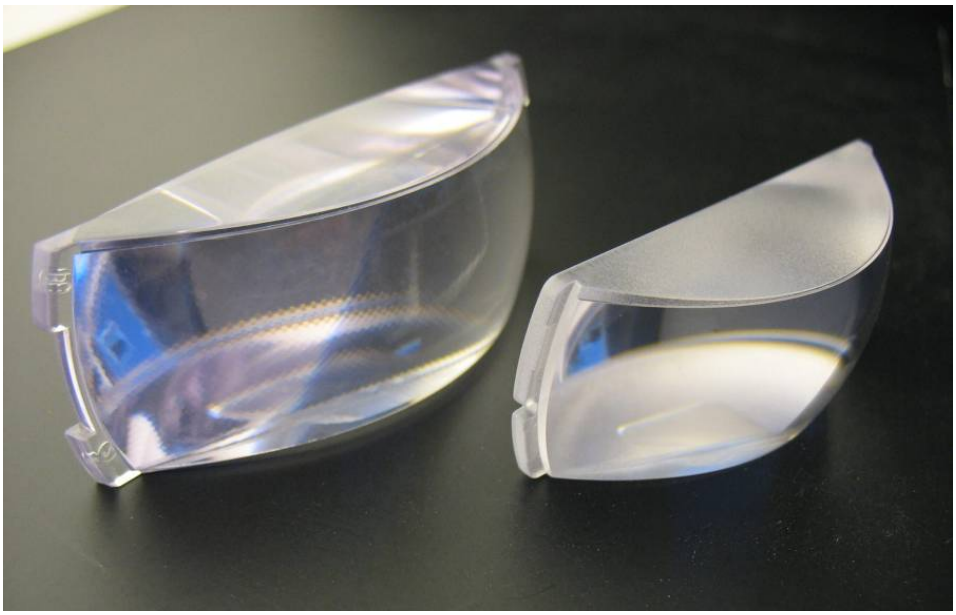

Figure 5.47: Examples for lenses with microstructures

5.6 Replication of Microstructures by Step-Embossing

Before the project, some machining trials of DO lightguides were completed, in order to achieve discontinuous grating grooves (pixels) by the use of a Fast Tool Servo. The result was, that groove quality varied, and the process was not stable enough to produce larger area machining. There were burr formation and tolerance issues, which were not acceptable. However, small areas of the lightguide structures offered a very good optical performance in collimation, which proves the basic functionality of the selected grating profile.

A new approach for the lightguide and other optical element fabrication was planned, due to critical topics in large area machining and its complexity. Small area microstructures were easier to machine in accordance with optical quality and requirements. This was one of the main reasons why the step-embossing process was considered to be a potential method for optically effective surface relief microstructures with deterministic grating designs. Modulated periodic blazed grating profiles were investigated and utilized in all replication trials and demonstrators.

The step-embossing process was implemented by means of a thermal embossing machine (ASE500) manufactured by Modines. This step & repeat machine is suitable for small and large area patterning. A fast cycle time enables large amount of imprinting steps (e.g. 30 000 – 60 000 steps). In **Figure 5.48** the step-embossing machine and specification is presented.

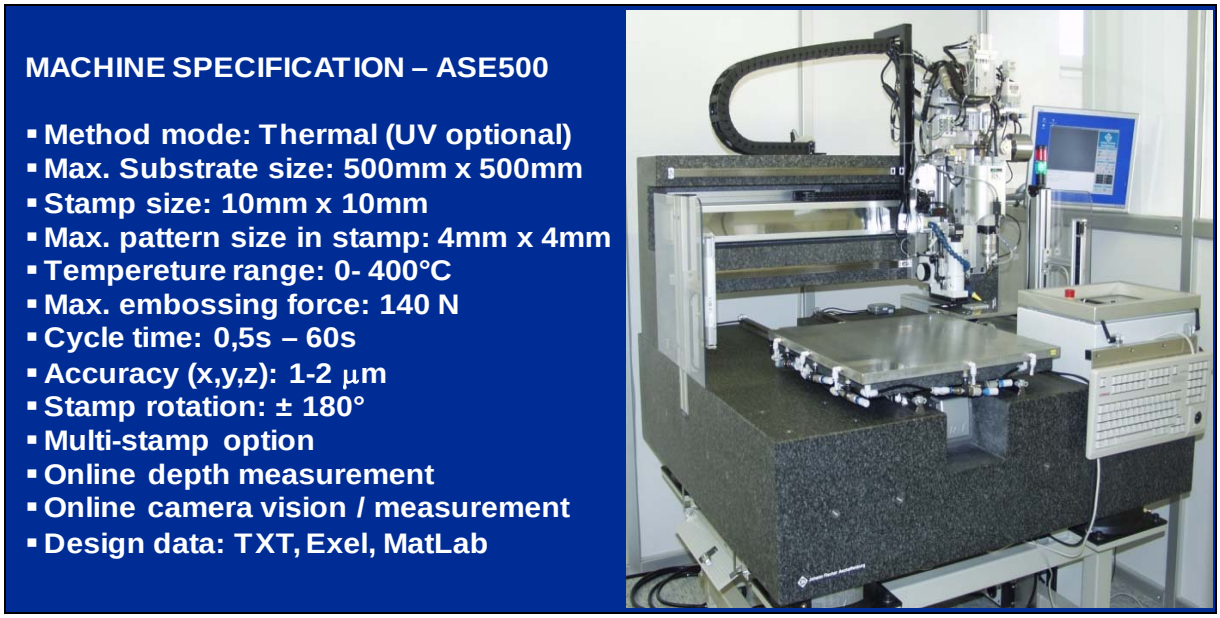

Figure 5.48: Step-embossing machine for microstructure replication in Modines

In order to prepare functional demonstrators, high quality stamper tools were required. The stamper and its preparation method was different in all demonstrators:

- Microdisplay backlight ⇔ direct electroplated stamper
- Keypad lightguide ⇔ resist electroplated stamper
- Frontlight ⇔ laser engraved stamper and

- LED illumination lens ⇔ PDMS stamper

All original microstructures were micromachined first. During the course of the project »ERANET-OPTICALSTRUCT«, the following main tasks were completed:

- High quality micromachined blazed grating structures, small and larger area relief structures
- Replication of machined master structures by direct nickel electroforming or by soft lithography
- Nickel stamper tool fabrication by laser engraving, both small and larger surfaces
- Surface treatments for stamper tools before the embossing process
- Embossing trials with stamper tools, single embossing and step & repeat embossing
- Endurance test for the stamper tool by embossing
- Demonstrator's structure fabrication, replication by step-embossing
- Demonstrator preparation by UV-replication and validations

5.6.1 Stamper Tool Manufacturing

High quality micromachined blazed grating structures have been produced as described in section 5.2 to 5.3 comprising A) single and small grating structures, pixels (e.g. 40 x 50 μm) and B) larger rectangular surface with discontinuous grating groove structures (e.g. 30 x 30 mm) and C) larger round surface with radial continuous grating groove structures.

Since the high quality blazed grating masters were machined, replication and nickel shim electroforming was required. Four methods were investigated, in order to ensure good replication quality and high quality nickel stamper tools:

1) Small micromachined structures on the nickel plate were electroplated directly. Only one chemical surface treatment was necessary before the electroplating. As a result, high quality nickel shims were achieved.

2) Another solution with small structures was to replicate the original structure on the PMMA resist by means of step-embossing, and carry out the electroplating, and as a result, nickel shims were achieved.

3) Larger surface structures on the copper and nickel plate could not be replicated with the above manner. So, first the copper was replicated by PDMS and template was prepared. This template was utilized in the imprinting process, in order to replicate the structure in the UV-resist layer (soft lithography). After this, nickel electroplating was completed. The resist layer was dissolved and the first generation nickel shim was achieved.

4) Continuous structural nickel shims were utilised for the stamper tool manufacturing. The tool was fabricated by laser engraving, which removed unnecessary surface/structures by femtosecond-pulse laser ablation (see **Figure 5.49**). This method allowed the provision of single structure stamper tools, as well as relatively large modulated optical structures with multi-structures. A small lightguide design was engraved on the large blazed grating surface (e.g. 30 x 40 mm²). This type of stamper tool formed a complete lightguide with single embossing step. The surface quality of laser engraving was improved during this project, with a protective coating.

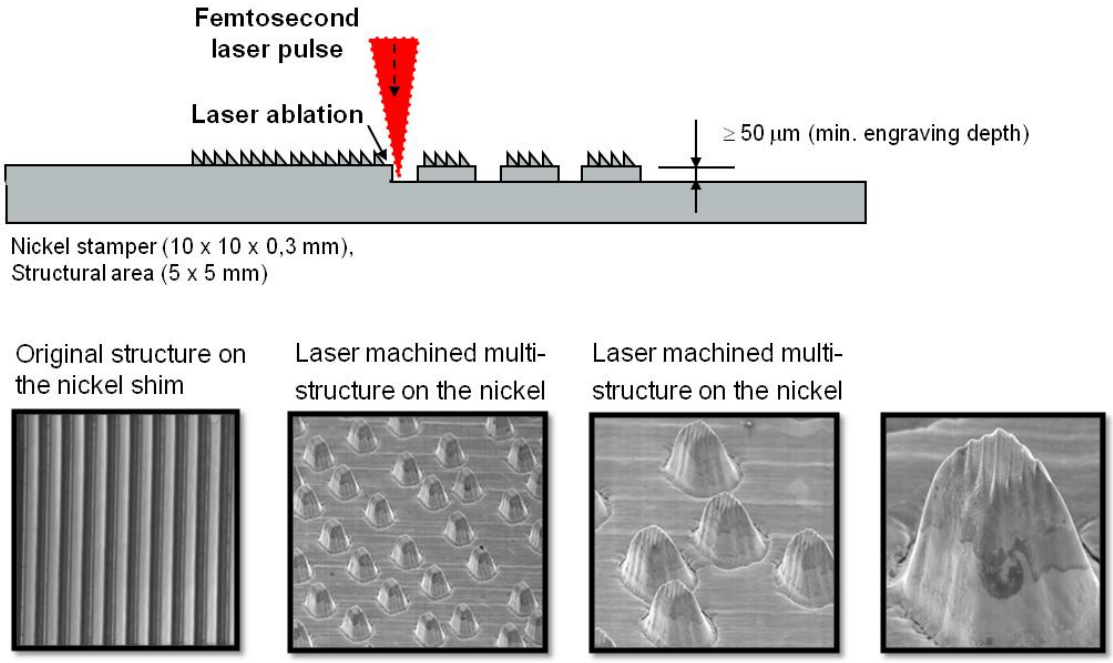

Figure 5.49: Stamper tool engraving by femtopulse laser

All final stamper tools were cut out of the nickel shim by laser. In **Figure 5.50** is described the stamper tool manufacturing process.

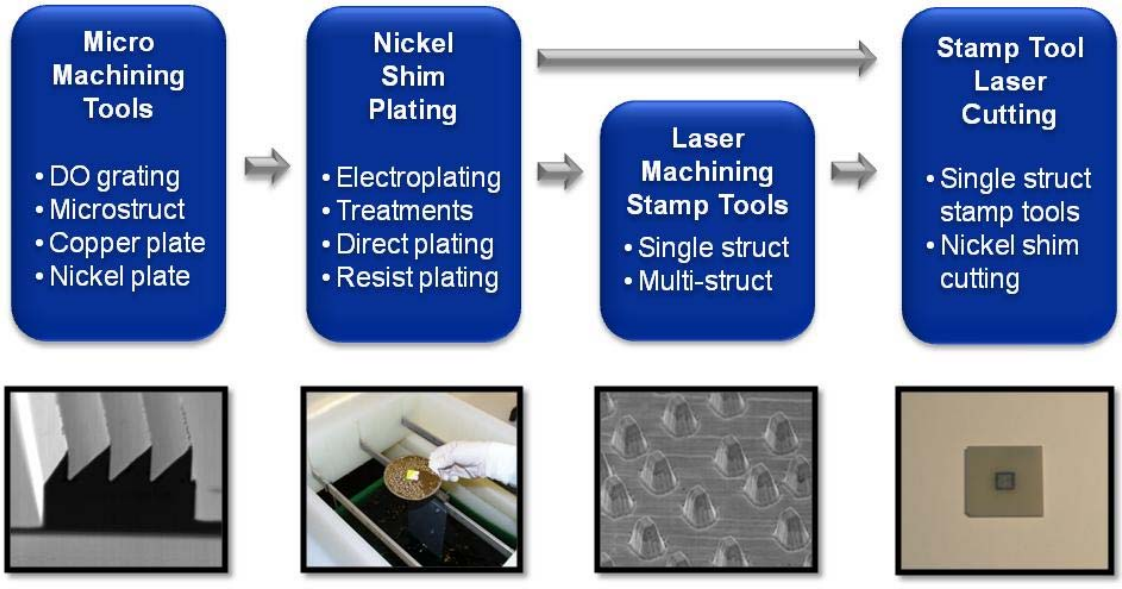

Figure 5.50: Principal process steps of stamper tool manufacturing

5.6.2 Stamper Tool Trials by Step-Embossing

Stamper tools were tested by means of step-embossing. Several thermo formable substrate polymer materials were investigated., as well as some resist materials. The most preferable material was PMMA and PC plate, with a thickness of 1 mm or larger, in order to provide sufficient thermal stability during the embossing. Single structure quality was always easy to achieve, but larger seamless surfaces, with a multi-structure (step & repeat) was more challenging. Several tests with Taguchi optimized parameters were completed, to ensure the best embossing quality without stitching lines. Such good results were made possible by controlled pressure, and a special stamper tool design, with overlapped structures on its edge. Also, additional cooling (air or liquid) was arranged and tested on the substrate surface during embossing (see **Figure 5.51**). This helped to prevent thermal deformation on the existing surface relief structures.

Larger stamper tools were also tested, in order to make complete demonstrators by single embossing with a high pressure (ref. frontlight). The lateral stability was always more critical when the stamper tool was enlarged. As a result, good embossing quality and alignment was achieved.

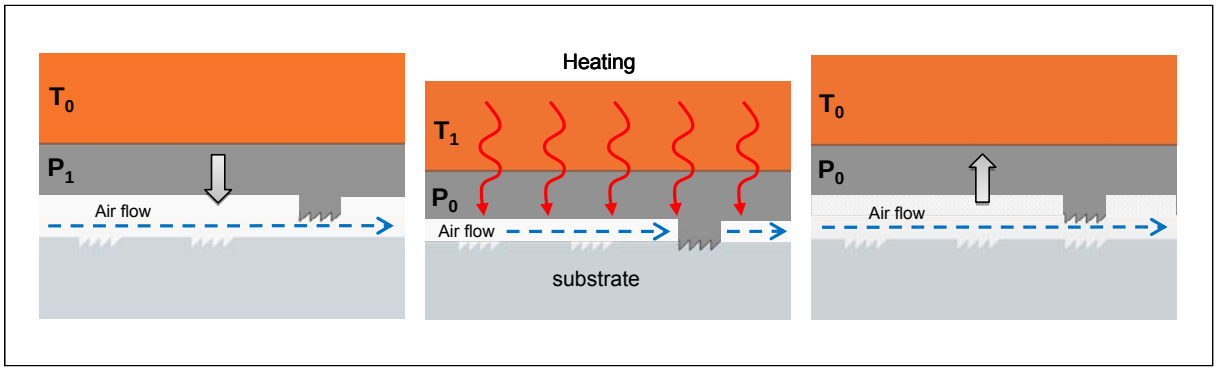

Figure 5.51: Step-embossing of single structure tool with additional air cooling

The stamper tools could be utilised directly for the embossing process, but surface contamination must also be considered. In order to avoid this, surface treatment is recommended. Two different treatments were tested, silica treatment and diamond coating. Both were good for helping to solve the contamination problem. However, the diamond treatment is long-last coating, which also stiffer than the surface of stamper tool. The cleaning step was also important, which surprisingly, caused some problems initially. Solvent did not help and some caused corrosion. In the end the most suitable cleaning solvent and method was achieved with the help of ultrasonics and standard detergent.

A long endurance test was completed for one nickel stamper tool. This tool was utilized in the embossing process and the structure was embossed over 100 000 times on the PMMA substrate. The stamper tool was still in good condition and suitable for the next embossing process. The surface of this tool was treated with a silane coating.

5.6.3 Backlight and Frontlight for Microdisplays

Two different demonstrators were prepared for the microdisplay illumination. The backlight was fabricated by means of step & repeat embossing with small electroplated tools, while the frontlight was fabricated by means of single step-embossing with larger laser-engraved stamper tool. These demonstrators were based on blazed grating profiles, which provides light collimating characteristics without the need for prismatic sheets. The backlight was the more focused demonstrator, as a result of the challenging multi-step-embossing process and highest efficiency target. The frontlight stamp tool was fabricated by laser engraving, and thus, some undesirable defects/roughness appeared. However the basic stamper concept was approved.

The backlight design was done for 1” single LED lightguide with a narrow light outcoupling angle. Only one type of stamper tool was utilised. The design contained 26 640 embossing cycles. Thus the cycle time needed to be minimized. **Figure 5.52** shows the basics of the step-embossing process, the matLab picture of embossing coordinates (blue matrix), distribution of the filling factor for the grating structures and the functional backlight demonstrator with a microscope picture of step-embossed structure.

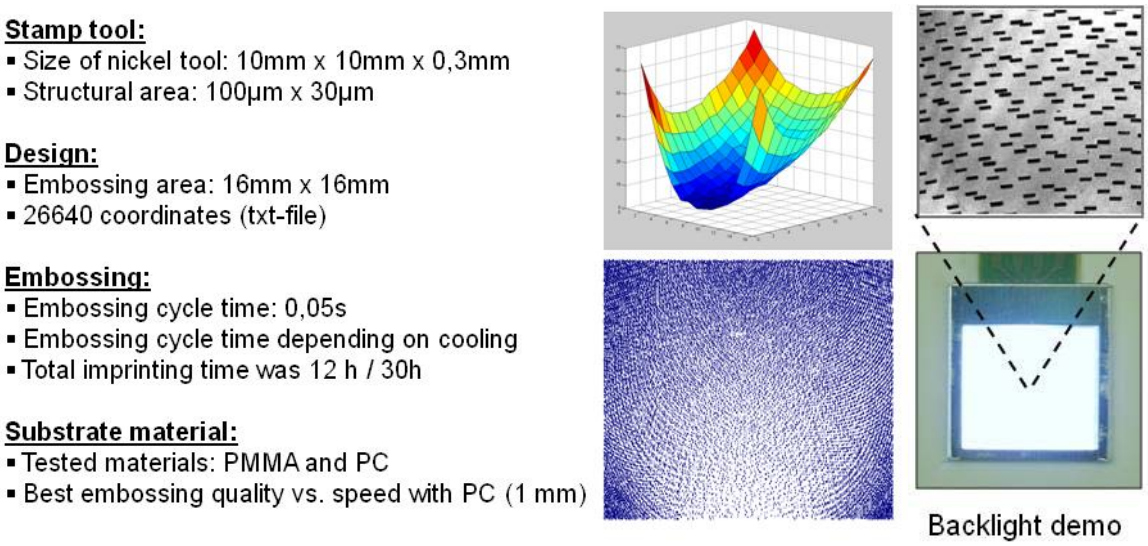

Figure 5.52: Specification for backlight step-embossing and demonstrator

Optical characteristics of the backlight demonstrator was validated. Typical methods are luminance and uniformity measurements, as well as conoscopic measurement of luminance angle. The uniformity was over 80%, which is a very good result. The luminance level was 20 000 cd/m^2, which is excellent, without any prismatic sheet. The luminance angle / light distribution was narrow as expected. Only one direction showed a small angular error, and light leakage, which was caused by small deformation of the tool and profile replication. This can be realized in **Figure 5.53**.

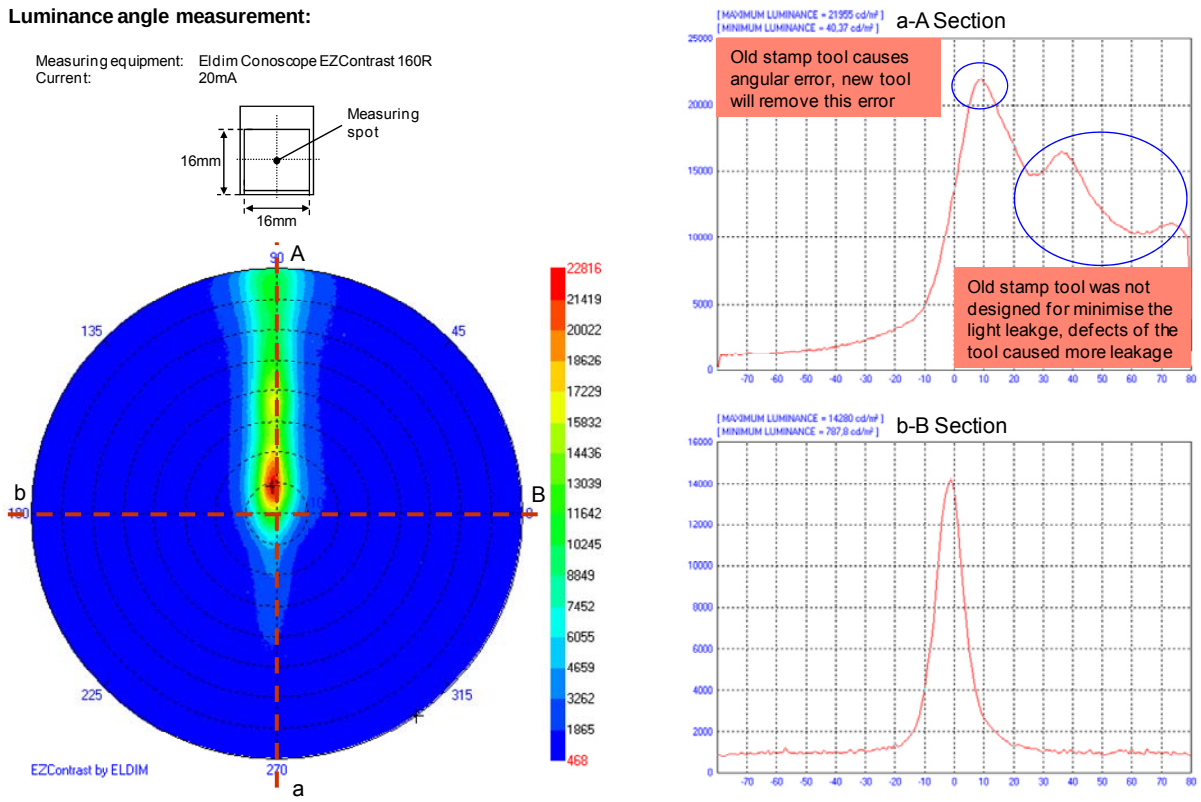

Figure 5.53: Conoscopic measurement of microdisplay backlight, single LED design

Both backlight and frontlight demonstrators could be utilised with the display. Optical performance and efficiency targets were exceeded, which led to lower power consumption. These demonstrators can be manufactured in high volumes by means of roll-to-roll embossing.

5.6.4 Lightguide for Keypad Illumination

One demonstrator was a new type of highly efficient lightguide for mobile phone keypads. Conventional lightguide (original) was done by micro lenses, which did not provide optimal efficiency. The new solution was again based on the blazed grating profiles and controlled light outcoupling angles. The lightguide was fabricated by means of repeated step-embossing with small electroplated tools.

A keypad lightguide is thin (0,2 mm) flexible film without any holes placed on its bottom areas (see **Figure 5.54**, left). Soft material, like silicone, provides good tactile feeling. This type of solution minimizes the amount of LEDs needed, and decreases total power consumption. This keypad lightguide demonstrator was designed and prepared for a commercially available mobile phone. The basic topic was to achieve clear comparison data between existing and new lightguide mounted in the similar mobile phone. Similar LEDs, power consumption, keypads and other components provided easy validation basics. Keypad lightguide design comprised discrete patterns and illumination areas. Additionally, two LED solutions formed a new challenge in optical design. In multi-LED solutions an important aspect is the alignment of each grating structure towards a specific LED. One example of a discrete keypad lightguide design is presented in Figure 5.54, right.

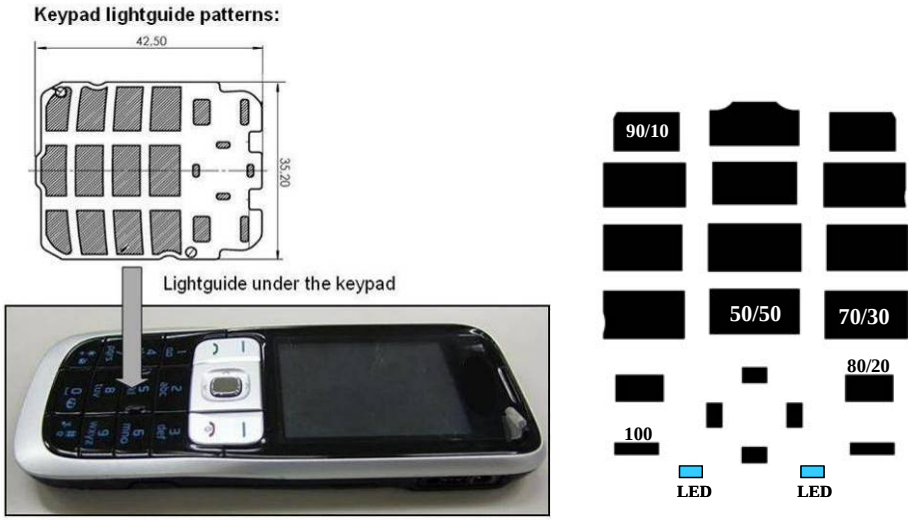

Figure 5.54: Mobile device with keypad lightguide (left), design rule (right)

The different rotation angles of grating structures, pixels were selected in terms of LED location in different discrete areas. The values in the picture indicate the proportions of grating pixels aligned with each LED with preferred rotation angles.

Design data for the lightguide was completed by fuzzy logic based software. The data comprised all coordinates of the step-embossing process in order to achieve the preferred luminance distribution with preferred stamper tool. The design contained 19 000 coordinates. Basic process phases of lightguide manufacturing are presented in **Figure 5.55**.

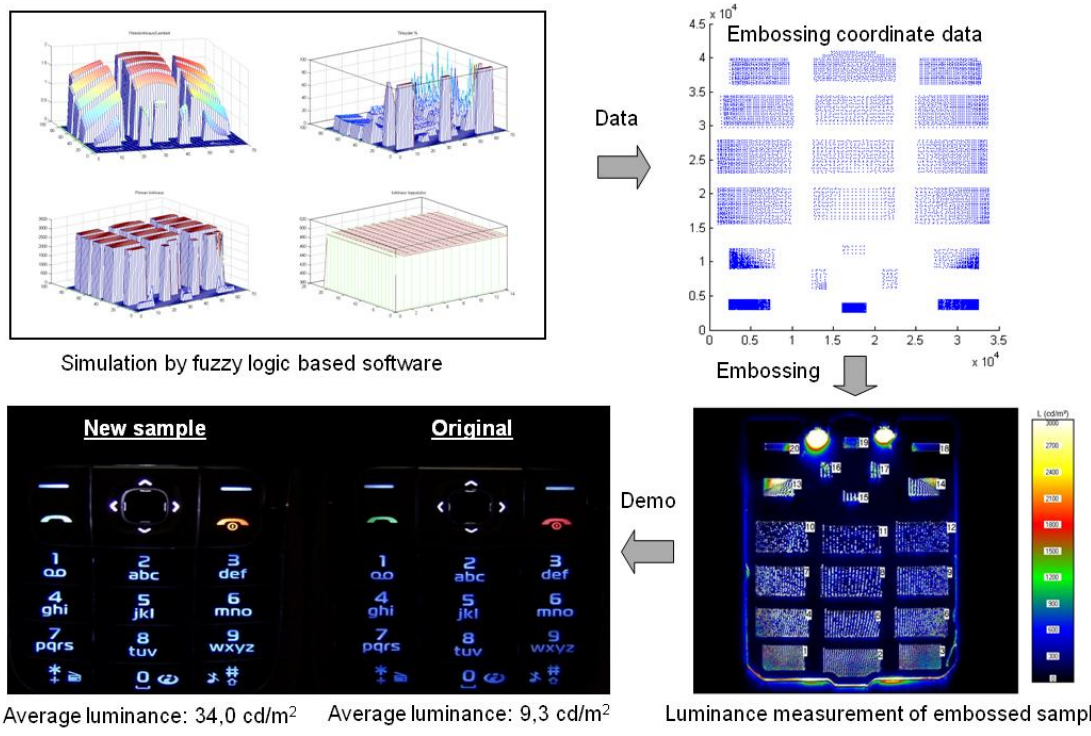

Figure 5.55: Manufacturing phases of keypad lightguide

The keypad lightguide was mounted in the mobile device. Optical performance, such as uniformity and luminance, were measured with both the original and the new lightguide. The new demonstrator achieved over 3 times higher luminance level than

original with better uniformity. This result has very good impact for energy saving and battery life time. Productivity of the demonstrator was also approved by means of roll-to-roll embossing.

5.6.5 Lens for LED Illuminator

The final demonstrator was related to LED lighting, - a high bright / high power LED illuminator with a flat diffractive grating lens. Today several LED lamps are available on the market. Unfortunately the majority of these lamps are not real illuminators. Those can be categorized as lights with purely entertainment value, due to low efficiency, or undesirable optical characteristics such as non-uniform illumination, hot spots, additional shadow, etc. Thus new optical efficiency is preferred. The idea behind in this demonstrator was to prepare halogen replaceable LED illuminator and complete illuminance measurement between halogen and an LED illuminator. White high-brightness four chips LED were selected and lens diameter was set at 45 mm. A periodic grating profile was machined, which was based on radial blazed grooves. The original nickel plate needed to be anti-adhesion treated with plasma before PDMS stamper manufacturing. This guarantees better replication quality and avoids defects. After PDMS replication, the stamper tool manufacturing followed the steps mentioned in point 3 (stamper tool section). Final lens samples were achieved through by single step-embossing. The lens profile structure was replicated directly on the thin PMMA plate (0,25 mm) by UV curing, utilizing a PDMS stamper (soft lithography). The lens was cut to the right size and mounted on the assembly frame, which was attached, together with the LED heat sink substrate. Inside the frame was a replaceable reflector. This was simple specular reflector film with two different angles, 120° and 80°. The total height of the LED illuminator was 11 mm. Surface relief grating profile of the lens was placed at the bottom, inside the illuminator.

The ready LED illuminator was measured and compared with different halogen lamps. Illuminance was measured with a conoscopic system, at different angles by lux meter at a distance of 1 meter. **Figure 5.56** shows the basic features of the LED illuminator and measurement jig.

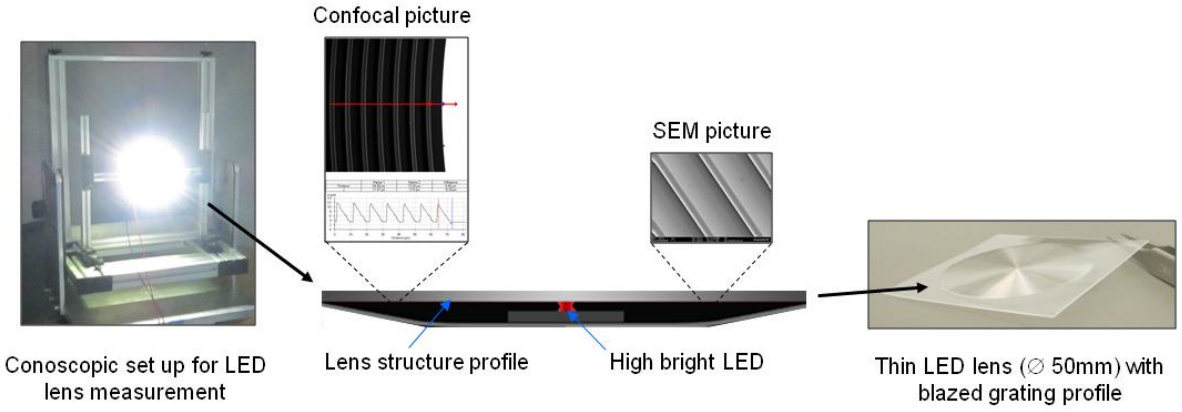

Figure 5.56: LED illuminator concept in illuminance measurement

The LED illuminator was measured with two different power levels (3,3 W / 10,6 W) utilizing two different angular reflectors. Naturally, the illuminance level increased

with a tighter reflector. All illuminance levels exceeded expected results. Additionally, visual inspection was very promising in terms of uniformity and progressive edge illumination at different angles. **Figure 5.57** shows illuminance and distribution curves with the same LED illuminator under different conditions.

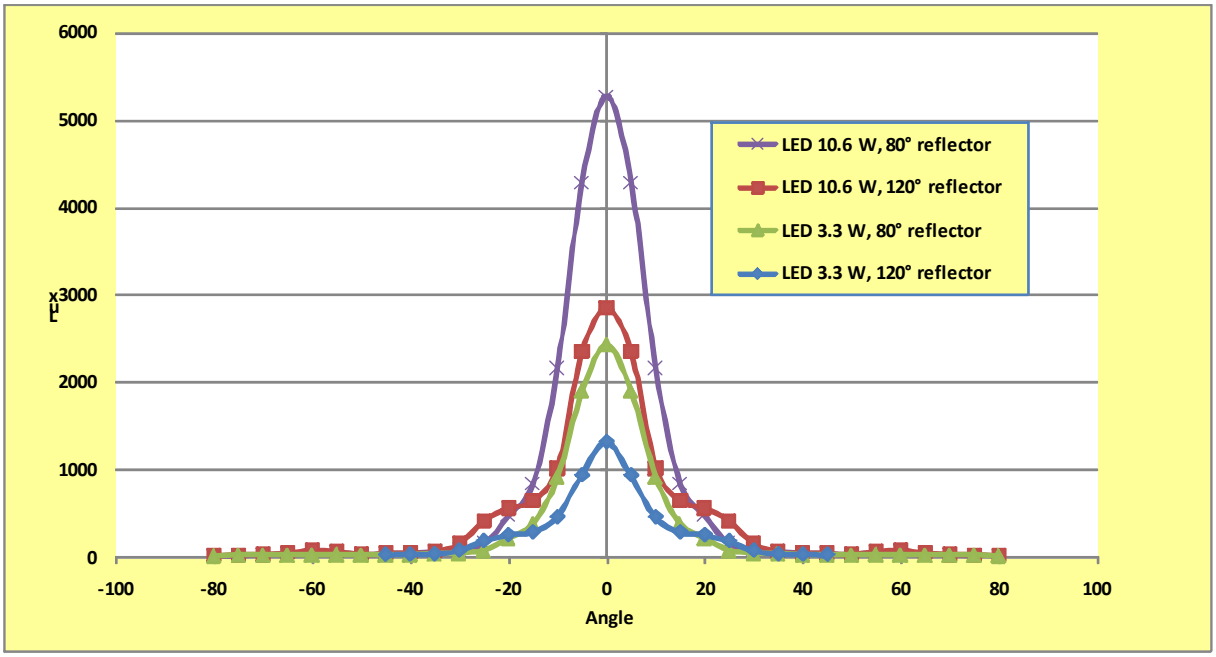

Figure 5.57: Illuminance and distribution of LED illuminator with blazed grating lens

Different halogen lamps were measured with the same method and set up. The most common halogen lamps, 50 W and 35 W were selected for comparison. **Figure 5.58** shows measurements of two halogen lamps and two measurements of LED illuminators with different power consumption.

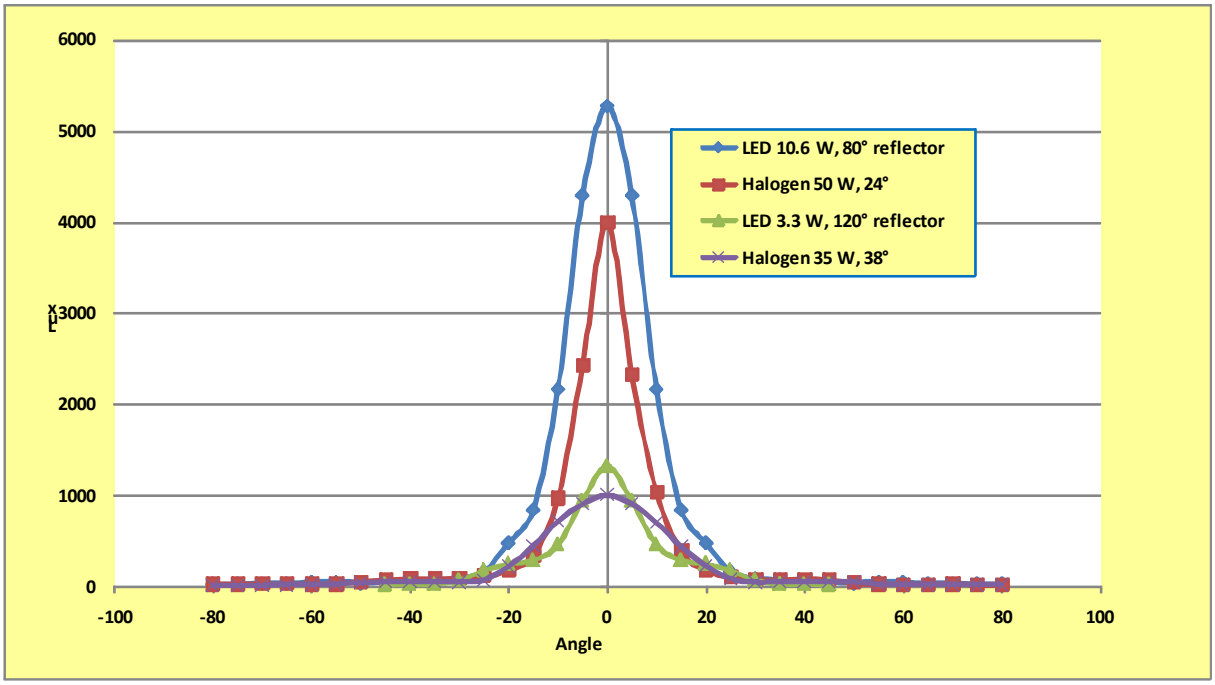

Figure 5.58: Illumination and power consumption of LED illuminator vs. halogen lamps

Illuminance curves indicate the efficiency benefit of LED illuminator vs. halogen lamps. Around 10 times less power consumption in the LED illuminator is enough to provide the same or higher illuminance level as a 35 W halogen lamp, while about 5 times less power consumption in LED illuminator provides 20% higher illuminance level and larger light distribution than a 50 W halogen lamp. These preliminary results are very promising, which will lead to great energy savings in the future.

This lens demonstrator can also be manufactured in high volumes by means of roll-to-roll embossing. Small material volume comparing refractive lenses can reduce material costs by around 80%, which is a remarkable benefit. Furthermore, production costs are lower due to faster manufacturing process. This is clearly one part of potential »Green Technology«.

6 Mechanical Design of the Machine Demonstrator

The manufacturing of hybrid optics by ultra-precision machining requires a new machine system. Therefore, in the following sections the concept of the machine is explained. Afterwards the design of the Fast Tool Servo, the base machine, and the dynamic axis as basis of the hybrid axis are discussed.

6.1 Concept of the Machine Demonstrator

State of the art are ultra-precision machines that use, if needed, only one dynamic axis for the machining of non-rotationally symmetric parts. This can be a Fast Tool Servo (FTS) system mounted on the Z-slide or the Z-slide is designed as Slow Tool enabling a large stroke of several millimeters at low frequencies. Current FTS systems can be divided into two groups that can be distinguished by the available stroke. Short stroke FTS allow for strokes up to 100 µm, are driven by piezo actuators and are guided by flexural bearings. They reach frequencies up to 1000 Hz. Long stroke FTS offer a travel range up to 10 mm. Those systems use aerostatic slides and are driven by linear motors. Dynamics up to 500 Hz can be reached. To enable the efficient machining of hybrid optics, a new, hybrid FTS system is required that combines the two kinds of dynamic axes. **Figure 6.1** shows the principle of the hybrid FTS. The FTS, carrying the cutting tool, is integrated into the front of a dynamic axis. Since the dynamic axis is less dynamic properties than the FTS, in this report the dynamic axis is also called Slow Tool axis. Usually Slow Tools are dynamic Z-slides of an ultra-precision machine offering all opportunities of a standard machine slide. In contrast, the dynamic axis (Slow Tool) as shown in Figure 6.1 is just able to carry the FTS or other cutting tools with adapters. The slide of the dynamic axis is guided by hydrostatic bearings and driven by a voice coil. The compact design of the hybrid FTS ensures that all centers of mass are in line with the cutting tool, which is reducing errors during dynamic movement. Finally the hybrid FTS will be used in combination of an ultra-precision turning machine (base machine).

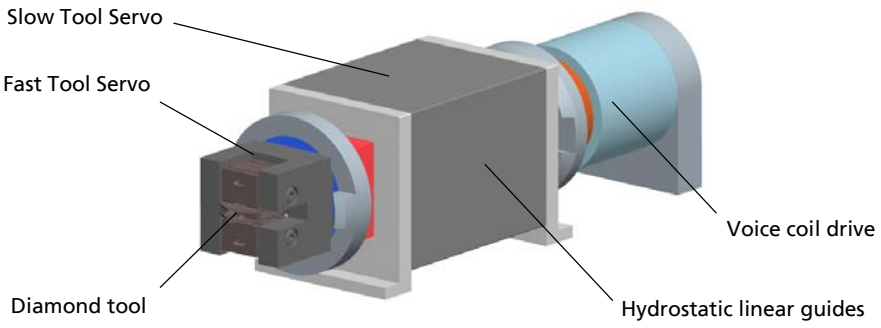

Figure 6.1: Principle of hybrid FTS

By the realization of the new machine system, both microstructures and free-form surfaces can be machined in one setup enabling new possibilities in ultra-precision machining. Nevertheless, the control of the machine has to consider the hybrid axis

system as well. Therefore, the description of the hybrid optic has to be decomposed (see **Figure 6.2**) to be machined separately by the two parts of the hybrid FTS.

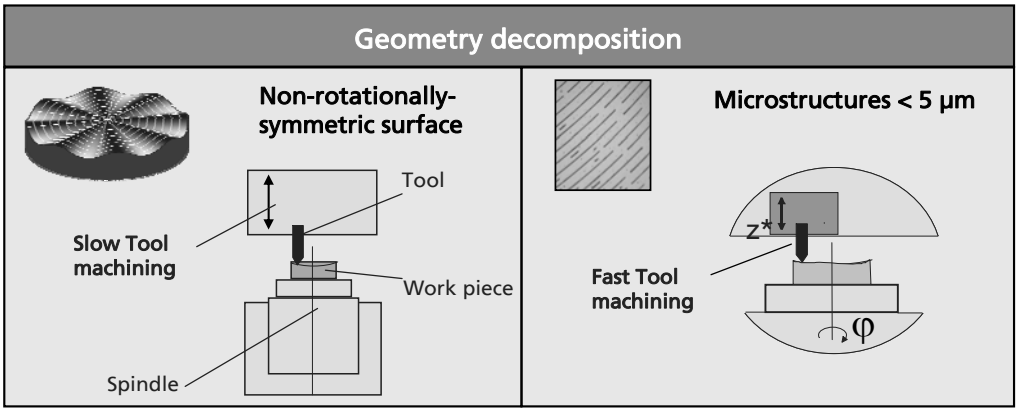

Figure 6.2: Geometry decomposition for the machining of hybrid optics

Beside the machining of hybrid optics the combination of the Fast and Slow Tool into one unit offers new possibilities. The FTS can support the machining at locations on the surface where the dynamic of the Slow Tool is not sufficient enough. This can be the case at sharp corners and transitions on the surface. The FTS can also be used to add other signals for example for the compensation of thermal drifts. It can further compensate deflections or vibrations of the tool which are may caused by non-continuous cutting.

Since the machining of microstructures is often time consuming further provisions regarding the measurement of thermal drifts at the tool tip or the work holding spindle along the Z-axis are done. As mentioned before these compensations can be added to the signal of the dynamic axes.

To efficiently use the new potential regarding machining strategies as well as the compensation of errors a connection between the control of the dynamic axes and the base machine is necessary. The integration into one machine control is described in chapter 7.

6.2 Development of Fast Tool Servo (FTS)

The following section describe the layout of the FTS and the tool guiding system. Afterwards the realized system is introduced. It has been tested and characterized by measurements and test part machining.

6.2.1 Layout of the FTS System

The objectives of the development of the new Fast Tool Servo system in the scope of »ERANET-OPTICALSTRUCT« are the achievement of high working frequencies (2 kHz @ 10 µm stroke), a sufficient long-time stability for machining operations of several hours and the possibility for the combination with another dynamic axis like a Slow Tool.

Typically, highly dynamic FTS systems are using flexural guides (e.g. combination of leaf springs) for the cutting tool and a piezo actuator as drive unit. Capacitive sensors

are applied for the position feedback (see **Figure 6.3**). The stroke of such a system is basically limited by the combination of the piezo actuator and the stiffness of the flexural guide. Both act as springs, that work in serial arrangement, and in that way limit the remaining stroke. According to Figure 6.3 the maximal possible stroke s_{max} is defined at the intersection of the piezo stiffness (k_P) and the spring stiffness (k_F). Nevertheless, the piezo actuator is the most suitable drive for a highly dynamic FTS system and shall be used for the new FTS. But to achieve maximum dynamics the properties of the guiding and the piezo actuator have to be adjusted thoroughly.

At first the requirements for the piezo stack are defined desired stroke. It shall reach in composition with that guiding system at least a stroke of s_{max} = 30 µm (see formula in Figure 6.3). Furthermore, a resonance frequency of at least 10 kHz and a low capacity, to decrease the requirements of the electrical power amplifier, is necessary.

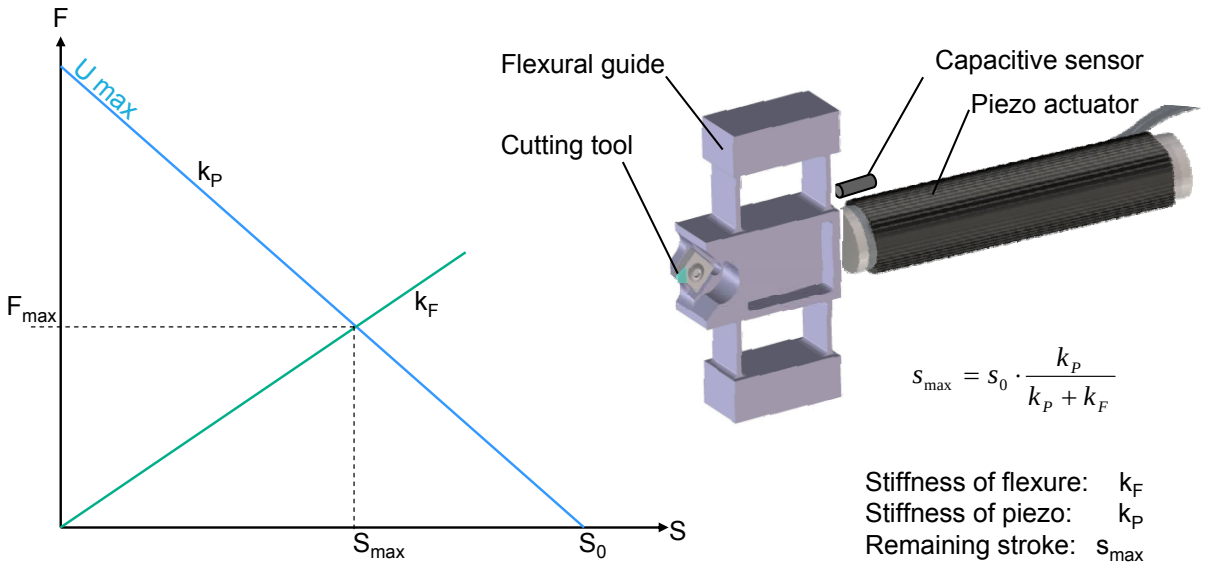

Figure 6.3: Principle of piezo driven FTS and limitation of stroke

The requirements have been fulfilled by a high voltage actuator (0-1000V). The nominal stroke of the piezo is 80 µm and the stiffness is 90 N/µm. The length is 72 mm and the ceramics have a diameter of 16 mm. Furthermore, it comes with an integrated PT1000 thermal sensor. The piezo actuator is shown in **Figure 6.4**.

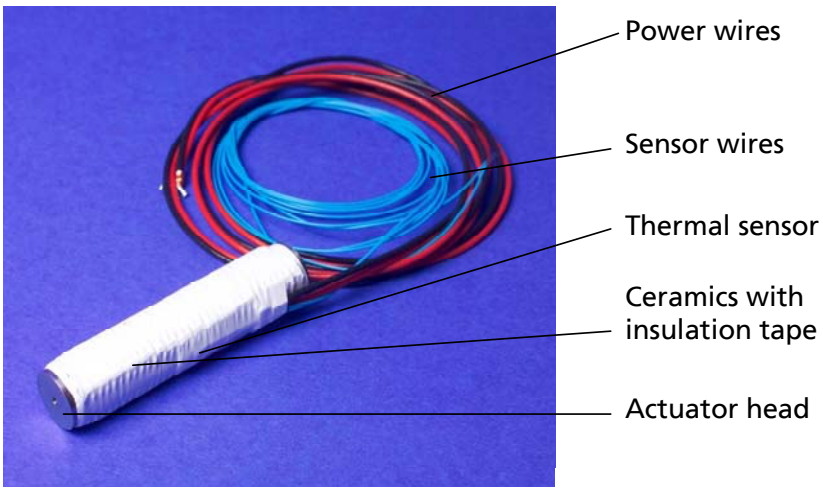

Figure 6.4: Chosen piezo actuator with integrated thermal sensor

In combination with the flexural guidings the stroke of the piezo is theoretically limited to about s_{max} = 50 µm. This value is further strongly depending on the stiffness of the FTS housing as well as the internal contact points between the piezo and the housing or the flexural guide. Examinations of the assembled FTS system provide the information about the specific value µm/V_{piezo} that defines the dynamic power consumption (see chapter 6.2.4). With the chosen piezo actuator, the crucial part of the FTS is defined and the following the further design of the FTS is described.

6.2.2 Tool Guiding System

The tool guiding system for the FTS shall be designed as monolithic flexural bearing which replaces leaf spring combinations used in older FTS designs. In that way, a higher stiffness can be achieved and the dynamic behavior can be adjusted and optimized more easily. The stiffness of the flexural bearings in moving direction is adjusted to the piezo stiffness and has a value of 45 N/µm. Depending on the final moving mass and the preloading an eigenfrequency of about 3 - 4 kHz can be reached.

Different designs of monolithic flexural bearings that vary in the layout of the flexures have been discussed. Flexures can be designed as simple leaf springs (see Figure 6.3) or as lever with small notches having a radius shape. Both types can be designed to match the proposed requirements concerning stroke and stiffness, but only the flexures with radius notches allow for the innovative design of the tool guiding system.

Since the FTS shall be combined with another dynamic, long stroke axis any interferences due to inertial forces have to be avoided. A moving mass of 100 g causes a force of 80 N at the aimed moving frequency. Hence, a mass compensation unit has to be integrated into the FTS. Mass compensation systems used in dynamic machine tools use an additional slide equipped with its own drive and linear scale. Due to limits in available space, weight, and costs such a system cannot be integrated into the new FTS. Hence, the movement of the tool guiding system has to be used as well for the mass compensation. A special design of the flexures allows to bypass and switch the motion of the tool guiding block in a way that a compensation mass performs the exact opposite movement. In that manner, no additional drive or measurement system is needed. The flexural guiding system is shown in **Figure 6.5**.

In the center of the guiding system, the actual tool guiding slide can be seen having the tool seat in the front (left) and the interface to the piezo on the right side. The center slide is guided by a set of levers and flexural bearings that are connected to the mounting blocks and the counter masses. The system of flexures is designed in that way that the counter mass slides do the same stroke than the center slide but in opposite direction. The masses of the two counter slides are adjusted to the moving mass in the center of the whole system. Furthermore, additional masses (correction masses) can be mounted to the counter slides to compensate also the mass of the moving part of the piezo stack.

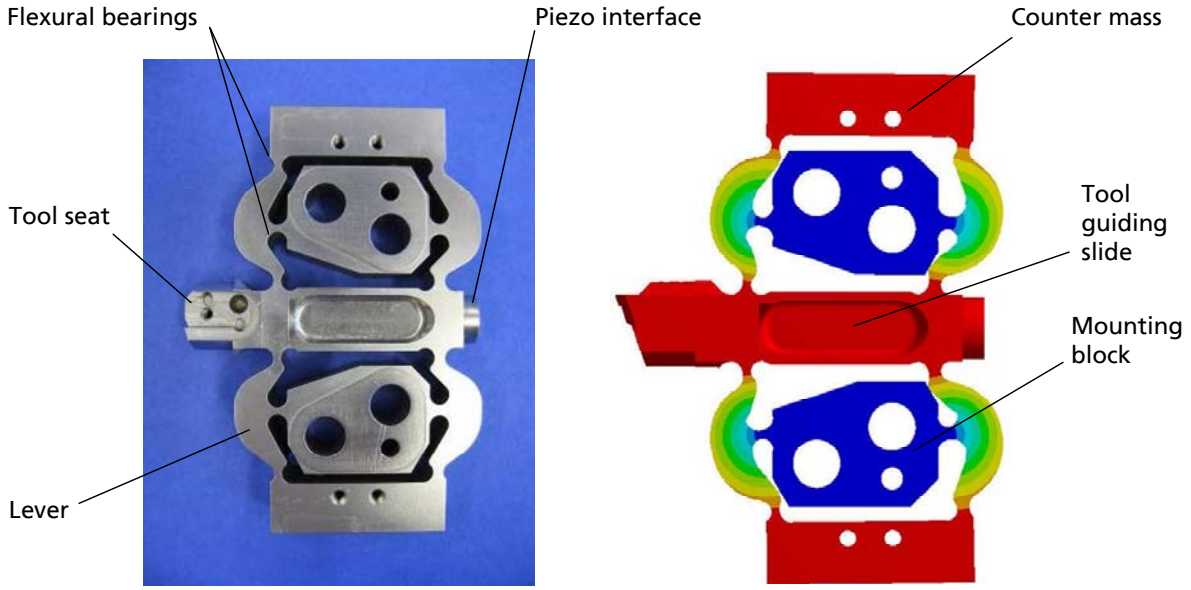

Figure 6.5: Design of the flexural guiding system

The size of the correction mass has been determined by tests using the hybrid arrangement of the FTS and the Slow Tool. Therefore, a step signal has been put on the FTS and the reaction at the Slow Tool has been monitored. Without additional masses, a peak in positive direction can be seen, while an extra mass of 2 x 19 g at the counter mass slides provokes a movement in opposite direction (see **Figure 6.6**). After optimization of the mass, nearly no reaction at the Slow Tool can be noticed anymore. This proofs the effect and functionality of the mass compensation.

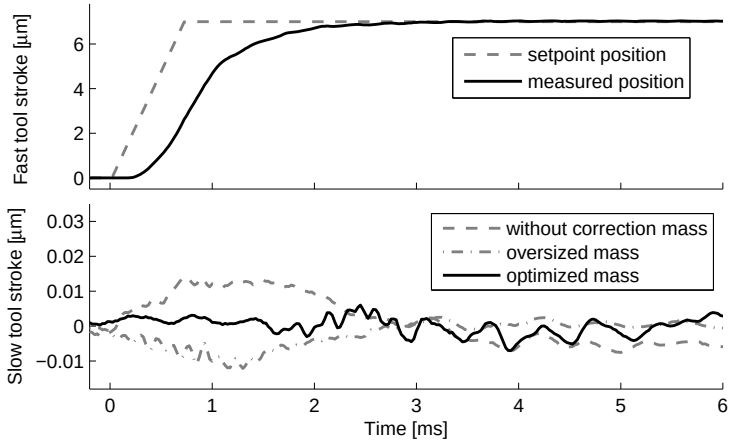

Figure 6.6: Reduction of FTS influence on Slow Tool by an optimized correction mass

The examination of the real flexural bearing on a test bench proved a stiffness of 42 N/µm which is very close to the simulated values of the 45 N/µm. The eigenfrequency has been determined to 2725 Hz. It is a bit lower than the aimed eigenfrequency. Due to a higher mass of the center slide which needed a stiff design to prevent deformation by the driving forces.

The standard type of a diamond cutting tool uses a square bare with 6 mm width and length of about 40 mm, which is too big for the new FTS. Hence, a diamond tool attached to a small tool insert has been used. Due to manufacturing reasons the tool

seat has been rotated by 90° and in cooperation with Contour a new tool has been designed (see **Figure 6.7**). The diamond is soldered to the flank of the insert so that it can be used also in vertical direction.

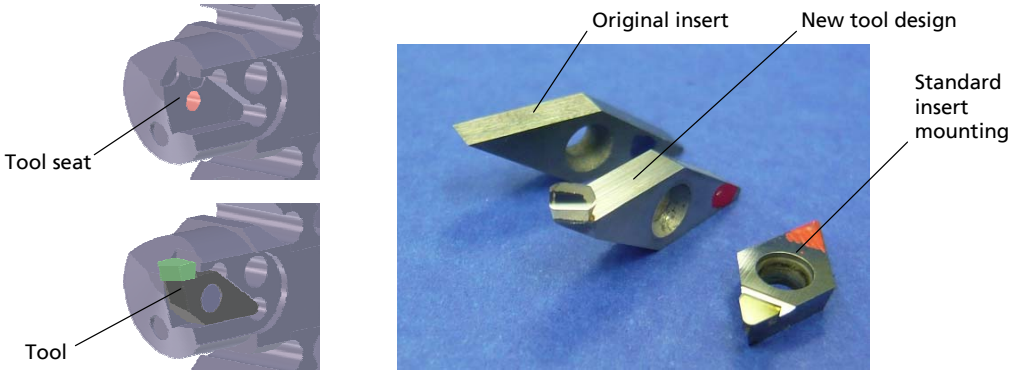

Figure 6.7: Integration of diamond cutting tool (left); Tool inserts with diamond cutting edge (right)

The tool guiding unit incorporates furthermore the reference surface for the capacitive measurement system. Ideally, the measurement system measures directly at the tool tip to reduce uncertainties due to thermal drifts. Since this has not been possible, a thermal sensor has been integrated close to the tool tip. In that way the compensation of thermal drifts is enabled.

6.2.3 Realization of the FTS

The design of the FTS is mainly influenced by the tool guiding unit and the piezo actuator. Furthermore, the FTS has to be able to be integrated into the slide of the Slow Tool to realize the aimed hybrid FTS. Therefore, it has to be compact and maximally reduced in its overall weight. Nevertheless, the FTS can also be integrated itself into an ultra-precision lathe to machine non-rotationally symmetric surfaces and structures.

The realized FTS is shown in **Figure 6.8** as photography and as CAD model. The dimension of the FTS at the front are 125 x 110 mm² (height x width). The length of the system is 230 mm.

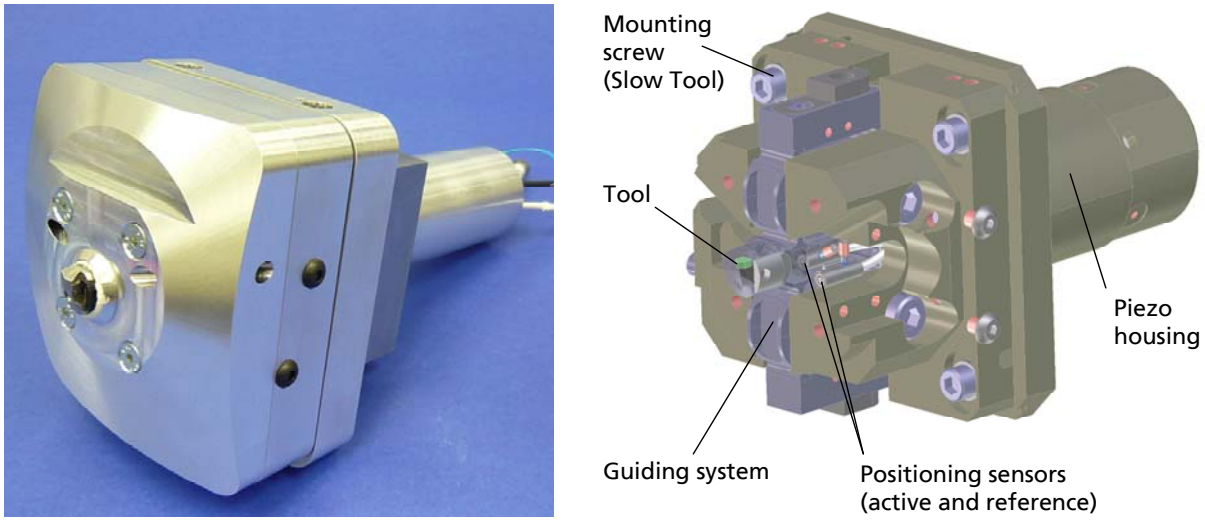

Figure 6.8: Picture of new FTS (left), CAD model of FTS without housing (right)

The overall weight of the FTS has reached 4.5 kg, due to the required stiffness of the housing, that is needed to reduce losses of the piezo stroke, and the Slow Tool interface. As material mainly steel is used and parts that are critical regarding the position measurement of the tool are made of Invar. The housing is made of aluminum and its conical shape allows for the machining of work pieces with a cone of 20°. If this is not sufficient, an extension can be used that is mounted to the tool seat. In that way steeper geometries can be machined.

The CAD model in Figure 6.8 (right) shows the integration of the flexural guiding system into the FTS. It is mounted vertically and the piezo actuator is placed behind the guiding system in the round back of the FTS. Next to the tool guiding system at the front a capacitive sensor is placed for the position feedback. The sensor has a measurement range of 50 µm and offers a resolution of 5 nm for a frequency range up to 15 kHz. Beside the use of Invar material, the long-time behavior of the FTS shall be enhanced by using a second capacitive sensor which is mounted next to the active sensor in the housing. It is producing a reference signal that will vary in the same way the main sensor will react on changes of the environment. This reference signal will be used for compensation strategies. Furthermore, several sensors are integrated into the FTS that monitor the piezo, the housing, and the tool seat temperature to prevent an over heating and enable compensation of temperature caused drifts.

Figure 6.9 shows a front and back view of the FTS. The lid at the front protects of cause the inside but gives also access for two spray mist nozzles. This is especially important, if the FTS is used in combination with the Slow Tool during the manufacturing of free-form surfaces requiring a large stroke. Due to the long stroke, it is not easy to adjust the spray mist efficiently from external. The small step in the upper part of the lid eases the tool referencing by the use of microscope objectives.

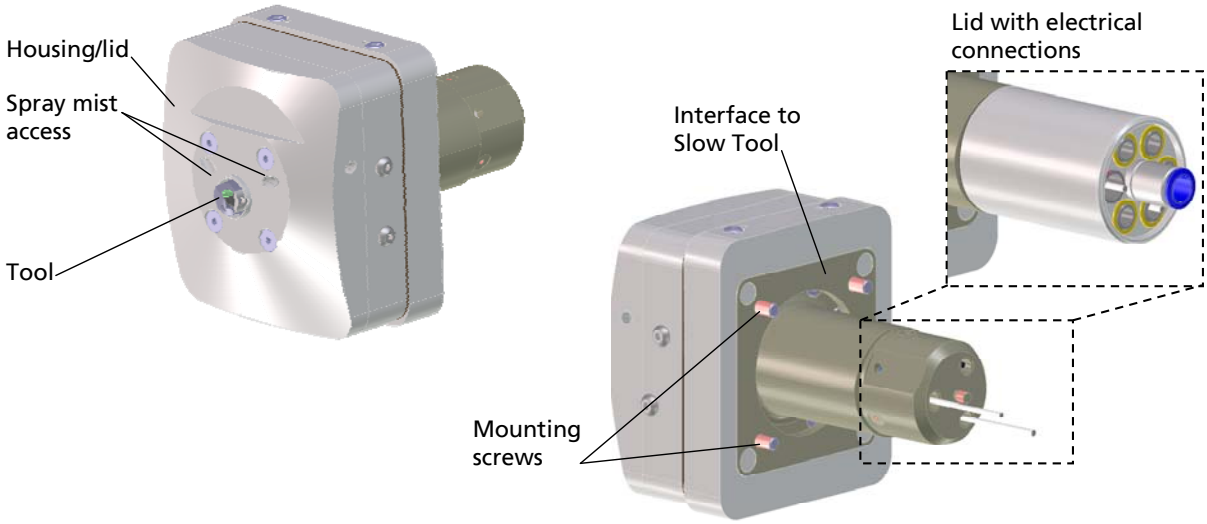

Figure 6.9: Interfaces of FTS systems at front and back side

At the back of the FTS, the bolt pattern for the connection with the Slow Tool slide can be seen. The slide has a cross section of 80 x 80 mm² and a bore diameter of 55 mm. The bore is required for the round piezo housing at the back of the FTS.

The cables of the sensors and the piezo are guided to the back side of the FTS. Since the FTS has to be mounted in the Slow Tool slide the electrical connections have to be pluggable (see Figure 6.9). Furthermore, a pneumatic connector can be seen that works as air outlet.

The FTS can also be used without the Slow Tool as stand-alone device. Therefore, an adjustment unit based on flexures is mounted at the interface to the Slow Tool. It allows for the fine tool height adjustment on a standard ultra-precision lathe. Hence, the FTS can be employed in several ways and be used flexibly for different machining tasks in the field of ultra-precision technology.

6.2.4 Characterization of the FTS

In the following, the important mechanical properties of the FTS and the transmission behavior of the control path are described.

The compliance of the FTS in working (or moving) direction indicates very good the realized stiffness at the interfaces between the piezo and the tool guiding unit, and between other components. Also the stiffness of the housing is included in the result. The frequency response has been derived using an impulse hammer and the integrated capacitive sensor, as shown in **Figure 6.10**. A stiffness of about $k_{stat,FTS}$ = 87 N/µm could be measured for the FTS in Z-direction. This is a very good value since the stiffness of the piezo actuator is nominal k_{piezo} = 90 N/µm. Furthermore, an eigenfrequency of $f_{eigen,FTS}$ = 3470 Hz has been determined, which demonstrates the good dynamic properties. This frequency is higher than the eigenfrequency of the single tool guiding unit. The reason for this is that the stiffness of the flexural guide and the piezo work parallel and are added, if the force is introduced by the impulse hammer from the front.

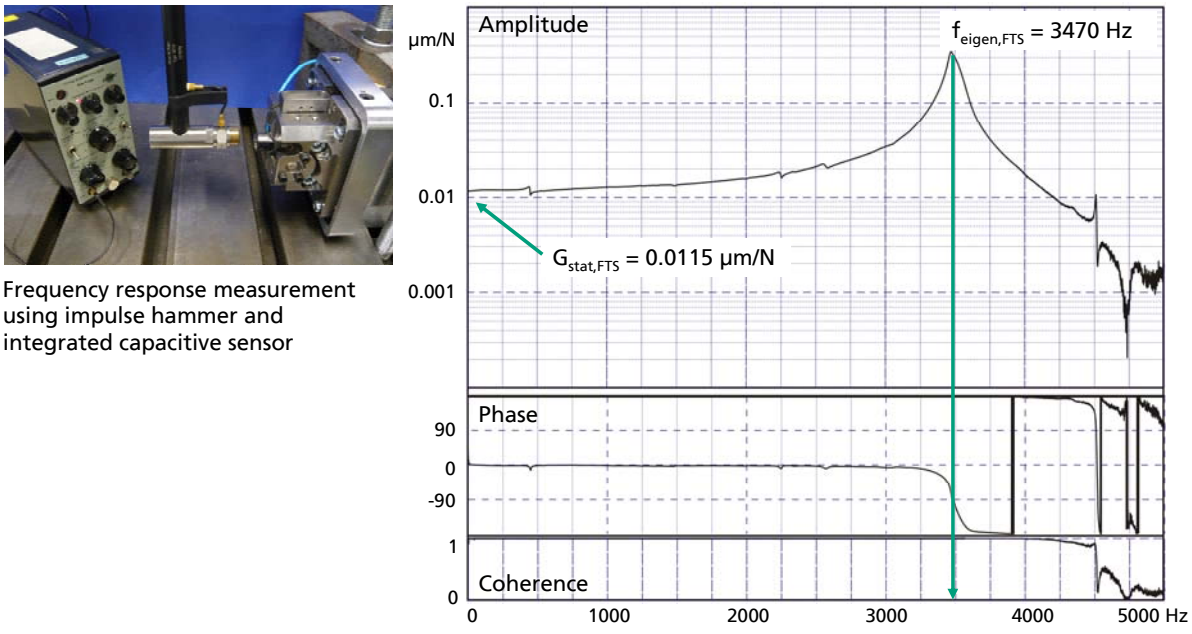

Frequency response measurement using impulse hammer and integrated capacitive sensor

Figure 6.10: Compliance of FTS in working direction (Z-direction)

For the machining process the stiffness of the tip at the tool guiding system in cutting direction (Y-direction) is important. This has been examined by establishing a

frequency response analysis. The force (chirp signal) is introduced using a piezo actuator. An external sensor measures the deflection. A static stiffness of $k_{stat,y,seat}$ = 20.4 N/µm could be determined, which is a sufficient value (see **Figure 6.11**).

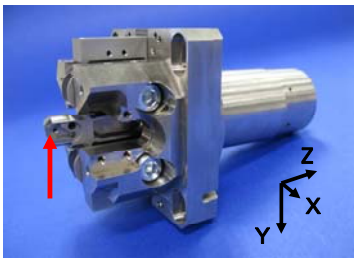

Frequency response in Y-direction using piezo actuator and external capacitive sensor

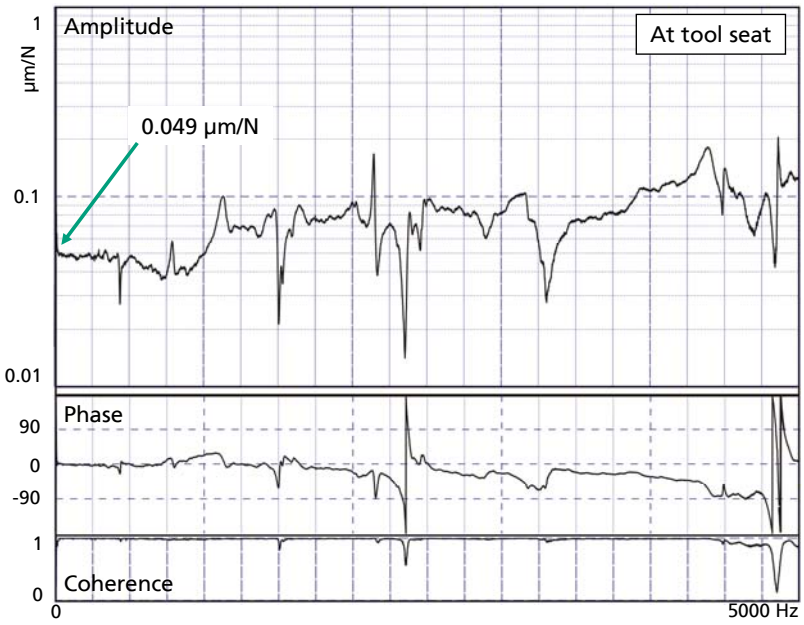

Figure 6.11: Compliance of FTS in Y-direction (cutting direction)

The transmission behavior of the FTS, which is relevant for the closed-loop control, has been examined in a further test. The control path consists of the FTS with its piezo actuator and the mechanics, the capacitive sensor with its amplifier, and the piezo power amplifier (PI-E481). The frequency response is determined between the input signal of the piezo amplifier and the measurement result (voltage signal) provided by the amplifier of the capacitive sensor. The result can be seen in **Figure 6.12**. The control path has an eigenfrequency of $f_{eigen,FTS}$ = 3532 Hz and a bandwidth of 1950 Hz, which is a bit lower than the aimed 2000 Hz.

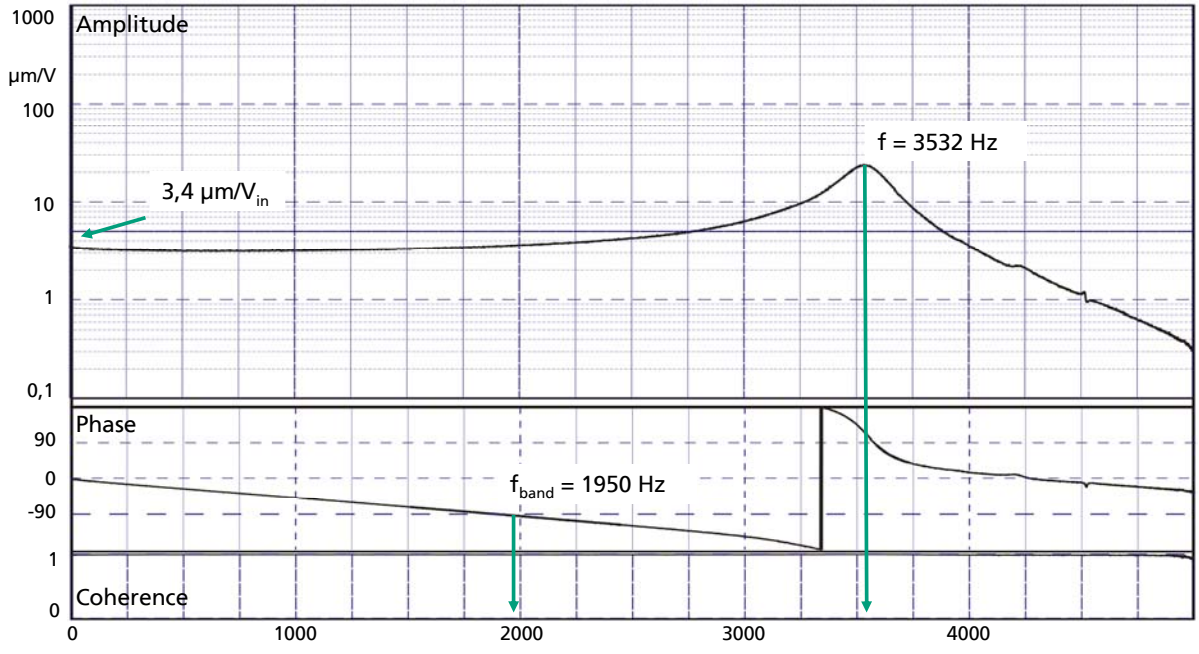

Figure 6.12: Transmission behavior of control path using amplifier PI-E481: stroke vs. U_{in}

The bandwidth is limited by an allowed phase decay of -90°. This value is influenced by dead times in the measurement amplifier (15° for each 1000 Hz) and in the piezo amplifier. A tested older amplifier model (PI-E480) has shown an even stronger phase decay. Nevertheless, the first characterization test has shown the potential of the developed FTS system.

6.2.5 Test Machining using the FTS

Figure 6.13 shows the FTS mounted as single device on an ultra-precision lathe. The picture in the lower left corner of the figure shows in detail the tool setting operation using a microscope camera.

At first, planar test parts have been machined in different conditions. The FTS has been used for the machining of the aluminum work piece without any electrical connection and also in position control. In both cases a surface roughness of 3 -4 nm Ra could be reached, which is sufficient and mainly influenced by the work piece material. The dynamic properties of the FTS have been tested by the machining of a sine wave structure. The FTS has been controlled using a frequency generator at 2 kHz. A stroke of 2.5 µm has been applied. Using a spindle speed of 50 rpm a wave length of 60 µm could be reached at the outer circumference of the work piece.

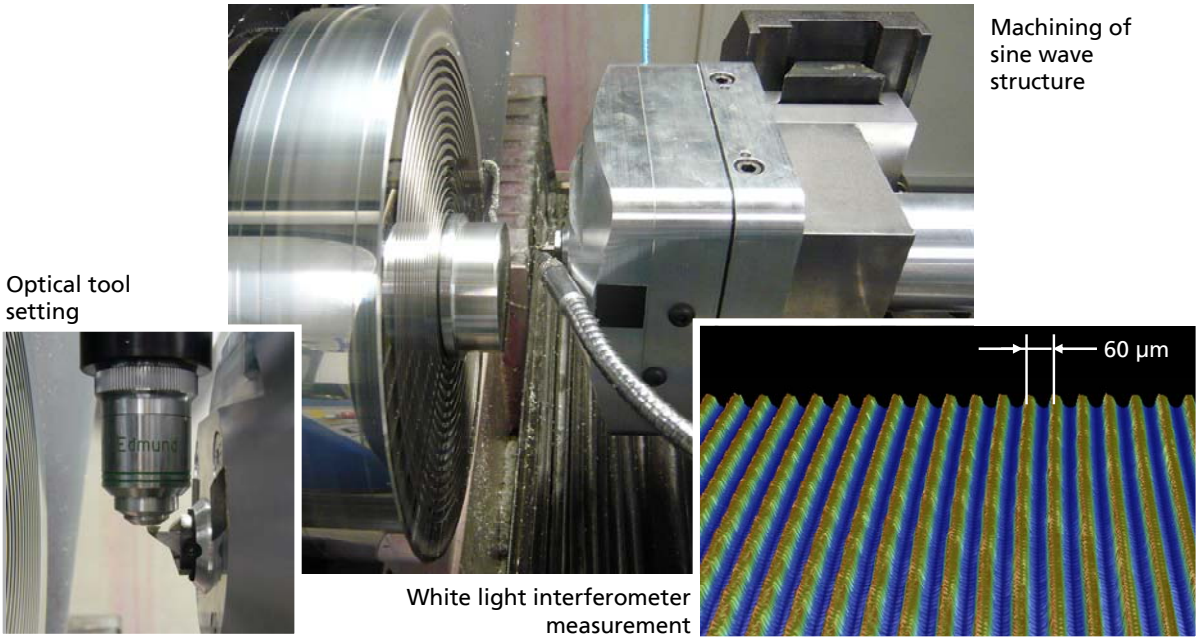

Figure 6.13: Test machining of waviness using 2000 Hz working frequency of FTS

By this machining the basic tests of the FTS have been finished. The capability of the new designed FTS has been proven. A more detailed analysis of the dynamic behavior of the FTS will be described in the chapter 7 in the scope of the machine control.

6.3 Design of the Base Machine

The design of the base machine is strongly influenced by the overall concept of the machine demonstrator. Hence, it is crucial to have the specifications of the hybrid FTS concept, described in chapter 6.1, in mind when discussing the base machine. To be able to machine hybrid optics within a reasonable time, 5 mm stroke at a frequency of 20 Hz have been defined as performance target for the dynamic of the long stroke part of the hybrid concept. To limit the reaction forces during acceleration, the need to reduce the moving mass as small as possible can be derived. To optimize the dynamic behavior, the use of linear direct drives has been inevitable. For ultra-precision machines the overall accuracy is a crucial feature and is affected by thermal stability and Abbé-errors.

Aiming for these specifications, different concepts of the machine demonstrator have been discussed in the beginning of the project. Two concepts have been further detailed. The first one has been a concept of a turning machine with a travel of about 200 mm for the X- and the Z-axis. Both linear axes built as lightweight as possible to enable a »slow but large travel« movement as part of the hybrid concept. Soon, first considerations showed that despite all lightweight construction, the slides would still be too heavy to reach the specified accelerations, at least at a commercially acceptable effort.

The second concept has been used in the end (see **Figure 6.14**). This concept is based on a machine with a large travel and limited dynamics and is called MTC 410.

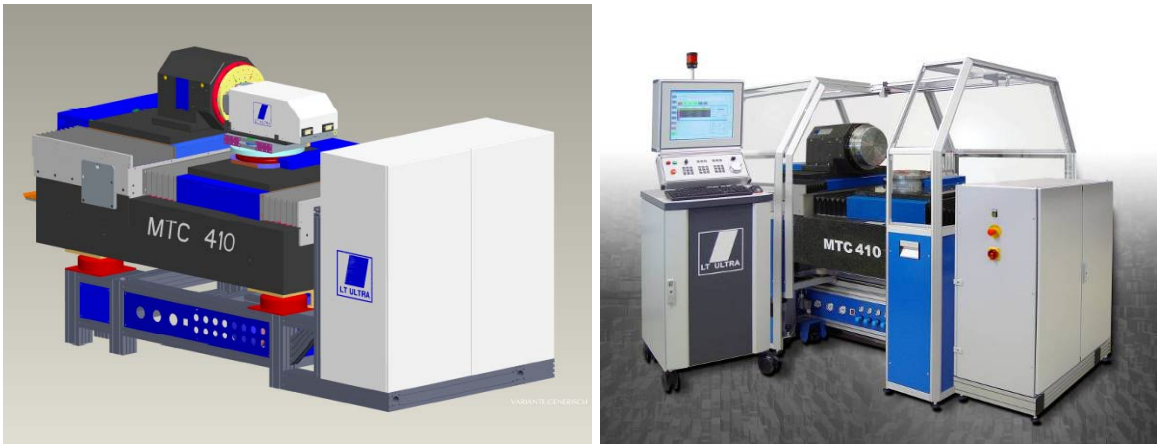

Figure 6.14: CAD model of base machine with hybrid FTS (left), Base machine MTC 410 (right)

Without considering a lightweight design for the slides, the machine allows for a travel of 410 mm in both axes and has a B-axis on top of the Z-slide. The hybrid axis concept is implemented as an on-top-solution.

Summarizing, the main parameters of the realized machine concept are:

- Hybrid axis as on top solution
- Stroke of dynamic slide in the hybrid FTS: 20 mm
- Additional axes allow for a lightweight slide
- Integration of FTS and dynamic slide into a hybrid FTS system
- Large travel of standard Z-axis with no need of highly dynamic performance
- No weight constraints of Z-slide enable the integration of a rotary axis

The MTC 410 is a 4-axes ultra-precision turning machine. Equipped with a C-axis, a main spindle with high resolution encoder and torque drive, synchronous multi-axis machining is possible. The air bearing spindle can handle payloads of up to 100 kg and has a speed range of 0 to 2500 rpm. It features a granite housing and active cooling facilities for a minimum of thermal spindle growth.

The second rotary axis in the machine is the B-axis. It is equipped with a torque drive and a high resolution encoder (< 0.004 arc seconds). High damping and stiffness are guaranteed by using hydrostatic oil bearing technology. Active cooling is also possible. Usually the B-axis should be clamped during the machining to offer high stiffness. But if the acceleration of the dynamic axis is reduced, the B-axis allows to pivot the hybrid axis, not only for adjustment but also during machining, offering some new machining options.

The integration of the B-axis in the Z-slide reduces the stack height and allows a center height of 325 mm regarding the machine bed and a center height of 190 mm over the rotary table of the B-axis. By adding distance pieces between X-slide and main spindle even bigger center heights can be realized.

The linear axes feature hydrostatic bearing technology and linear direct drives. Both slides are equipped with optical linear encoders. The feedback resolution is 33 pm (picometer). The slides are made of granite which, due to its low thermal expansion coefficient, helps to provide thermal stability. Additionally, both linear motors are indirectly cooled by the oil and provide facilities for direct water cooling.

The machine base is made of a massive block of granite (as shown in **Figure 6.15**) with a mass of around 2300 kg. The overall weight of the machine is about 4000 kg. An active vibration isolation system decouples the machine base from ambient noise. The machine is designed to be as compact as possible. The overall dimensions without housing and control panel are 1900 x 1500 x 1500 mm³.

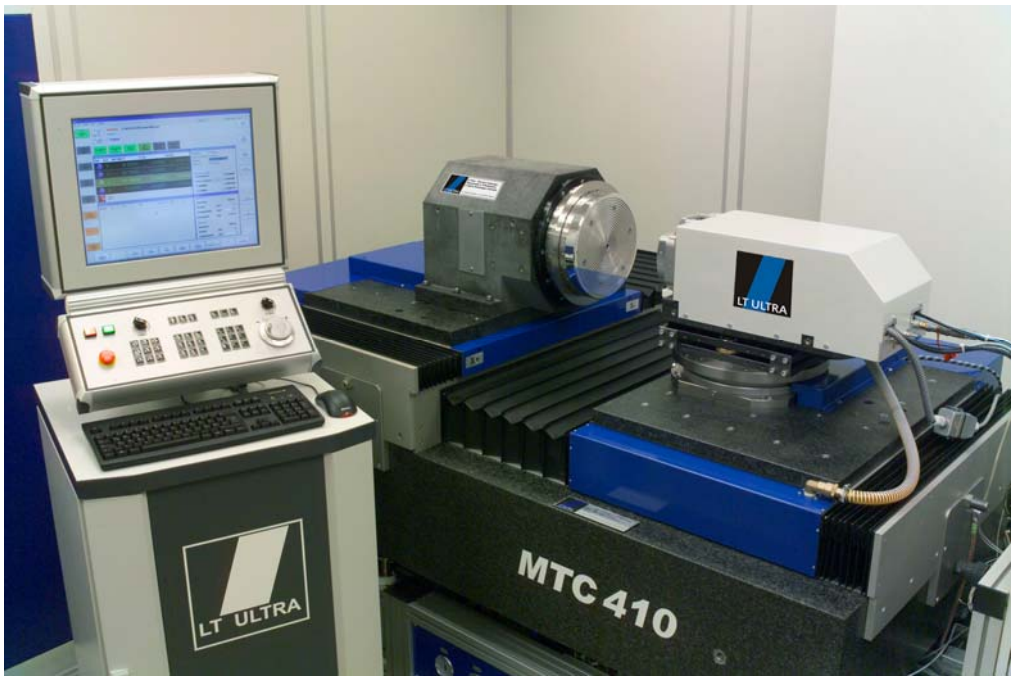

Figure 6.15: Machine demonstrator with hybrid FTS at Fraunhofer IPT

6.4 Design of the Dynamic Axis

The dynamic axis is the basis of the hybrid FTS system developed in the scope of »ERANET-OPTICALSTRUCT«. The concept of the hybrid FTS introduced before and shown in **Figure 6.16**, defines that the dynamic axis (Slow Tool) has to move the FTS. The FTS is integrated into the front of the slide. The aim of the dynamic axis is the realization of large strokes, if free-form surfaces with non-rotationally symmetric shapes of several millimeters have to be machined.

A Slow Tool usually is the Z-slide of a two axis ultra-precision machine, which has better dynamic properties than a conventional slide. But for the design of the hybrid system a classic Slow Tool slide with an FTS system on top cannot be used since dynamics of 20 Hz at 5 mm stroke shall be reached. Hence, a compact and integrated solution has been realized.

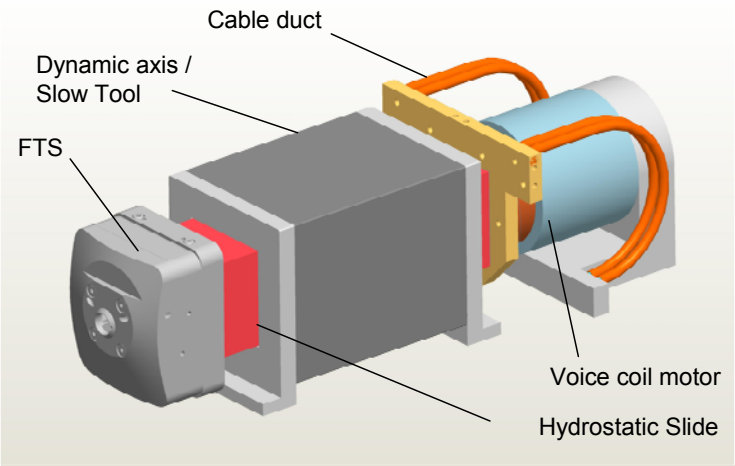

Figure 6.16: Concept of dynamic axis with integrated FTS

Beside the compact layout, the drive is the most crucial component of the dynamic axis. Accelerations for a sinusoidal motion 5 mm of stroke at 20 Hz are in the range of 40 m/s². For 5 mm and 25 Hz it takes 62 m/s². Another limiting factor is the speed that is reached, moving the slide with such high accelerations at comparatively large amplitudes. The maximum speed is limited by several factors such as the maximum speed of the motor or the linear scale. **Figure 6.17** shows the amplitude against the frequency for a speed limit of 0,7 m/s and an acceleration limit of 62 m/s². While at lower frequencies the maximum velocity is the limiting factor, more dynamic movements with frequencies above 15 Hz are bounded by the maximum acceleration.

A voice coil motor has been chosen to drive the dynamic axis, not only for its high power but also for its ease of use and the possibility to mount it aligned with the center of mass of the slide. It easily accelerates the slide with 65 m/s². Without the FTS, the maximum acceleration of the slide will be even higher.

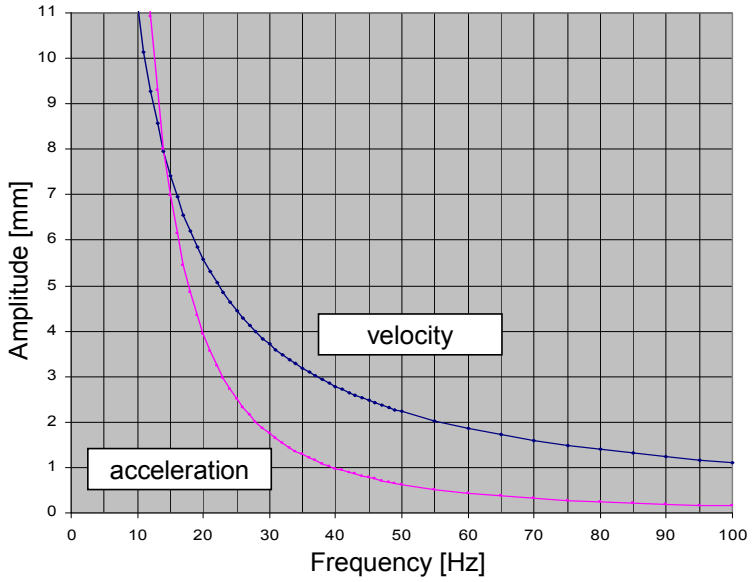

Figure 6.17: Amplitude against frequency, speed and acceleration limits

The moving mass of the system has been reduced to about 10 kg including the FTS to decrease the forces that are needed to accelerate. This reduction is possible by using special alloys for the slide. The slide has a sleeve like design and is supported with hydrostatic bearings for high stiffness and damping. This design in combination with the voice coil drive enables overall strokes of 20 mm.

Sleeve and voice coil motor are fixed to a granite base plate, all covered by an aluminum housing to protect the system against dirt and chips. Underneath the base plate the hybrid system is fixed to the B-axis via the tool adjustment unit (see **Figure 6.18**). Using flexural bearings, it allows for an adjustment in a range of a few hundred microns. After the adjustment is finished, the mechanism is clamped to fix the position. The rough height adjustment of the cutting tool is provided at the interface between the FTS and the slide of the dynamic axis. The overall weight of the hybrid FTS is about 90 kg, that has to be carried by the B-axis.

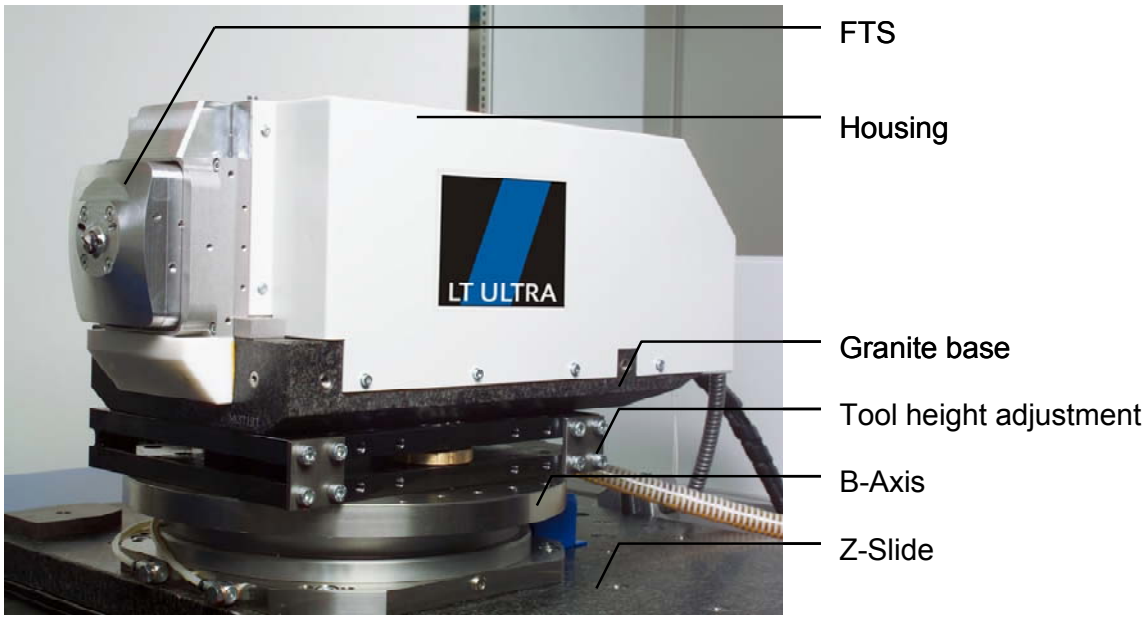

Figure 6.18: Realized hybrid axis mounted on B-axis

As the accuracy of the overall machine demonstrator has to be very high, heat management plays an important role not only in the base machine but in the hybrid axis as well. Therefore, it is possible to cool the voice coil. Furthermore, the oil of the hydrostatic bearings is temperature controlled to allow for stable conditions. Beside the possible temperature control, further precautions have been done. The linear scale, measuring the movement of the sleeve, is mounted as close as possible to the interface of the FTS and in that way to the tool tip. Additionally, Invar fixtures are used to reduce possible displacements that cannot be measured with the scale.

The dynamic axis (or Slow Tool) is working in combination with the FTS as hybrid FTS system, but can also be used as stand-alone device. Therefore, an adapter is replacing the FTS and carries the cutting tool. Without the FTS better dynamic properties are reached, due to the significantly lower moving mass.

7 Control System

The main focus of the developments related to the machine control is layed onto the implementation of a combined servo system (FT/ST servo control system) for the mechanically coupled highly-dynamic axes of the Fast Tool and the Slow Tool. These developments include high bandwidth feedback control loops, the compensation of systematic positioning errors and the synchronization with the control system of the basis machine with an interpolation error minimized setpoint generation.

7.1 Control System of the Machine Demonstrator

The machine control environment for the turning kinematic bases on a modular system of Delta Tau Data Systems, a UMAC rack (Universal Motion and Automation Controller) with a Turbo-PMAC2 processor board. The processor board integrates a Motorola processor with a word width of 24 bit and a system clock of 400 MHz. All feedback control loops of the turning kinematic are implemented on dedicated axis control boards. The setpoint generation, in most cases the interpretation of G-code, is realized in the same processing environment like the PLC functions of the machine like safety functions, supervising the machine status and the control of auxiliary units for cooling and others. On the one hand this architecture has the advantage to by design execute all feedback control loops in the same clock without the need to synchronize them. On the other hand the central processor can be overloaded by moderately complex mathematical calculations needed for setpoints or additional control algorithms or a higher control clock. This overload can easily result in a crash of the whole system which has to be prevented in any case. The HMI (Human Machine Interface) software is implemented on a Windows PC and communicates over USB (Universal Serial Bus) with the hardware controller. The HMI software itself, shown in **Figure 7.1**, does not affect the realtime performance of the control hardware significantly.

Figure 7.1: Human Machine Interface (HMI) of the machine demonstrator

7.2 FT/ST Servo Control System

The control of the dynamic axes of the Hybrid-FTS (FT/ST servo control system) bases on an FPGA (Field Programmable Gate Array) system for the feedback control and a PC-based system for low level setpoint generation. This system enables position control clocks of above 100 kHz for the piezo-driven FTS. The system is connected to the system bus of the basis machine's control system to synchronize both controls.

7.2.1 Platform Architecture

The basic platform for the development of the FT/ST servo control system is a hybrid system, consisting of a microprocessor based high level part and an FPGA-based low level part. Logically higher application layers are implemented in the microprocessor-based part of the control system. These layers include for instance parameterization and supervision interfaces to the human machine interface, which do not need to be real-time capable. Further, low bandwidth control loops for compensation purposes which might be computationally demanding are implemented in the high level part. The high bandwidth position control loops of the axes are implemented in the low latency FPGA based part of the servo system to achieve the best possible dynamics and accuracy. The control system which implements the control algorithms in this setup does not constrain or limit the dynamic performance of the overall feedback system consisting furthermore of power electronics, mechanics and sensors.

In a microprocessor system the digital hardware structure of the computation system is fixed. Hence, in such a system the subset of available elementary arithmetic operations usually is restricted. In addition, the system peripherals, to which the sensors and actors are connected, in most microprocessor architectures are not connected to the arithmetical unit directly, but over a peripheral bus system. This implies a significantly high latency time from the input to the output signals which dominates the dynamic performance of the control loops. Beyond that, the latency is not constant in time, which, if not taken account of, causes additional noise in the control loop, leading to a poor positioning performance.

Compared to a microprocessor, the digital hardware structure of a computation system, which can be implemented within an FPGA, is freely programmable and reconfigurable. The hardware structure can be adapted to the application. Especially, critical paths in the digital algorithms can be optimized. While programs on a microprocessor based system are as a matter of principle sequentially processed, on an FPGA based system calculations which are adjusted to the application can be executed in parallel. Parallelizations of this kind are especially effective in the case of modules, which are directly communicating with the electronic peripherals of the system, like measurement interfaces or control value outputs. With these techniques the overall latency of the control algorithms can be optimized to a minimum.

However, while it is technically possible, FPGAs are not suited for the implementation of mathematically complex algorithms, in contrast to microprocessors, whose highly clocked digital logic is exceedingly optimized for these tasks. The implied performance discrepancy particularly applies for algorithms using floating point arithmetic. For this reason, the mathematically complex algorithms for the calculation of surface-based setpoints are processed in the microprocessor based part of the system. On the other hand, the mathematically quite elementary feedback control algorithms for the highly dynamic axes benefit from the achievable extremely low latency of the FPGA.

Figure 7.2 shows the actual implementation of the FT/ST servo control system. The microprocessor based high level layer is realized by an embedded control PC which is connected to the HMI (Human Machine Interface) PC of the basis machine control. The low level FPGA based part of the system is connected to the highly dynamic axes and the realtime control system of the basis machine control, the PMAC control system. The FPGA system implementation can be debugged over JTAG (Joint Test Action Group – IEEE 1149.1), the common method to debug ICs (Integrated Circuit) and embedded systems.

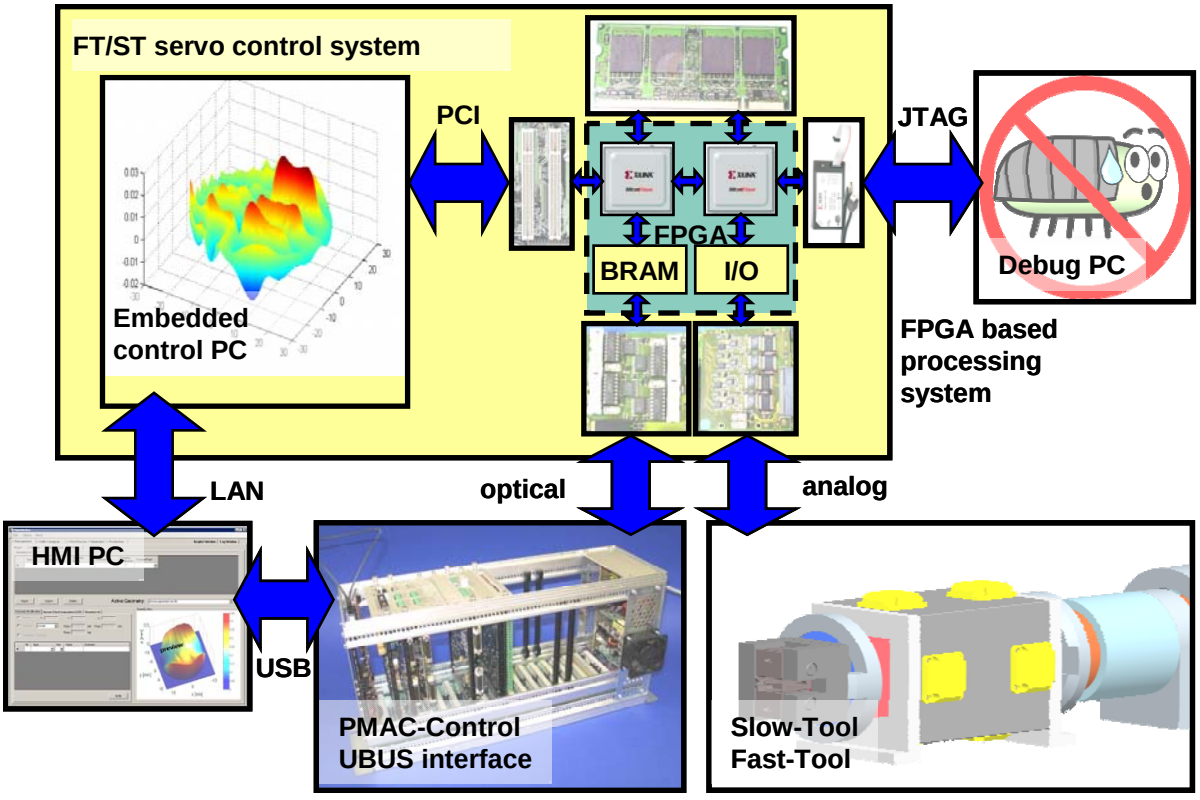

Figure 7.2: Block diagram of the FT/ST servo control system and its interfaces

7.2.2 FPGA Hardware

Figure 7.3 shows the applied FPGA hardware. The system bases on a PCIe board distributed by the company Cesys with a Xilinx Virtex-4 FPGA. The board integrates local volatile memory of 512 MB DDR2 (Double Data Rate) SDRAM (Synchronous Dynamic Random Access Memory), which is used for setpoints representing structures for the Fast Tool axis. The hardware I/O which was customized in the

scope of the »ERANET-OPTICALSTRUCT« project is directly connected to the FPGA. The I/O consists of an AD/DA board with fast ADC (Analog Digital Converter) and DAC (Digital Analog Converter), an extension board with TTL quadrature inputs for positioning sensors, optical transmitters and receivers to connect the servo system to the basis machine's control and TTL I/O to enable and supervise the power electronics of the drive system.

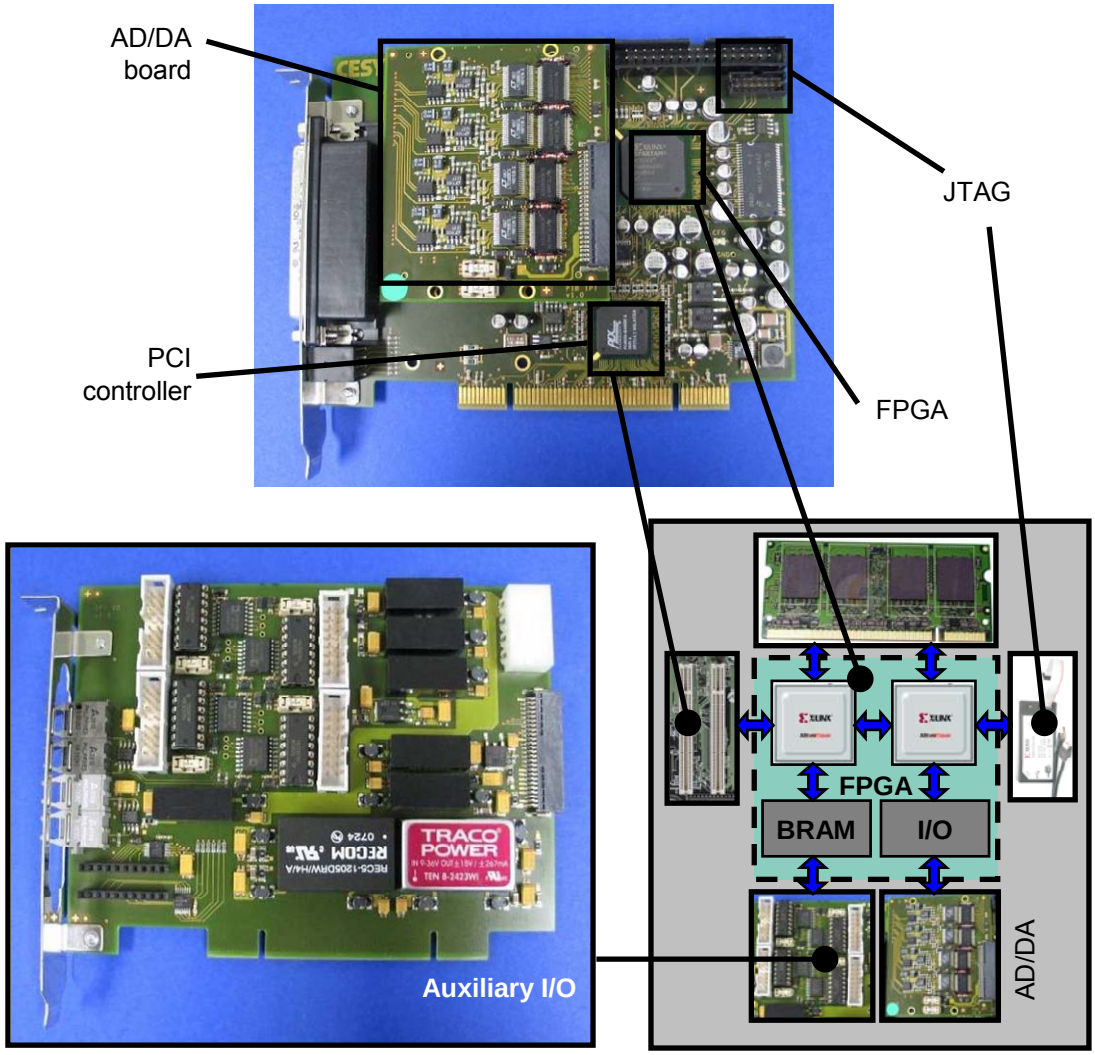

Figure 7.3: I/O hardware of the FT/ST servo control system

To keep the system reconfigurable without having to alter the hardware implementation permanently, two soft processor cores are instantiated in the FPGA fabric. These MicroBlaze processor softcores provided by Xilinx are programmed with C code and are capable to execute single precision 32 bit wide floating point operations (IEEE 754). Both processors together use roughly half of the available FPGA logic blocks and are connected to the SDRAM memory over a memory controller which consumes around 20 % of the FPGA logic blocks. The remaining 30 % are used for user I/O logic and parallel signal processing. A block diagram of the implemented system is shown in **Figure 7.4**. The two processors share the tasks of the calculation of the feedback control and the setpoint generation and user interface. Thus, the processor µBlaze1 is connected over PCI to the embedded PC

and the PMAC machine control system to synchronize the setpoint generation for the FT/ST servo control system with the G-Code generation. The interface to the PMAC control using DPRAM (Dual Ported RAM) is explained later on in chapter 7.3. The other processor µBlaze2 executing the control algorithms for the Fast Tool and the Slow Tool is connected to the AD/DA board. Both processors communicate over so called mailbox registers for fast synchronization and share a memory region in the SDRAM for setpoint data. Setpoint algorithms which are mathematically not complex like non-continuous structures are processed in the softcore processors with a rather low latency. Mathematically complex algorithms need to be calculated in the embedded PC system. The necessary data exchange over the PCI bus causes higher latency which can however be tolerated for the Slow Tool system due to its lower dynamics.

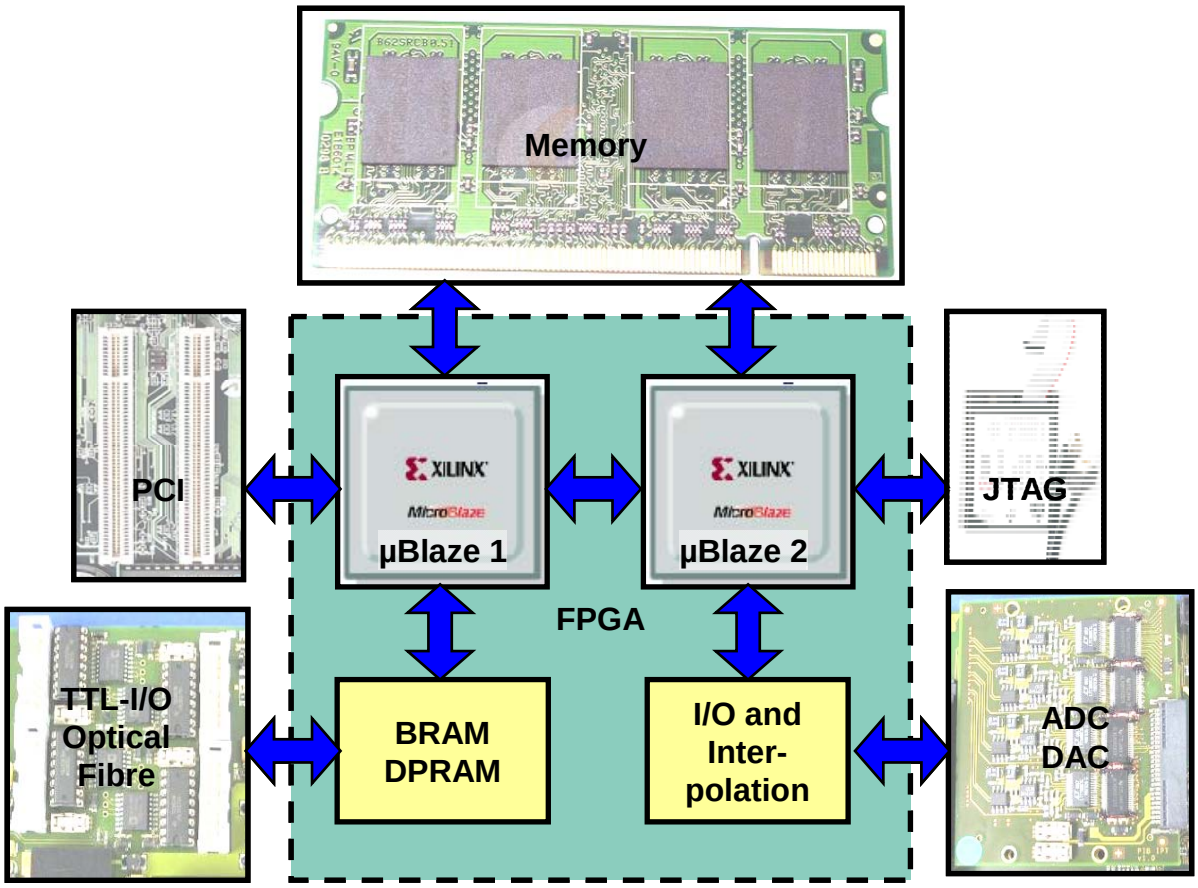

Figure 7.4: FT/ST servo control system – FPGA layer

7.2.3 Hardware and Software Layers

Beside the partition of the system's hardware platform into a microprocessor and an FPGA based part, the FT/ST servo control system furthermore is organized in several hardware and software layers. A rough overview of these layers is shown in **Figure 7.5**. The sensors and actors of the Fast Tool and Slow Tool are connected over electronically analog interfaces. The *hardware I/O layer* is the interface between the analog physical signals of the sensors and actors and their digital representation in the digital control hardware. The main components of this layer are electronic ADC and DAC chips with a minimal latency of 20 ns as well as the related control

hardware containing oversampling and clock adaption algorithms. For connecting a sin/cos encoded optical linear scale, which is used to measure the actual position of the Slow Tool system, a counter and interpolation module also is implemented in low latency FPGA logic. The *low level computation layer* is implemented completely in the FPGA itself, using two softcore processors, which are instantiated in the FPGA fabric and programmed with C code. The design of the FPGA takes place in VHDL (Very High Speed Integrated Circuit Hardware Description Language). The derived FPGA binary image has to be downloaded onto the FPGA on system start since the FPGA memory cells are volatile. A PCIe bridge (PCI-Express – Peripheral Component Interconnect) provides the connection of the FPGA and the microprocessor system. The FT/ST servo control system uses an industry PC configured with Debian Linux and the realtime system kernel extension Xenomai, able to provide setpoint generation clocks of more than 40 kHz.

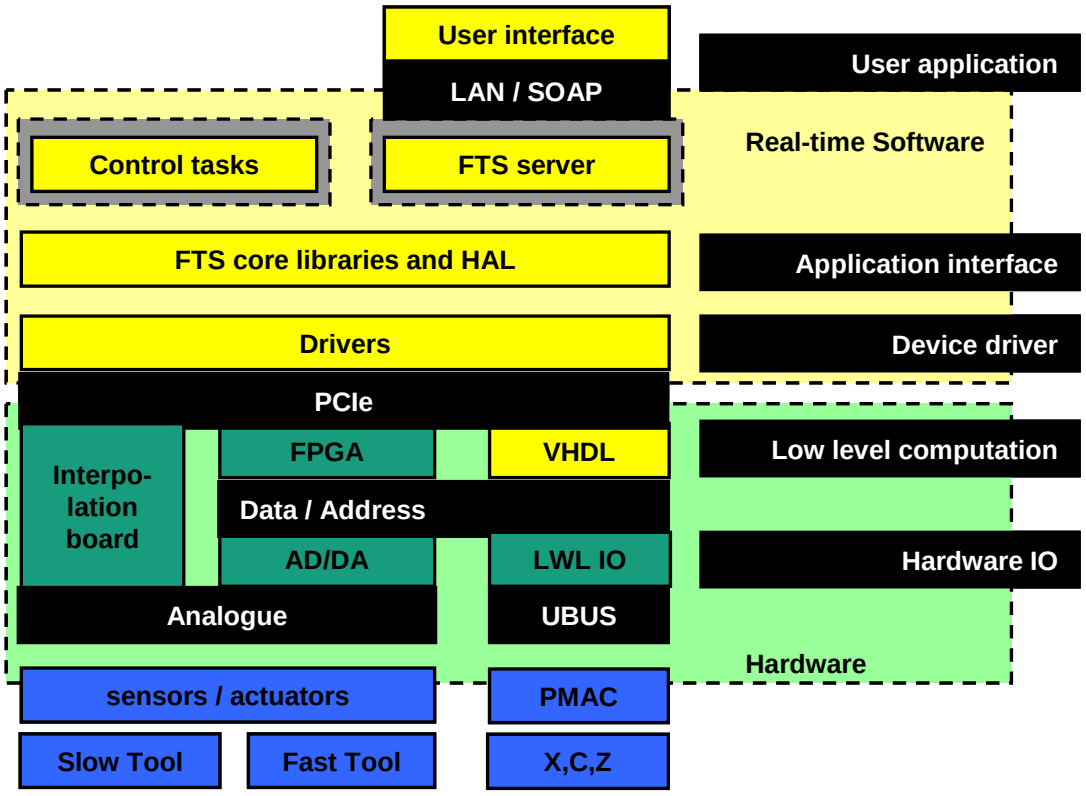

Figure 7.5: Hardware und software layers in the FT/ST servo control system

The *device driver layer* in the microprocessor system connects the electronic hardware with the *FTS core libraries* and the *hardware abstraction layer (HAL)*. These system components (*application interface*) provide the applications with a uniform interface to the signals transmitted to and received from the device drivers. Applications on the one hand are realtime algorithms for feed forward control and slow feedback control loops. On the other hand, the application interface is used by non-realtime management modules, which provide the machine operator with a signal and parameter interface for supervision and modification of control parameters.

Additionally to a character based terminal, a platform independent interface basing on SOAP (Simple Object Access Protocol) is implemented to access the application interface over LAN (Local Area Network) even on a machine with another operating system like Microsoft Windows XP. Using this interface, the FT/ST servo control system can be parameterized from an arbitrary client in the local network. Primarily, it is intended to connect the FT/ST servo control system to the control PC of the basis machine. For this purpose a GUI (graphical user interface) was implemented which integrates the user interface for the control parameters for the highly dynamic axes and the CAM (Computer Aided Manufacturing) modules developed by the project partner ModuleWorks and discussed in chapter 8.

7.3 Synchronization of the Highly Dynamic Axes

In a machine tool, a position synchronous movement of the axes in most applications is mandatory, at least desirable, to achieve the demanded accuracy of the work piece geometry. In conventional turning applications, the rotational machine axis, on which the work piece is clamped, is not operated with a closed position control, but only with a closed speed control loop. This operating mode is naturally suitable for work pieces with a rotationally symmetric geometry, since the position of the linear Z-axis is only dependent on the position of the X-axis, but not on the spindle angle. Though, machining work pieces with non-rotationally symmetric geometries requires the geometric coupling of all axes of the machine tool. This requirement can be satisfied by different techniques.

If the rotational axis cannot be position controlled and operation in spindle mode is retained, it is possible to accomplish a synchronization of the axes by using the measurement signals of the spindle and the Z-axis. In a couple of old Fast Tool systems, where the highly dynamic axis is developed as an auxiliary axis, this synchronization approach is applied, especially, if a direct intervention into the basis machine control was either not possible or difficult to achieve. The major disadvantage of the introduced synchronization approach is the insufficient coupling of the servo control system of the highly dynamic axes to the basis machine control. Due to the missing information feedback, both systems cannot be optimally operated regarding their limits. The missing functionality is a shortcoming, particularly, if safety functions need to be implemented in the machine system. The main machine control will not react on overload or failures of the highly dynamic axes in the process, if the feedback channel is missing. In that case, only the highly dynamic axes would switch off, the basis machine would continue.

This drawback can be corrected by closer coupling the FT/ST servo control system to the main machine control. **Figure 7.6** shows the configuration of the complete machine control as a block diagram on the left. Before the machining, the geometry data supplied by CAD (Computer Aided Design) is processed in the CAD/CAM (Computer Aided Manufacturing) chain which produces G-Code for the main machine control and a synchronized geometry part for the highly dynamic axes.

Already in the CAM the original geometry is split into a rotationally symmetric part for the basis machine and a non-rotationally symmetric part for the highly dynamic axes. Within the scope of this machining strategy, the rotational movement of the work piece is realized with a position controlled C-axis. The control loops of the different axes are decoupled regarding their setpoints. A decoupling of the control loops of the Z-axis and the FT/ST axes needing a cross communication, with a disturbance variable feed forward for instance, can be realized with this implementation, though.

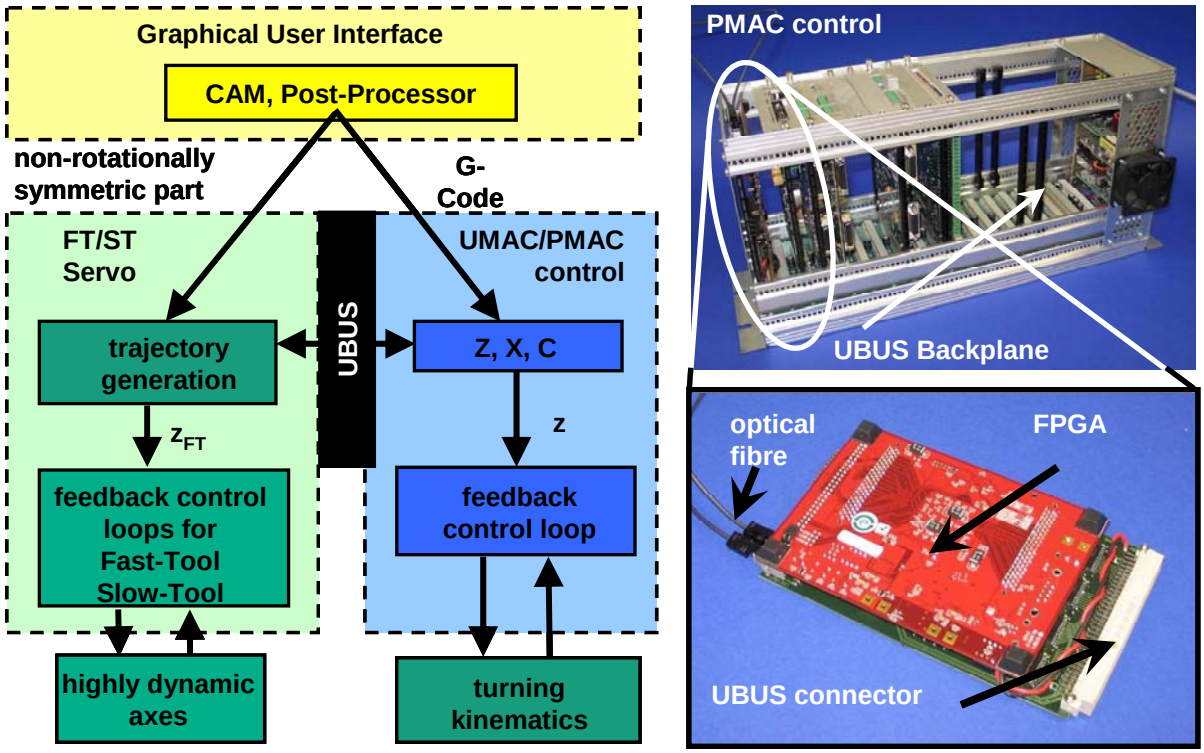

Figure 7.6: Synchronization of PMAC control and FT/ST servo control system

The right side of Figure 7.6 shows photos of the PMAC main machine control with the I/O board, which was developed in the scope of the project »ERANET-OPTICALSTRUCT«, needed for communicating with the FT/ST servo control system. The PMAC control system bases on a backplane, which connects a processor board to different I/O modules and axis control boards. The processor communicates with the other boards, which are connected to the backplane, over UBUS (Universal BUS), a proprietary bus system developed by Delta Tau. In this architecture, the processor board is the master, which initiates all data transfers. Like in other bus systems for similar applications, the electronic parts of the bus system itself can be assigned to the data bus, the address bus and the control signals.

The I/O board developed in the »ERANET-OPTICALSTRUCT« project operates as a bridge between the PMAC's UBUS backplane and a serial digital optical interface which connects galvanically isolated to the FT/ST servo control system. The board consists of an adapter board, which is electronically and mechanically fit to the UBUS system, and a standard board with programmable FPGA logic. The FPGA (Xilinx Spartan 3) contains the UBUS protocol, local block memory for the exchange data

and a digital serial transceiver representing the interface to the FT/ST servo control system. The developed board is mapped into the address space of the PMAC processor and can be operated in the same manner as other I/O boards connected to the UBUS backplane. Two line codes like were tested for the serial communication on the optical fiber. The start/stop method (e.g. used in EIA-232) directly applies the serialized data stream onto the transmission line without any encoding which turned out to be a problem using higher data rates (>1 MBit/s) and word lengths of 32 Bit since the synchronization regarding the baud rate was lost. To solve this problem, the Manchester line code (used in the physical layer of the Ethernet standard IEEE 802.3) was introduced. Like **Figure 7.7** shows, that the encoded data has at least one edge transition per bit from which the baud rate can be restored in the receiver. With this property the Manchester line code is self-clocking and needs no synchronization regarding the baud rate. Around 8 MBit/s can be achieved getting a stable serial communication.

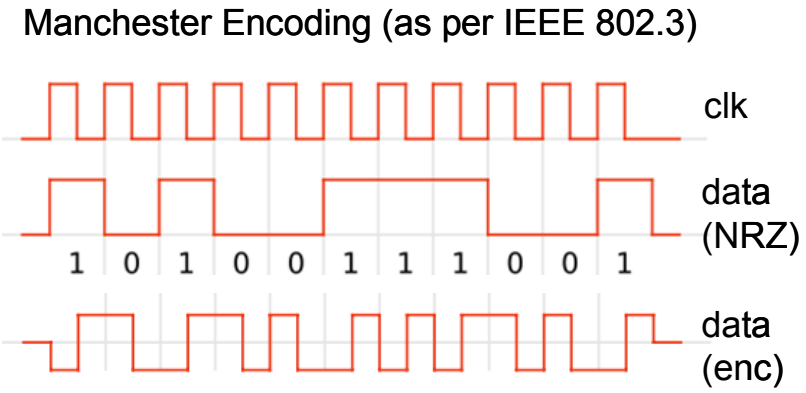

Figure 7.7: Line code of optical I/O between PMAC and FT/ST servo system

The data transfer between the PMAC control and the FT/ST servo control system is bidirectional. The PMAC control transmits synchronization information like the actual position of the C- and the X-axis of the basis machine. On the feedback channel the actual position of the highly dynamic axes and status information is transmitted which can be processed in the main machine control, or at least displayed in the HMI (Human Machine Interface). The direct connection to the UBUS backplane guarantees the lowest possible latency between the PMAC and the FT/ST servo control system. Furthermore, both systems are synchronized with UBUS system clock signals regarding the position control clocks of the axes.

7.4 Control Loops and Compensation

Figure 7.8 shows the information flow of the fundamental control signals between the FPGA based FT/ST servo control system and the electromechanical axes containing sensors and actors. The position control loop for the Fast Tool is closed over a voltage controlled output stage for the piezo actuator and a capacitive position sensor with processing. The position control loop of the Fast Tool reaches a control clock of 100 kHz. The transfer behavior of the electro-mechanical system is limited to

2 kHz due to mechanical eigenfrequencies. A sampling control demands at least the factor 10 as minimum limit for the control clock. To utilize the full bandwidth of the mechanics, a minimum control clock of 20 kHz is required. The desired control clock is specified higher, though, to provide a phase decay which is as low as possible in the range of higher frequencies. This phase decay is critical for the performance of the transfer behavior of the axis.

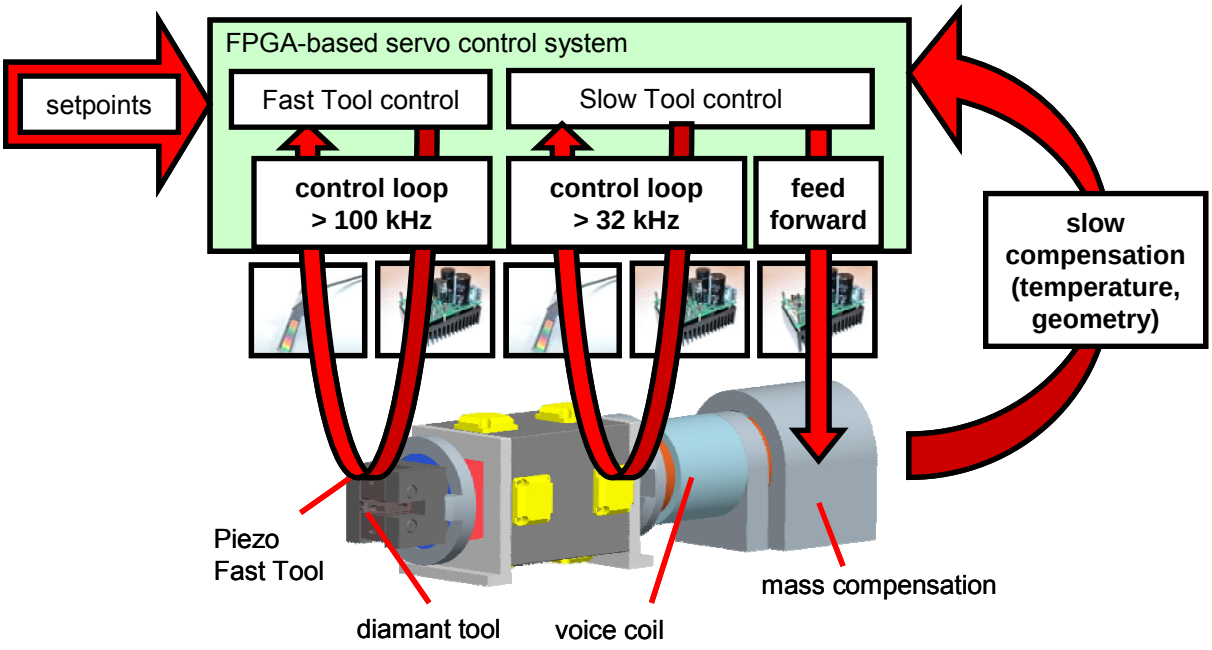

Figure 7.8: Information flow and control loops of the FT/ST servo control system

Due to the higher mass which has to be moved, the Slow Tool system has clearly lower dynamics than the Fast Tool system. Especially for the velocity control loop for the implemented system a clock of higher than 32 kHz is desired. The effect of the mechanical coupling of the Fast Tool and the Slow Tool can be reduced by a control oriented feed forward decoupling which is parallel to the feedback controls of the axes. The control clocks should be chosen multiples of each other to facilitate such an implementation.

Compensation strategies which are slow in terms of the mentioned control clocks, for geometrical or thermal deviations can be implemented with a significantly slower clock then the control loops. Depending on the mathematical complexity, these algorithms are implemented in the microprocessor based part of the system.

7.4.1 Servo Control Algorithms

To close the position control loop in the servo amplifier, the cascaded P/PI control algorithm, depict in **Figure 7.9**, is applied. The input signal of the position controller is the position error, the difference from the interpolated position measurement and the position setpoint. The pre-control in the feed forward control branch of the setpoint adjusts the amplitude and the phase of the control system by means of the inverse transfer function of the closed loop.

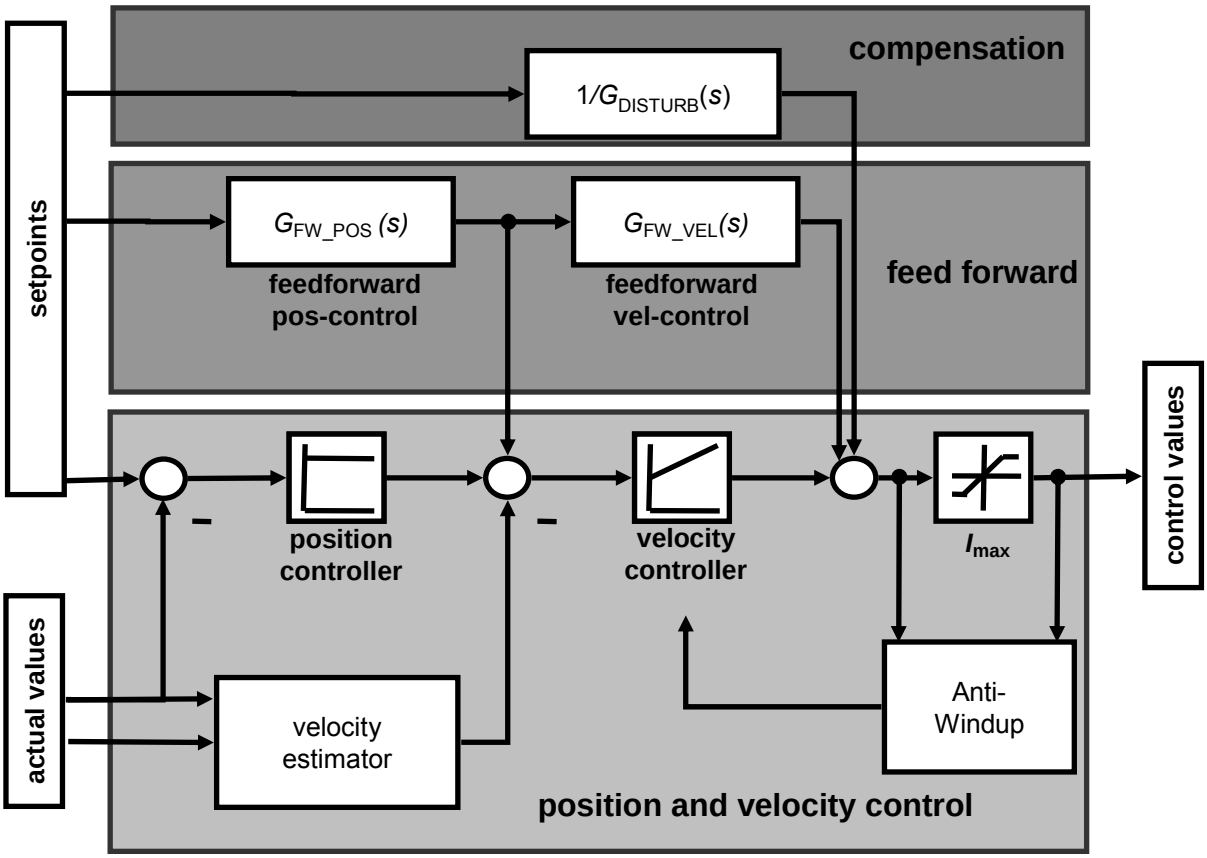

Figure 7.9: FT/ST servo control system – block diagram of the control algorithm

In the case of the Slow Tool control, the velocity estimator is realized by an observer structure which computes the current velocity from the acceleration proportional electrical current of the voice coil and the actual position from the interpolated glass scale signal. A velocity signal can both be calculated by integrating an acceleration or by differentiating a position signal. While the dominant error resulting from the integration is in the low and quasi-static frequencies, differentiations turn out to be noisy in the high frequencies. The observer mixes the signal in the frequency domain. A time constant determines a cut-off frequency which separates the frequency ranges for the acceleration and the position signal with a transition frequency range for a smooth switch. **Figure 7.10** shows the improvement achieved by the velocity observer. The velocity gained from just differentiating the position signal contains much more noise than the velocity signal obtained by the observer. The drawback of the observer is the additional phase decay visual in the figure as delay in the signal. Even so, the dynamic effect onto the position control bandwidth is negligible for the Slow Tool system.

The velocity error, that is calculated by subtracting the output signal of the position controller and the actual velocity from the observer, serves as the input signal of the PI velocity controller. The output signal of the velocity controller is restricted to the output range of the output stage's input signal. The AntiWindup circuit detects a saturation of this signal and inhibits further increases in the integral part of the velocity controller which would lead to instabilities of the control loop. To prevent an algebraic loop, the calculation of the AntiWindup is delayed for one control clock.

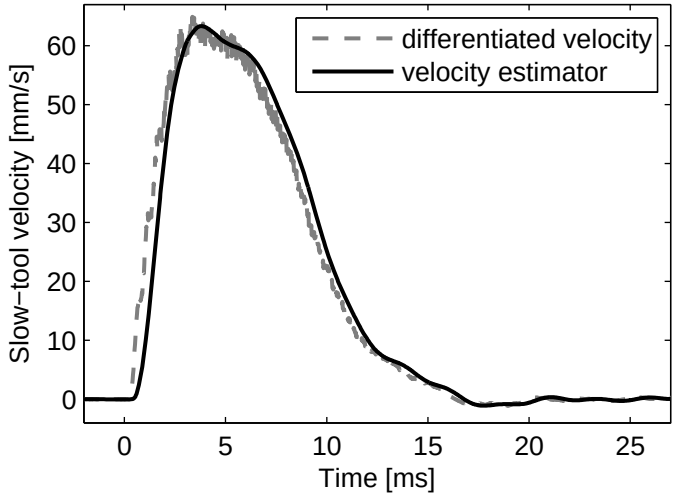

Figure 7.10: Comparison of differentiated and estimated velocity (Slow Tool)

7.4.2 Operating Area of the Axes

The Slow Tool Axis' area of operation is upper-bounded by position, velocity, acceleration and jerk limits. The individual limits are shown in **Figure 7.11** in a double logarithmical plot displaying the maximal frequency for each amplitude of stroke.

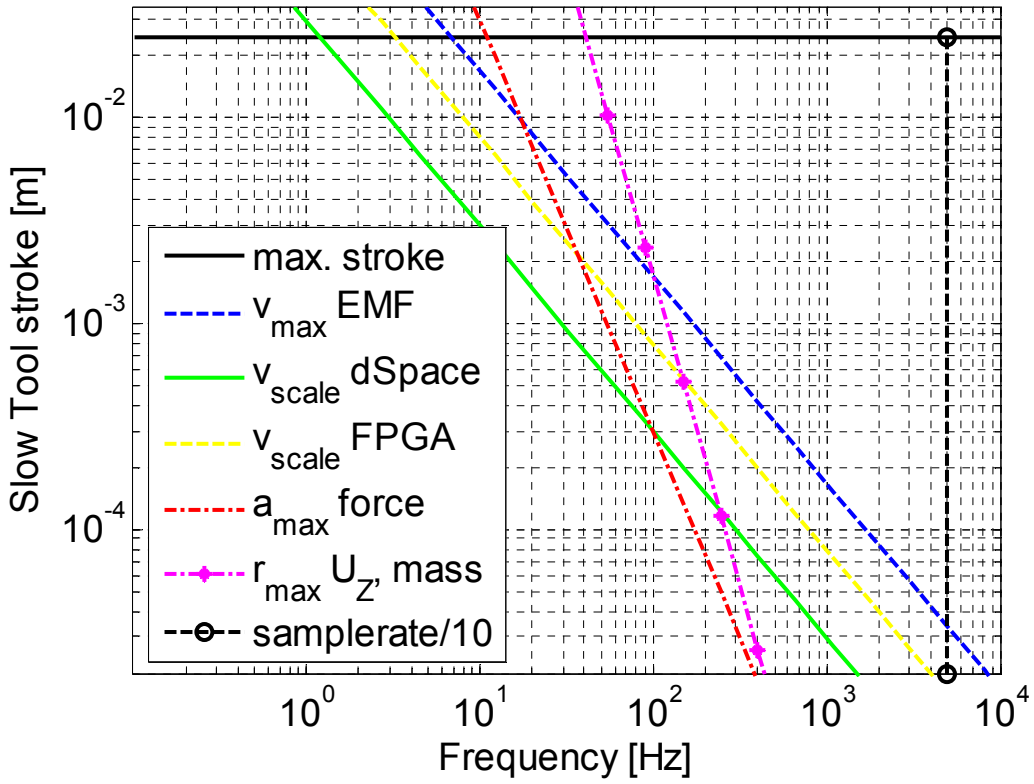

Figure 7.11: Slow Tool – area of operation

The dead stop positions of the axis constrain the area of operation with a hard boundary at 25 mm. The bandwidth of the cascaded position control loop is a soft boundary. Using a position control clock of 50 kHz, it is estimated one decade below at 5 kHz. The applicable maximum velocity results from the division of the glass scale r = 250 nm which is used for position measurement and the bandwidth of the

interpolation circuitry of f_{Int} = 700 kHz in the case of the prototyping dSpace system and f_{int} = 2 MHz in the case of the FPGA interpolator module to

$$v_{\max} = r \cdot f_{\text{int}} = \begin{cases} 175\,\frac{mm}{s} \\ 500\,\frac{mm}{s} \end{cases} \text{ for } \begin{matrix} f_{\text{int}} = 700kHz \\ f_{\text{int}} = 2MHz \end{matrix} .$$

The velocity limit resulting from the back-EMF plotted in the diagram is covered by the velocity limit resulting from the linear scale interpolation and, thus, can be neglected. The maximum amplitude of the stroke at sinus excitation

$$s_{\max}(f) = \frac{v_{\max}}{2\pi f}$$

is shown for both scale divisions in Figure 7.11. At the maximum amplitude of 25 mm, the frequency range of the dSpace prototyping system is 1 Hz. Higher dynamics with a frequency range up to 3 Hz at the same amplitude need the FPGA interpolator module with f_{int} = 2 MHz. The maximum acceleration of the highly dynamic axis is dependent on the power dissipation of the motor which mostly consists of ohmic loss and, Hence, is a quadratic function of the current. The nominal force of the voice coil of F_N = 605 N determines the maximally possible continuous acceleration. With the moved mass of m = 10 kg the maximum frequency-dependent amplitude in stroke can be calculated to

$$s_{\max}(f) = \frac{F_{\text{N}}}{m \cdot (2\pi f)^2} .$$

In lower frequency ranges, the amplitude limitation is dominated by position and velocity constraints. The limitation of the dynamics, resulting from the continuous maximal power consumption of the motor, turns out to be significant for frequencies up from 100 Hz regarding the dSpace prototyping system or 40 Hz regarding the FPGA system. A duplication of the frequency maintaining the same amplitude of stroke would mean the 16-fold increase of power according to $P \sim F^2 \sim f^4$, which points out the power dissipation P derived from the necessary force F for a frequency f of a harmonic excitation. The final considered boundary in Figure 7.11 concerns the jerk j of the axis which is dependent on the intermediate circuit voltage u. The dependencies for the jerk can be deduced from

$$u = L \cdot \frac{\partial i}{\partial t} + R \cdot i - k_{\text{EMK}} \cdot v \quad \text{with} \quad j = \frac{\partial a}{\partial t} = \frac{k_{\text{MOT}}}{m}$$

with the inductance L and the resistance R of the coil, the force constant of the motor k_{EMK} and the current i. Setting the velocity v and the current i to zero in the initial state and in the reversal points of a sinus excitation, the maximally possible jerk of the axis appears with the maximum voltage. The maximum jerk j then can be calculated to

$$j_{\max} = \frac{k_{\text{MOT}}}{L \cdot m} \cdot u_{\max} .$$

Applying a force constant of $k_{MOT,ser}$ = 104 N/A and a motor inductance of L_{ser} = 3.2 mH for a serial connection of the coil windings and using a maximal intermediate circuit voltage of u_{MAX} = 110 V lead to the jerk boundary charted in Figure 7.11, which turns out to be the significant boundary for frequencies from around 500 Hz. To increase the dynamics, the coil is separated and connected in parallel.

Summarized, the dynamics of the axis controlled by the FPGA system is constrained by the mechanic stops in the quasi static frequency range. From 3 to 30 Hz the amplitude of the stroke is restricted by the maximal velocity to 2 mm. The maximum force which results from the maximum power is the dominating constraint up to 500 Hz. Only beyond 500 Hz effects from the maximal jerk become significant.

7.4.3 Control Parameters and Measurement Results

The velocity estimator and the feed forward control applied, the Slow Tool axis shows the transfer behavior of the position that is shown in **Figure 7.12** for small signals. The cut-off frequency which is defined as the frequency at the phase crossover at 90° lies between 40 and 60 Hz without pre-control. The pre-control filter is derived from the closed-loop position transfer function and enhances the frequency response behavior of the axis. The filter is based on the low order poles and zeros of a simulation model which is matched to the measured frequency response of the axis. The filter is stabilized by adding a sufficient number of poles in the higher frequency domain. The cut-off frequency with pre-control is increased to 100 to 200 Hz. The measurement shows good coherence of the measured input and output signals.

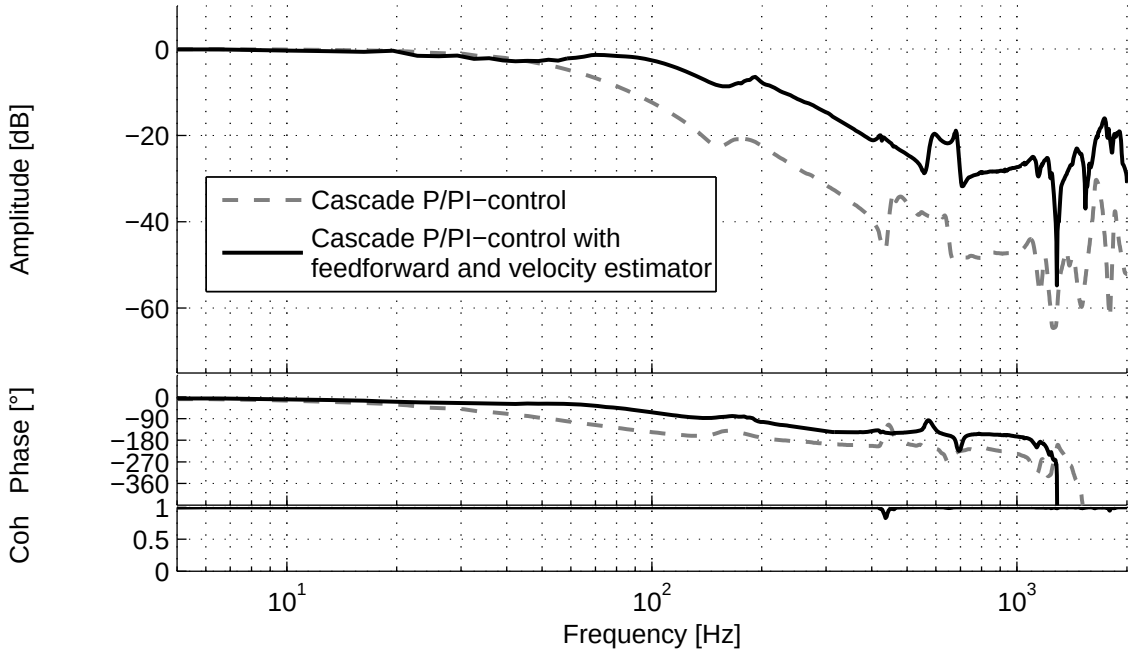

Figure 7.12: Slow Tool – transfer behavior of the position control loop

The control algorithm for the Fast Tool also uses a feed forward pre-control filter. Additionally to the standard PI controller a notch controller was tested. **Figure 7.13** shows the position transfer behavior for small signals for the different configurations.

The cut-off frequency as criteria, the notch control has no clear advantage. At least the amplitude curve shows a better performance than the standard PI control. With the feed forward pre-control filter the cut-off frequency is increased from around 450 Hz to around 1 kHz. Up to 2 kHz the measurement shows a good coherence of the input and output signals. The bad coherence beyond 2 kHz results from the mechanic eigenfrequencies in this range.

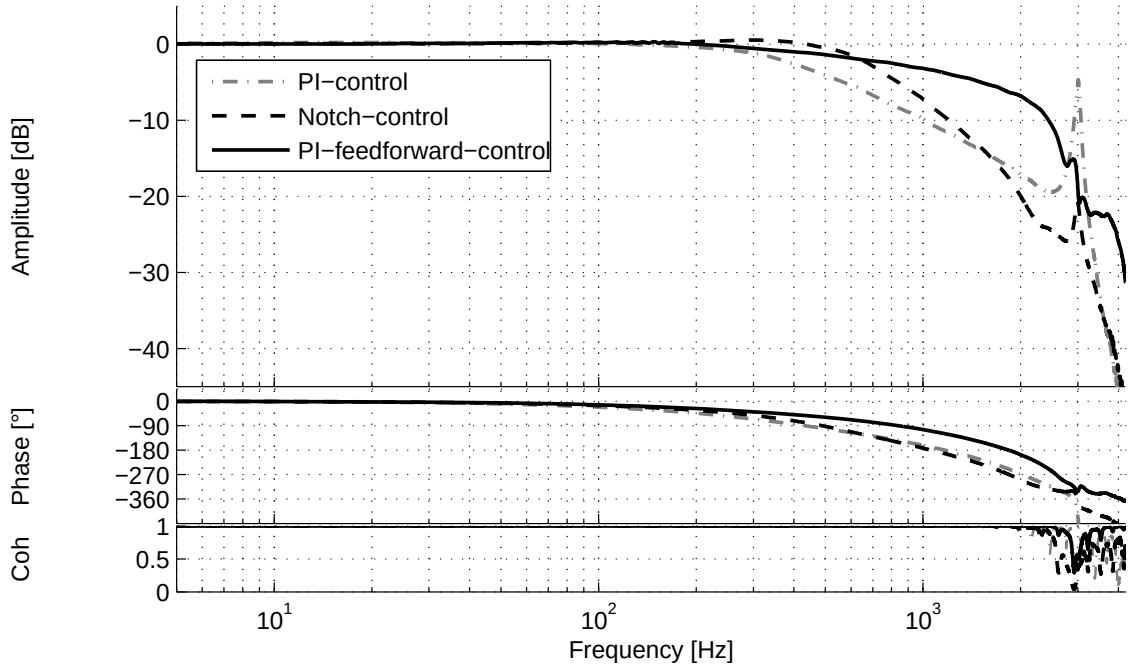

Figure 7.13: Fast Tool – Transfer behavior of the position feedback control loop

Figure 7.14 shows the derivation of the feed forward control with the intermediate data needed. The shown frequency response (measured frequency response) is measured with a sine signal with a linearly ascending frequency and a hyperbolically descending amplitude. This signal stimulates all frequencies in the desired band width. The measurement is transformed from the time domain to the frequency domain with the aid of the H1/H2-method for transfer behavior which bases on the power density spectrum of the input and the output signal. While the H1-method minimizes noise on the input, with the applied H2-method the output noise is minimal. The coherence signal shows the significance of the measurement regarding the correlation of the input and output signals.

Using the real system's frequency response, the parameters for the linear model of the Slow Tool and the Fast Tool, shown in the diagram, are verified and corrected. The accuracy of the frequency response of the system with the estimated model parameters relating to the measured curve is quantified with the weighted squared discrete error sum

$$e(b_i) = \sum_{\omega=0}^{\omega_g} \alpha(\omega) \cdot (\Delta A^2(\omega, b_i) + \Delta\Phi^2(\omega, b_i))$$

with the differences of the amplitude A and the phase Φ which are functions of the angular frequency $\omega = 2\pi f$ and the parameters of the estimated linear model b_i. The

square function is preferred to the absolute function, due to the fact that it is not singular in the zero-point. The weighting factor α allows for measuring the estimation error for the model parameters differently in designated frequency ranges. The endpoint of the summation of the error is the cut-off-frequency of the measured system ω_g.

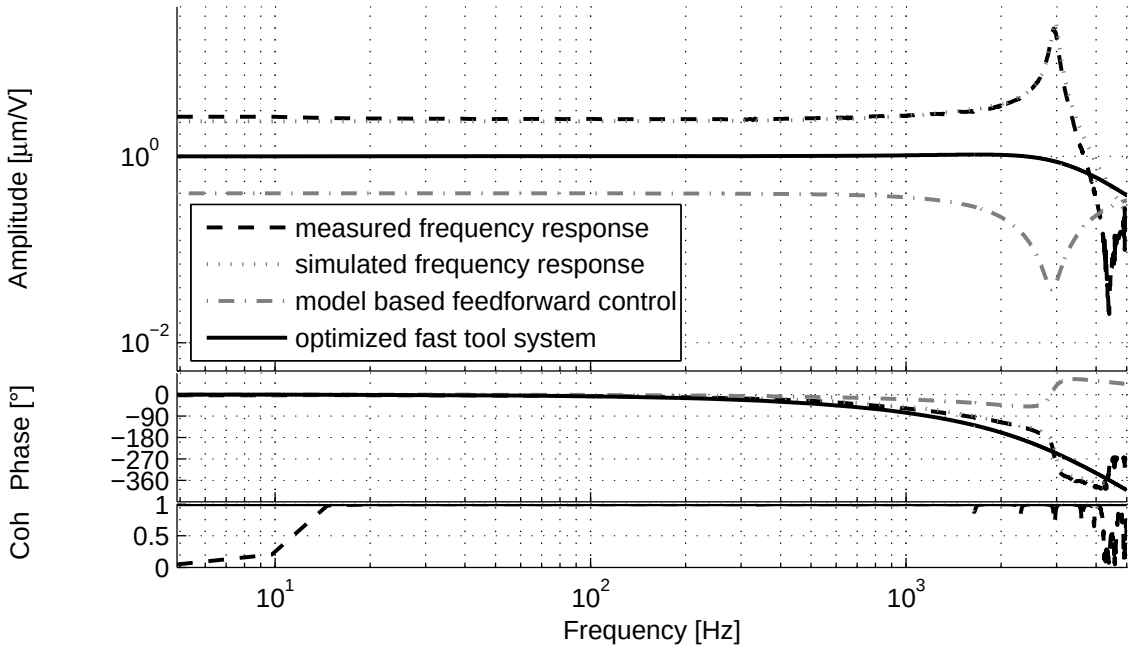

Figure 7.14: Fast Tool – designing feed forward control

The model parameters are tuned automatically with an optimization algorithm based on Newton's method with the error function $e(b_i)$ as objective function. The minimum of the function is found with the iteration step containing the gradient and the Hessian of the error $e(b_i)$

$$\delta_i = -H^{-1}(b_i) \cdot \nabla e(b_i) \text{ with } H(b_i) = \nabla^2 e(b_i)$$

which results from a Taylor approximation truncated after the second term. δ_i points to the minimum in the multidimensional room spanned by the parameter vector b_i and is used for the update for the next iteration step applying

$$b_{i+1} = b_i + \beta \cdot \delta_i ..$$

The weighting factor β which is found with a linear search stabilizes this iteration step. With appropriate starting points, the algorithm converges super-linear in the surrounding area of the minimum value. Though, the stability of a pure Newton algorithm depends heavily on the preset starting point of the iteration b_0. To produce a feasible starting point for the Newton algorithm from suboptimal starting points, a simplex algorithm which converges maximally linear, but is generally more stable, with parameter values more distant from the minimum point is used in a pre-process.

The model based feed-forward control filter is derived from the simulation model of the transfer behavior of the closed loop system by inverting the model, and adding a

low pass filter with a sufficient order. The resulting filter is shown in Figure 7.14 as *model based feed forward control*. The optimized transfer behavior of the response to position setpoint changes with the filter applied, shows better amplitude characteristics. Due to the low pass filter needed for the feed forward control, the phase has a higher decay in the range of the resonance frequency compared to the original system. The disturbance reaction of the control loop is not affected from this extension.

The standard deviation of the position resolution in quiescent state for the Slow Tool is 2 nm and for the Fast Tool is 7 nm (see **Figure 7.15**, right). This value is a good measure for the noise in the system accounting for the resulting surface roughness of the work piece. Machining experiments with the introduced control parameters in deed show that the surface roughness on the work piece with 5 nm Ra was in the range of the values measured in the control system.

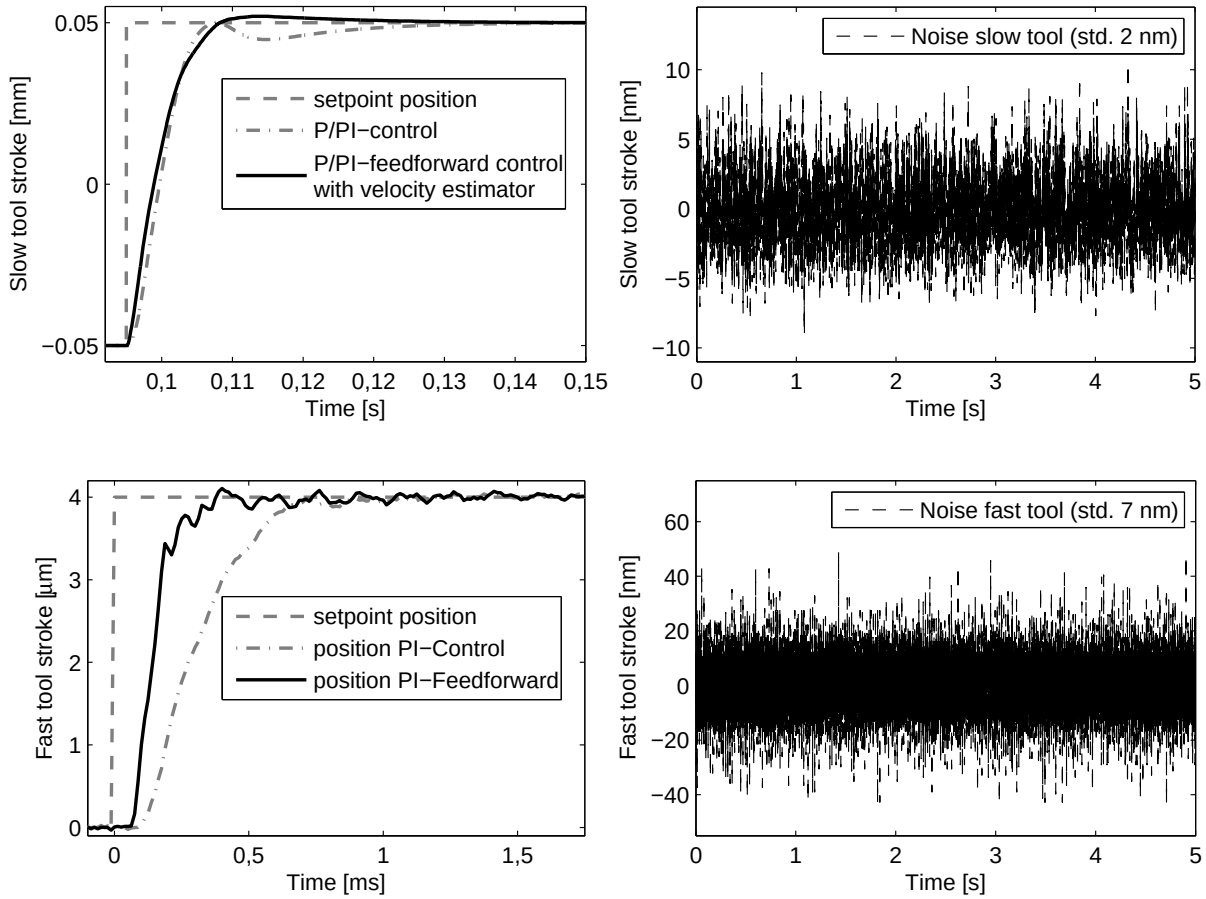

Figure 7.15: Step response and position noise

The figures on the left show the step responses of the two dynamic axes. It is clearly visible that the feed forward filter improves the positioning behavior. Regarding steps, the Fast Tool system due to the lower damping capability of the mechanical design, is more susceptible to vibrations caused by mechanical eigenfrequencies.

8 Data Processing and Graphical User Interface

The hybrid FTS offers a lot of new machining possibilities. Hence, the tool path programming of hybrid optics is getting more complicated. Therefore, an easy to handle human machine interface is needed. The user interface needs to support the regular data formats used to encode surface information in industrial environments. In contrast to spherical and rotationally-symmetric geometries, data processing for non-rotationally symmetric geometries and free-form surfaces as well as microstructures can prove to be fairly complex. To avoid interpolation errors resulting from transformation between different data formats, the concept is to modify the geometry data given from CAD as little as possible. Especially in the case of free-form geometries this concept is far from the traditional CAD/CAM chains, where the surface data is transformed into curve trajectories in a very early step of the machining process. Free form geometries encoded in NURBS (Non Uniform Rational B-Splines) are directly processed by the Fast Tool Servo system and are not modified in the CAM step to inhibit such interpolation errors. In addition to their ability to describe smooth free-form surfaces with a minimum number of coefficients, the mathematical description of NURBS is capable to represent structured geometries with sharp edges in a closed form without the need to include explicit case differentiations into the data format.

8.1 Geometry Data

In the CAM process geometry setpoint data is separated into curve-based trajectory data for the basis machine axes and surface-based geometry data for the dynamic axes. While lower order surface-based geometry data is represented in a polynomial representation, higher order surface-based geometries or free-form geometries are represented in NURBS or the data format used in CAD. **Figure 8.1** shows the data processing for free-form geometries using a demonstrator geometry. The low order part of the surface with a total stroke of 0.5 mm is realized by the low dynamic Slow-Tool system and the high order part with a total stroke of around 20 µm is done by the FTS.

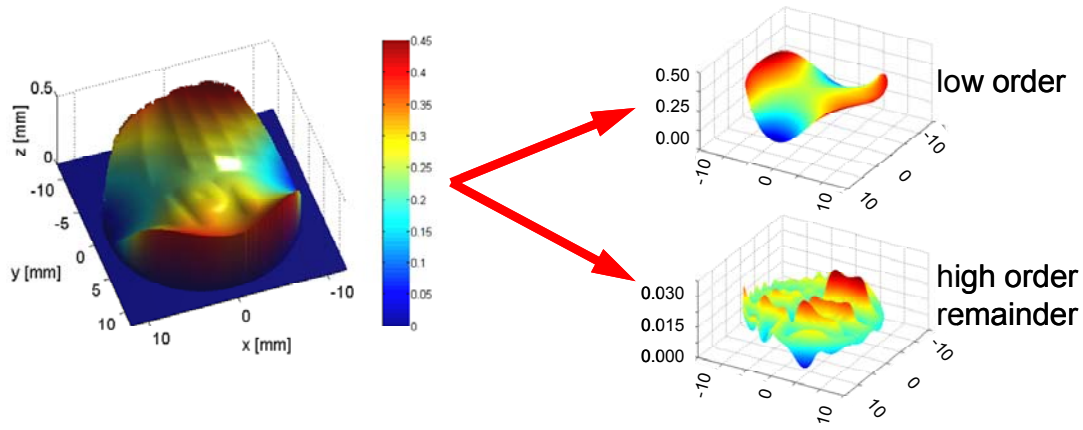

Figure 8.1: Surface based geometry splitting

To support the machine operator, the machine interface integrates simulation and analysis methods which check and verify the manufacturability of the geometries and structures according to the given tools and process parameters. This check includes the simulation of the dynamic behavior of the axis system in terms of control. The optimal setpoint calculation satisfies a compromise between the achievable surface roughness and form accuracy. The control parameters are directly updated with actual parameters from the machine system's control chain to support the dynamic simulation. The dynamic behavior of the machine includes the simulation of following errors resulting from the dynamic behavior of the axes. Geometrical effects from different tool geometries are also simulated, either in the case of continuous surfaces which are machined with radius tools and in the case of structured surfaces which can be manufactured with structured tools. The simulation presents the resulting surface geometries in a 3D view to allow the machine operator to recognize errors from the manufacturing process at an early stage.

8.1.1 Data Formats and Transformations

The mathematical representation and the data format of setpoint geometries in most cases is determined in the design process. The characteristics of the setpoint data handling in the machining process of the work piece or the molding tool are often not considered in the selection of the setpoint representation. Most machine tools need a machine internal preprocessing where the setpoints are converted into a data format which can be processed by the machine control system. These conversions not only include the encoding of the setpoints in a specified data format like IGES (Initial Graphics Exchange Specification) or STEP (Standard for the Exchange of Product model data), but particularly the mathematical representation. Machine control system usually cannot process surface geometries directly. Hence, these geometries are transformed into one-dimensional curves or even clouds of discrete ordered points. If required, interjacent information is interpolated in a later step to retrieve acceleration, velocity or even position continuity.

This type of data processing chain which is the standard accumulates interpolation errors and deviations in every transformation step and can result in significant errors at the end of the chain depending on the complexity of the original setpoints. In conventional machining systems, these interpolation errors disappear partly in the permitted tolerances of the workpiece geometries and partly in the surface roughness. In ultra-precision machining of free-form geometries, the transformations contained in the data processing lead to significant errors in form accuracy and surface roughness on the work pieces. On the one hand these errors result from the interpolation errors themselves. On the other hand the loss of mathematical continuity in higher orders leads to dynamic errors in the control loops of the axes. Especially, losing continuity of the slope (1^{st} order) influencing the axis velocity as well as the curvature (2^{nd} order) regarding acceleration proves to be a critical issue for the Fast Tool and Slow Tool axes. Discontinuous geometries due to physical limits cannot be followed by the axis kinematics which leads to dynamic errors in the

axis position. Finally, these correlations lead to higher surface roughness or form errors on the machined work piece.

8.1.2 Handling Geometry Data

In the scope of the project »ERANET-OPTICALSTRUCT«, several strategies to display and process setpoint geometries were developed with the objective to eliminate or at least reduce the impact of setpoint transformations onto the machining accuracy. The basic philosophy for all these strategies is to modify the specified mathematical geometry description, provided by the design process, as little as possible. At the best, the original geometry representation can be retained deeply in the hierarchy of the control layers down to the servo control system of the highly dynamic axes. For free-form geometries, which are mathematically specified by an optical design process as NURBS, an evaluation algorithm was developed. This algorithm is able to process such kind of surface information in realtime, which is required by the servo system. By directly accessing the original information no transformations are necessary in the geometry processing chain.

For the turning production of free-form work pieces enabled by highly dynamic axes moving the diamond tool, in the CAM process the geometry usually is split into a rotationally symmetric (rs) part for the basis machine and a non-rotationally symmetric (nrs) part for the highly dynamic axes, like it is shown in **Figure 8.2** on the left side.

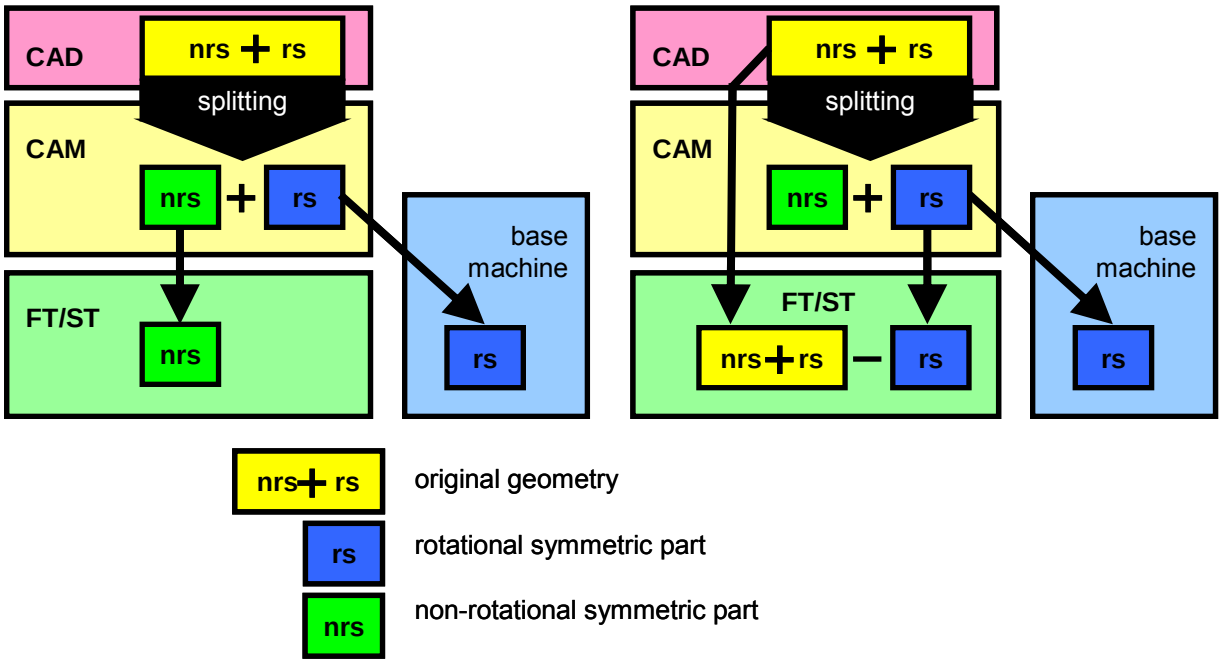

Figure 8.2: Strategies to prevent interpolation errors while processing free-form geometries in the CAM (Delayed Splitting Method)

The rotationally symmetric part can pretty exactly be represented as one-dimensional curve. Yet, the non-rotationally symmetric remainder in most cases cannot be exactly represented with NURBS, hardly ever with the same number of coefficients. The solution to this problem is to represent the non-rotationally symmetric geometry part analytically as a difference of the original geometry and the rotationally symmetric

part. With this approach, the geometry can be represented exactly. The geometry flow to be implemented in the control system is shown in Figure 8.2 on the right side. Unlike the rotationally symmetric part, the non-rotationally symmetric part is not explicitly calculated in the CAM process, but transferred implicitly as the mentioned difference to the FT/ST servo control system. The real calculation of the difference is done, when it is needed during the machining process (Delayed Splitting Method). The important difference of both methods is the mathematical representation of the calculation result. In the CAM, the explicit difference would need to be calculated for the whole surface geometry with the result of a new surface. In the FT/ST servo control system it is sufficient to calculate the difference point-wise in the servo control clock without interpolation errors and without significantly higher computation costs.

Another difficulty, when processing setpoint geometries provided by the mechanical or optical design, is the heterogeneity of the data formats and mathematical specifications common in these domains, especially regarding free-form geometries and structured surfaces. Particularly, in the optical design setpoint geometries often are defined by mathematical functions. In the majority of cases, these functions can be specified by an explicit dependency of the component of the surface geometry in Z-direction from two coordinates in the orthogonal X/Y- or X/C-plane. However, implicit surface specifications like NURBS are popular, where the Cartesian points on the surface (X,Y,Z) depend on two parameters (u,v), which span the surface. The direct analytical inversion of the surface specification as function Z(X,Y) in this case is not possible in general.

At least onto the case of an explicit geometry specification, the information technology oriented paradigm of abstraction and encapsulation can be applied. Among others, functions implemented in C or Simulink used in older Fast Tool Servo Systems are examples for explicit geometry specifications. Using abstraction and encapsulation provides a uniform interface for functional units which use and process the geometry information. Furthermore, this technique enables the construction of objects as a composition of other objects to avoid explicit computations, which contain irreversible interpolation errors.

Figure 8.3 shows the implementation of this method for the setpoint generation in the CAM and the simulation. The geometry data is encapsulated in an ADE object (Abstract Data Encapsulation) and can alternatively be utilized as shared library (e.g. Microsoft Windows DLL – Dynamically Linked Library) or over a LAN connection with an RPC (Remote Procedure Call) protocol (e.g. SOAP – Simple Object Access Protocol). To provide a uniform interface, ADE provides geometry access functions like z(x,y) as well as get and set functions for parameters and settings. Supporting the SOAP protocol optionally to the DLL interface allows for connecting remote geometry processing systems to the CAM and the simulation. This technique allows for directly embedding the setpoint geometry processing of the FT/ST servo control system into the simulation processes of the CAD/CAM tool. The direct calculation of the setpoints during the CAD/CAM process in the servo control system provides the opportunity to early recognize deviations or errors in the implementation of the

setpoint algorithms themselves. Deviations may occur due to varieties of the computational hardware, the software libraries or the compiler. The described setpoint processing strategies were implemented as software modules by the IPT and are integrated into the development of the CAD/CAM tool and the GUI (Graphical User Interface).

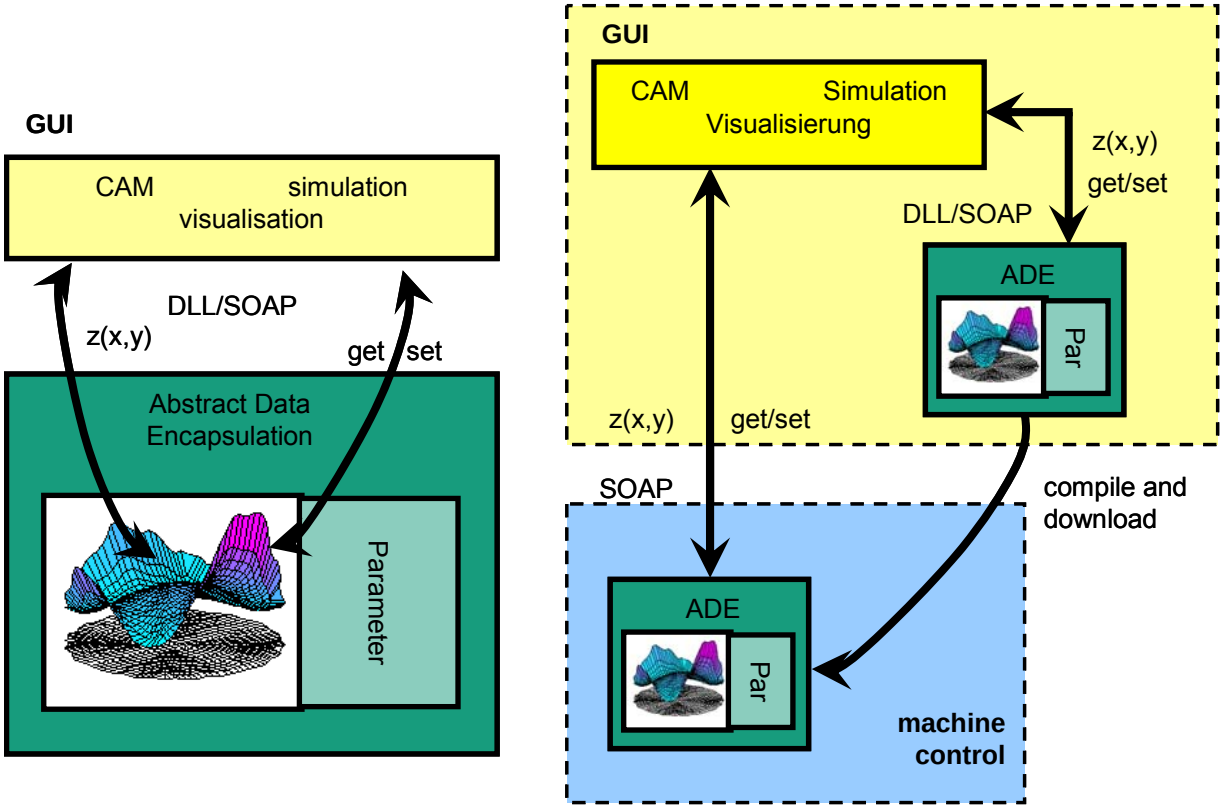

Figure 8.3: Using abstraction and encapsulation to handle setpoint geometries

With the experiences gained in the project »ERANET-OPTICALSTRUCT« regarding the process chain for manufacturing optical surfaces with free-form geometry and structures a specification for a geometry data processing system with a graphical user interface (GUI) was created. The different modules shown in **Figure 8.4** are partially implemented by ModuleWorks and partially implemented by Fraunhofer IPT: These modules contain libraries for processing, visualizing and simulating geometry information and communicating with the machine control. The internal system data like geometries, axes or machine cycles are consistently stored in extendable list structures.

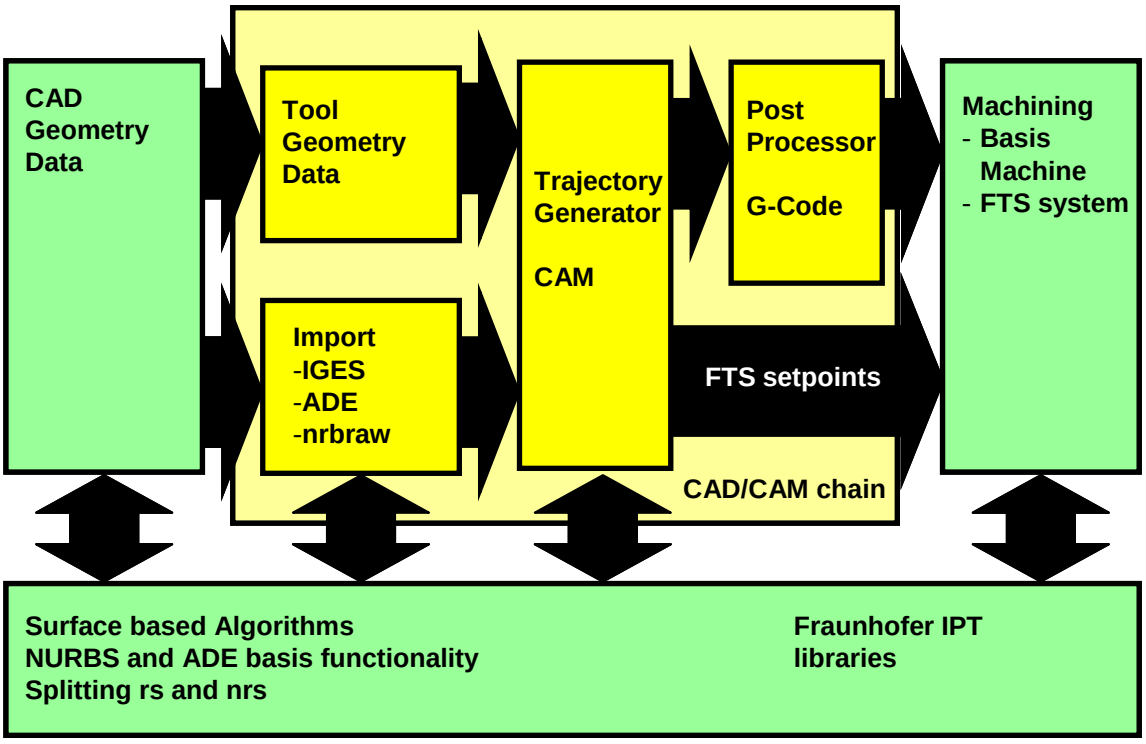

Figure 8.4: Geometry data processing chain

8.2 CAD/CAM Chain

The output of the CAD/CAM chain has to describe the actual tool path and the needed process parameters in such way that both the manufacturing quality and a maximum of productivity is reached. Therefore, each production process has its own needs and constraints for the CAD/CAM chain. The chain for the ultra precision turning process is different to other CAD/CAM chains like the chain for a milling operation. The two main differences are the way of how the surface which should be produced is described and the influence of the CAD/CAM chain on the main tool movement pattern.

The CAD part of the current established CAD/CAM chain of the ultra precision turning process describes the surface to be machined either as a set of asphere formulas or as an implied radius-angle formula (look-up table). This means that the CAD part is less a design than a programming part due to the lack of an intuitive surface description. Current ultra precision turning CAD/CAM systems only have a poor or no support of NURBS surfaces which will lead to a more intuitive surface description. Therefore, one goal of the »ERANET-OPTICALSTRUCT« project was to implement a CAD/CAM system that is able to compute tool paths on arbitrary NURBS surfaces, such that the design of the surface to be machined can be done by a standard CAD program. Current ultra precision turning CAD/CAM systems do not directly support the structure description files by Modines. Therefore, a lot of human interaction is needed to manufacture them. So, a strategy has been implemented in the CAM system to support all needs for manufacturing the structures with as less

human interaction as possible. Instead of just following the coaxial circles given by the structures itself, a de-burring strategy was implemented to get a high surface quality.

Supporting arbitrary NURBS surfaces for the ultra precision turning process is a big challenge. The main issue is the quality of the CAD system output. Certainly, it describes the surface to be machined in a defined tolerance, but in general, the output is not a single surface but a set of surfaces or a surface patch. Having a set of surfaces means that the CAM system has to deal with defective data. There are gaps and intersections between surfaces or the surface orientation might flip. This is a big difference and disadvantage compared to until now used asphere formulas and implied radius-angle formulas because the surface is no continuous surface anymore. One approach to solve this problem is to just sample the given surface but this will lead to a huge amount of data and the problem of the gaps is still not solved. Therefore, it was decided to do the whole tool path computation directly in NURBS. Because tool paths are created for a turning process it can be assumed that there is always a midpoint of rotation. Starting from this midpoint, a line segment is projected along a certain angle on the surface. Doing this in circular manner several times leads to a kind of star shape. If each projection result is interpreted as a curve which lies in plane, the normal vector will have no z component. By displacing the curve in z-positive direction by the tool radius two needs are achieved at once: the tool radius compensation and the small gaps are closed automatically. Taken the displaced curve as a guide curve of the tool center point, the tool path points can easily be created by translating them by the tool radius along the negative z-axis. **Figure 8.5** shows a sample with projected line segments and their offsets. The beginning of the star shape also can be recognized.

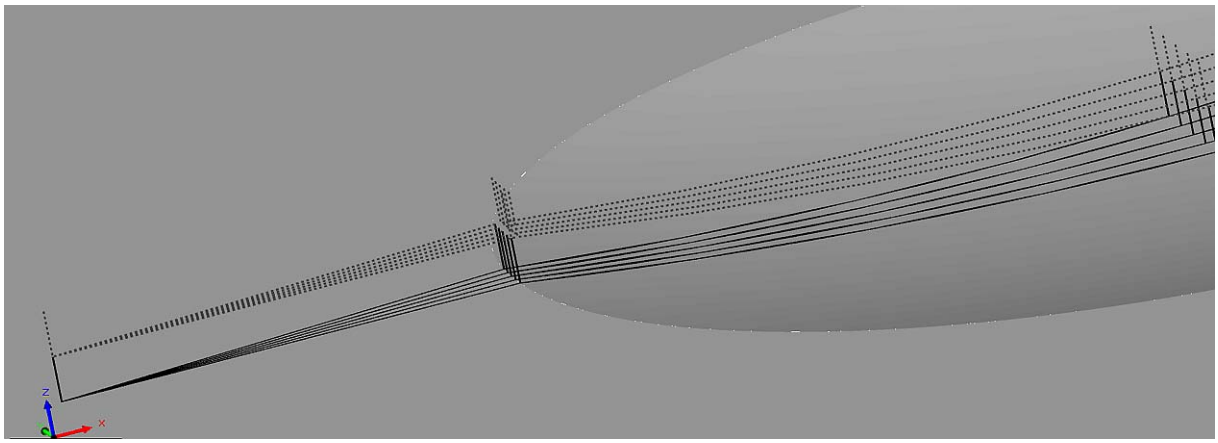

Figure 8.5: A sample part with the projected line segments (solid black) and their offsets (dash grey)

To improve both the programming and the surface finishing quality, a new base machine strategy with de-burring capabilities was implemented for Modines structure description files. The main tool path pattern is already given by the structures themselves because they lie on several coaxial circles. While machining these structures, the machine has to turn at each radius of a circle several times because otherwise it is impossible to reach the depth of a structure at once. Instead of just

following the radius of each circle, the algorithm starts with a bigger radius and reduces it with each depth step, such that the tool movement looks like an upside down cone. Simultaneously, the infeed speed is verified, until it reaches a user given depth. While the first part of the grove is machined with a (higher) so called roughing infeed, for the last micrometers a (lower) finishing infeed is used. By this, both a minor machining time and a better surface quality can be reached. **Figure 8.6** shows the upside down cone formed by the base machine structure tool path. The cone starts at a higher level at an outer radius and smoothly decreases the radius until the final radius and level is reached. The variations in infeed values used for roughing and finishing can be seen at the different distances of the different z levels of the toolpath becoming smaller with a lower z component.

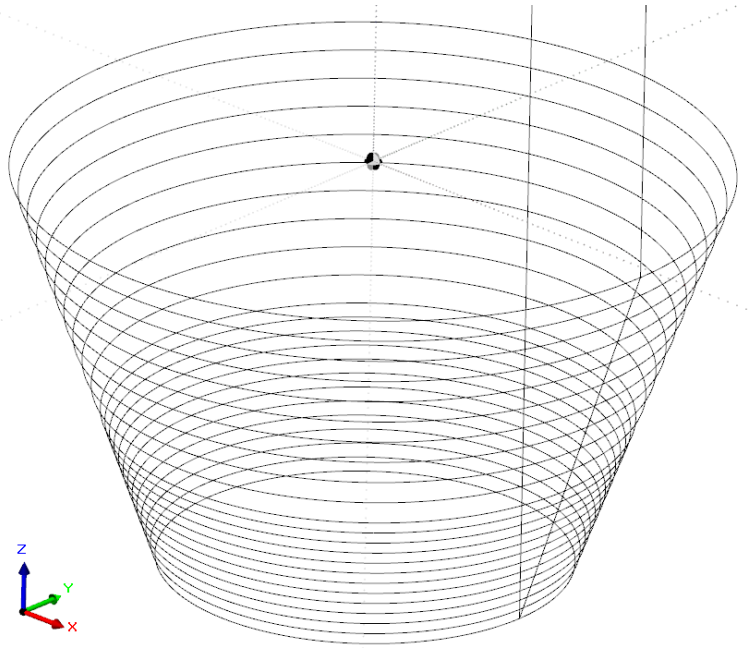

Figure 8.6: The upside down cone formed by the base machine structure tool path

8.3 Graphical User Interface

Instead of using a standard CAM integration into a common CAM host application, it was decided to implement an own user interface, to be able to integrate the software directly into the control of the machine. The target system was a constraint for the definition of the development platform. The basic implementation of the algorithms was done in C++ under Microsoft Visual Studio 2005. The open source alternative wxWidgets was used for the implementation of the graphical user interface (GUI) itself. The wxWidgets library provides an easy way to develop a lean interface with a high amount of controls, which does not follow classic document view paradigms, without spending the majority of the time budget on creating and connecting user controls. For the 3D views a standard version (1.3) of the OpenGL library was used to achieve a maximum of compatibility.

To achieve a maximum of flexibility and extensibility which is obviously needed for developing a technical prototype, the wxWidgets event handling mechanism was

extended. Therefore, a global event handler is added on the top of the highest wxWidgets event handler. This global event handler distributes all high level events to the whole program. High level events in this context are user interactions regarding logical components of the user interface like machine, geometry or even cycles. To receive such a high level event, a registration has to be done to the corresponding event at the global event handler. This registration is also done by events. For example, the program part, which is responsible for displaying geometries, is registered to the geometry-change-event. When the user selects a new active geometry a geometry-change-event is triggered. This event is forwarded up by the wxWidgets event mechanism to the global event handler, which informs any module which is registered to the geometry-change-event. By this technique it is easy to extend the program. Whenever an extension needs information about the current active geometry it just has to be registered to the geometry-change-event and by this means gets all it needs.

The graphical user interface is a tab based program. All major and sub tasks are organized in tabs. By this decision, the logical steps of creating a tool path cycle are also separated in the user interface. The machine and the to be machined surface are independent from each other. Therefore, they are accessible through different tabs, namely Machine and Geometry. In the following, some screen shots of the user interface are shown and explained. **Figure 8.7** shows the start up screen of the »ERANET-OPTICALSTRUCT« CAM system.

Figure 8.7: The start up screen of the graphical user interface

The tab »Management/Machine« offers the capability to setup the machine which is used for manufacturing. All axes of the machine and their limits can be defined. Linear and rotary axis can be selected and their coordinate naming can be given (see **Figure 8.8**). This machine description is transformed to an input for the ModuleWorks MultiXPost library, which does the actual post processing. Therefore, the here defined machine kinematic together with the computed tool path is needed.

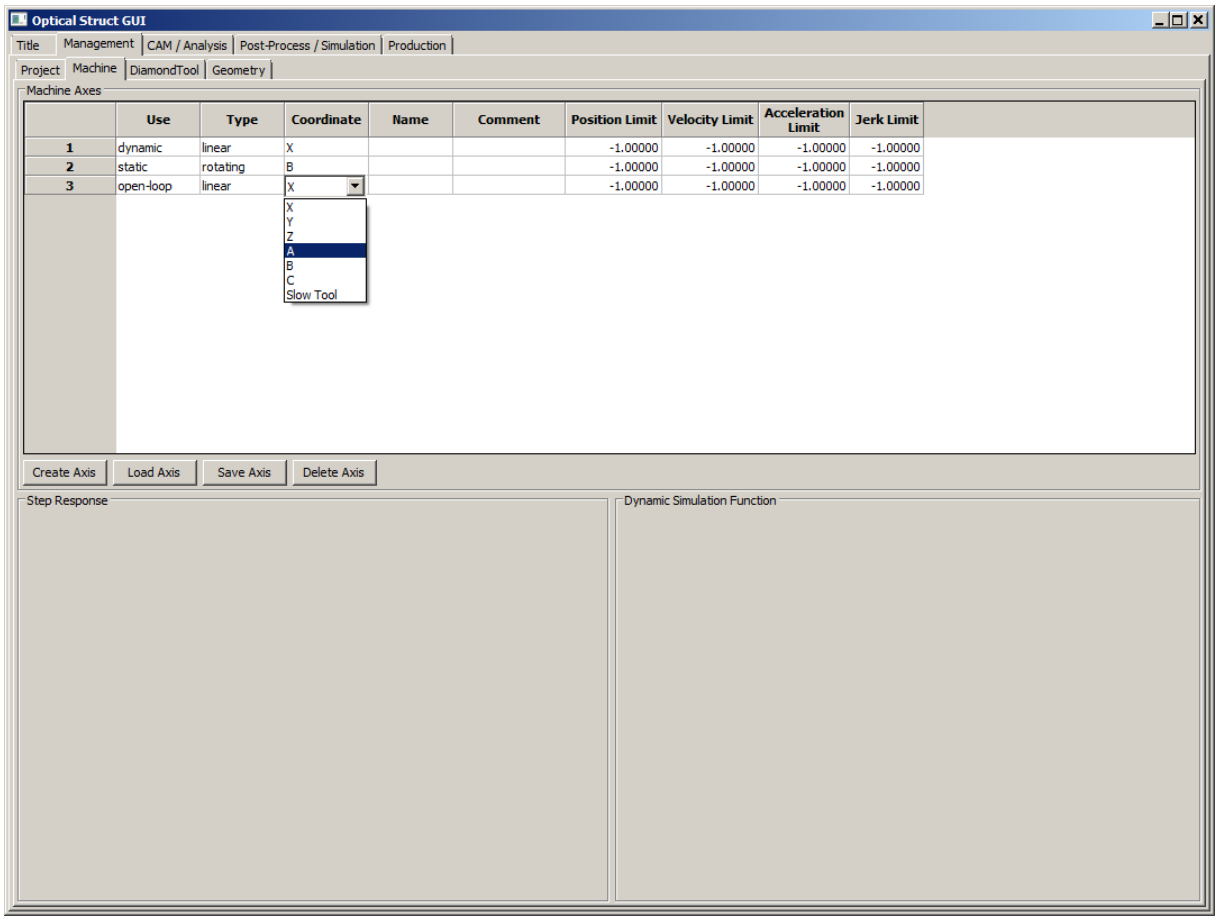

Figure 8.8: Tab Management/Machine

To create a new axis the »Create Axis« button has to be pressed first. By this, a create-axis-event is triggered. The responsible handler catches the event and creates a new default (dynamic, linear, nameless) axis, which will be listed at the end of the grid view. Now the values of the axis can be changed by simply clicking into the corresponding cell. For the properties use, type and coordinate a combo box with the corresponding predefined values will pop up, while all other properties have no limitation in value.

In the tab »Management/Diamond Tool« a tool can be defined by choosing between several types of tools (radius, half-radius, V-shaped or facet) and the clearance types (conical and cylindrical). Naturally, all angles and the radius of the tool can be defined as well. Beside of this, the tool name and a comment can be specified, e.g. »used already 2 times« (see **Figure 8.9**).

A new tool will be created by just pressing the »Create« button. By this a create-tool-event is triggered. The responsible handler will catch the event and create a new default (radius) tool with a unique name (»Tool_X« where X is some number), which will be listed at the end of the grid view. To change the values of the tool, the corresponding row in the grid view needs to be selected. By this all its current values will be displayed in the lower part of the »Diamond Tool tab«. After editing the tool values, the »Apply« button has to be pressed to take over the changes.

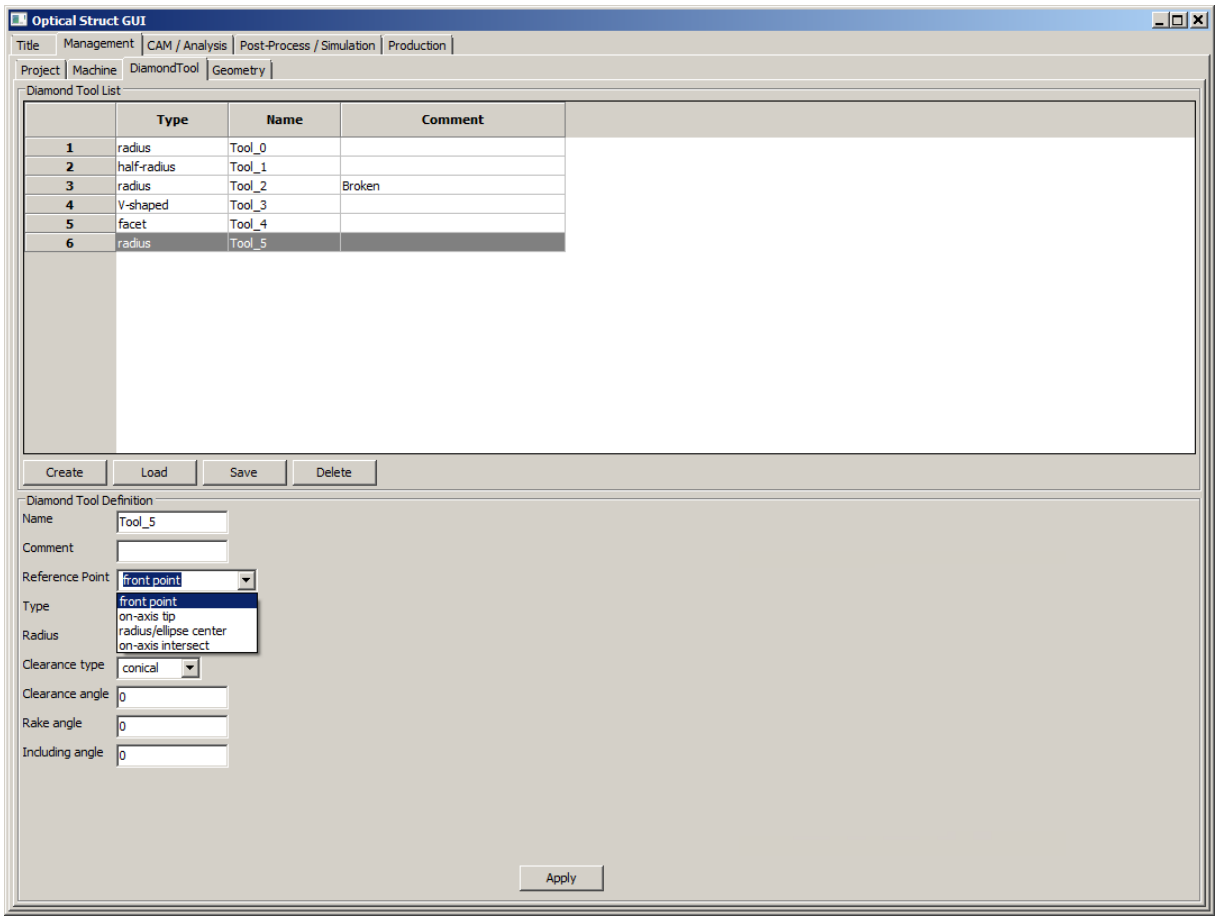

Figure 8.9: Tab Management/Diamond Tool

The tab »Management/Geometry« deals with geometries. Different types of geometry data formats can be loaded and activated for further processing. For easier identifying a geometry, it can be given a name and displayed in the lower right corner in an OpenGL based preview (see **Figure 8.10**).

To add a new geometry to the program the »Import« button must be pressed. By this a standard file browser dialog will pop up and the wanted file can be chosen. The import module supports the formats IGES (Initial Graphics Exchange Specification), an IPT internal NURBS description, the Modines structure format and the Abstract Data Encapsulation format (ADE) defined by the IPT and ModuleWorks. The ADE comes as a dynamic linked library and is capable to handle arbitrary information. Currently, ADE is used to provide a function z(x,c) or a radius/angle lookup table.

Pressing the button »Import« once again triggers an event (import-geometry-event). The corresponding file will be loaded and a new-geometry-event is triggered which forces the corresponding handler to add the new geometry to the end of the grid view, where the values of the geometry can be changed by a simple click into the corresponding cell. The special column »Diamond Tool« provides a combo box, which includes all tools defined in the »Diamond Tool tab«. By selecting a tool it is indicated that the corresponding surface should be machined with the chosen tool.

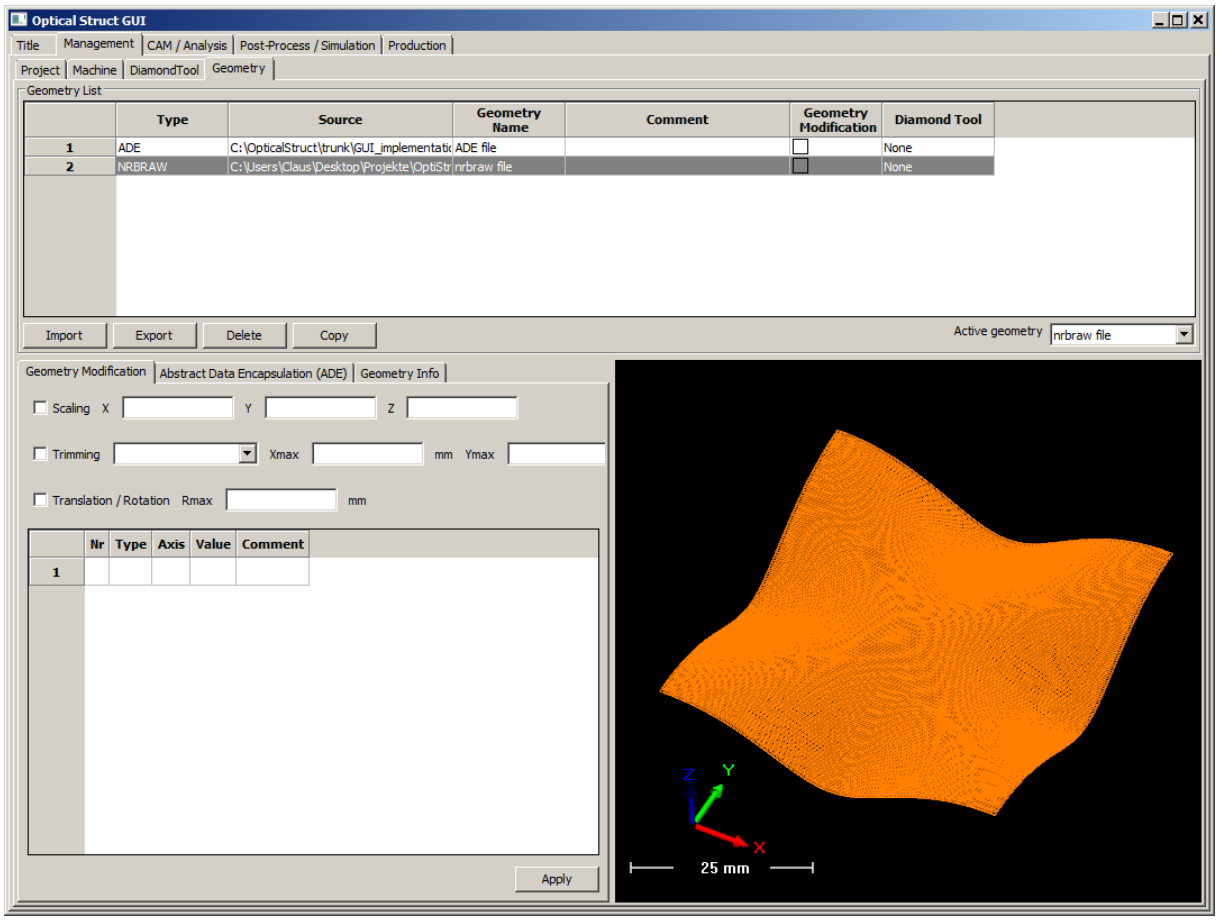

Figure 8.10: Tab Management/Geometry

The tab »CAM/Analysis/Machining cycles« gives the capability to define the cycles to be machined. Depending on the active geometry and the machining strategy, the user can choose between the basic path patterns »spiral«, »coaxial circles«, or »inherited« for Modines structure files where the tool path is implicitly defined by the structure specification. Naturally, all cycle parameters like spindle speed or feed rate can be configured as well (see **Figure 8.11**). When a new cycle is defined in this tab, all needed information for the tool path calculation is collected and converted to an input for the ModuleWorks tool path calculation core (mwGeoLib). Depending on the different geometry types, the basic path pattern and the tool (-radius) selected for this particular surface the algorithm for computing the tool path is chosen. Whenever something unexpected happens, an exception is thrown to indicate the failure.

The tab »Post-Process/Generate Program« is the step before starting machining. The post processor is triggered to generate a NC-file/program for each cycle which has been defined in the tab »Machining cycles« (see **Figure 8.12**). The tab also provides the capability to define additional NC-program parts by hand for auxiliary tasks. When the »Create« button is pressed, the machine kinematic model defined in the tab »Machine« and the computed tool path of the current selected cycle are exported to the ModuleWorks post processor »MultiXPost«. This module creates an NC file with the name of the current cycle and loads it into a simple editor.

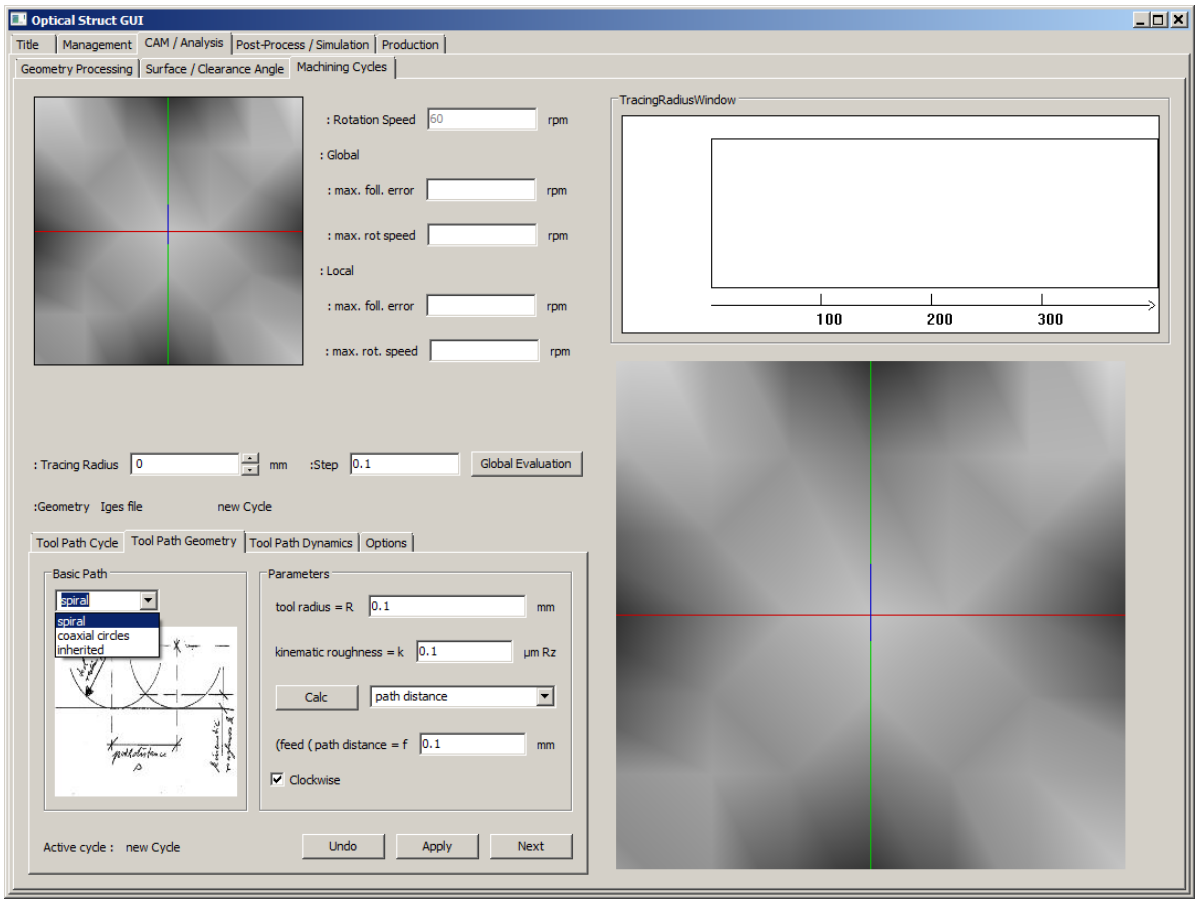

Figure 8.11: Tab CAM/Analysis/Machining cycles

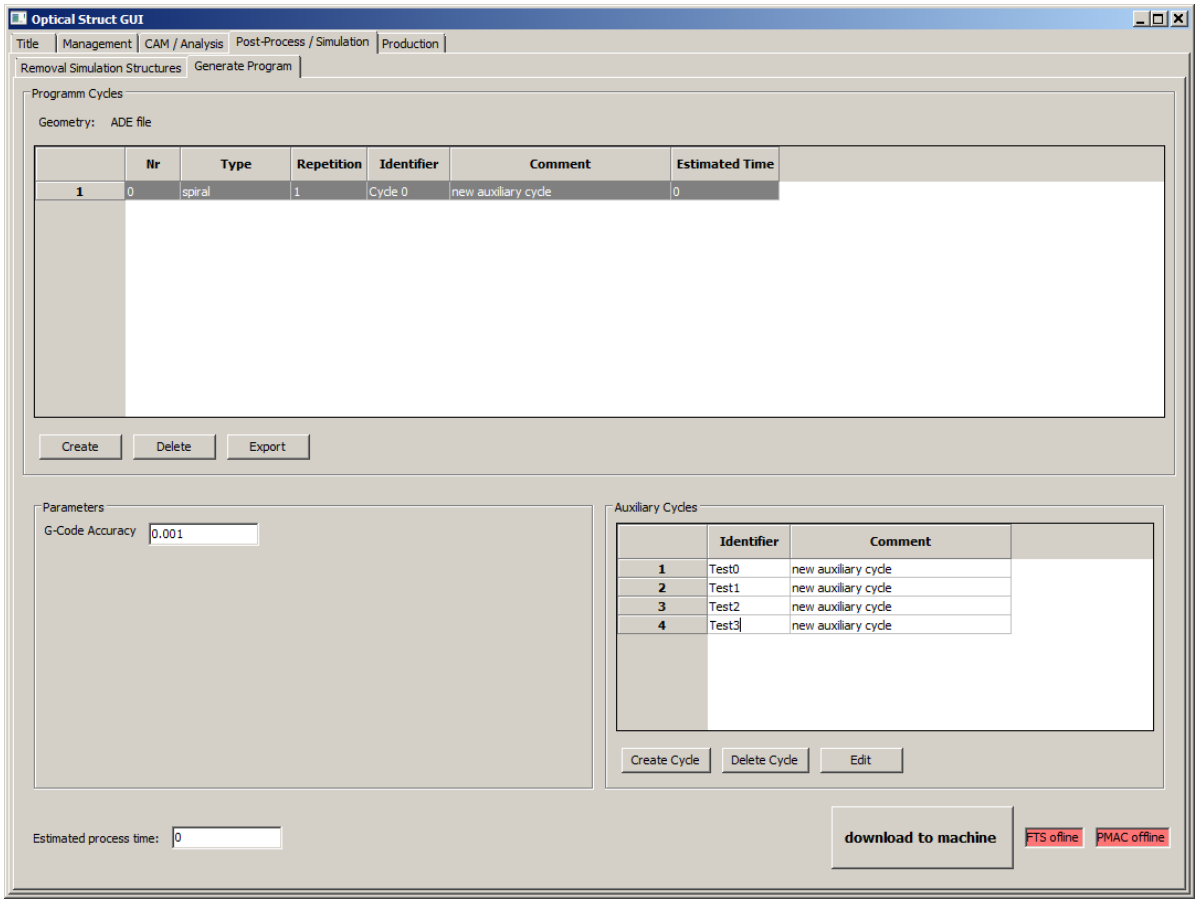

Figure 8.12: Tab Post-Process/Generate Program

8.4 Simulation Techniques

Integrating the processing of complex structured free-form surfaces into a CAD/CAM chain, dramatically increases the complexity of the created machining processes. Processes with their different parameter sets are combined and new ways of creating process data are introduced. The new process contains the combination of Slow Tool and Fast Tool control paths and the underlying workpiece data, now extended from regular function based surfaces to free defined NURBS (Non-Uniform Rational B-splines) based surfaces. In addition to that, the data no longer is generated and controlled by the machine control itself, but it is generated one step before in the CAM chain. Thus, errors cannot be fixed by the machine control when they occur, besides the fact that they may cause additional costs, if work pieces or tools get damaged because of these errors. Because of this risen complexity, there is a high demand for a previous simulation of the process to avoid such error conditions. This is comparable to the step between shop floor programming and the switch to a CAM process with five axis simultaneous tool movements (see **Figure 8.13**).

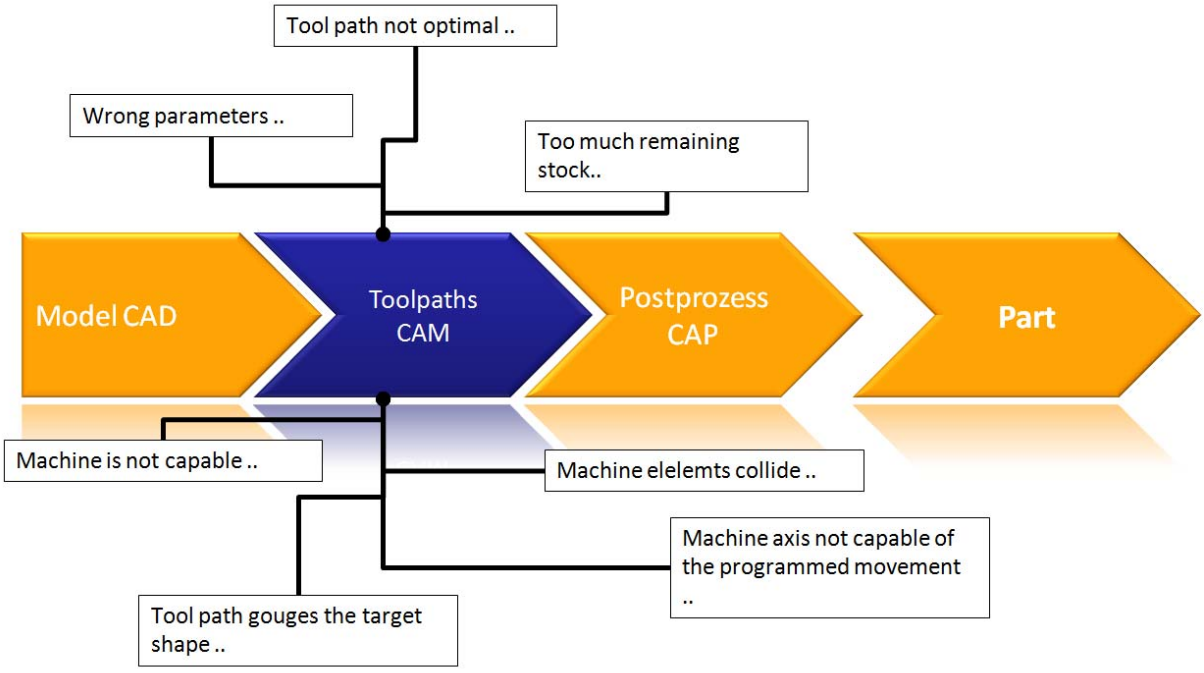

Figure 8.13: Possible problem causes in the new process chain

8.4.1 State of Classic Process Simulations

In the classic process chain the simulation can be split into three different parts as shown in **Figure 8.14**. It is split up into the user interface (SimUI), the kinematics simulation, where possible collisions of machine elements can be detected, and the material removal simulation (CutSim), where the resulting remaining stock can be verified and checked, if it is free of errors.

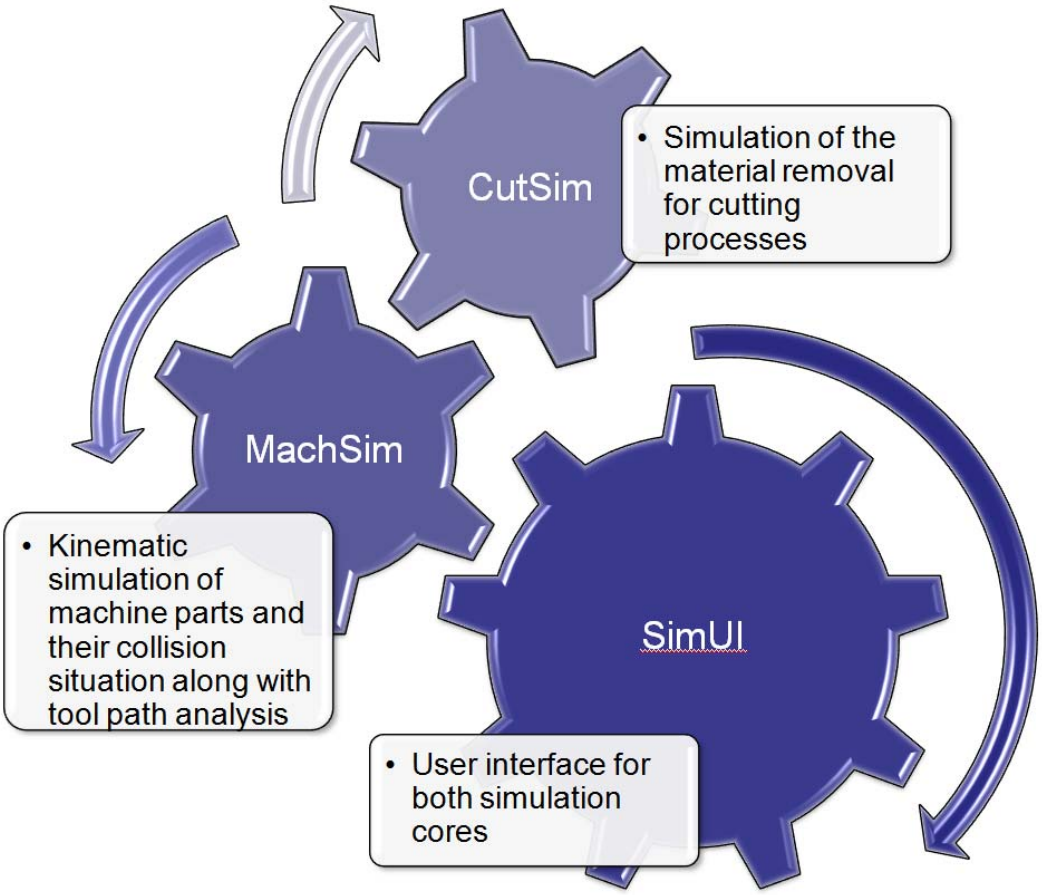

Figure 8.14: The three different parts of a complete simulation component

The processes which are simulated in this project are different to these »classic« processes. Here, a full machine simulation is not needed because kinematic problems are not likely to occur. Because of this, a complex user interface is not needed to handle machine axes and controls. The removal simulation provides this basic functionality and is working with the following simple communication concept with the »ERANET-OPTICALSTRUCT« user interface (the host application).

The removal simulation receives the definition of the initial stock as a triangulated mesh from the host application. Further, the application needs to set a tool. The next step is to define the motion of the tool in the coordinate system of the initial stock that was provided. The application calls the »Cut« method of the interface.

The application should create an OpenGL context and call the »Draw« method of the Verifier Interface to get the resulting work piece visualized. If OpenGL transformations are done in the OpenGL context, the visualization will respect this transformations. E.g. in a machine simulation environment, the rotary table can rotate for every NC line, causing the work piece to rotate as well. In that case, the visual rotation of the current machined work piece can be done by the application, using an OpenGL transformation or a rotation of the OpenGL context before the »Draw« method of the verifier API (Application Programming Interface) is called. The application is responsible for reacting on mouse and keyboard interaction. It is

possible to call the »Cut« method multiple times before doing the visualization. This will reduce the total time of the material removal simulation since visualization in OpenGL is taking more time than the actual »Cut«.

If the target work piece is available as a triangle mesh with a good accuracy, the verifier library can use this information to make a comparison between the currently machined stock model and the work piece at any time of the material removal calculation and display the results in different colors, e.g. red for gouges and blue for excess material. Further, the simulation can send a notification in case of a non-cutting portion of the tool or the holder is colliding with the current stock definition. The resulting work piece after material removal can be returned as a triangle mesh any time during or after the simulation.

8.4.2 Modifications and Improvements on the Simulation

As a basis for the removal simulation component, a simulation for milling of dies and molds was used. The processes for dies and molds differ in two major points from the processes created in this project.

One difference is scale. In conventional milling machining, dies and molds can have the size of meters, where the optical components created in the scope of the project »ERANET-OPTICALSTRUCT« have an average size of centimeters or even lower. This implies a scaling of all simulation algorithms by a magnitude of at least 100 times. During the project all components were investigated and checked, if they scale correctly with the changed process parameters. But this difference is not only the static scale. It is also the dynamic scale of the process. Where in die and mold milling processes the user needs an overview of the full workpiece, here in addition to this overview a detailed look onto the workpiece structures is needed. With this detailed zoom it is possible to verify the arrangement of the detailed microstructures on the workpiece.

To handle this difference and dynamic in scale, between centimeter parts and micro / nano structures, a dynamic zoom capability was added to the simulation (see **Figure 8.15**). This zoom capability enables the user to interactively zoom into the area of interest on the workpiece to investigate the microstructures on the free-from surface. The developed solution uses basic 3D hardware, accessed by the internal OpenGL driver of the target system. The demanded version of the OpenGL driver implementation is 1.3. By using such a low version we can assure a wide compatibility, when the host application is based on machine controls.

The second difference of the process is the number of distinct tool paths. In regular milling a standard tool path contains from 1000 up to 100000 distinct moves. The process which should be simulated in this project origins from turning which does not resolve discrete axis positions. Due to the fact that free-form shapes together with microstructures are simulated, the turning tool path needs to be discretized. The need for micro precision can lead to about 10 million single movements to be simulated in one run.

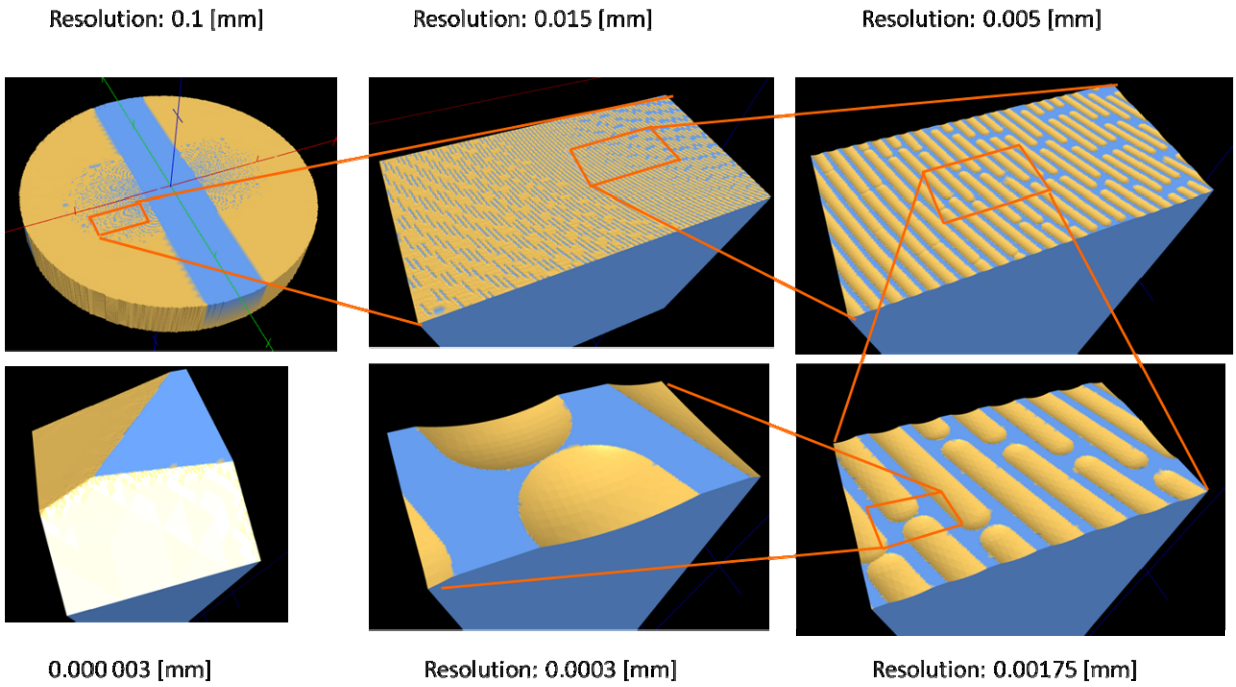

Figure 8.15: Dynamic target geometry simulation, zoom on microstructures

To reach a good performance for this huge amount of single moves, the internal simulation technique was completely rewritten. In order to get good performance and correct details in the microstructures, an analytical approach was used, which does not induce additional sampling errors into the simulated result. Thus, result quality depends only on the used precision of the workpiece model and this can be overcome via the zoom function.

The goal was the 1 million moves should be simulated in about 10 sec to give the user the ability to use the simulation as a debug tool. To achieve the high needed performance during the simulation, the code for the calculation of the surface points that were changed during the removal needed to be specially optimized. In the final version the simulation is now able to simulate 3 million tool paths in less than 30 sec.

9 Measurement Technology for Microstructures

9.1 Validation of Suitable Measurement Principles

Production of high precision optical structures is requiring accurate dimensional measurements as a crucial source of information to improve and monitor both the processes and the products.

The diffractive microstructures developed in »ERANET-OPTICALSTRUCT« have the following geometrical characteristics:

- Structures with 45° or 90° vertical walls
- V-groove structures with very small pitch and depth values until 5 µm
- Micro lens arrays with depth of 100 - 150 µm and lens radius of few mm

The complexity of the measurement of structures of this size and shape is demanding an advanced approach in terms of measurement sensor technology, machine technology and metrological calibration of the measurement instrument. Particularly, the geometrical characteristics of the diffractive structures require the following metrology capabilities:

- True 3D measurement capabilities, to be able to acquire information in walls and holes of the very small diffractive structures
- Lateral resolution better than 1 µm, to be able to measure structures of 5 µm
- 3D accuracy better than 0.2 µm

The aim of the metrology system is to develop an »off-line« laboratory solution to measure the diffractive 3D structures and to validate the manufactured optical structures in »ERANET-OPTICALSTRUCT«.

9.1.1 State of the Art of Nano and Micro Scale Metrology Systems

For conventional products, classical metrology instruments like Coordinate Measurement Machines (CMMs) allow to deliver flexible off-the-shelf solutions for most R&D and process control problems. Although high precision CMMs provide accuracies in the range of 0.5 - 1 µm, the 3D resolution is highly constrained by the sensor technologies. **Figure 9.1** shows state-of-the-art sensors for micro and nano-scale metrology. For tactile probes, the smallest tip diameters are over 30 µm, reducing the capabilities of the CMM to measure narrow holes and structures.

Scanning Probes Microscopy (SPM) provides good uncertainty (better than 0.1 nm) and lateral resolution (better than 10 nm), but are not providing 3D measurement and are not capable of measuring steep slopes or holes. SPM is normally used for measurement of roughness profiles, deviations from ideal flat form and molecular structures.

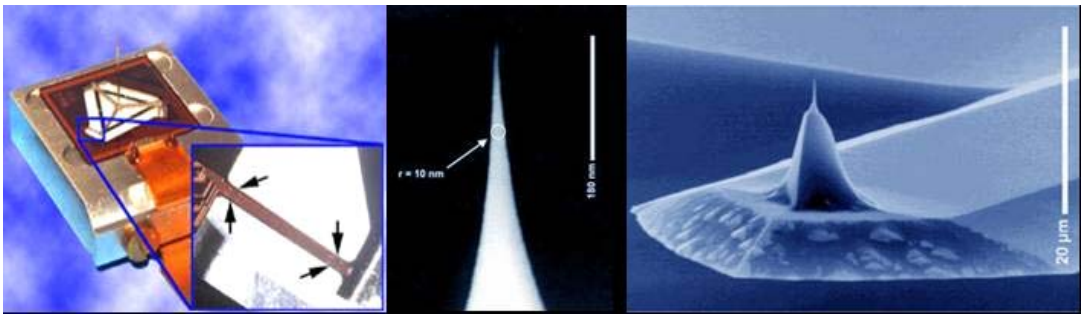

Figure 9.1: State of the art 3D sensors stripe-membrane tactile stylus (courtesy IBS PE / Philips) and SPM tip of silicon.

Optical sensors based on confocal or interferometric principles are providing high accuracy in the axial direction, lateral resolution over 0.5 µm, but are not able to measure on vertical walls of 3D structures.

Figure 9.2 summarizes the state-of-the-art and the limitations of the actual existing probing systems, and the opportunities to develop a new technology for the project.

Geometric Measurement Task	Features, complications	Uncer-tainty	Struct.r resolut.	Preferred probe type	Availability
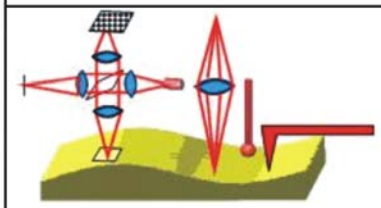	Soft profiles (<10°), flat objects ...."that's basically what today's nano metrology manages"	>1nm	>1-2µm	Optical probes (point & area): con-focal, white light interferometer (coherence radar), fringe projection; Scanning Probe Microscopes (SPMs)	In this case only a highly accurate 2D motion stage is needed (no real 3D Nano CMM, like in all the following cases)
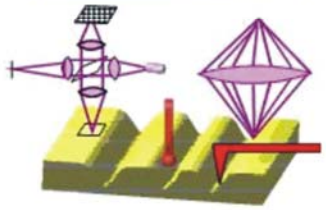	Steep profiles (<45°);	>1-2µm	>1-2µm	SPM; optical confocal point probe;	
	very steep profiles (<80°), reflexes, no diffuse back-scattering	**<300nm**	**<300nm**	**SPM; optical probe (point & area) with high lateral resolution (using UV) and big aperture**	**NOT AVAILABLE**
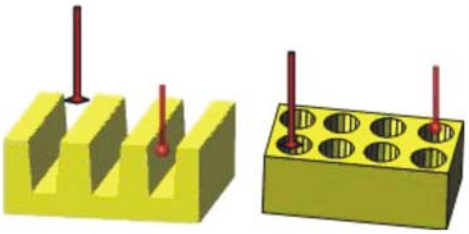	Holes, grooves, very steep slopes	>1µm	>30µm	Tactile micro probes, tactile-optical micro probes;	Real 3D Nano CMM is needed
		<100nm	**<100nm**	**Tactile nano probes: nano materials as probe tips on high gain MEMS circuits**	**NOT AVAILABLE**
	Holes, grooves, very steep slopes with high	>3µm	>50µm	Tactile micro probes, tactile-optical micro probes;	Rotary stage to individually align features;
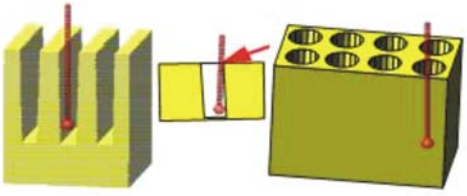	aspect ratios (depth to diameter) and/or with different orientations	**<200nm**	**<200nm**	**Tactile nano probes: nano materials as probe tips on high gain MEMS circuit**	**NOT AVAILABLE**

Figure 9.2: State-of-the-art of probing systems for 3D metrology

Considering this requirements, the development of a new type of measurement system, using a tactile 3D probe is the challenge of this project, with the following features:

- True 3D uncertainty significantly below 200 nm
- Tip diameter below than 100 nm
- Capability to measure 90° vertical walls

9.1.2 Components of the Measurement System

Figure 9.3 shows the metrology machine concept, based on the Abbé-principle, where the probing sensor is in the point of intersection of the three interferometer axes. This structure guarantees minimum Cartesian errors. The sample is located in a moving stage consisting of three faces of a cube, where three mirrors are used to reflect the laser of the interferometers. By measuring the distance to the mirrors, the position of the stage is estimated. The probing sensor is utilized to touch the part and measure the exact position of surface points of the sample. From the obtained 3D surface points the dimensions of the geometrical features could be estimated.

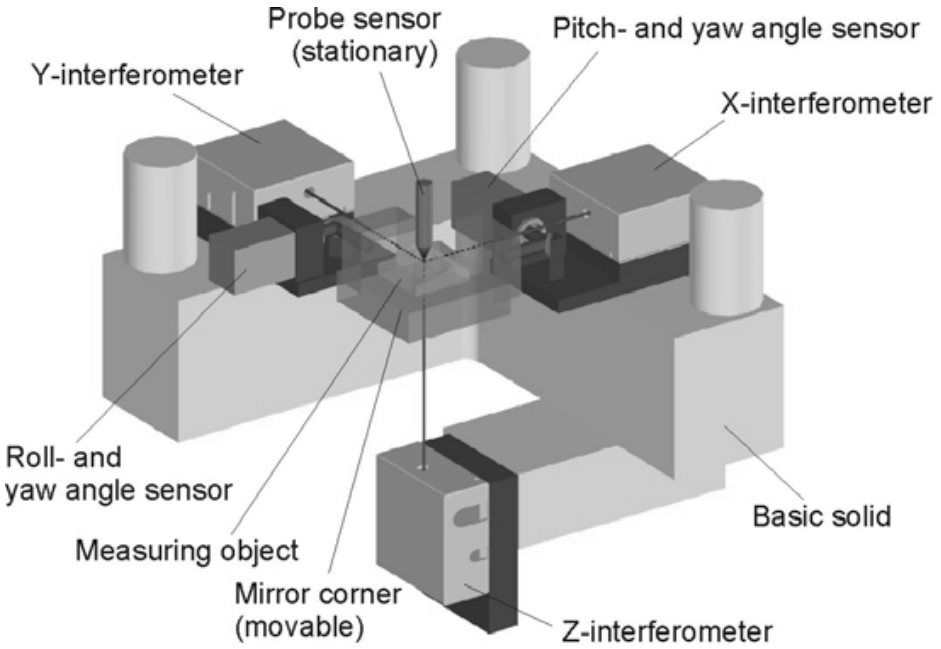

Figure 9.3: Basic setup of the metrology frame based on Abbé principle

Figure 9.4 presents the components integrated in the measurement system.

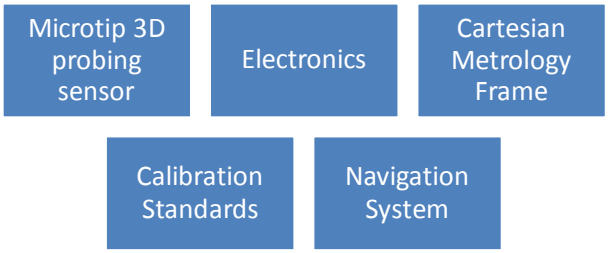

Figure 9.4: Components of the metrology system

Microtip 3D probing system

The microtip 3D probing system is the sensing component of the metrology system, consisting on a microtip mounted on a stylus coupled to a 3D force sensing device. The working principle consists on measuring the force or deflection of the stylus when the tip is touching the measured sample. **Figure 9.5** shows the schematics of the probing system.

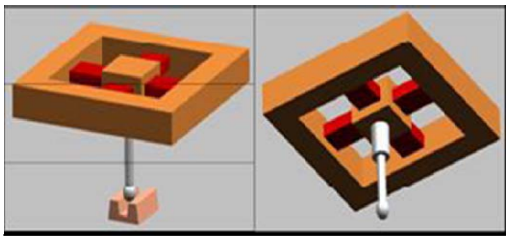

Figure 9.5: Schematics of the probing system

In order to be able to measure structures as small as 5 µm, the size of the tip has to be below 1 µm. The sensor has to be able to measure deflection in 3 directions X,Y, and Z.

Electronics

The probing system needs an electronic design to amplify and condition the analog force signals. Additionally, the recording of the deflection signals need to be synchronized to the movement of the Cartesian metrology frame.

Cartesian Metrology Frame

In order to move the stage and touching the part with the tip, a robotic Cartesian system able to position the sensor in 3D with a very high accuracy will be used. The Cartesian Metrology Frame has to provide uncertainty below 0.2 µm, what is a big constraint to the system. After a review of the existing nano systems in Europe, the commercial machine developed and supplied by the German company SIOS (see **Figure 9.6**) has been selected for pilot implementation.

Figure 9.6: Metrology Frame supplied by SIOS

Calibration standards

A calibration artifact is needed to calibrate and verify the measurement system. Thinking on the accuracies and resolution of the metrology system of the »ERANET-OPTICALSTRUCT« project, development of the calibration system is a very important challenge. The problem is not only to manufacture a 3D object stable and precise, but to have an accredited laboratory to certify and calibrate the object. For the project, the cooperation with the Physikalisch-Technische Bundesanstalt (PTB, national metrology institute in Germany) has been requested.

Navigation system

Because both the probing tip as the structures to be measured are too small to be seen with human vision of the machine operator, a navigation system consisting on a visualization video microscope is needed. The aim of the navigation system will be to assist the operator while performing the measurements seeing both the tip and the part when moving the machine, and avoiding collisions of the probing sensor.

9.2 Development of a 3D Measurement Sensor

9.2.1 Requirements of the 3D Measurement Sensor

Considering the requirements of the measurement system, the following requirements for the probing system have been defined:

- Tip size no longer than 30 µm and probing tip diameter below 50 nm
- Miniaturize cantilever-optimum design
- Cross section of the cantilever: 1 x 1 to 3 x 3 µm²
- Length of cantilever: 1000 µm
- Deflection range better than 10 µm
- 3D force probing signals in X,Y, and Z
- True 3D uncertainty better than 0.1 µm
- Different angles tip possible
- Sensitivity in all the three dimensions with low and equal stiffness
- Resonant frequencies higher than 1 kHz
- Develop tip holder-changer

Additionally, a critical requirement is that minimum heat is to be dissipated in the measurement volume. This is a strong requirement both for the electronics of the sensor and for any other device to be used during measurement, for example, the navigation system.

9.2.2 Manufacturing Technology of the Probing System

The technology selected for the design and development of the probing system is a combination of SPM and micro-probe technology, where a silicon tip similar to the SPM systems is integrated with a cantilever based force sensing micro device.

When the tip is deflected when touching the measured object, a force signal is generated by the sensing device. The recording and analysis of the force signal allow estimating the position of the measured surface point.

Initially a structure based on a L-shaped sensing device was conceived, but that structure has been refined to another more effective, based in a H-type sensing system presented in **Figure 9.7**.

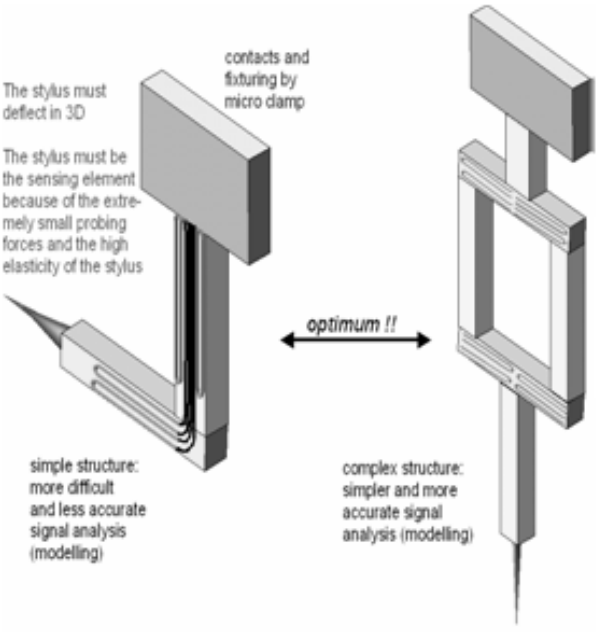

Figure 9.7: L and H sensing probes

Two possibilities of force probing have been selected: using capacitive sensors or using resistive sensors. Of the two options, a first development of capacitive sensors has been chosen, with the possibility to develop a resistive sensor in the future as an evolution of the design.

The technology chosen for the manufacturing is based on wet etching of silicon wafers. This is a well known technology for the manufacturing of AFM probes. The manufacturing has been requested to the company Nascatec, what is owner of a patented technology to manufacture tilted tips. The technology is having the following advantages:

- Probing end of the sensor can be functionalized and customized by wet silicon etching, with pyramidal, V-line shapes or L-shaped
- All the traditional techniques of an AFM tip formation are available
- 10 nm radius of curvature is a possible value

- Tips could be created on upper and lower sides of the probe
- Care with customized ending of the rod is not too soft, which would cause loss of sensitivity (stiffness must be equal to the probe's stiffness)
- Standard etching process favors tip clusters with the positions and angles of the tips at the cantilever end as they are beneficial for universal micro parts' measurement

Figure 9.8 shows the incremental steps of the etching process, where material is removed until obtaining the desired geometry of the tip.

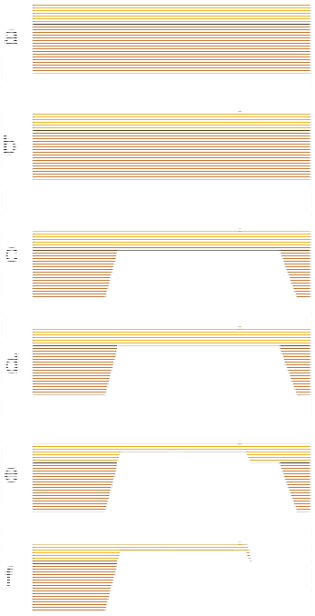

Figure 9.8: Silicon wet etching steps

With this technique, both capacitive or resistive probing systems can be manufactured. When the tip is deflected, a force is applied to the sensing devices, and a signal is generated. The structure of the sensing devices allow to measure deflection in 3D, proportional to the deformation of the sensor arms, as shown in **Figure 9.9**.

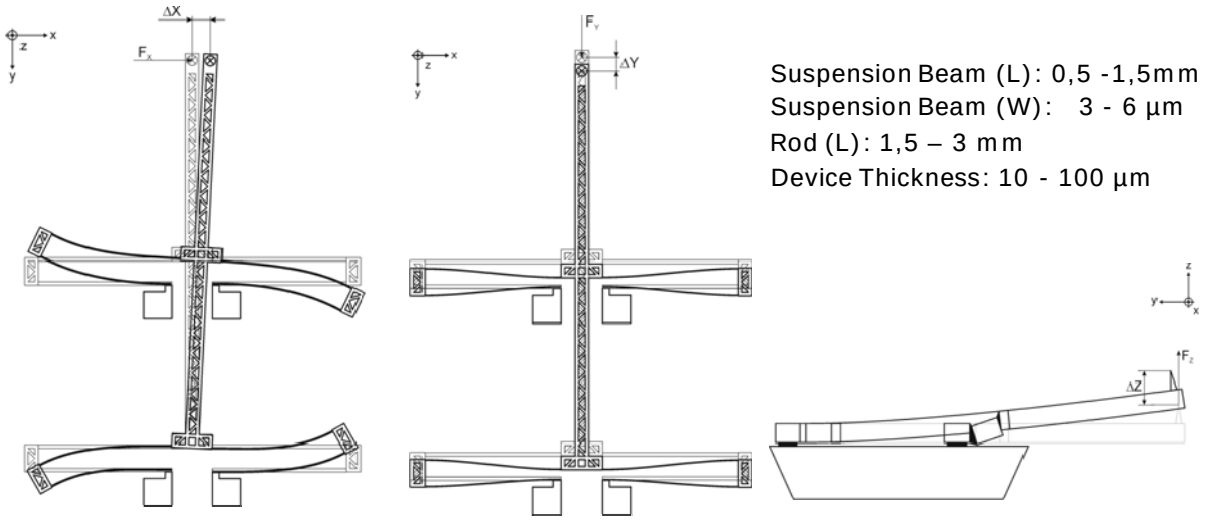

Figure 9.9: 3D deflection and sensing

9.2.3 Prototype Manufacturing

A prototype of the probing system has been manufactured for the »ERANET-OPTICALSTRUCT« project. **Figure 9.10** presents the design dimensions of the probing system.

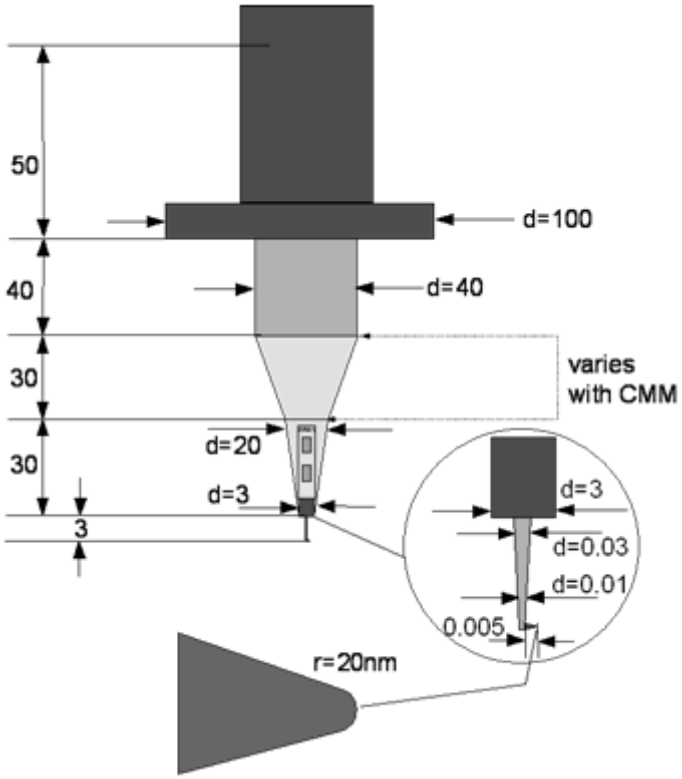

Figure 9.10: Design of the tactile probing sensor

The tactile metrology sensor is integrated by a sensor holder, to be able to exchange different sensors in the machine, the sensor electronics and the silicon tip.

The silicon tip to be integrated into the measurement system has been supplied by Nascatec. **Figure 9.11** shows an image of the prototype sensor (image obtained by an optical microscope).

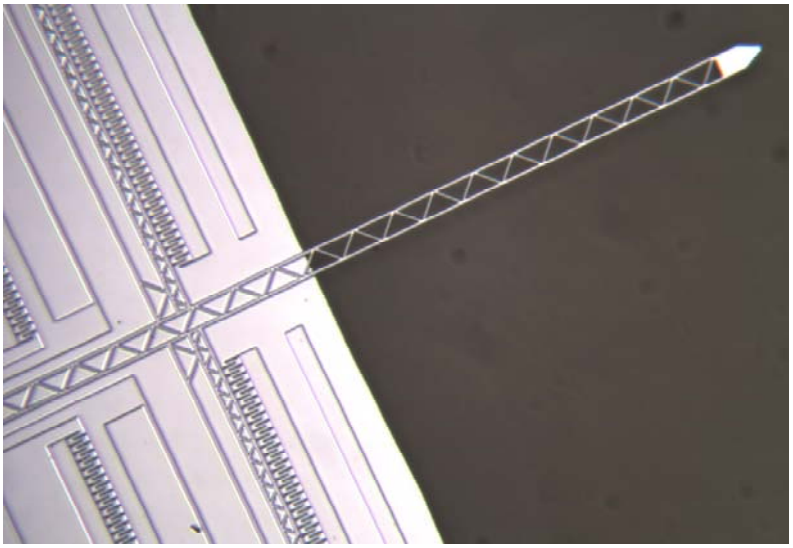

Figure 9.11: Tactile microprobe showing the cantilever and the sensor tip

Characterization of the probing system has included two aspects: repeatability of the holding system and performance of the silicon probing sensor. For the repeatability of the holding system, a laboratory setup has been developed as shown in **Figure 9.12**.

Figure 9.12: Holder of the tactile probe

The holder has been coupled with a kinematic mount to guarantee the repeatability when placing the sensor in the machine. An experiment of several repetitions has been performed in order to estimate the repeatability of the kinematic mounting, proofing that the repeatability is better than +/- 2.5 µm (see **Figure 9.13**). Position has been measured with a CMM.

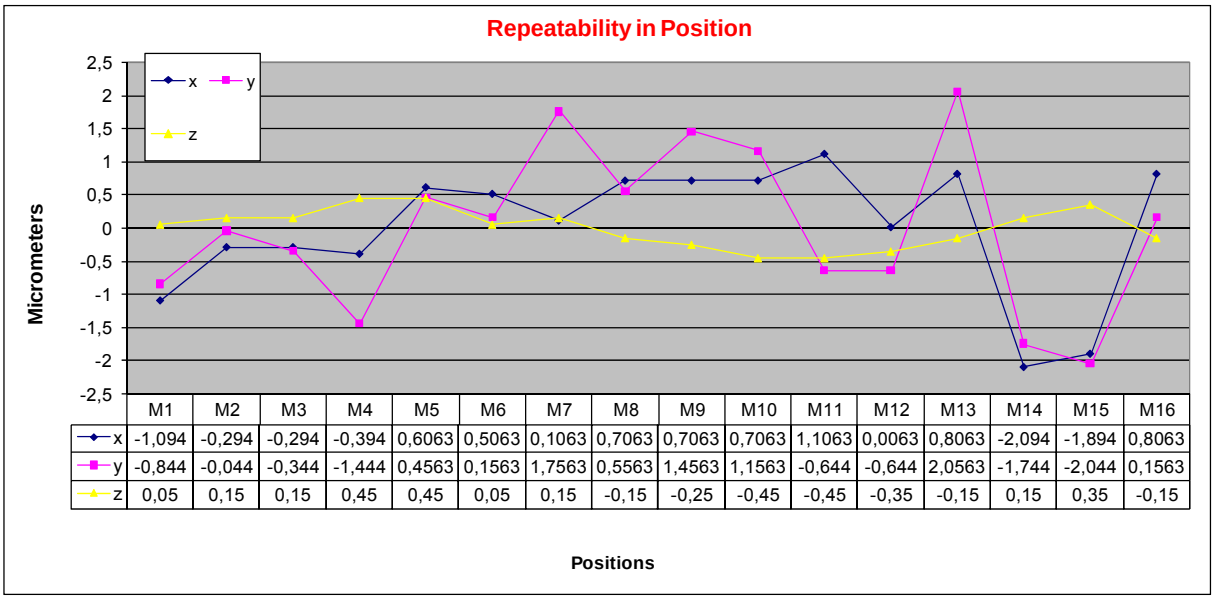

	M1	M2	M3	M4	M5	M6	M7	M8	M9	M10	M11	M12	M13	M14	M15	M16
x	-1,094	-0,294	-0,294	-0,394	0,6063	0,5063	0,1063	0,7063	0,7063	0,7063	1,1063	0,0063	0,8063	-2,094	-1,894	0,8063
y	-0,844	-0,044	-0,344	-1,444	0,4563	0,1563	1,7563	0,5563	1,4563	1,1563	-0,644	-0,644	2,0563	-1,744	-2,044	0,1563
z	0,05	0,15	0,15	0,45	0,45	0,05	0,15	-0,15	-0,25	-0,45	-0,45	-0,35	-0,15	0,15	0,35	-0,15

Figure 9.13: Repeatability in position of the holding system

On the other hand, experiments show the capacity of the sensing system to provide a deflection signal. For this purpose an experimental setup to calibrate and characterize SPM systems with a piezoelectric stage and three interferometers has been utilized at the PTB, as it is showed in **Figure 9.14**.

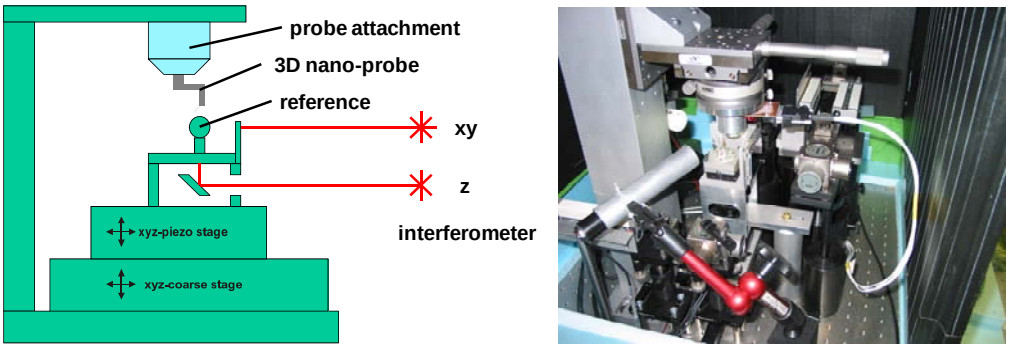

Figure 9.14: Experimental setup of the SPM characterization system

Additionally, a setup for temperature characterization has been prepared, as shown in **Figure 9.15**.

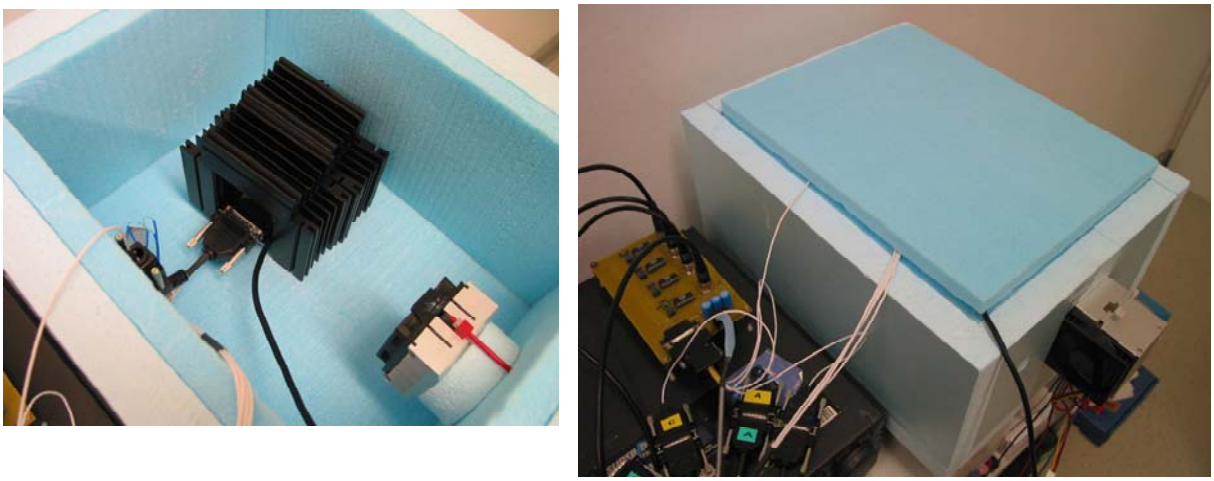

Figure 9.15: Setup for SPM temperature characterization (PTB)

9.2.4 Nanoscale Calibration Artifacts

A critical element of the development of the metrology system for micro and nanoscale measurements is the design and development of artifacts for calibration purposes. There is a lack in the market of calibration standards for this level of metrology performance and resolution, and a specific development has been conducted.

The basic requirements of a calibration standard are the following:

- Mechanical stability
- Stability in temperature
- Low form error of the shape (ball, plate, …)
- Possibility to be calibrated by the national institutes and accredited laboratories

Additionally, for the »ERANET-OPTICALSTRUCT« project, it is needed for the calibration standard to have real 3D shapes, and not only 2D shapes as other existing standards for microscopy.

Three types of standards have been designed and evaluated for the project:

- Ball plate
- Silicon plate
- Silicon 3D pyramid

Ball plate

A ball plate is a piece where several very small balls are fixed and distributed on a flat plate. The positions of the balls are calibrated.

For the ball plate different types of ball materials and plate materials have been selected and studied, as shown in **Figure 9.16**.

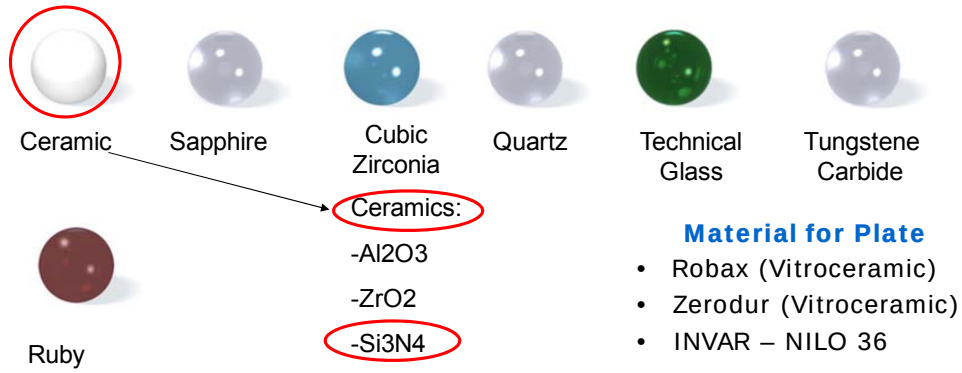

Figure 9.16: Ball plates sphere and plate material possibilities

For the balls the best options are ceramic and ruby, showing a good form factor. For the plate, Robax has been selected. **Figure 9.17** shows the first prototype of the artifact.

Figure 9.17: Ball bar artifact standard

Silicon Plate

The second proposed artifact is based on flat small pieces of silicon that have the property of a very low form error, to be oriented in different directions to be able to have a real 3D object. The idea is to use a mechanized part as a base and plates of silicon glued to the base. Different designs are proposed to have to possibility to obtain different plate orientations, as shown in **Figure 9.18**.

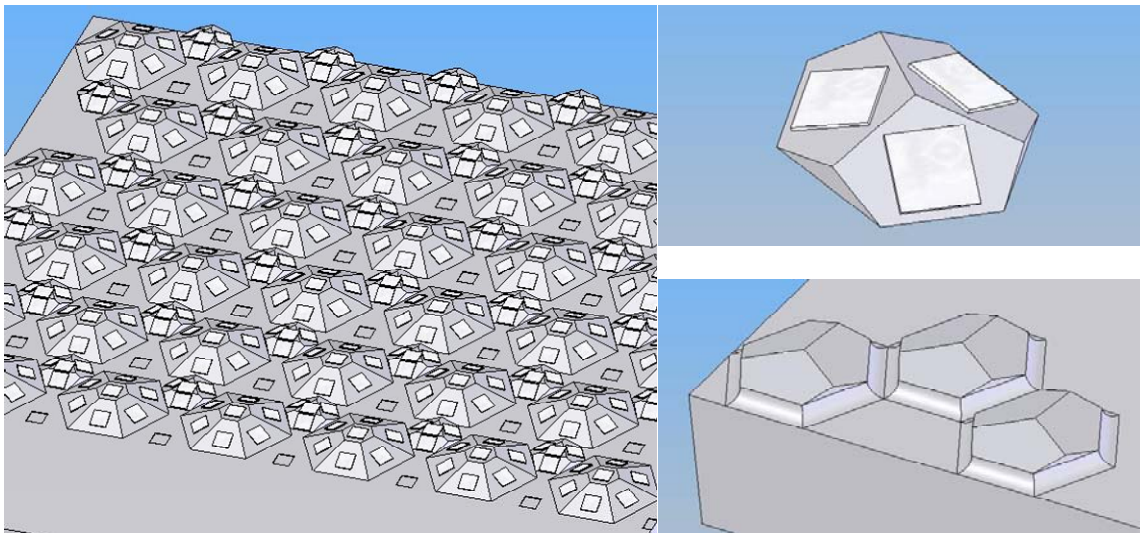

Figure 9.18: Silicon plate artifacts

The first prototype has been manufactured in zerodur, in cooperation with Tekniker (Spain) with silicon plates glued to it, presented in **Figure 9.19**.

Figure 9.19: Standard of silicon plates oriented in different directions

Silicon 3D Pyramid

The third object has been developed with the cooperation of the PTB. It is based in the idea of wet etching of a silicon wafer in order to obtain different levels of silicon, that glued will provide a pyramid shape.

Figure 9.20 shows the design of the silicon pyramid.

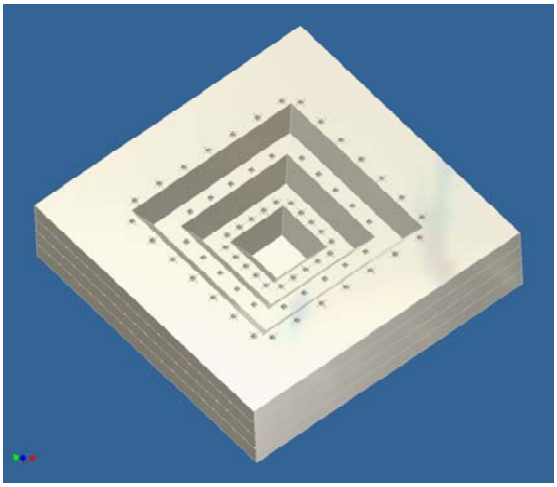

Figure 9.20: Silicon pyramid standard

The manufacturing process developed at the PTB consist on etching the silicon plates, and making a pile of the different plates aligning the wafers, represented in **Figure 9.21**.

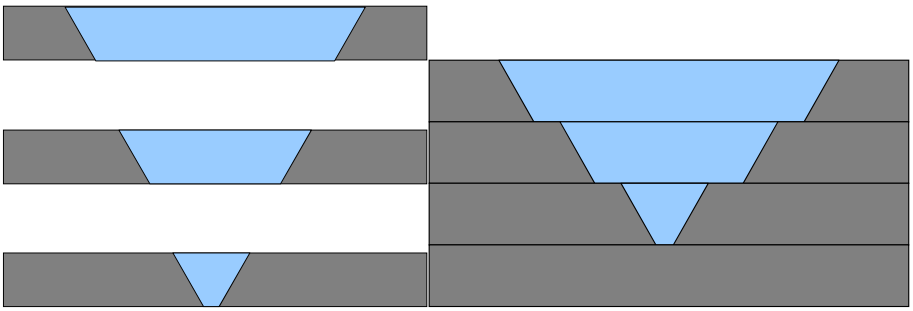

Figure 9.21: Silicon pyramid standard manufacturing

Figure 9.22 shows the prototype of the standard that has been manufactured.

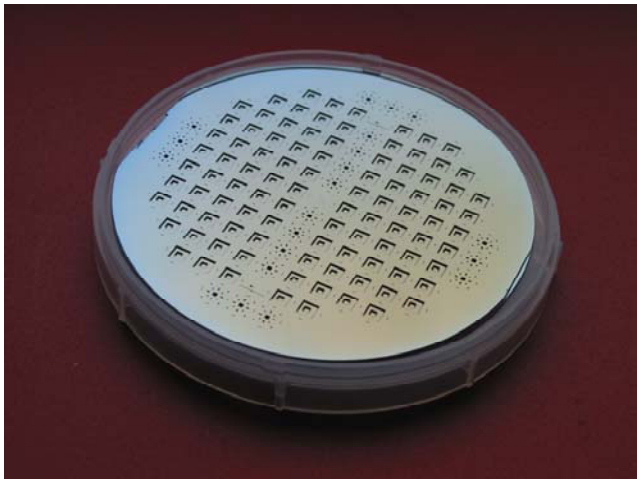

Figure 9.22: Silicon calibration standard

9.3 Electronics for the Measurement System

The development of the electronics of the measurement system include the following systems:

- Electronics of the microprobing system
- Customization of the electronics and software of the Cartesian machine

9.3.1 Electronics of the Microprobing System

The developed micro tactile probing system is requiring an electronics subsystem for the integration with the metrology frame. A specific electronic design to be integrated into the holder of the probe has been performed. The design is basically a multiplexed system to perform readout of the different sensors and a capacitance to voltage converter, according to **Figure 9.23**.

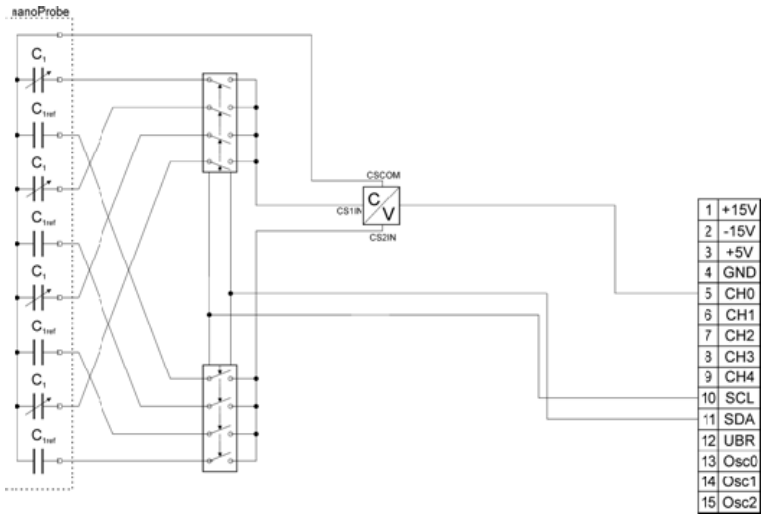

Figure 9.23: Electronic design for the microprobe system

Figure 9.24 shows the prototype of the electronics that has been manufactured and integrated into the probing system.

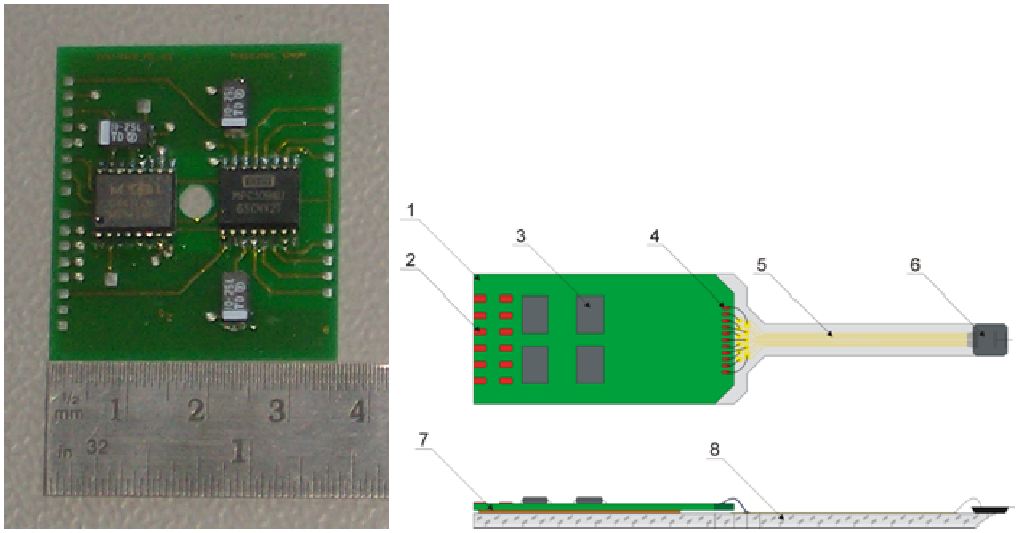

Figure 9.24: Prototype of the sensor electronics and integration on the microtip

9.3.2 Electronics and Software of the Cartesian Machine

The integration of the probing system to the machine requires a synchronized reading of the deflection of the sensor and the readings of the position of the machine. The SIOS machine integrates three interferometers to measure the position of the frame. Additionally, signal processing of the readings of the sensor is needed. For this purpose, a data processing unit has been integrated, to calculate the parameters of the sensing process, as shown in **Figure 9.25**.

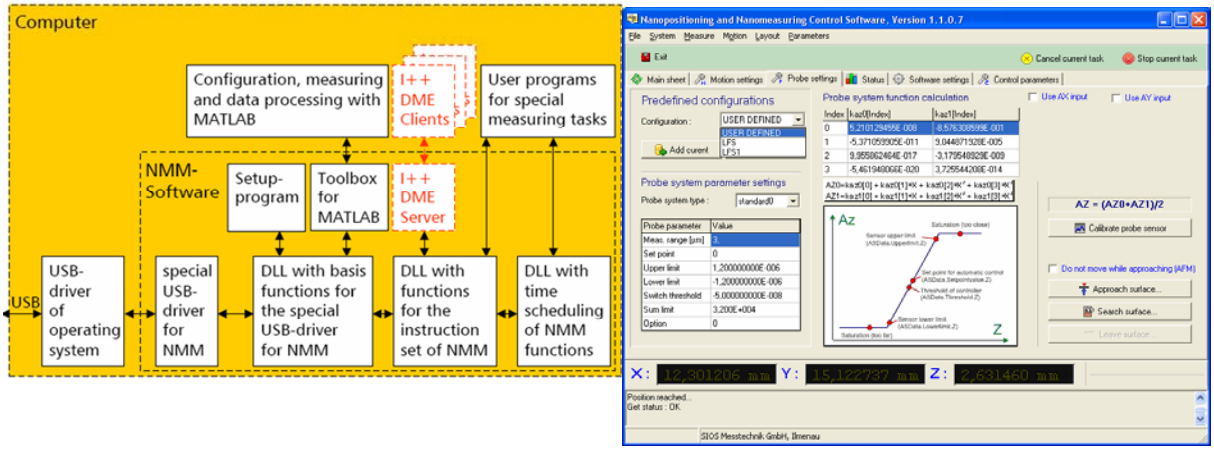

Figure 9.25: Software modules for signal processing of the SIOS machine

9.4 Assembling the Prototype

A prototype of the measurement system have been integrated for the project, consisting on:

- The 3D tactile microprobing system
- The sensor electronics
- The Cartesian metrology frame with software (SIOS machine)
- Navigation system

9.4.1 Navigation System

Because the size of the tip sensor and the structures to be measured, it is not possible to use normal human vision to assist the measurement process. It is crucial to have a subsystem able to magnify the vision of the elements to be used by the operator when measuring.

For the navigation system a video microscope has been designed, integrated by a digital video camera, a lighting system and a microscope lens. The requirements of the system are the following:

- Long working distance to avoid heat in the measurement volume
- Use of optical fiber for lighting is required to avoid heat source of the light system

- High optical resolution
- Axial illumination
- Zoom (digital could be preferred to avoid using electrical optics that dissipate heat)
- Telecentric objective (if possible)
- Considering the size of the tip, a field of view of 1 mm is required for the navigation system

In order to guarantee image quality, a high resolution video camera (see **Figure 9.26**) has been selected, providing 5 Megapixel with real video.

	Image Resolution	Pixel Size	Sensor size	Sensor size	Sensor
UI-1480SE	2560x1920	2.2 µm x2.2 µm	6.5x4.9mm	1/2"	CMOS

Figure 9.26: Navigation system digital video camera

The resulting magnification for 1 mm FOV and the 1/2” CMOS sensor is 1:5. With this magnification, a long distance microscope lens with high resolving power has been selected (see **Figure 9.27**).

		Working distance	FOV 1/2" sensor	Deph focus
Acrovid 5X	5X	37 mm	1.28 x 0.96 mm	16 µm

Resolving power: 1.7 µm

Figure 9.27: Long distance microscope lens

Finally, a coaxial illumination system has been integrated into the system, as shown in **Figure 9.28**. The navigation system prototype has been evaluated, and finally integrated into the machine.

Figure 9.28: Prototype of the navigation system

9.4.2 Integration of the Prototype

The integration has been performed in the measurement machine, with the sensor system and the navigation system, as shown in **Figure 9.29**.

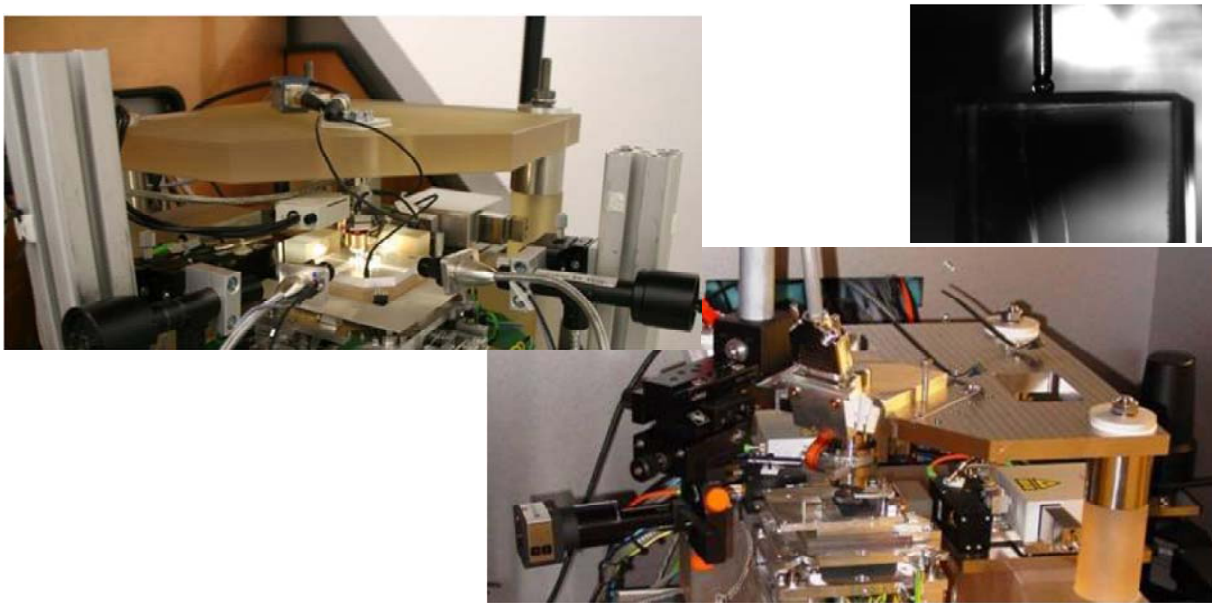

Figure 9.29: Integration in the machine

9.5 Measurement of Test Parts Machined in the Project

9.5.1 Manufacturing of Samples for Testing

For the purpose of testing the measurement system, a set of machined samples has been manufactured. Particularly, a blazed grating with 10 µm until 7 µm grooves has been prepared, as shown in **Figure 9.30**.

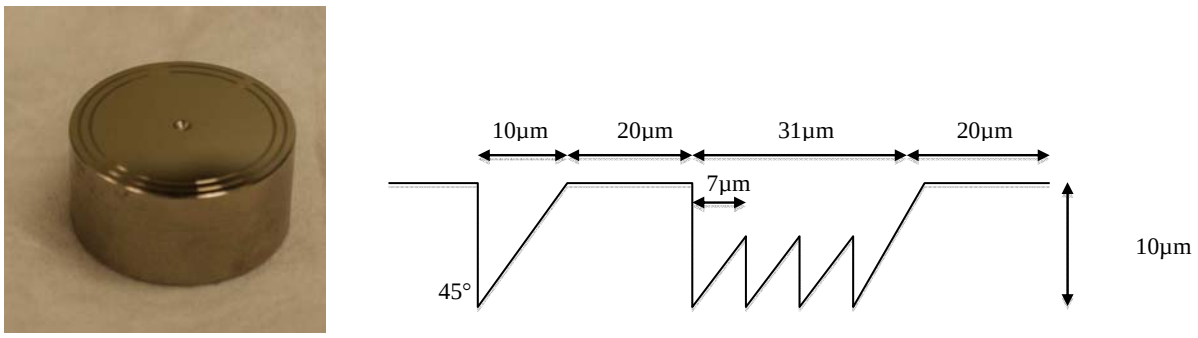

Figure 9.30: Sample 1 (left), V-groove pattern (right)

9.5.2 Measurement Results

Some measurements have been performed with the developed prototype. The following is a summary of the obtained results.

A radial direction has been selected to perform the measurement. **Figure 9.31** shows the results for the measured section.

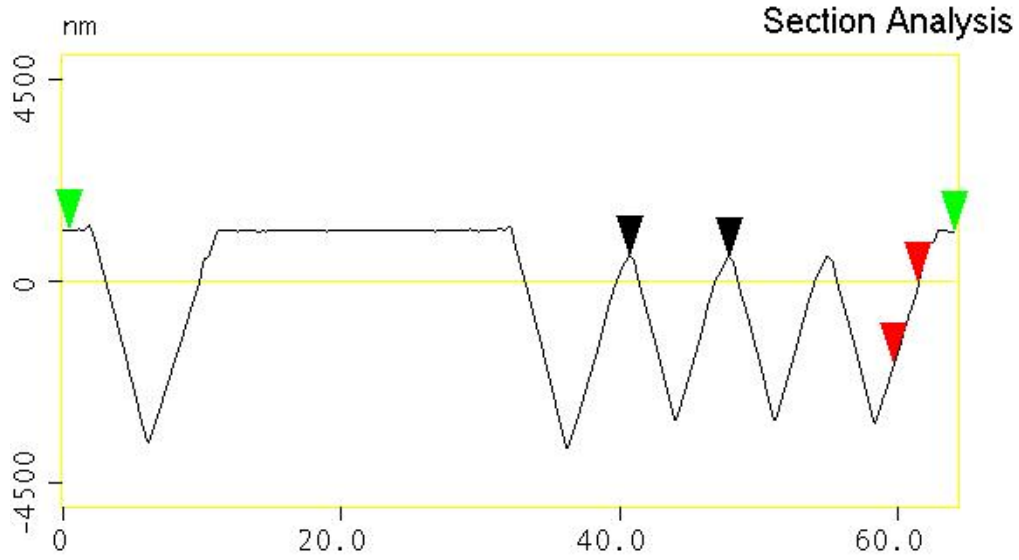

Figure 9.31: Measurement of V-groove pattern

The following dimensions have been extracted from the section.

Pitch distance:

Distance between 2 peaks	Horizontal	7.2 µm
	Vertical	32.9 nm

The distance between the highest corners is around 7 µm with a really small height difference. This result indicates a very good dimensional quality of the machined structure.

45º vertical walls:

The slope of the desired structures should be 45°, obtaining the following result.

Angle of v-groove 45º wall	Angle	45.7º

This is a very good result in terms of quality of the geometry and the machining process. The vertical tip orientation of the sensor is also good to measure vertical walls at 45º.

90º vertical walls:

We notice that the probe is not totally capable of measuring the 90º vertical walls and instead is leaving the shape of the tip used. This problem is derived from the orientation of the tip (vertical) regarding the surface. The way to solve this problem is to develop different sensors with the tip in a non-vertical orientation. **Figure 9.32** shows the possible crystallographic orientations for the tip.

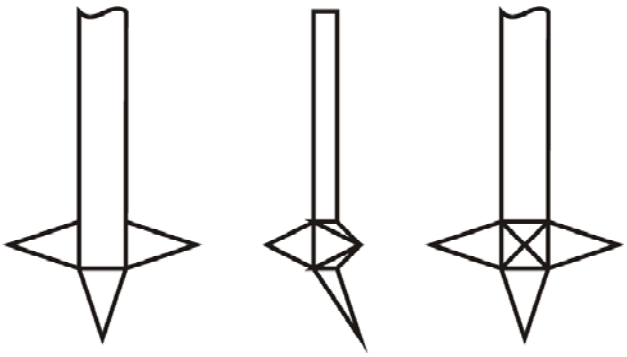

Figure 9.32: Possible crystallographic orientations for the microprobe tip

In future prototypes of the tip, another orientations will be implemented, solving the problem of optimizing the tip orientation to the measured geometry.

Pattern width:

The distance of the pattern is being measured (green triangles), and shows a good result from the theoretical 61 µm.

Total distance of the pattern	Horizontal	63.6 µm
	Vertical distance	10.4 nm

9.5.3 Conclusions from the Measurements

From the experiments, the following conclusions can be extracted:

- The quality of the machined geometries in terms of dimensions is correct.
- The measurement system performance is very good in terms of measurement uncertainty and noise level.
- Tip dimensions are compatible with the very narrow dimensions of diffractive structures.
- The direction of the tip of the manufactured sensor prototype is critical. For the application is important to have several sensors with different tip orientations, and an automatic sensor exchange device to be able to use the best tip orientation for different vertical walls (45º or 90º). This will be checked in future prototype developments.
- The use of the system requires a high level of expertise. Future software development has to be oriented to simplify operation of the equipment.

10 Machining of Large Area Microstructures and Hybrid Optical Surfaces

10.1 Large Area Microstructures

In the scope of the project »ERANET-OPTICALSTRUCT«, many studies have been conducted to improve the quality of microstructures. Therefore, small test parts have been used and each time a few gratings have been machined. By this optimization of the process the burr formation has been reduced to a minimum for stamper tools, as **Figure 10.1** shows. Now these results and strategies have to be transferred to the manufacturing of structured areas with several 100 mm² in size. Applications can be the machining of concentric, continuous blazed gratings on discs with diameters up to 100 mm or the machining of non-continuous blazed gratings on a restricted area, as shown in Figure 10.1 (right).

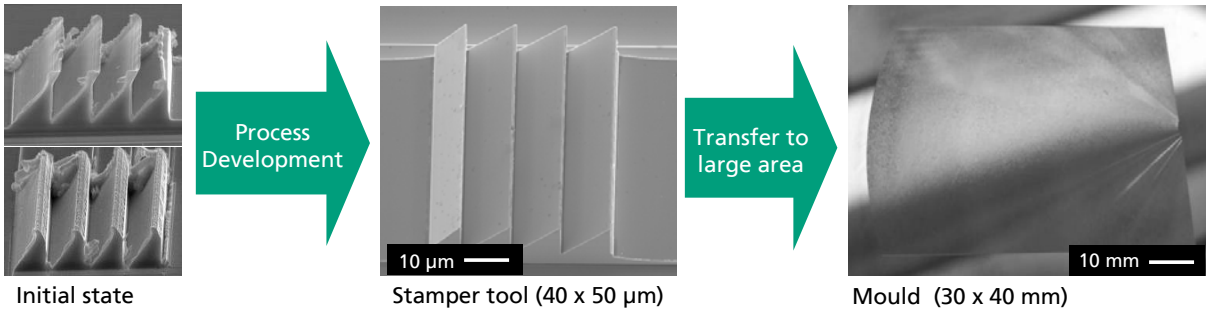

Figure 10.1: Transfer of process development to large area machining

In both cases the process is characterized by long machining times (up to several days, depending on radial structure density), tool wear due to long cutting distances, and the risk of temperature changes, which cause depth variations in the structure.

Due to the long machining times, the conditions have to be very stable during the machining procedure. This is achieved by using temperature controlled cabins as well as by sufficient warm-up runs of the machine. This is especially necessary for the spindle due to possible axial drifts which result directly in a depth variation of the machined grooves. Considering these precautions, different work pieces have been machined. This is described in the following chapters.

10.1.1 Machining Continuous Blazed Gratings on a Large Surface

The optimized machining strategy and process parameters have been used for the machining of a large disc with a NiP-coating (see **Figure 10.2**). The structure starts at a diameter of 0.9 mm and ends at a diameter of 100 mm. The machining time and the cutting length are the critical issues in this process. The pitch and the depth of the v-grooves determine the number of grooves, but a stronger influence on the machining time has the depth of cut. The smaller the depth of cut the more rotations of the work piece are needed in the plunge cutting process until the final depth is reached. Figure 10.2 (right) shows the influence of different structure designs (A or B) on the machining time and the cutting length. In both examples the same

depth of cut of 0.25 µm has been used for the finish cut. A larger infeed has been utilized for a kind of roughing step until a certain depth has been reached. For the plate shown in Figure 10.2 the structure type »B« has been used.

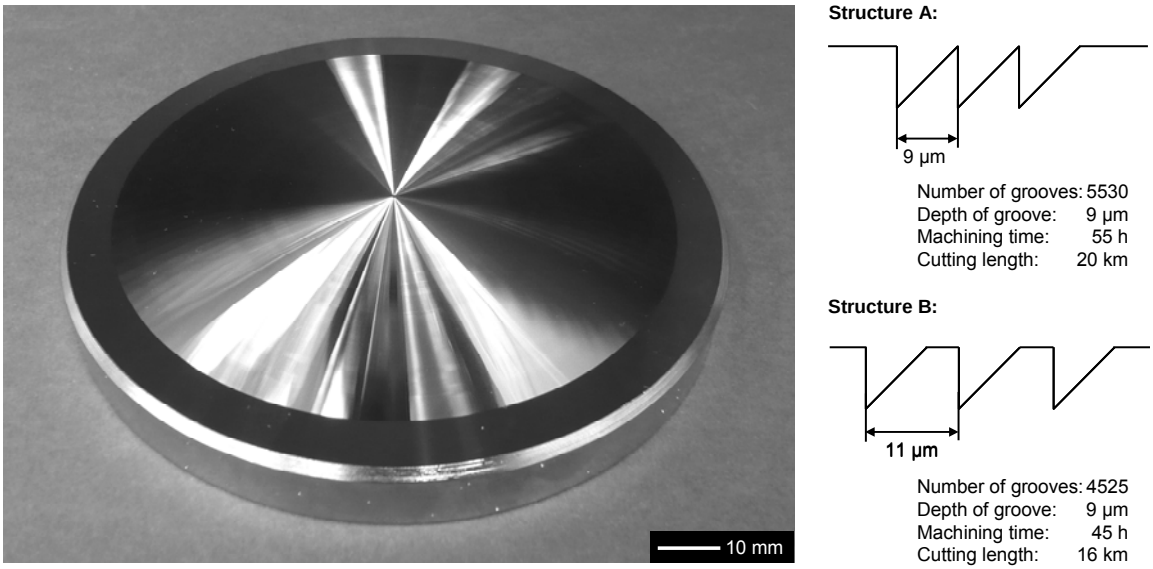

Figure 10.2: Continuous groove structure (blazed gratings) and variation of groove pitch

The machining of the plate shown in Figure 10.2 has been very successful. The burr formation could be avoided throughout the whole diameter by using the diagonal infeed direction. No in-process de-burring has been applied. The depth variation has been minimized to values of below 1 µm. Further improvements of the depth variation can be reached by the implementation of the temperature compensation in the machine control.

Another disc has been machined with blazed gratings (structure type: B) up to a diameter of 50 mm (see **Figure 10.3**). It has been used as mold for the LED illumination, which is described in chapter 5.6.5. The large SEM pictures demonstrate the quality and the stability of the process.

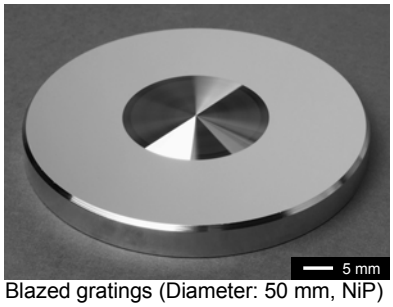

Blazed gratings (Diameter: 50 mm, NiP)

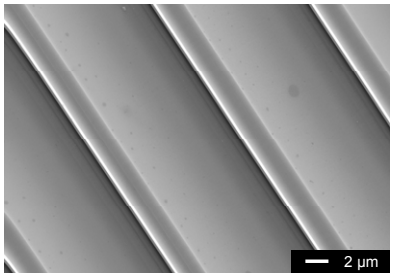

Detailed view into burr free grooves

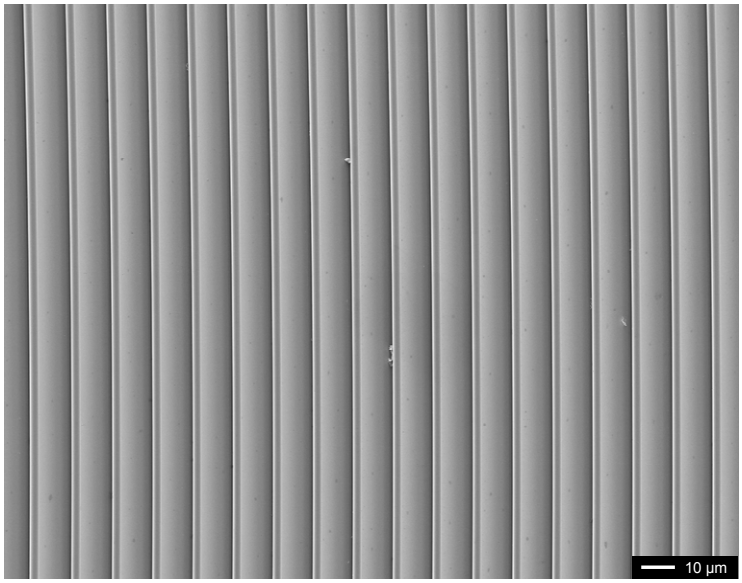

SEM picture showing constant groove characteristics

Figure 10.3: Continuous groove structure of blazed gratings

The detailed view in the lower left corner of Figure 10.3 reveals the smooth slanted surfaces of the blazed grating that is absolutely necessary for the optical function of the structure. It can only be reached by machining using diamond cutting tools.

10.1.2 Machining Discontinuous Blazed Gratings

By the use of the FTS the blazed gratings can be machined as discontinuous grooves. In that way, the length and the distance of the grooves can be adjusted freely. Further, the area of the structures can be regulated to certain area, as shown in **Figure 10.4**. Two squares are structured and can be used as master structure for lightguides in backlights for displays. So far, the structure density has been adjusted in the step & repeat embossing process by the distance between each embossing step using a small stamp. Now this pattern can be directly machined into the mold surface.

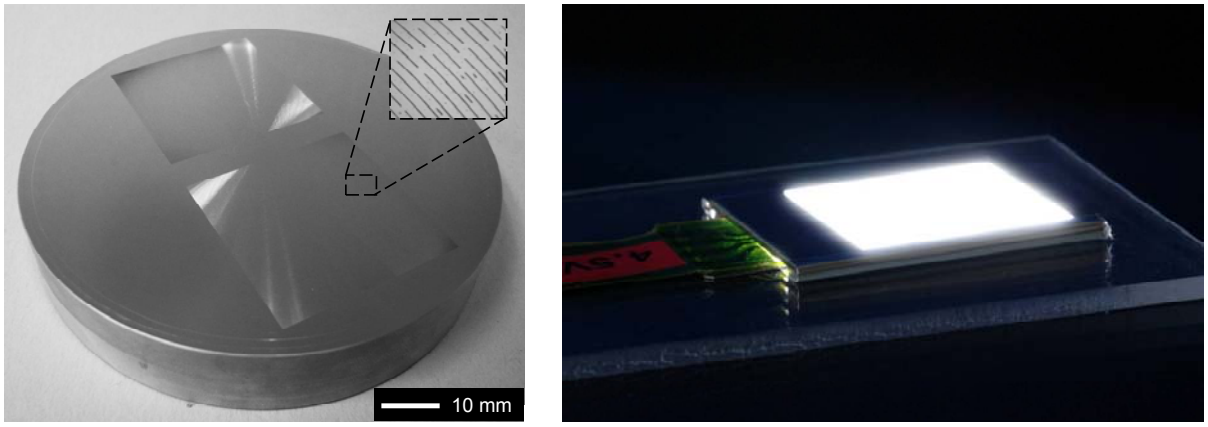

Microstructured mold for lightguide (30 x 30 mm²) Backlight sample using LED and microstructured lightguide

Figure 10.4: Microstructured mold for lightguides in backlight units

The final machining of the work piece, illustrated in Figure 10.4, has taken about 20 h and a radius range from 3 to 36 mm has been processed. The machining time is less compared to the previously presented example because of the lower structure depth and density in radial direction. Further, the use of the aluminum RSA-905 allowed for a larger depths of cut.

The given examples showed that the process development has been transferred successfully to large area work pieces. Due to thorough warm-up cycles, the accuracy of the structure can be enhanced. Further, the tool wear does not affect the machining of micro grooves significantly and cutting distances of 20 km could be achieved even in machining NiP-coatings.

10.2 Examples of Hybrid Optical Surfaces

In chapter 4.1 the use and the opportunities of hybrid optics for automotive headlights have been explained. In that case, a microstructure has been machined on a free-form surface. The free-form is required to compensate for the shrinkage in the mold during the injection molding process. Since the non-rotational part of the free-form is only small, two different demonstrator work pieces are introduced in the following.

The first demonstrator work piece is a sine wave surface that carries a facet structure on top. It is shown in **Figure 10.5**. The diameter of the work piece is 50 mm. The sine wave as basic shape of the work piece consists of four sine waves with an amplitude of 0.5 mm. Therefore, a stroke of 1 mm is needed which is allocated by the dynamic axis. The small picture in the upper left corner of Figure 10.5 shows a non-structured sine wave. The sine wave curve is constant in the angular orientation on the work piece. The hole in the work piece is needed because of the increasing slope angle of the surface towards the center (stroke keeps constant but circumference is reduced). In this case, the slope was limited by the diamond tool to 12.5°. The applied facet structure originally is used for laser mirrors to form/integrate the laser beam. A facet mirror on a planar work piece can be seen in the lower left corner in Figure 10.5. Each facet has an aspherical shape. The specific arrangement on the surface results in small rectangular facets. The structure depth is about 15 µm. Due to the highly dynamic requirements of the surface geometry, it has been machined by the FTS system.

The machining of the aluminum work piece has been done using a spindle speed of 150 rpm. For the finishing cut a feed rate of 0.5 mm/min and a depth of cut of 4 µm have been adjusted. A surface finish of 5 nm Ra has been achieved.

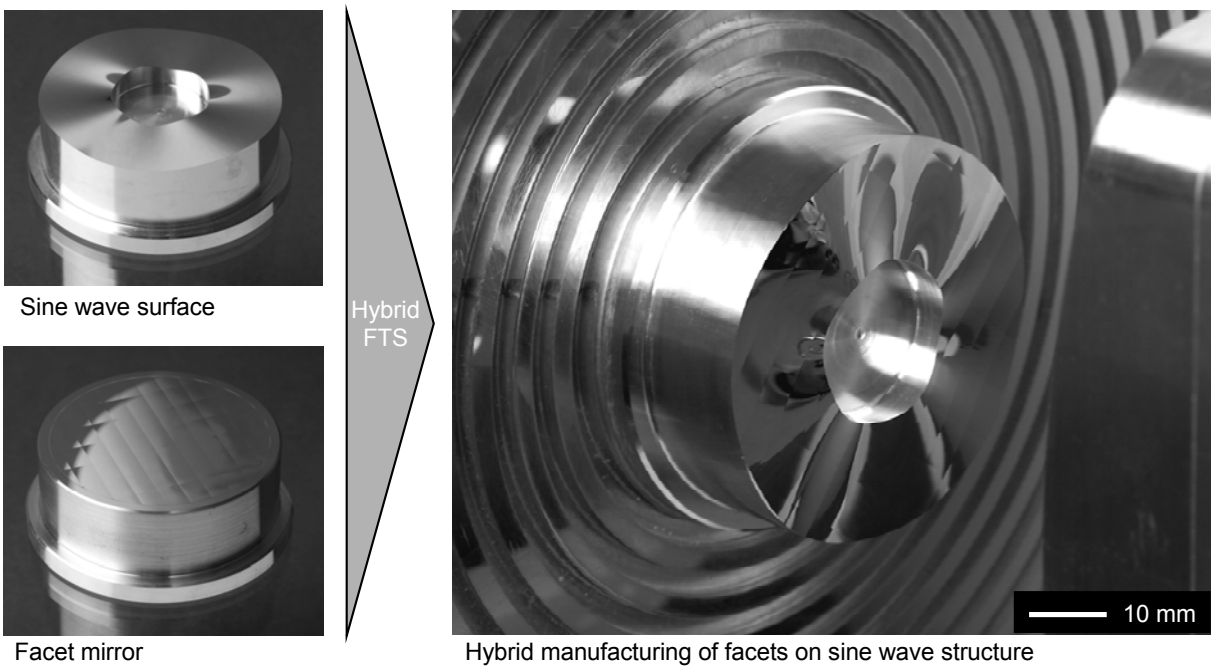

Figure 10.5: Hybrid machining: facets on sine wave surface

The second demonstrator work piece is shown in **Figure 10.6**. The basic geometry of this hybrid optic is a sloped surface, which has the same facets on top that have been described before. The work piece has a diameter of 80 mm and a slope of 10% has been adjusted. Hence, the required maximum stroke of the Slow Tool is 8 mm. The machining has been done with a rotational speed of 150 rpm using a cutting tool with 500 µm radius. The finishing has been done adjusting a feed rate of 0.5 mm/min and a depth of cut of 4 µm. A surface finish of 5 nm Ra has been achieved.

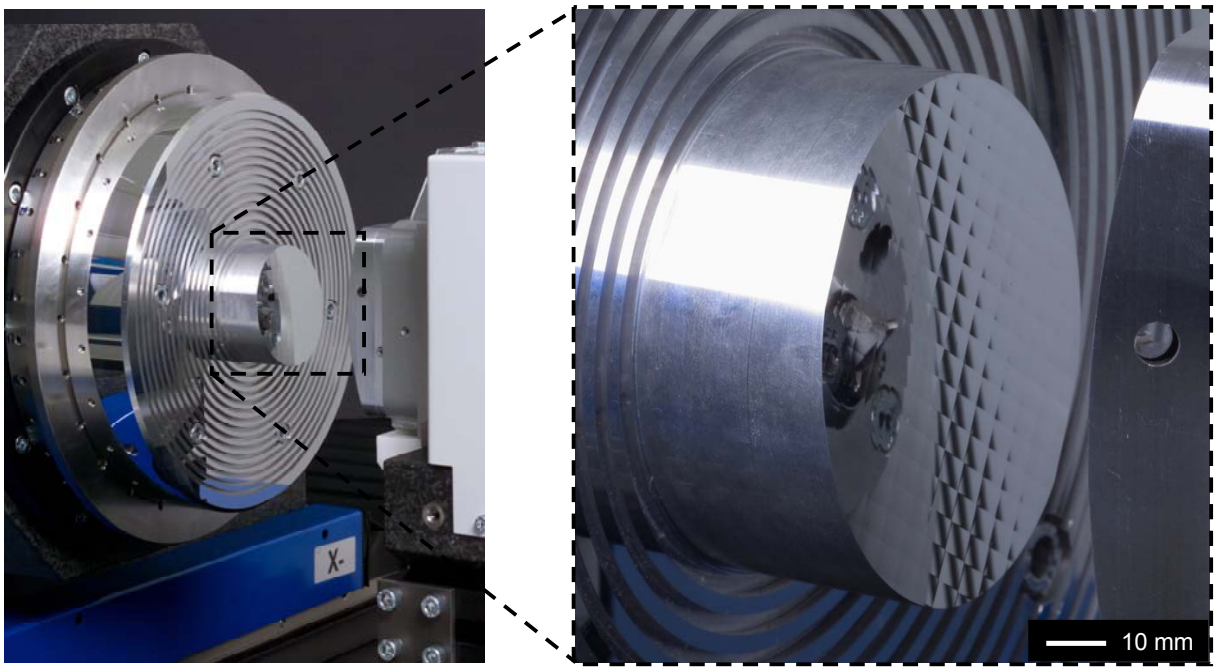

Figure 10.6: Hybrid machining: facets on sloped surface

The movement of the dynamic axis is a sine with one period per revolution and in that way less complex than the demonstrator described before. Exemplarily, **Figure 10.7** shows the set point data for the Fast and Slow Tool axis during the machining of the hybrid optic explained before. Easily, the highly dynamic signal for FTS can be recognized. Furthermore, the Slow Tool movement is very homogeneous while the FTS has to realize sharp peaks at the transition from one facet to another.

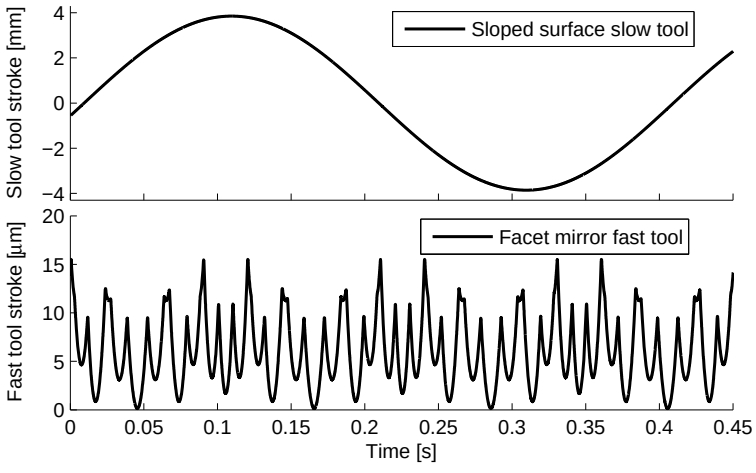

Figure 10.7: Set point data for the machining of facets on sloped surface

The machining of the sloped surface requires also a radius compensation for the cutting tool, which is integrated into the control of the hybrid FTS. In that way, it is possible to machine a flat, sloped surface or even by the use of the FTS system a sloped surface with facets on it.

These examples demonstrate the machining possibilities that the new hybrid FTS offers. Applications can be found in the field of reflective optics, where structured free-form surfaces are needed or in the area of injection molding, where structured mold inserts with free-form shape are needed for the compensation of shrinkage. But the new system is also relevant for precision parts that do not have an optical function. For the calibration of CMM in measurement technology, multi-wave standards are used. Such standards use superimposed sine wave structures that now can be machined which a larger variety offering larger strokes.

11 Summary

Many new developments in optical systems are driven by the quick improvements of LEDs as light source. The LED technology allows for new lighting systems for example in headlights for automotive applications or in miniaturized illumination systems in the field of display technology. In both cases highly sophisticated polymer optics are required to realize these new lighting applications. The research conducted in the scope of the project »ERANET-OPTICALSTRUCT« strongly contributed in enabling these new and innovative lighting solutions based on hybrid optics. The aim of the project was to improve the whole process chain starting with the optical design, the mold machining, and ending with the manufacturing of the final product by replication.

Beside the replication as final manufacturing step, ultra-precision machining using diamond cutting tools is the key technology for the production of hybrid optics and the corresponding molds. However, the ultra-precision machining systems as well as the process technology needed improvements to enable the production of hybrid optics.

Therefore, within this project a new ultra-precision turning machine using a hybrid Fast Tool Servo (FTS) system was developed. The hybrid FTS system combines a long stroke dynamic axis with a highly dynamic FTS. The dynamic axis was designed to machine the free-form part of the hybrid optics while the FTS is producing the microstructures simultaneously. The control system for the hybrid FTS was improved strongly within the project. Applying FPGA (Field Programmable Gate Array) technology for the feedback control platform of the system, allows for minimal latency times that are negligible for the control loop bandwidth. It was achieved that the control hardware itself is not the limiting factor in bandwidth anymore.

Advances in setpoint processing focus on the idea to preserve the original setpoint geometry from the CAD system as far as possible in the geometry processing chain. This strategy both includes preventing mathematical transformations and conversions of the data format. For the programming of the machine, a CAD/CAM module offering 3D-visualization was implemented. It supports the machinist in choosing the right spindle speeds and feed rates, or checking the tool capabilities. The visualization enables diagnostics of microstructured surfaces up to smallest details.

To enable the robust machining of hybrid optics with finite microstructures by diamond machining, a deep understanding of the relevant process and material parameters was generated. Now, it is possible to machine burr free v-groove structures with high precision, which is defined by the optical surface quality and constant structure dimensions. Furthermore, a new diamond cutting tool was developed that has a clearance angle of 40° and offers new possibilities in the design and machining of free-form surfaces.

The new process and machining technology was used to realize molds and master structures for the replicative production of hybrid optics and microstructures.

Especially the high quality replication of thick-walled plastic optics by injection molding processes requires the knowledge of the influencing process parameters. Within the project the quality of hybrid lenses used in head-lights for the automotive industry was significantly improved. Furthermore, microstructured stamping tools and large area molds were used for the production of light guiding foils and diffractive optical elements. These foils are used in mobile phones to lighten the display or the keypad as well as for the replacement of halogen bulbs achieving a reduction of energy consumption of 60% while offering the same brightness. The characterization of the microstructures is enabled by a new miniature tactile measurement probe that was developed and tested within the project.

The results of the research project »ERANET-OPTICALSTRUCT« were achieved by a strong cooperation between all partners. Due to the special structure of the MNT ERA-NET program it has been possible to integrate European technology leaders in the project consortium. This supported strongly the accomplishment and quality of the project results.

The consortium wants to thank the different national funding agencies for supporting the project. The Finish company Oy Modines has been funded by Tekes. The work of Unimetrik has been supported by the Basque Government Innobasque. The German consortium has been funded by the German Federal Ministry of Education and Research (BMBF) and managed by the Project Management Agency Forschungszentrum Karlsruhe (PTKA). Further, the consortium wants to thank the companies Kanigen Works Benelux and Contour Fine Tooling for their cooperation.

12 Publications

Articles

Brecher, C.; Merz, M.; Niehaus, F.; Wenzel, C.: *Microstructuring of Free-Form Surfaces by the Use of a Hybrid Fast-Tool-Servo-System.* In: Proceedings of the euspen International Conference - Zürich - May 2008, Eds.: Brussel, H.; Brinksmeier, E.; Spaan, H.; Burke, T., Copy & Druck Wien, Austria 2008, ISBN 978-0-9553082-5-3, S. 518-522

Brecher, C.; Niehaus, F.; Merz, M.; Wenzel, C.: *Mikrostrukturierung von Freiformflächen Maschinen- und Prozessoptimierung im Forschungsprojekt "Eranet-Opticalstruct".* In: Werkstattstechnik - wt online 98 (2008), 3, S. 195-199

Brecher, C.; Niehaus, F.; Merz, M.; Schmidt, K.: *Machining Microstructures on Free-Form Surfaces.* In: Tagungsband »MiNaT-Hotspots«, 2008

Brecher, C.; Niehaus, F.; Merz, M.; Wenzel, C.: *Diamantzerspanung mit mehr Dynamik*. In: Mikroproduktion, 05/09, Hanser Verlag, 2009, S. 8-12

Presentations

Schmidt, K.: *Trends in der Ultrapräzisionszerspanung*, Workshop - Mikrozerspanung für den Werkzeug und Formenbau, Fraunhofer IPK, Berlin, 2007

Niehaus, F.: *ERANET-OPTICALSTRUCT - Microstructuring of Free-Form Surfaces*, »MiNaT-Hotspots«, 2008

Poster Presentations

Brecher, C.; Niehaus, F.; Merz, M.; Wenzel, C.: *Mikrostrukturierung von Freiformflächen.* Karlsruher Arbeitsgespräche, 2008

Brecher, C.; Niehaus, F.; Merz, M.; Wenzel, C.: *Microstructuring of Free-Form Surfaces by the Use of a Hybrid Fast-Tool-Servo-System (FTS)*. euspen International Conference, Zürich, 2008

Brecher, C.; Niehaus, F.; Merz, M.; Wenzel, C.: *Mikrostrukturierung von Freiformflächen.* MiNaT - Internationale Fachmesse für Feinwerks-, Ultrapräzisions-, Mikro- und Nanotechnologien, Stuttgart, 2008

Brecher, C.; Niehaus, F.; Merz, M.; Wenzel, C.: *ERANET-OPTICALSTRUCT - Mikrostrukturen auf Freiformen*. Hannover Messe, 2009

13 Contacts

Forschungszentrum Karlsruhe GmbH
Project Management Agency Forschungszentrum Karlsruhe (PTKA)
Mr. Stefan Scherr
Hermann-von-Helmholtz-Platz 1
D-76344 Eggenstein-Leopoldshafen, Germany
Phone: +49 7247 82 5286
Fax: +49 7247 82 5456

Eschenbach Optik GmbH + Co
Mr. Erik Schalle
Andernacher Straße 29 B
D-90411 Nürnberg, Germany
Phone: +49 911 3600 450
Fax: +49 911 3600 5450

Fraunhofer Institute for Production Technology (IPT)
Mr. Michael Merz, Mr. Frank Niehaus
Steinbachstraße 17
D-52074 Aachen, Germany
Phone: +49 241 8904 0
Fax: +49 241 8904 198

LT Ultra-Precision Technology GmbH
Mr. Richard Widemann
Afterholderberg, Wiesenstraße 9
D-88634 Herdwangen-Schönach, Germany
Phone: +49 7552 405 99 0
Fax: +49 7552 405 99 50

ModuleWorks GmbH
Dr. Marc Stautner
Ritterstrasse 12a
D-52072 Aachen, Germany
Phone: +49 241 400 6020
Fax: +49 241 400 6019

Modines Ltd.
Mr. Kari Rinko
Matalasalmenkuja 1
FI-00150 Helsinki, Finland
Phone: +358 9 6226 550
Fax: +358 9 177 866

UNIMETRIK - INNOVALIA Metrology
Mr. Toni Ventura-Traveset
San Blas, 11
ES-01170 Legutiano-Álava, Spain
Phone: +34 93 663 3043
Fax: +34 93 663 1838

Contour Fine Tooling BV
Mr. Eric van Hal
De Vest 1C
NL-5555 XL Valkenswaard, The Netherlands
Phone: +31 40 208 2363
Fax: +31 40 208 2313

Kanigen Works Benelux
Mr. Mark Decker
Wolfsbergstraat 57
B-3600 Genk, Belgium
Phone: +32 89 3801 26
Fax: +32 89 3804 32